PhD program in Environmental Engineering

Doctoral thesis by compendium of publications

Dynamics of ultrafine particles and tropospheric ozone episodes

Cristina Carnerero Quintero

Barcelona, 2021

Thesis advisors:

Dr. Xavier Querol Carceller
IDAEA-CSIC

Dr. Andrés Alastuey Urós
IDAEA-CSIC

Tutor:

Dr. Santiago Gassó Domingo
Universitat Politècnica de Catalunya

“There is not a particle of life
which does not bear poetry within it.”

GUSTAVE FLAUBERT

ACKNOWLEDGEMENTS

I would like to express my most sincere gratitude to my supervisors, Dr. Xavier Querol and Dr. Andrés Alastuey for their invaluable support. Most of all, I would like to thank them for allowing me to come up with new ideas and strengthening my personal development with no limitations. I am also grateful for their attitude towards me, which has always been humble and caring. I have always felt respected and valued by them, for which I am thankful above all.

I am especially thankful to each and all of my colleagues at IDAEA. You were always happy to help and offer advice whenever I asked, but most importantly, I always felt at home with you. I would like to thank Dr. Noemí Pérez and Dr. Cristina Reche for maintaining the instrumentation at Barcelona and Montseny and providing data used in this thesis. Special thanks to Jesús Yus, Marta Via, Adolfo González, Jordi Massagué, Pedro Trechera and Amaia Fernández for all the talks, lunches, coffees, memorable meetings outside of work and, in recent times, very much needed virtual support. My warmest thanks to Dr. María Cruz Minguillón and Diana Blanco for teaching me things that are far more important than science. Gracias.

This thesis would not have been possible without Dr. Maria Rosa Soler Duffour (Universitat de Barcelona), to whom I will always be grateful for introducing me to air quality and recommending me to my supervisors. Gràcies per l'oportunitat.

Special thanks to Professor Kang-Ho Ahn and his team from the University of Hanyang for being involved in the filed measurement campaigns and contributing with state-of-the-art instrumentation.

I would also like to thank colleagues at INAR who received me and helped me in many ways during my visit in Helsinki, especially Dr. Lubna Dada and Dr. Pauli Paasonen, who guided my first steps in this thesis with great patience. Kiitos.

During this thesis, I met numerous people that have helped and inspired me in many ways. To keep it short, I would like to thank everyone who helped me during campaigns, collaborated in my publications, and joined or imparted courses, workshops or conferences I attended.

I would also like to thank the administrations that supported the measurement campaigns, long-term measurements, research projects and contracts in the framework encompassing this doctoral thesis. This work was supported by the Spanish Ministry of Agriculture, Fishing, Food and Environment; the Ministry of Economy, Industry and Competitiveness; the Madrid City

Council and Regional Government; FEDER funds under the project HOUSE (CGL2016-78594-R). The measuring stations of Barcelona and Montseny received the support of the Government of Catalonia.

This doctoral thesis received the financial support of a predoctoral fellowship "*Ayudas para contratos predoctorales para la formación de doctores*" (BES-2017-080027), awarded by the *Ministerio de Economía, Industria y Competitividad* (Spanish Government) and funded by the European Social Fund (European Commission).

On a more personal note, I must highlight the unwavering support received by Iolanda, Araceli, Sara and Marina, with whom I ventured into science more than 10 years ago. Shortly after, I met Sergio, who has been my source of strength ever since. Without their encouragement and love, I would never have succeeded. Us estimo.

A mi madre y a mi padre les doy las gracias por enseñarme a pensar siempre de manera independiente y animarme a aprender sin límites.

ABSTRACT

Atmospheric aerosol particles, particularly ultrafine particles (UFPs; particles with less than 100 nm in diameter), and tropospheric ozone (O_3) are atmospheric pollutants highly influenced by photochemical reactions, i.e., processes initiated by the absorption of solar radiation. High concentrations of ambient UFPs and O_3 have important adverse effects on human health and impact on climate.

Areas with high insolation and atmospheric dynamics favoring the accumulation of pollutants by vertical recirculation of air masses, such as the Western Mediterranean and other regions of Southern Europe, often register episodes with high concentrations of UFPs and O_3, especially in spring and summer. UFPs episodes might be caused by the emission and accumulation of particles or by the photochemical formation of particles from gaseous precursors (new particle formation; NPF).

The objective of this thesis is to characterize the relationship between UFPs and O_3 in areas and periods with important photochemical activity. More specifically, this thesis aims at (i) identifying the atmospheric patterns causing the episodes, (ii) establishing whether these pollutants are driven by the same processes or occurring in parallel and (iii) describing how UFP concentrations have evolved over the last years.

Based on these objectives, we analyzed data gathered during intensive field campaigns of simultaneous surface-level and vertical measurements, as well as long-term series of continuous measurements. Combining these, we focus on evaluating the seasonality and simultaneity of UFPs and O_3 episodes, identifying the key contributing atmospheric factors and providing insights on the influence of NPF on the concentration of UFPs.

We found that two distinct scenarios govern the formation and transport of UFPs and O_3: recirculation of air masses and venting. The occurrence of either scenario is determined by large-scale meteorology, whereas the magnitude of concentrations is modulated by the availability of precursors and local atmospheric and orographic conditions. Our results indicate that acute UFPs episodes are undoubtedly linked with O_3 episodes. Yet, the episodes may or may not be simultaneous on the same day. The occurrence of an O_3 episode seems to be always concurrent with an UFPs episode caused by accumulation of primary and secondary particles during

recirculation periods. However, high UFPs concentrations caused by NPF are mainly occurring with lower (but relatively high in absolute values) O_3 concentrations during venting periods.

When considering the average annual UFPs concentrations in urban locations, primary traffic emissions have a greater contribution to the total number of particles than NPF. Yet, on days with NPF events, the contribution from NPF to UFPs might be higher than that from primary emissions.

Although NPF events do not occur in most of the days, the number of days with NPF events is increasing, probably due to a decreasing trend in the anthropogenic atmospheric emissions in recent years, which caused a decline in the particle sinks. Thus, the contribution of NPF to the number concentration of UFPs is increasing as well. The total concentration of UFPs may either increase or decrease, depending on the local conditions and precursor emissions. In urban environments, the decline in anthropogenic emissions causes a direct decrease in the concentration of UFPs. In rural environments, NPF becomes more favorable and the concentration of UFPs increases. This might be related to increasing local biogenic emission of precursors caused by rising temperatures, as well as a reduction of sinks due to a decline in transported anthropogenic emissions.

Abatement policies implemented in recent years aiming at decreasing anthropogenic emissions of atmospheric pollutants have had a major impact in the number concentration of UFPs at urban environments. However, these policies have not had a significant impact in the regional background, where the concentration of UFPs has increased.

RESUM

Els aerosols atmosfèrics, particularment partícules ultrafines (UFPs per les seves sigles en anglès; partícules de menys de 100 nanòmetres de diàmetre), i l'ozó troposfèric (O_3) són contaminants atmosfèrics molt influenciats per reaccions fotoquímiques, i. e., processos iniciats per l'absorció de radiació solar. Concentracions elevades d'UFPs i O_3 en l'ambient tenen importants afectes adversos en la salut humana i impactes en el clima.

En àrees amb una alta insolació i dinàmiques atmosfèriques que afavoreixen l'acumulació de contaminants degut a recirculacions verticals de masses d'aire, com el Mediterrani occidental i altres regions del sud d'Europa, sovint s'enregistren episodis d'altes concentracions d'UFPs i O_3, especialment a la primavera i a l'estiu. Els episodis d'UFPs poden estar causats per l'emissió i acumulació de partícules o per la formació fotoquímica de partícules a partir de precursors gasosos (formació de partícules noves; NPF per les seves sigles en anglès).

L'objectiu d'aquesta tesi és caracteritzar la relació entre UFPs i O_3 en àrees amb una activitat fotoquímica important. Concretament, aquesta tesi té com a objectiu identificar els patrons atmosfèrics que causen els episodis, determinant si aquests contaminants estan regits pels mateixos processos o bé ocorren en paral·lel, així com descriure l'evolució de les concentracions d'UFP en els darrers anys.

Basant-nos en aquests objectius, hem analitzat dades recopilades durant campanyes de mesures intensives de mesures simultànies a nivell de superfície i en altura, així com sèries de dades de mesures contínues de llarg termini. Mitjançant la combinació d'aquestes dades, s'ha avaluat l'estacionalitat i la simultaneïtat dels episodis d'UFPs i d'O_3, identificant els factors que hi contribueixen i aportant informació sobre la influencia de la NPF en les concentracions d'UFPs.

Hem trobat que hi ha dos escenaris que controlen la formació i el transport d'UFPs i O_3: la recirculació vertical de masses d'aire i la ventilació. L'ocurrència d'un o altre escenari ve determinada per les condicions meteorològiques a escala sinòptica, mentre que la magnitud de les concentracions ve donada per la disponibilitat de precursors i les condicions atmosfèriques i orogràfiques locals. Els nostres resultats indiquen que els episodis aguts d'UFPs estan indubtablement vinculats amb els episodis d'O_3. Tot i així, els episodis poden ser simultanis en un mateix dia o no ser-ho. Un episodi d'O_3 sembla ser sempre simultani amb un episodi d'UFPs causat per acumulació de partícules primàries i secundàries durant períodes de recirculació.

Tanmateix, altes concentracions d'UFPs causades per NPF tenen lloc principalment amb concentracions baixes (però relativament altes en valor absolut) d'O_3 durant períodes de ventilació.

Quan es consideren les concentracions mitjanes anuals d'UFPs en àrees urbanes, les emissions primàries del trànsit tenen una major contribució al nombre total de partícules que la NPF. No obstant, en dies amb episodis de NPF, la contribució de la NPF al nombre total d'UFPs és més gran que la de les emissions primàries.

Tot i que en la majoria dels dies no es detecten episodis de NPF, el nombre de dies amb NPF està incrementant, probablement degut a una tendència a la baixa de les emissions atmosfèriques antropogèniques en els darrers anys, que han causat una disminució en les embornals de condensació i coagulació de partícules. En conseqüència, la contribució de la NPF al nombre d'UFPs també està augmentat. La concentració total d'UFPs pot augmentar o disminuir, depenent de les condicions locals i les emissions de precursors. En àrees urbanes, la disminució d'emissions antropogèniques causa una disminució directa de la concentració d'UFPs. En canvi, en ambients rurals, la NPF esdevé més favorable fins al punt que la concentració d'UFPs creix. Això pot ser degut a un increment de les emissions biogèniques locals de precursors causades per l'augment de les temperatures, així com una reducció de les embornals de partícules degut a la disminució del transport d'emissions antropogèniques.

Les polítiques implementades en els darrers anys amb l'objectiu de reduir les emissions antropogèniques de contaminants atmosfèrics han tingut un gran impacte en la concentració del nombre de partícules en ambients urbans. Per contra, aquestes polítiques no han tingut un impacte significatiu en el fons regional, on el nombre de partícules ha augmentat.

RESUMEN

Los aerosoles atmosféricos, en particular las partículas ultrafinas (UFPs por sus siglas en inglés; partículas de menos de 100 nanómetros de diámetro), y el ozono troposférico (O_3) son contaminantes atmosféricos muy influenciados por reacciones fotoquímicas, i.e., procesos iniciados por la absorción de radiación solar. Concentraciones elevadas de UFPs y O_3 en el ambiente tienen importantes efectos adversos en la salud humana e impactos en el clima.

En áreas con una alta insolación y dinámicas atmosféricas que favorecen la acumulación de contaminantes debido a recirculaciones verticales de masas de aire, como en el Mediterráneo occidental y otras regiones del sur de Europa, a menudo se registran episodios de altas concentraciones de UFPs y O_3, especialmente en primavera y verano. Los episodios de UFPs pueden estar causados por la emisión y acumulación de partículas o por la formación fotoquímica de partículas a partir de precursores gaseosos (formación de nuevas partículas; NPF por sus siglas en inglés).

El objetivo de esta tesis es caracterizar la relación entre UFPs y O_3 en áreas y períodos con una actividad fotoquímica importante. Concretamente, esta tesis tiene como objetivos identificar los patrones atmosféricos que causan los episodios, determinando si estos contaminantes están regidos por los mismos procesos o bien ocurren en paralelo, así como describir la evolución de las concentraciones de UFPs en los últimos años.

Basándonos en estos objetivos, se han analizado datos recopilados durante campañas de medidas intensivas simultáneas a nivel de superficie y en altura, así como series de datos de medidas continuas a largo plazo. Mediante la combinación de estos datos, se ha evaluado la estacionalidad y la simultaneidad de los episodios de UFPs y O_3, identificando los factores que contribuyen a ellos y aportando información sobre la influencia de la NPF en las concentraciones de UFPs.

Hemos encontrado que hay dos escenarios que controlan la formación y el transporte de UFPs y O_3: la recirculación vertical de masas de aire y la ventilación. El acontecimiento de uno u otro escenario viene determinado por las condiciones meteorológicas a escala sinóptica, mientras que la magnitud de las concentraciones viene dada por la disponibilidad de precursores y las condiciones atmosféricas y orográficas locales. Nuestros resultados indican que los episodios agudos de UFPs están indudablemente vinculados con los episodios de O_3. Aun así, los episodios pueden ser simultáneos en el mismo día o no serlo. Un episodio de O_3 parece ser siempre

simultáneo con un episodio de UFPs causado por acumulación de partículas primarias y secundarias durante períodos de recirculación. Sin embargo, altas concentraciones de UFPs causadas por NPF tienen lugar principalmente con concentraciones relativamente bajas (pero altas en valor absoluto) de O_3 durante períodos de ventilación.

Cuando se considera el promedio de las concentraciones anuales de UFPs en áreas urbanas, las emisiones primarias del tráfico tienen una mayor contribución al número total de partículas que la NPF. No obstante, en días con episodios de NPF, la contribución de NPF al número total de UFPs puede ser mayor que la de las emisiones primarias.

Aunque en la mayoría de días no se detectan episodios de NPF, el número de días con NPF está incrementando, probablemente debido a una tendencia a la baja en los últimos años de las emisiones atmosféricas antrópicas, que han causado una disminución en los sumideros de condensación y coagulación. En consecuencia, la contribución de la NPF al número de UFPs también va en aumento. La concentración total de UFPs puede aumentar o disminuir, dependiendo de las condiciones locales y las emisiones de precursores. En áreas urbanas, la disminución de emisiones antrópicas causa una disminución directa de la concentración de UFPs. En cambio, en ambientes rurales, la NPF se hace más favorable, hasta el punto de aumentar las concentraciones de UFPs. Esto puede ser debido a un incremento de las emisiones biogénicas locales de precursores debido al aumento de temperaturas, así como a una reducción de los sumideros de partículas debido a una disminución del transporte de emisiones antrópicas.

Las políticas implementadas en los últimos años con el objetivo de reducir las emisiones antrópicas de contaminantes atmosféricos han tenido un gran impacto en las concentraciones del número de UFPs en ambientes urbanos. Por el contrario, estas políticas no han tenido un impacto significativo en el fondo regional, donde la concentración de UFPs ha aumentado.

TABLE OF CONTENTS

List of Acronyms

Note that this list does not include the acronyms used in the compendium of scientific publications.

a.s.l.	Above sea level
a.g.l.	Above ground level
ACTRIS	Aerosols, Clouds and Trace gases Research InfraStructure
AIS	Air Ion Spectrometer
ATN	Attenuation coefficient
BC	Black Carbon
CH_4	Methane
CIEMAT	Centro de Investigaciones Energéticas, MedioAmbientales y Tecnológicas. English: Research center for energy, environment and technology
CLTRAP	Convention on Long-range Transboundary Air Pollution
CO	Carbon monoxide
CoagS	Coagulation Sink
CPC	Condensation Particle Counter
CS	Condensation Sink
CSIC	Consejo Superior de Investigaciones Científicas. English: Spanish national research council
DEG	Diethylene Glycol
DMA	Differential Mobility Analyzer
D_p	Particle diameter
ELVOC	Extremely low-volatile organic compound
GR	Growth Rate
H_2SO_4	Sulfuric acid

HO_2	Hydroperoxyl radical
HOMs	Highly oxygenated organic molecules
IDAEA	Instituto de Diagnóstico Ambiental y Estudios del Agua English: Institute of environmental assessment and water research
IQFR	Instituto de Química Física Rocasolano English: Institute of Physical Chemistry Rocasolano
ISCIII	Instituto de Salud Carlos III. English: Carlos III Health Institute
$J_{\Delta Dp}$	Formation rate
LVOC	Low-volatility organic compound
MAAP	Multi-Angle Absorption Photometer
NH_3	Ammonia
NO	Nitric oxide
NO_2	Nitrogen dioxide
NO_3	Nitrate radicals
NOx	Nitrogen oxides
NPF	New Particle Formation
O_3	Ozone
OH	Hydroxyl radical
PMF	Positive Matrix Factorization
PSM	Particle Size Magnifier
PTR-TOF-MS	Proton-Transfer-Reaction Time-Of-Flight Mass Spectrometer
RB	Regional Background
RO_2	Organic peroxide
SB	Suburban Background
SMPS	Scanning Mobility Particle Sizer
SO_2	Sulfur dioxide
SR	Solar Radiation or Shrinking Rate (see footnote on page 30)

U	Urban
UB	Urban Background
UFP	Ultrafine Particle
VOC	Volatile Organic Compound
WHO	World Health Organization
XVPCA	Xarxa de Vigilancia i Prevenció de la Contaminació Atmosfèrica. English: Atmospheric pollution monitoring and forecasting network

LIST OF TABLES

Note that the scientific publications included in the compendium have their own numbering of tables and are not listed here.

LIST OF FIGURES

Note that the scientific publications included in the compendium have their own numbering of figures and are not listed here.

STRUCTURE OF THE DOCTORAL THESIS

This doctoral thesis is presented as a compendium of publications. The dissertation is composed of a general introduction including the state of the art and objectives of the thesis (Section 1), followed by a description of the methodology with details of the instrumentation and techniques used (Section 2). Copies of the three research publications are reproduced in Section 3, preceded by a brief summary of their contents and the contributions of the author to each of them. Section 4 provides a global discussion of the results published in the research publications. Finally, conclusions and suggestions for future research are included in Sections 5 and 6. Throughout the dissertation, the publications are cited with roman numerals according to the following numeration:

Paper I **Carnerero, C.**, Pérez, N., Reche, C., Ealo, M., Titos, G., Lee, H.-K., Eun, H.-R., Park, Y.-H., Dada, L., Paasonen, P., Kerminen, V.-M., Mantilla, E., Escudero, M., Gómez-Moreno, F. J., Alonso-Blanco, E., Coz, E., Saiz-Lopez, A., Temime-Roussel, B., Marchand, N., Beddows, D. C. S., Harrison, R. M., Petäjä, T., Kulmala, M., Ahn, K.-H., Alastuey, A. and Querol, X.: Vertical and horizontal distribution of regional new particle formation events in Madrid, *Atmospheric Chemistry and Physics*, 18(22), 16601–16618, doi:10.5194/acp-18-16601-2018, 2018.

Paper II **Carnerero, C.**, Pérez, N., Petäjä, T., Laurila, T. M., Ahonen, L. R., Kontkanen, J., Ahn, K.-H., Alastuey, A. and Querol, X.: Relating high ozone, ultrafine particles, and new particle formation episodes using cluster analysis, *Atmospheric Environment: X*, 4, 100051, doi:10.1016/j.aeaoa.2019.100051, 2019.

Paper III **Carnerero, C.**, Rivas, I., Reche, C., Pérez, N., Alastuey, A. and Querol, X.: Trends in primary and secondary particle number concentrations in urban and regional environments in NE Spain, *Atmospheric Environment*, 244, 117982, doi:10.1016/j.atmosenv.2020.117982, 2021.

1 INTRODUCTION

The Earth's atmosphere is a mixture of gases and particles in all states of matter. In a cubic centimeter of air, the number of gas molecules is of the order of 10^{19} (assuming ideal gases in standard conditions), whereas the number of particles varies greatly in time and space. In order of magnitude, typical particle concentrations range from 10^2 cm^{-3} in Arctic environments (Tunved et al., 2013), to 10^6 cm^{-3} in polluted urban areas (Vu et al., 2015). The most abundant gas in the atmosphere is nitrogen (78%), followed by oxygen (21%), and other gases in much lower quantities (Seinfeld and Pandis, 2006). Some of these trace gases are of great importance because, together with particulate matter, constitute major components of air pollution and are, therefore, of special relevance for health and climate (EEA, 2020).

The composition of the atmosphere is controlled by physical, chemical and biological processes. Of special interest are photochemical reactions, initiated when molecules absorb electromagnetic radiation in the ultraviolet, visible or infrared range in the form of photons with energy $h\nu$ (IUPAC, 2009). This thesis focuses on two atmospheric constituents that are influenced by photochemical reactions: aerosol particles and tropospheric ozone (O_3).

This section is organized as follows. First, an introduction on atmospheric aerosols (Section 1.1), focusing on ultrafine particles (UFPs) and their formation pathways, as well as O_3 (Section 1.2) is presented. The effects on climate and health of both pollutants are also summarized in their respective subsections. Section 1.3 provides a list of the legal standards and guidelines set for the regulation of these pollutants. Section 1.4 includes an overview of the state of the art, including the gaps of knowledge and motivation of this thesis. The objectives of the thesis are presented in Section 1.5. Finally, Section 1.6 describes the area of study.

1.1 Atmospheric Aerosols

Atmospheric aerosol particles are defined as solid, liquid or mixed-phase particles suspended in air that may have diverse chemical composition, structure, sources and formation mechanisms (Seinfeld and Pandis, 2006). The diameter of these particles is generally considered to range between one nanometer to tens of micrometers (10^{-9}–10^{-5} m). In the lower levels of the atmosphere, aerosols have a typical lifetime of hours or days (Jaenicke, 1993).

Aerosol particles can be classified according to their formation mechanisms into primary or secondary. Primary particles are emitted directly into the atmosphere in solid or liquid state, whereas secondary particles are formed in the atmosphere from gaseous precursors (Kulmala et al., 2004).

Based on their source, aerosols fall under two categories: natural or anthropogenic. Natural aerosols result from natural emission processes, including sea salt and spray, resuspension of dust by wind, wild forest fires, volcanic emissions, plant debris and secondary aerosols formed from the oxidation of biogenic volatile organic compounds (VOCs), amongst others. Anthropogenic aerosols have their origin on human activity, including combustion processes, industrial emissions, construction, farming, agriculture and others. Natural primary aerosols dominate the global annual mass fluxes of particulate matter (Figure 1.1; Giere and Querol, 2010), although the global number concentration of aerosols is dominated by secondary particles (Gordon et al., 2017). At local scale, the contributions are diverse in different environments and the number concentration remains poorly quantified (Kerminen et al., 2018). In general, aerosol models suggest that secondary particles formed from both natural and anthropogenic precursors dominate the particle number concentrations in remote continental environments (Spracklen et al., 2006), whereas the concentrations in polluted environments are dominated by primary anthropogenic particles (Spracklen et al., 2006; Vu et al., 2015). Figure 1.2 shows an example of an urban environment where primary anthropogenic particles dominate the particle number concentrations.

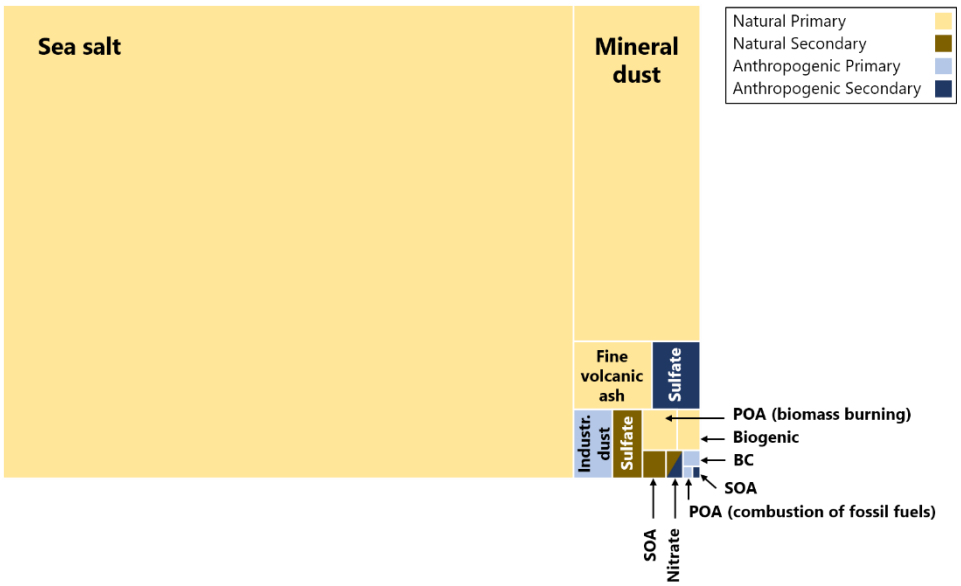

Figure 1.1: Types of atmospheric aerosols proportionally sized to the flux of mass emission/production and colored according to their type. POA = primary organic aerosol; SOA = secondary organic aerosol; BC = black carbon. Adapted from Gieré and Querol (2010).

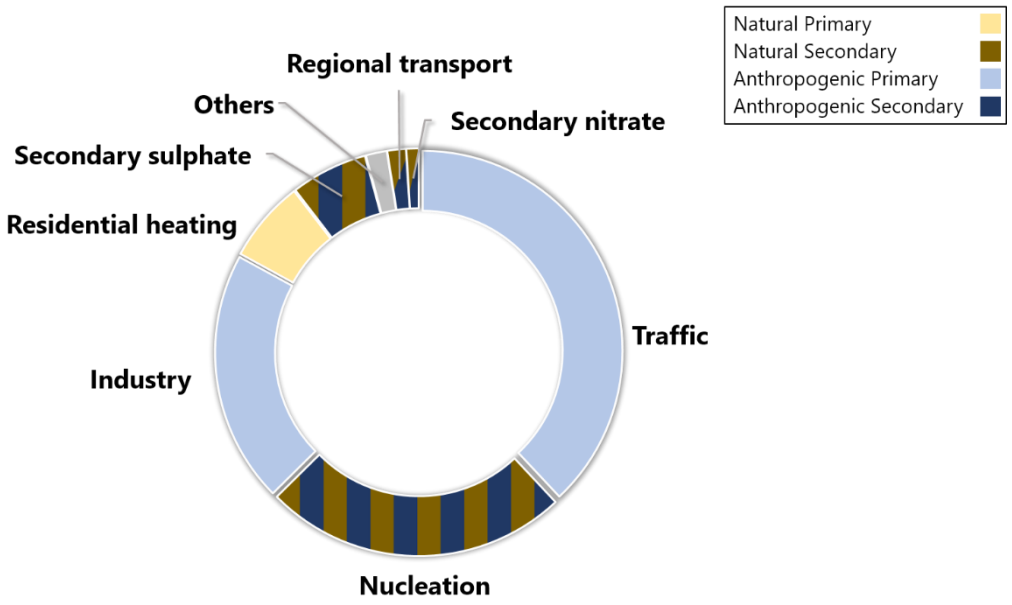

Figure 1.2: Average source contributions to particle number concentrations measured in an urban environment in Rochester, NY (USA), colored according to their type. Compiled from Ogulei et al. (2007).

Aerosol concentrations are commonly described by either the number of particles per unit of volume, mass per unit of volume, surface area or volume. The number concentration is usually dominated by smaller particles, whereas mass or volume concentrations are dominated by coarser particles (Seinfeld and Pandis, 2006). The aerosol size distribution varies with local conditions. According to their size, aerosol particles can be categorized into several groups. These groups, called modes, are not universally defined, and different studies might consider different size ranges for a given mode. In this thesis, the modes are defined as follows unless stated otherwise: the *nucleation* mode is used to refer to particles with less than 25 nm in diameter; the *Aitken* mode designates particles ranging from 25 to 100 nm; the *accumulation* mode refers to particles between 100 nm and 1 µm in diameter; and the *coarse* mode refers to particles larger than 1 µm. The term *ultrafine particles* (UFPs) commonly refers to atmospheric particles with less than 100 nm in diameter and are measured in number concentration. However, this definition is sometimes used loosely referring to quasi-ultrafine particles to include particles larger than 100 nm but substantially smaller than 1 µm and are measured as number concentration. In this thesis, the term UFP is used according to the later definition, including particles in the nucleation, Aitken and accumulation modes. Given that throughout this thesis the metric describing aerosols will be the number concentration and size distribution, our definition includes mostly particles with less than 100 nm, although a range accumulation mode particles might be included too, depending on the measuring range of the instrumentation used (see Section 2.2). According to Charron and Harrison (2003), particles with less than 100 nm make up to 70–90% of the total particle number

concentration. Therefore, despite including accumulation mode particles, the particle number concentration can be assumed to be a good representation of that of UFPs.

The order of magnitude of UFP concentrations in remote areas, rural or urban backgrounds, roadsides and street canyons or tunnels are 10^2, 10^3, 10^4 and 10^5–10^6 cm^{-3}, respectively (Cassee et al., 2019). In general, the main source of UFP number concentration in urban areas is road traffic (Brines et al., 2015; Kumar et al., 2014; Paasonen et al., 2016; Vu et al., 2015), followed by secondary aerosol formation (Dall'Osto et al., 2013; Ogulei et al., 2007; Rivas et al., 2020). Other sources include non-road traffic, industrial emissions, residential heating and secondary particles (Ogulei et al., 2007). At regional scales, new particle formation (NPF) is a major source of UFPs (Kerminen et al., 2018 and references therein). Fossil fuel-burning emissions from power stations, refineries and smelters are also an important source of regional UFPs (Junkermann and Hacker, 2018).

1.1.1 New Particle Formation

New particle formation is the main pathway for the secondary formation of particles. It involves the formation of molecular clusters with less than 2 nm in diameter via photochemical reactions in the gas phase, and the following growth of those clusters to sizes up to 100 nm (Kulmala et al., 2004). It is a worldwide phenomenon and has been observed to occur from pristine environments to highly polluted megacities, in urban, suburban, rural, marine and mountain environments, and at various altitudes inside the troposphere (Kerminen et al., 2018 and references therein).

NPF contributes to a major fraction of the global budget of atmospheric aerosols (Gordon et al., 2017; Spracklen et al., 2006). Atmospheric conditions such as irradiance, temperature, humidity and mixing conditions have a direct effect on factors controlling NPF. They influence the availability of molecular clusters, the concentration of vapors involved in the formation and growth processes or the amount of larger particles that act as a sink of those vapors inhibiting NPF (Kulmala and Kerminen, 2008; Zhang et al., 2012). For this reason, the local and regional contributions of NPF to the total aerosol number concentrations may vary greatly within small spatial and temporal scales (Kerminen et al., 2018).

A large number of studies have described the formation mechanism and growth of secondary atmospheric particles. Based on historical theoretical understandings, advances in measurement techniques and recent observations, Kulmala et al. (2014) proposed a gas-to-particle conversion scheme that, combining molecular and clustering dynamics with atmospheric chemistry, provides the theoretical foundations of our current understanding of atmospheric NPF (Figure 1.3).

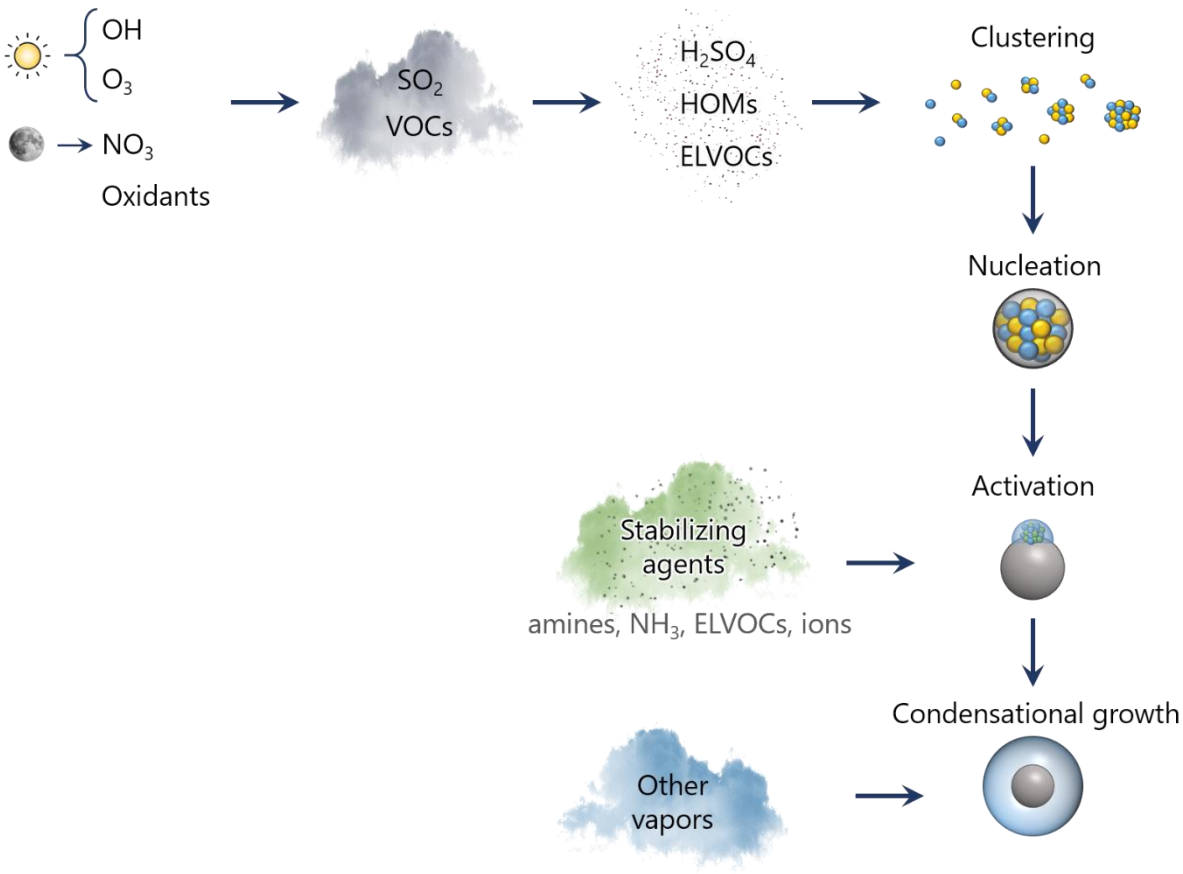

Figure 1.3: Schematic of the formation and growth of nanoparticles according to the gas-to-particle conversion scheme proposed by Kulmala et al. (2014). OH = hydroxyl radicals; NO_3 = nitrate radicals; SO_2 = sulfur dioxide; H_2SO_4 = sulfuric acid; HOMs = highly oxygenated organic molecules; ELVOCs = extremely low-volatile organic compounds; NH_3 = ammonia.

Sulfuric acid (H_2SO_4) and extremely low-volatile organic compounds (ELVOCs, molecules that condense onto any pre-existing particle; Donahue et al., 2012) are the key components in NPF (Kulmala et al., 2017) because of their low saturation vapor pressure that facilitates the formation of small clusters and subsequent condensation onto them. Molecular clusters are constantly forming in the atmosphere but they have very short lifetimes because they are constantly colliding to larger particles that absorb them (scavenging). Only under specific conditions, molecular clusters are able to form particles capable of growing (Kulmala et al., 2013). Particularly, before forming particles, clusters containing H_2SO_4 need to be stabilized by agents that decrease cluster evaporation rates (Kulmala et al., 2017), such as gaseous amines and ammonia (NH_3) that form acid-base complexes with inorganic or organic acids (Kirkby et al., 2011; Sipila et al., 2010), ELVOCs, water molecules or air ions that can form clusters through electrostatic interactions. Consequently, gaseous precursor sulfur dioxide (SO_2) and VOCs are required to be available in the system to form H_2SO_4 and low-volatility complexes via atmospheric oxidants favored by high

insolation and temperatures, such as hydroxyl radicals (OH) during the day and nitrate radicals (NO_3) at night, and O_3.

Specific combinations of these constituents lead to the formation of critical size stable clusters that form nanometric aerosol particles (nucleation). Once formed, these nanoparticles require the presence of additional vapors to enhance their growth rates (activation). Then, activated nanoparticles grow via condensation of multiple vapors (Kulmala et al., 2014) up to sizes at which they can influence climate (50–100 nm) by contributing to the concentration of cloud condensation nuclei (Merikanto et al., 2009).

Recently, highly oxygenated organic molecules (HOMs), formed via autoxidation involving peroxy radicals from VOCs (Bianchi et al., 2019), have gained interest for being involved in NPF. HOMs are mainly ELVOCs and LVOCs (low-volatility organic compounds; Donahue et al., 2012), thus they condense onto almost every pre-existing particle. HOMs have been proven to contribute to particle growth (Riccobono et al., 2012; Riipinen et al., 2012; Schobesberger et al., 2013; Yan et al., 2021), and even be required for particle growth over 10 nm (Brean et al., 2020). HOMs have also been observed to contribute to early stages of NPF even under low H_2SO_4 concentrations (Ehn et al., 2014; Kirkby et al., 2016; Rose et al., 2018; Yan et al., 2018).

Whether the newly formed particles grow up to several nanometers or not depends on the balance between precursor sources and sinks. Freshly formed particles need to grow by condensing vapors onto their surface, but small particles have more probabilities to be lost to scavenging by larger pre-existing particles. High concentrations of NOx also suppress NPF and initial growth (Lehtipalo et al., 2018). Eventually, only a small fraction of freshly formed particles survive to climatically relevant sizes (Vehkamäki and Riipinen, 2012). Nonetheless, NPF has been reported to be a dominant contribution to the aerosol number and mass even in highly polluted Chinese megacities, which have large aerosol loads (Kulmala et al., 2021; Qi et al., 2015; Wu et al., 2007; Xiao et al., 2015; Yao et al., 2018). This is in contrast with our current understanding: the high aerosol loads in those environments should rapidly scavenge fresh particles, which would have very few probabilities of surviving. Although there are still uncertainties regarding NPF in highly polluted environments, recent observations and chamber experiments point to much higher growth rates than those observed in clean environments, enhanced by high anthropogenic gas-phase precursor emissions. These would allow freshly nucleated particles to rapidly grow past size ranges that are most vulnerable to be lost to scavenging, thus being able to grow further and increase their survival rates (Kulmala et al., 2021; Wang et al., 2020; Yao et al., 2018).

1.1.2 Effects on health and climate

Despite a lack of general consensus regarding the specific chemical or physical characteristics of aerosol particles that are hazardous to human health, there are strong evidences of severe health effects arising from short-term and long-term exposure to particulate matter. These include an increase of premature mortality and morbidity, as well as an increased risk for cancer (Hoek et al., 2013; WHO, 2013, 2016). In general, smaller particles are able to penetrate deeper into the respiratory system before depositing and, therefore, are more dangerous than coarse particles. For this reason, UFPs are particularly hazardous for human health due to their small size. Moreover, it is well established that UFPs may translocate from the lungs and reach the circulatory system, and from there the brain and other organs (Cassee et al., 2011; Schraufnagel, 2020).

In regards to climate effects, aerosols have a net negative radiative forcing by reflecting incoming solar radiation, thus leading to a cooling effect (IPCC, 2013). UFPs may act as condensation or ice nuclei for clouds, thereby indirectly affecting climate by increasing the scattering effect of clouds (indirect cooling effect), modifying cloud dynamics and altering precipitation patterns (IPCC, 2013). Exceptionally, mineral dust, black carbon (BC) and brown carbon particles absorb radiation and have a warming effect, which reduces the net cooling effect of aerosols (IPCC, 2013).

1.2 Tropospheric Ozone

Tropospheric O_3 is a gaseous secondary pollutant formed in the lower atmosphere from photochemical reactions of natural and anthropogenic gaseous precursors, mainly NOx and VOCs (Monks et al., 2015 and references therein). Methane (CH_4) and carbon monoxide (CO) also contribute to O_3 formation, especially in long-range transport processes. Tropospheric O_3 constitutes around 10% of the total O_3 in the atmosphere, with the remaining 90% in the stratosphere forming the O_3 layer (Seinfeld and Pandis, 2006). The concentration of O_3 in the troposphere is determined by the balance of stratospheric intrusions, i.e., downward transport of stratospheric O_3 into the troposphere, local photochemical formation, regional and long-range transport, and removal by deposition or aerosol uptake (Monks et al., 2015). High O_3 concentrations in the lower troposphere are hazardous to human health, vegetation and materials (WHO, 2008). In the upper troposphere, O_3 contributes to global warming (IPCC, 2013).

1.2.1 Ozone formation and precursors

In the troposphere, VOCs, CH_4 and CO emitted from biogenic and anthropogenic sources react with OH radicals in the presence of solar radiation to generate organic and hydroperoxyl radicals (RO_2 and HO_2), very strong oxidizing agents that oxidize NO into NO_2 (1.1) (U.S. EPA, 2006). The solar radiation dissociates NO_2 into NO and activated oxygen (O*) (1.3), which in turn reacts with molecular oxygen (O_2), resulting in the formation of O_3 (1.4) (Figure 1.4). Thus, the formation of O_3 in the troposphere requires the presence of NOx.

$$NO + HO_2 \rightarrow NO_2 \quad (1.1)$$

$$NO + RO_2 \rightarrow NO_2 \quad (1.2)$$

$$NO_2 + h\upsilon \rightarrow NO + O^* \quad (1.3)$$

$$O^* + O_2 \rightarrow O_3 \quad (1.4)$$

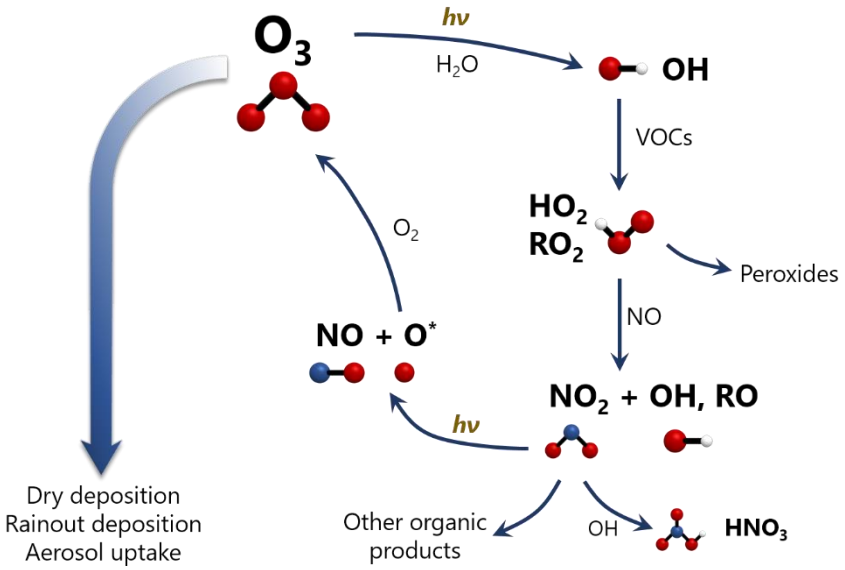

Figure 1.4: Schematic of the photochemical formation of ozone (O_3) in the troposphere. Adapted from U.S. EPA (2006). hν = photons (solar radiation); H_2O = water (vapor); OH = hydroxyl radicals; VOCs = volatile organic compounds; HO_2 = hydroperoxyl radical; RO_2 = organic peroxide; NO = nitric oxide; NO_2 = nitrogen oxide; RO = ; HNO_3 = nitric acid; O* = activated oxygen; O_2 = molecular oxygen.

At the end of the process, there is still NO available to start the reaction again without a major loss, i.e., NO acts as a catalyst in the formation of O_3. The extraction of NOx from the atmosphere occurs by deposition and formation of nitrate aerosols (Figure 1.4). NOx are mostly anthropogenic

emitted around urban areas, whereas VOCs emissions are more evenly distributed and have a wide range of origins. NOx are also involved in the removal of O_3 by titration (1.5):

$$O_3 + NO \rightarrow NO_2 + O_2 \,. \tag{1.5}$$

The photochemical reactions driving O_3 formation are nonlinear. Thus, the initial VOCs and NOx concentrations are not proportional to the final concentration of O_3 formed. The VOC/NOx ratio (Figure 1.5) plays a major role in determining how changes in VOC and NOx concentrations affect the concentrations of O_3 (Sillman, 1999):

- In NOx-limited systems (high VOC/NOx ratios), decreasing NOx concentrations at constant VOCs concentrations might result in lower O_3 concentrations. However, a decrease in VOCs concentrations might not necessarily cause a decrease in O_3 levels, and can even cause an increase.
- In VOC-limited systems (low VOC/NOx ratios), lowering VOCs concentrations at constant NOx concentrations might cause a decrease in O_3 levels. Conversely, decreasing NOx concentrations might not necessarily lead to lower O_3 concentrations, and can even cause an increase under certain conditions.

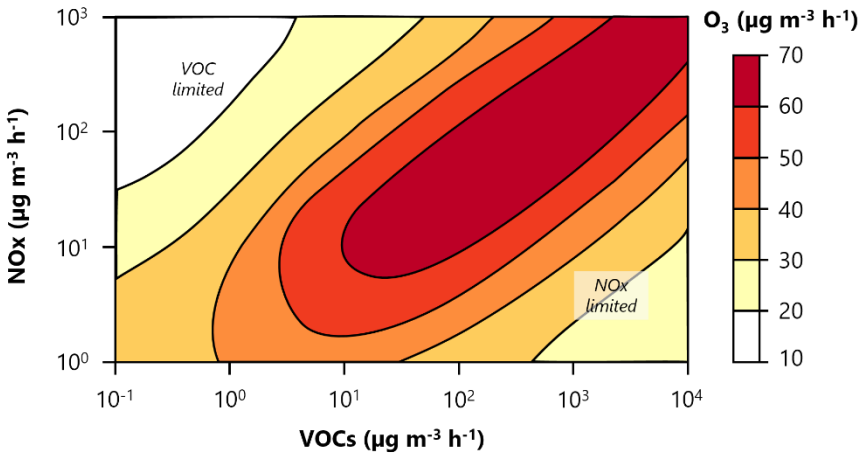

Figure 1.5: Schematic of the rates of O_3 production as a function of VOCs and NOx emissions. Adapted from Monks et al. (2015). Note that the numerical values are only provided for a qualitative understanding and are not accurate. The dependence varies with time and local conditions.

The strong variability of VOC/NOx ratios from one location to another, with time of day and with altitude makes it difficult to design efficient abatement measures to reduce O_3 concentrations. Additional factors driving O_3 concentrations are meteorological and climatic conditions. Peak O_3 episodes are usually registered with high temperatures and insolation, and in conditions of light

winds and lack of vertical mixing leading to stagnation and the recirculation of air masses (Monks et al., 2015).

1.2.2 Effects on health, vegetation and climate

Due to its highly oxidative properties, tropospheric O_3 is one of the most harmful ambient pollutants for human health. According to EEA (2020), exposure to O_3 caused over 20.000 premature deaths in Europe in 2018. This represents a 20% increase compared to 2009 and is related to rising temperatures in summer. Thus, increasing O_3 concentrations should be expected in a scenario with increasing temperatures in the coming years.

There is strong epidemiological evidence that daily short-term exposures to high concentrations of O_3 increase cardiovascular, respiratory and all-cause mortality and morbidity rates, especially in sensitive population (WHO, 2008, 2013). Short-term exposure can also affect cognitive development and reproductive health (WHO, 2013). Long-term exposure to O_3 has been linked to respiratory mortality and all-cause mortality in vulnerable population (WHO, 2013).

Additionally, high O_3 concentrations have harmful effects on vegetation at cell levels, damaging agricultural crops, plants and forests. Foliage crops, such as lettuce, spinach or cabbage that are exposed to high O_3 concentrations during peak episodes develop acute leaf damage that reduces the quality and economic value of the crop. On the other hand, crops exposed to high background concentrations of O_3, even without peak episodes, suffer chronic damages that lead to decreased production and reduced quality, yielding to important economic losses (ICP Vegetation, 2011). Global yield losses for 2030 due to O_3 pollution are predicted to range from 5–26% for wheat, 15–19% for soybean and 4–9% for maize, with total agricultural losses of €14–29 billion annually globally (Avnery et al., 2011). It must be noted that these calculations account only for the quantity of yield loss. The economic losses derived from the reduction in the quality of crops is not accounted for in these predictions.

Materials exposed to high concentrations of O_3 may suffer decolorization, decomposition and corrosion (Kucera and Fitz, 1995), which may yield important economic losses. Of particular concern are the impacts of O_3 on cultural heritage buildings, monuments and works of art, including the indoor of museums and conservation storages, which result in additional inestimable cultural losses.

With regards to climate, tropospheric O_3 is one of the most effective contributors to greenhouse radiative forcing (IPCC, 2013). Thereby, it has a significant effect on climate, contributing to global warming. Moreover, under greenhouse gas forcing, higher temperatures lead to increased O_3 formation, resulting in an intricate positive feedback loop.

Overall, the effects of O_3 on health, vegetation and climate result in significant economic costs associated with decreased worker productivity, increased health expenses, reduced agricultural growth rates, degraded ecosystems and climate change.

1.3 Air Quality Standards and Guidelines

Current EU air quality standards do not contemplate UFP as a regulated ambient air quality metric. The lack of standardized measurement protocols and scarce long-term measures pose a major problem in the comparison of results from different studies, thus making it difficult to establish regulatory measures (Cassee et al., 2019). Nevertheless, monitoring programs are being implemented across Europe in preparation of future regulations, and the World Health Organization's (WHO) plans to review UFP indicators in future guidelines (WHO, 2016).

Table 1.1: Tropospheric ozone standards given in the EU Ambient Air Quality Directive 2008/50/EC, the CLRTAP and WHO guidelines.

Source	Averaging period	Guideline	Value
Directive 2008/50/EC	Maximum daily 8-hour mean	Target value	120 μg m^{-3}
	1 hour	Long-term objective	120 μg m^{-3}
		Information threshold	180 μg m^{-3}
		Alert threshold	240 μg m^{-3}
	AOT40(*) May–July averaged over 5 years	Target value	180000 μg m^{-3} h
		Long-term objective	6000 μg m^{-3} h
CLRTAP	AOT40(*) April–September	Critical level	10000 μg m^{-3} h
WHO 2005 guidelines	Maximum daily 8-hour mean	Air quality guideline	100 μg m^{-3}
		Interim target-1	160 μg m^{-3}

(*) AOT40 is calculated as the sum of concentrations exceeding 80 μg m^{-3} (40 ppb) accumulated from 8:00 to 20:00 CET.

In regards of ground-level O_3, the Directive 2008/50/EC on Ambient Air Quality and Cleaner Air for Europe of the European Parliament and of the Council (EC, 2008) sets 4 standards for the regulation of O_3 concentrations, which are listed in Table 1.1. These standards are target values, which require the implementation of measures to ensure that the standard is met, in contrast to the limit values set for most pollutants, which are legally binding under EU law. The target value fixes the maximum daily 8-hour mean of 120 μg m^{-3} to prevent harmful effects on human health and the environment, and is not to be exceeded on more than 25 days per year, averaged over 3

years. When concentrations above the hourly information threshold (180 μg m^{-3}) are registered, the health of sensitive population is at risk, and the authorities shall inform the public. If concentrations exceed the hourly alert threshold (240 μg m^{-3}) there is a risk to human health for all the population, and immediate action shall be taken by the authorities. The Air Quality EU Directive and the Convention on Long-range Transboundary Air Pollution (CLTRAP; UNECE, 2011) also set standards for the protection of vegetation. On the other hand, the WHO air quality guidelines (WHO, 2006) set the guideline for the maximum daily 8-hour mean to never exceed 100 μg m^{-3} for an adequate protection of public health. An interim target value of 160 μg m^{-3} is proposed for a progressive reduction in highly-polluted areas.

1.4 State of the Art

In recent years, UFPs have emerged as a pollutant of great interest because of their effects on human health and climate (Cassee et al., 2019; Ohlwein et al., 2019). Still, crucial information needed to design effective regulating and abatement measures, such as the precise contribution of different sources and precursors to UFP concentrations, remains unclear to this day. The response of NPF to variations in UFP concentrations is of particular interest. Generally, when UFP concentrations are low, NPF is more favored (Birmili et al., 2003; Pikridas et al., 2012; Salma et al., 2016), but efforts directed at decreasing primary emissions may lead to an increase in NPF and, consequently, in UFP concentrations (Spracklen et al., 2006; Wichmann et al., 2000). Therefore, implementing actions to decrease UFP concentrations might be ineffective or even counterproductive, posing a threat to human health and climate if the formation of particles increases the initial UFP concentrations. On the other hand, the observation of NPF in highly polluted environments with high aerosol loads (see Section 1.1.1) evidences the diversity of circumstances that may lead to an increase of UFPs.

Solar irradiance is a fundamental factor driving NPF (Kerminen et al., 2018) and, consequently, influencing UFP concentrations. In areas with high insolation, the contribution of photochemical NPF episodes add to primary emissions of UFPs and to episodes of other photochemical pollutants, thus entailing major health and climate concerns. This is the case of the larger part of southern Europe, where clear skies, high temperatures and recirculation dynamics lead to intense photochemical formation of O_3 in spring and summer (Gangoiti et al., 2001; Millán et al., 1991; Querol et al., 2016), when UFPs episodes are also common in the same area (Brines et al., 2015; Pey et al., 2009). However, the underlying relationship between UFPs episodes and O_3 episodes is not fully understood yet. Previous studies worldwide have reported high concentrations of UFPs or NPF to be concurrent with high O_3 concentrations (e.g., Brines et al., 2015; Fernández-

Camacho et al., 2010; Minoura and Takekawa, 2005; Park et al., 2008; Pey et al., 2009; Squizzato et al., 2019; Wang et al., 2016; Wonaschütz et al., 2015). However, most of these results were based upon the examination of yearly or seasonal data, and they fail to specify whether the UFP and O_3 episodes occurred simultaneously on the same days, or simply the atmospheric conditions in spring and summer favor high concentrations of the two pollutants separately. There are several explanations that could justify the coincidence reported in previous studies. These are:

(a) The conditions that favor UFPs episodes on a specific day also favor O_3 episodes, and/or vice versa, so the episodes can be simultaneous. In addition to the well-known high insolation favorable conditions, the conditions leading to the emission and accumulation of precursors of both pollutants may be similar.

(b) The formation pathways of UFPs have a direct effect on the chemical and physical reactions leading to O_3 formation, and/or vice versa, so the episodes can be simultaneous. For example, it has been previously observed that ELVOCs, which are involved in gas-to-particle conversion and are essential for the formation of UFPs, are produced in the α-pinene ozonolysis (Ehn et al., 2012; Zhao et al., 2013). Additionally, the reaction of O_3 with alkenes forms compounds that lead to H_2SO_4 formation, which enhances NPF (Kulmala et al., 2014).

(c) The conditions that favor UFPs episodes on a specific day inhibit O_3 episodes, and/or vice versa, so the episodes cannot occur simultaneously. For instance, the recirculation of air masses that may cause O_3 episodes lead to high aerosol loads, which generally disfavor the formation of particles. In this scenario, the coincidence reported in previous studies may be merely due to the solar cycles inducing similar seasonal patterns for both pollutants. Yet, when looking at yearly data without focusing on daily occurrences, the analysis may reveal that both pollutants episodes take place during the same season or even the same month. This may be because the occurrence of the episodes is directly influenced by the intensity of solar radiation and availability of their respective precursors, which make the most favorable conditions for both pollutants around late spring and summer.

(d) The formation processes of UFPs and O_3 are unrelated and the coincidence is only associated to the solar cycles, as in (c).

As explained in Section 1.1.1, the chemistry of atmospheric gas-to-particle conversion involved in the formation pathways of UFPs is still not completely understood (Kulmala et al., 2014; Lehtipalo et al., 2018). Furthermore, the exact precursors of particle formation are not fully identified, and might vary largely depending on the regions and environments (Kulmala et al., 2014). The dynamics of O_3 episodes is complex as well: in addition to the local emission of precursors, regional and long-range transboundary transport are thought to have important contributions to

the local O_3 concentrations (Syri et al., 2001). Stratospheric intrusions and mesoscale recirculations of the air masses add to the intricacy of O_3 episodes (Gangoiti et al., 2001; Kalabokas et al., 2008; Millán et al., 2002).

One of the main obstacles to broadening our current understanding of the relationship between these two pollutants is the scarcity of precise measurements of UFPs and their precursors, as the instrumentation is highly complex and expensive, and usually unavailable for most researchers. Additionally, the lack of consensus in the instrumentation and measurement techniques used to measure UFPs worldwide make it difficult to analyze long-term datasets and compare the results in different areas. Another significant limitation during the measurement of UFPs is the large influence of chemical and physical atmospheric conditions in the formation pathways of the particles. The characteristics of NPF may vary greatly within small areas and short periods of time, thus hindering the observation of such events with standard fixed instrumentation. Portable instrumentation allows obtaining a more thorough representation of the atmosphere during the episodes, providing the observations with a vertical dimension. However, such instrumentation is usually not available due to its high cost and difficult implementation, requiring several people to manually control the instruments, and often depending upon coordination with airfield authorities.

Moreover, the majority of detailed studies on atmospheric NPF processes and precursors are located in only a few locations, e.g., boreal forests or heavily polluted Asian megacities, and the situation in different environments remains poorly quantified (Kerminen et al., 2018). In general, different locations have different atmospheric conditions and pollutant concentrations, which in turn regulate the behavior of key NPF precursors, such as H_2SO_4 (Dada et al., 2020). Therefore, the processes observed in a specific environment might not be directly applicable to other locations. In particular, urban and rural areas in the Mediterranean might have very different precursors and ambient conditions yielding NPF compared to most of the environments studied in the literature, due to their particular geographical and climate characteristics.

1.5 Objectives

The objective of this thesis is to characterize the relationship between UFPs episodes and O_3 in areas with significant photochemical activity. The specific research objectives of this thesis are:

1. To characterize the dynamics of UFPs episodes and their connection with O_3 episodes.
2. To establish whether UFPs and O_3 episodes are driven by the same processes or occurring in parallel with the same seasonality pattern.

3. To describe how UFP concentrations have evolved over the last decade and to identify the factors driving potential changes.

1.6 The Area of Study

The studies included in this thesis are set in areas of the western Mediterranean in northeastern Spain and central Spain. In these areas, the influence of the Azores anticyclone and the complex topography of the western Mediterranean favor the production, accumulation and vertical recirculation of photochemical pollutants and their precursors (ETC/ACM, 2018; Gangoiti et al., 2001; Kalabokas et al., 2017; Millán et al., 2002; Toll and Baldasano, 2000).

Figure 1.6: Relief map of the Iberian Peninsula and Balearic Islands showing the areas of study of this thesis. Source: Cartography Service of the Autonomous University of Madrid (UAM).

To analyze the complexities of the relationship between UFPs and O_3 episodes, two areas of study are considered in this thesis (Figure 1.6): urban and suburban areas in Madrid, central Spain (**Paper I**), and urban and regional backgrounds in the western Mediterranean in northeastern Spain: Barcelona (**Paper III**) and Montseny (**Papers II** and **III**) (Figure 1.7).

The selection of the locations owes to (a) their inclusion in the two regions registering the highest O_3 episodes and the most exceedances of the O_3 information threshold in Spain according to Querol et al. (2016): northern Barcelona and the Madrid basin; and (b) several studies reporting photochemical particle formation to have a significant contribution to UFP concentrations in

these two areas (Brines et al., 2015; Minguillón et al., 2015; Pey et al., 2009; Querol et al., 2017; Reche et al., 2011).

Madrid is the capital and largest city of Spain with 3.3 million inhabitants (6.6 million inhabitants considering the metropolitan area). It lies in the geographical center of the Iberian Peninsula in a plateau at an altitude of 667 m above sea level (a.s.l.), with the Guadarrama mountain range limiting to the north, with a maximum altitude of 2428 m, and 300 km from the Mediterranean Sea coast. Road traffic is the main source of pollution in the area, with additional contributions from residential heating, industries and aircraft emissions (Salvador et al., 2015). Anabatic and katabatic winds driven by the surrounding mountain ranges and river basin lead to mesoscale recirculations that may accumulate pollutants for several days, causing intense pollution episodes (Plaza et al., 1997). An average of 4 annual exceedances of the O_3 hourly information threshold are registered per station in the city and neighboring areas (Querol et al., 2016).

Barcelona is the second most populous city in Spain with over 1.6 million inhabitants (5.6 million inhabitants considering the metropolitan area), located on the northeastern coast of Spain. It lies in a plain facing the Mediterranean Sea to the southeast and is surrounded by the Llobregat River to the southwest, the Besòs River to the northeast and the Coastal mountain range to the northwest, with a maximum altitude of 512 m a.s.l. The Pyrenees mountain range, with a maximum altitude of 3404 m a.s.l., lies 120 km to the north of the city (Figure 1.7). The main sources of pollution in Barcelona and its metropolitan area are road traffic and industries, with important contributions from shipping, power generation, aircraft, biomass burning and livestock. The geographical characteristics of the city, together with strong sea breezes caused by the warm temperatures of the Mediterranean Sea, drive the urban plume inland. The complex topography channels the air masses northwards to the Montseny natural area (50 km to the northeast; Figure 1.7) and the Vic plain (60 km to the north), one of the most important O_3 hot spots in Spain (Querol et al., 2016). Large scale recirculations with a return flow at upper levels may transport pollutants back towards the coast (Gangoiti et al., 2001; Soler et al., 2011). If the conditions persist for several days, pollutants and precursors accumulate in the area, leading to intense pollution episodes. In the areas north of Barcelona, the O_3 information threshold is exceeded an average of 15 times per year and station (Querol et al., 2016).

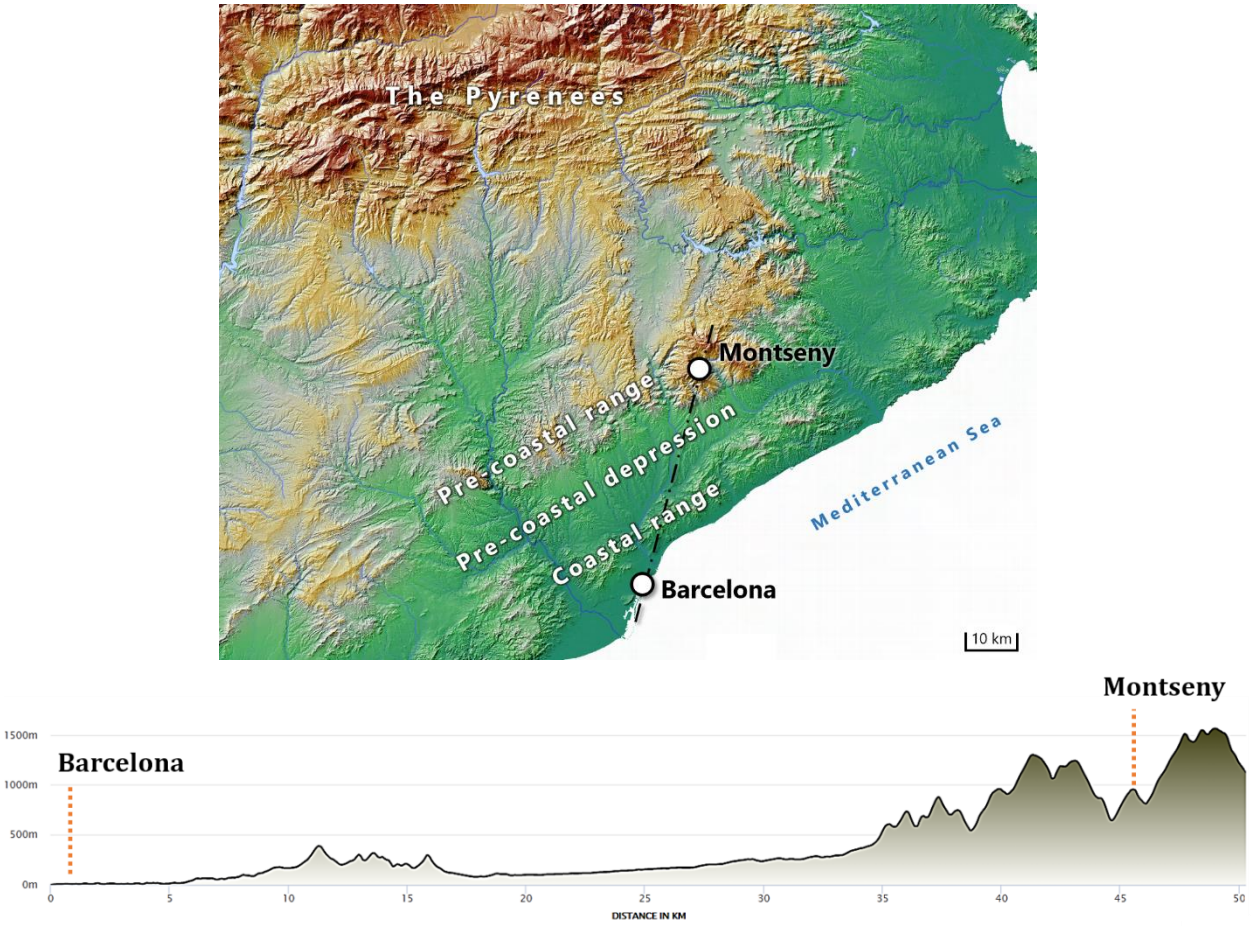

Figure 1.7: Above: Relief map of the Barcelona-Montseny area of study. A dash-dotted line indicates a cross section between the two measuring locations used in this thesis. Below: Elevation profile between the measuring locations Barcelona and Montseny in the cross section marked in the map above.

2 METHODOLOGY

2.1 Methodological Approach

The methodological approach taken in this thesis is a combination of intensive campaigns and long-term measurements, based on the main objectives of the research:

(i) With the aim of characterizing the dynamics of UFPs episodes and their relationship with O_3 episodes (Objective 1), intensive field campaigns were designed in collaboration with other institutions that provided instruments that are usually routinely unavailable at our monitoring sites due to their cost. These campaigns consisted of simultaneous measurements during a few weeks in early summer (June and July), coinciding with the highest photochemical activity that drives both NPF and O_3 episodes in the areas of study. Vertical measurements with a balloon sounding system expanded the data gathered at ground level. The results of these campaigns are reported in **Papers I** and **II**.

(ii) To determine whether UFPs and O_3 episodes are interconnected or merely occurring with the same seasonality (Objective 2), it is crucial to identify the time of occurrence of UFP and O_3 episodes. For that purpose, it is also crucial to understand how NPF regulates UFP episodes and concentrations. Data gathered during intensive campaigns (**Papers I** and **II**), as well as the analysis of long-term data on fixed location provided information on the temporal and spatial connection between the episodes (**Papers II** and **III**).

(iii) To assess how UFP and O_3 concentrations have evolved in recent years (Objective 3), a series of statistical analysis were performed in **Paper III**. Using long-time series of continuous measurements on fixed locations, trends of UFP, O_3 and other pollutants were evaluated in different environments.

Section 2.2 includes a list of all the instruments used and summarizes their working principles. Section 2.3 describes the locations chosen for the intensive campaigns, as well as the measurement sites that are used for the long-term measurements and indicates the instruments used in each case. Section 2.4 details the data analysis techniques used for the identification of NPF and the calculation of particle sinks and parameters during NPF events.

2.2 Instrumentation

Data for this thesis were collected using the instruments summarized in Table 1.1 during intensive campaigns and long-term measurements. This section briefly describes the measuring principles of the instrumentation used for each variable. Further details on the configuration of the instruments for each study and measuring location are given in the corresponding publications.

Table 2.1: Characteristics of the instrumentation used during the experimental measurements. U = Urban; UB =Urban Background; SB = Suburban background; RB = Regional Background.

Metric	Instrument	Manufacturer and model	Range	Contributor	Papers (environment)
Vertical profiles	Balloon sounding system	University of Hanyang	0-2000 m a.g.l.	University of Hanyang	I (SB), II (RB)
Particle number conc.	CPC	TSI 3776	2.5–3000 nm	CIEMAT	I (UB)
		University of Hanyang Hy-CPC	3.0–3000 nm	University of Hanyang	I (SB), II (RB)
Particle size distribution	SMPS	TSI 3082	8–120 nm	IDAEA	I (U)
		TSI 3080	15–660 nm	CIEMAT	I (UB)
			9–360 nm	Aix-Marseille Université	I (SB)
			10–478 nm	IDAEA	III (UB)
		TSI 3938E77	1–30 nm	CIEMAT	I (UB)
		University of Hanyang Hy-SMPS	8–245 nm	University of Hanyang	I (SB), II (RB)
		Tropos-SMPS	9–856 nm	IDAEA	II, III (RB)
Particle size distribution	PSM	Airmodus A10	1.2–2.5 nm	University of Helsinki	I (U), II (RB)
		Airmodus A11	1.2–4.0 nm	University of Helsinki	I (SB)
Ion size distribution	AIS	Airel Ltd AIS	0.8–40 nm	University of Helsinki	II (RB)
O_3 conc.	Ultraviolet photometry analyzer	Thermo Scientific 49i	0–2x10^5 ppb	CIEMAT	I (UB)
		MCV 48AV	0–2x10^4 ppb	IDAEA	II, III (RB)
		2B Technologies POM	0–10^4 ppb	IDAEA	II (RB)
BC conc.	Aethalometer	Magee Scientific AE33	0–100 μg m^{-3}	CIEMAT	I (U and UB)
	MAAP	Thermo Scientific MAAP 5012	0–180 μg m^{-3}	IDAEA	II (RB), III (UB and RB)
VOCs conc.	PTR-TOF-MS	Ionicon Analytic PTR-TOF 8000	1–5x10^4 amu	Aix-Marseille Université	I (SB)
NOx conc.	Chemiluminescence analyzer	Teledyne API 200EU	0–2x10^4 ppb	IQFR	I (U)
		Thermo Scientific 17i	0–100 ppb	CIEMAT	I (UB)
		Thermo Scientific 42i-TL	0–200 ppb	IDAEA	III (UB and RB)
SO_2 conc.	Ultraviolet fluorescence analyzer	Teledyne T100	0–2x10^4 ppb	IDAEA	II (RB), III (UB and RB)
CO conc.	Gas filter correlation analyzer	Teledyne T300EU	0–1000 ppm	IDAEA	III (UB and RB)

2.2.1 Balloon sounding system

In **Papers I** and **II**, a sounding system was used during intensive measuring campaigns to study the vertical distributions of particle concentrations and size distributions, as well as O_3 concentrations and meteorological variables. The system consisted of two latex balloons filled with helium and tied one on top of the other with a separation of a few meters. The maximum diameter of the balloons when fully inflated was 3.5 m. The balloon in the bottom was tethered to a winch system that allowed the balloons to ascend and descend at a controlled velocity, which could be fixed or varied by the operator. The sounding system could perform a complete vertical profile (ascension up to about 2000 m a.g.l. and descent) in around an hour. A metallic frame containing the instruments was hooked on the cable that connected the balloons with the winch. The total weight of the sounding system including the instrumentation was around 6 kg.

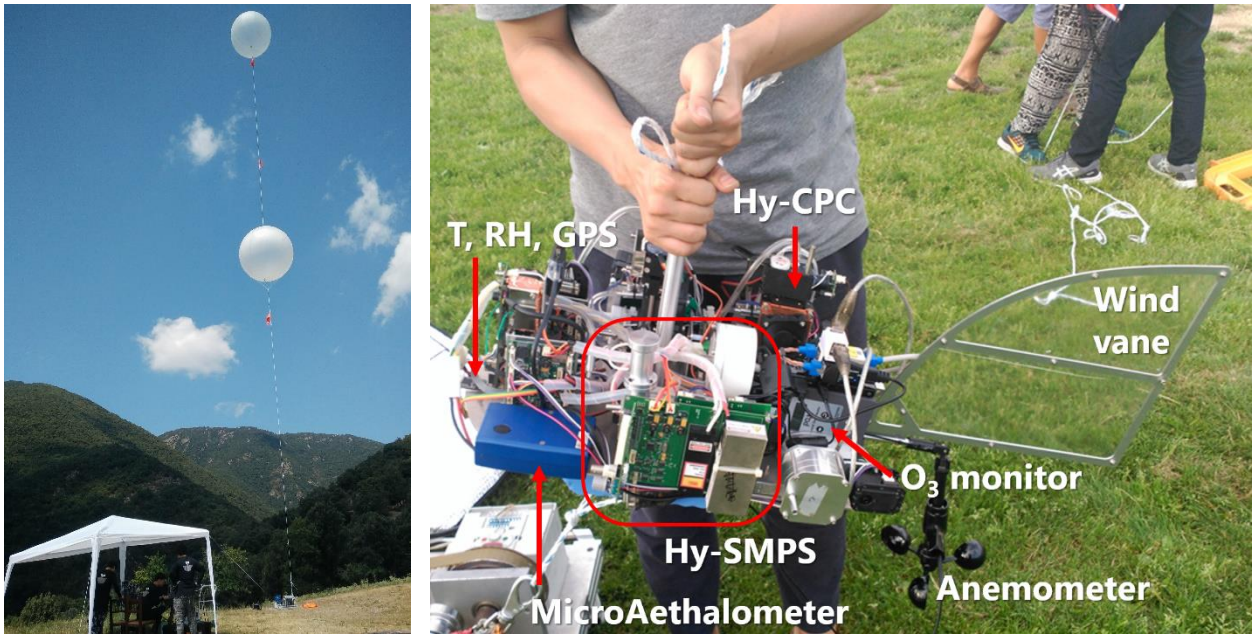

Figure 2.1: Left: Balloon sounding system at Montseny (**Paper II**) at ground level, before hooking the frame that contained the instrumentation (right). Note that only the instruments used for this thesis have been labeled.

2.2.2 Particle number concentration

Condensation Particle Counters (CPCs) measure the total number of particles in an aerosol sample by condensing a working fluid into the particles in the sample (Stolzenburg and McMurry, 1991). All CPC models used in this thesis operate with butanol as the working fluid. Other models operate with water or isopropyl alcohol.

The sample is carried through a heated saturator in which the butanol is vaporized and diffuses into the sample. A cooled condenser supersaturates the vapor, which condenses into the surface of the particles in the sample that have a starting diameter higher than the instrument lower-size-detection limit, in the order of 3–10 nm, depending on the CPC model. The particles grow in size up to a few μm, to a point that they can be counted with an optical detector: the droplets are guided to a laser beam, and a photodetector registers a light pulse for every particle that crosses the beam. Counting the light pulses and knowing the aerosol flow rate and sampling time, the total number of particles is calculated.

The total number particle concentration reported in **Paper I** was measured with a CPC at ground level. Additionally, in **Papers I** and **II**, a miniaturized CPC (Hy-CPC) was installed in the balloon sounding system to obtain vertical profiles of total number particle concentration. CPCs were also utilized in **Papers I, II** and **III** as part of other instruments that require CPCs to measure the particle size distribution of aerosols, as is described in the respective subsections.

2.2.3 Particle size distributions

2.2.3.1 Ultrafine Particles

Scanning Mobility Particle Sizer (SMPS) spectrometers measure the size distribution of particles with diameters greater than a few nm (Wang and Flagan, 1990). The working principle of SMPSs is based on the inverse relation between the diameter of a particle *(D_p)* and its electrical mobility *(Z;* Knutson and Whitby, 1975):

$$Z = \frac{q\ C_c}{3\ \pi\ \eta\ D_p}, \tag{2.1}$$

where q is the electric charge of the particle, C_C is the Cunningham correction factor to the friction of particles that depends on the particle diameter and its mean free path, and η is the dynamic viscosity of air. Z determines the velocity of a particle in an electric field E:

$$v = Z\ E \tag{2.2}$$

SMPS spectrometers consist of an electrostatic classifier that separates particles according to their sizes and a CPC that counts the number of particles in each size range (see Section 2.2.2). Upon entering the instrument, particles are neutralized using a radioactive or x-ray source so that the charge distribution of the sample is stationary. The sample is then directed to a Differential Mobility Analyzer (DMA).

The DMA consists of a cylinder with a central rod and grounded walls. By applying a high voltage to the central rod, thus creating a difference in voltage, an electrical field is generated between the rod and the walls. The polydisperse sample enters the DMA alongside the outside wall, and particles move towards the central rod at a velocity that is directly proportional to their Z (2.2), thus inversely proportional to their diameter (2.1). Therefore, particles with the same diameter impact the rod at the same point. By varying the voltage applied to the rod, particles of a certain diameter will impact the rod at the base of the cylinder, where a slit guides the monodisperse aerosol to a CPC that counts the number of particles. Particles that do not impact the rod at the slit exit the DMA with the exhaust flow. By scanning a range of voltages, the complete particle size distribution of the sample is obtained.

In **Papers I**, **II** and **III**, SMPS spectrometers at ground level provided the size distribution of particles during both long term and intensive campaigns. In **Papers I** and **II**, a miniaturized SMPS (Hy-SMPS), in combination with a miniaturized CPC (Hy-CPC), was placed on board of the balloon sounding system to measure the vertical size distribution of particles during intensive campaigns.

2.2.3.2 Sub-3 nm Particles

Particle Size Magnifiers (PSMs) are used in combination with CPCs to detect particles with diameters starting at 1 nm (Vanhanen et al., 2011). PSMs use diethylene glycol (DEG) as a working fluid to grow the particles in the aerosol sample. By turbulently mixing the heated saturated DEG with colder sample air, supersaturation is generated and particles grow up to around 90 nm. Then, the sample is grown further with a CPC, which also performs the optical particle counting. The cut-off diameter of particles in PSMs can be varied by modifying the DEG flow rate, as opposed to CPCs, in which the cut-off diameter is fixed and depends on the model. Thus, PSMs can provide size-resolved particle distributions by operating in scanning mode, as in **Papers I** and **II**. This instrument was used during intensive campaigns only.

2.2.3.3 Air Ions

An Air Ion Spectrometer (AIS; Mirme et al., 2007) measured the size distributions of positive and negative air ions with diameters ranging 0.8–40 nm during the intensive campaign reported in **Paper II**.

When the sample air enters the instrument, the flow is split to two DMAs, one for each polarity, that classify the ions according to their size. The DMAs generate radial electrical fields in which

the ions move until they precipitate onto different sections of one of the mobility analyzers, according to their electrical mobility. The AIS has two mobility analyzers, one for each DMA, with a total of 42 channels. In each channel, an electrometer registers the changes in the concentration of deposited ions. Finally, the electrometer signals are converted to ion mobility distributions. By combining the information of all electrometers, the size distribution of positive and negative ions is determined.

2.2.4 Ozone

Ultraviolet photometry analyzers measure O_3 concentrations based on the maximum absorption of O_3 molecules of ultraviolet light at a wavelength of 254 nm and Beer's Law (2.3), which defines how light of a certain wavelength is absorbed by an absorbing gas while travelling a distance L:

$$I = I_0 e^{-\alpha LC}, \tag{2.3}$$

where I is the intensity of the light after the absorption, I_0 is the intensity of the light if there was no absorption, α is the absorption coefficient and C is the concentration of the absorbing gas, in this case O_3.

When the sample gas enters the instrument, it is split into two streams. Part of the sample goes through an ozone scrubber that converts the O_3 into O_2 before being directed to the measuring chamber. A detector measures the intensity of radiation emitted at a wavelength of 254 nm (I_0). This step takes into account the absorption by gases other than O_3 or particulate matter in the sample. The other part of the sample is guided directly to the measuring chamber. The intensity of radiation emitted at a wavelength of 254 nm by this sample (I) takes into account the absorption by the O_3 present in the sample. Finally, the concentration of O_3 in the sample is calculated using (2.3).

In **Papers I, II** and **III**, ultraviolet photometry analyzers were used to measure O_3 concentration at ground level. Additionally, in **Paper II**, a portable analyzer was placed in the balloon sounding system to measure the vertical distribution of O_3 concentrations.

2.2.5 Black Carbon

2.2.5.1 Aethalometer

Aethalometers calculate mass concentrations of light-absorbing aerosols based on the absorption of light, such as the concentration of BC, as in **Paper I**.

In an Aethalometer, the optical absorption is measured at seven wavelengths, ranging from 370 to 950 nm, one of which (880 nm) is used for the calculation of BC mass concentrations, assuming an absorption cross section of 7.77 $m^2\ g^{-1}$. At this wavelength, all absorption can be attributed to BC (Drinovec et al., 2015 and references therein). The remaining wavelengths can be used for source apportionment or the calculation of the single scattering albedo.

The instrument measures the intensity of the light transmitted to the sample deposited in a filter *(I)* and to a reference portion of the filter with no sample *(I_0)*. Defining the attenuation coefficient (ATN) as

$$ATN = -100\ ln\left(\frac{I}{I_0}\right), \tag{2.4}$$

the BC mass concentration is calculated assuming that a change in ATN is caused by an increase in the BC deposited in the filter during a time interval Δt:

$$BC = \frac{A \cdot \Delta(ATN)}{\alpha_{ATN} \cdot Q \cdot \Delta t}\ , \tag{2.5}$$

where A is the filter area, α_{ATN} is the attenuation cross section (7.77 $m^2\ g^{-1}$ for the 880 nm wavelength) and Q is the flow rate.

2.2.5.2 Multi-Angle Absorption Photometer (MAAP)

In **Papers II** and **III**, a MAAP was used to measure BC concentrations based on the absorption and scattering of light in aerosols.

Within the instrument, the sample is deposited onto a glass fiber filter tape, where the aerosol will accumulate. In the detection chamber, the aerosol-filter layer is exposed to a light source that emits radiation at a nominal wavelength of 670 nm, at which most absorption can be attributed to BC. Multiple photodetectors located above the sample (back hemisphere) at different angles measure the back scatter of the incident light. A photodetector placed below the sample (forward hemisphere) measures the transmission and forward scatter of the light.

The absorption coefficients of the sample are derived with a radiative transfer model. The actual wavelength emitted by the instrument is 637 nm instead of 670 nm (Müller et al., 2011) and, consequently, the absorption coefficients needs to be multiplied by a correction factor of 1.05. Finally, the BC mass concentration is derived by assuming that the aerosol light absorption and BC mass concentration are correlated, with a mass absorption cross section of 6.6 $m^2\ g^{-1}$ for rural and urban aerosol (Bond et al., 2013).

2.2.6 Volatile Organic Compounds

Proton-Transfer-Reaction Time-Of-Flight Mass Spectrometers (PTR-TOF-MSs) are composed of a proton transfer reaction (PTR) ion source and a time-of-flight mass spectrometer (TOF-MS) and measure the online concentration of a range of VOCs in an air sample (Graus et al., 2010; Hansel et al., 1995), as in the intensive campaign in **Paper I**.

Within the instrument, protonated water (H_3O^+) collides with the sample and transfers protons to those molecules that have a higher proton affinity than water. The mass spectrometer then separates different ions according to their mass-to-charge ratio m/z, based on the principle that charged particles with the same m/z travel with the same velocity in an electrical field and, therefore, cover a given distance in the same amount of time. By counting the individual signals that the ions generate when they reach the detector system, the concentration of each compound is calculated.

2.2.7 NO and NO_2

Chemiluminescence analyzers measure NO and NOx (NOx = NO + NO_2) concentrations and calculate NO_2 concentrations, as reported in **Papers I** and **III**. The principle of operation of these analyzers is based on the reaction between NO and O_3, which emits photons with an intensity linearly proportional to the concentration of NO.

$$NO + O_3 \rightarrow NO_2 + O_2 + h\nu \tag{2.6}$$

The instrument operates in two different modes. In the NOx mode, NO_2 is converted to NO with a molybdenum converter. In the NO mode, this conversion is omitted. In both modes, the sample is then guided to the reaction chamber. There, the sample reacts with the O_3, generated with an ozonator inside the instrument. A photomultiplier tube detects the photons generated in the reaction (2.6) and the NO concentration is computed. Finally, NO_2 concentrations are calculated subtracting NO concentrations from NOx concentrations.

2.2.8 SO_2

Ultraviolet fluorescence analyzers were used in **Papers II** and **III** to determine SO_2 concentrations in ambient air. Within the instrument, the sample gas is exposed to 190–230 nm ultraviolet radiation. The SO_2 molecules in the sample gas absorb part of this radiation, which causes one of their electrons to change to an excited state. The molecules quickly return to a lower

energy state by emitting photons with a wavelength of 330 nm (fluorescence). By measuring the amount of photons emitted with a photomultiplier tube, the instrument calculates the concentration of SO_2 in the sample gas.

2.2.9 Carbon monoxide

A gas filter correlation analyzer was used in **Paper III** to measure the concentration of CO. The measurement fundamentals of gas filter correlation analyzers are based on Beer's Law (2.3) and the absorption of CO molecules of light at a wavelength of 4.7 μm.

The analyzer generates a beam of infrared light with a known intensity that is directed to a cell filled with sample gas (sampling chamber). A set of mirrors reflect the light back and forth to lengthen the absorption path *L*. After leaving the cell, the beam is guided to a band-pass filter that only transmits light at 4.7 μm to a photodetector that quantifies the intensity of the light after being absorbed.

Given that water vapor also absorbs light at 4.7 μm, a gas filter correlation wheel is added to the light path in the analyzer. The wheel contains two chambers, one filled with pure N_2 gas (measurement cell) and another one with a mix of CO and N_2 (reference cell). As the wheel rotates, the light passes through the cavities alternatively, producing a square wave with two alternating amplitudes: the infrared light does not interact with the N_2 in the measurement cell, whereas the CO in the reference cell absorbs part of the light.

If no sample air is introduced in the sampling chamber, the ratio between the two pulses is 0.6. When ambient CO is added to the sampling chamber, the ratio increases and tends to 1. The instrument calculates the concentration by transforming the ratio using a look-up table and interpolation. Finally, the concentration is normalized to account for changes in the sampling pressure.

2.3 Measurement Sites and Locations

2.3.1 Madrid

The observations reported in **Paper I** were made in four different locations in and around Madrid, central Spain, during an intensive field campaign in July 2016. Four different locations were used to represent urban, urban background and suburban environments in the area:

Urban site: Instrumentation installed temporarily at the Institute of Agricultural Sciences (Spanish: Instituto de Ciencias Agrarias, CSIC; 40.4404° N, 3.6880° W, 713 m a.s.l.), located 200 m from one of the busiest streets in the city, provided observations of urban air in central Madrid. The instrumentation, installed in the 6th floor of the building, measured BC, NOx and particle size distributions using an Aethalometer, a chemiluminescence analyzer and an SMPS and a PSM, respectively.

Urban background: The research center for energy, environment and technology (Spanish: Centro de Investigaciones Energéticas, MedioAmbientales y Tecnológicas, CIEMAT; 40.4564 N, 3.7256 W, 669 m a.s.l.) is an urban background station in the outskirts of Madrid. Located 9 km NW from the city center and surrounded by green areas, the station is not directly influenced by traffic emissions. The instrumentation used for the measurements of BC, NOx, O_3, total particle concentrations and particle size distributions consisted of an Aethalometer, chemiluminescence and ultraviolet photometry analyzers, a CPC and two SMPSs, respectively.

Suburban site: In Majadahonda, a residential city bordering Madrid, an SMPS, a PSM and a PTR-TOF-MS were temporarily deployed in a suburban environment at the Carlos III Health Institute (Spanish: Instituto de Salud Carlos III, ISCIII; 40.4574° N, 3.8651° W, 739 m a.s.l.), located 15 km from central Madrid. In addition, a balloon sounding system was set in the Majadahonda athletics and rugby field (40.4749° N, 3.8818° W, 728 m a.s.l.) to measure the vertical distribution of aerosols and O_3 in the suburban environment, at 17 km from the center of Madrid.

2.3.2 Barcelona

The observations at the urban background location reported in **Paper III** were made at the Institute of Environmental Assessment and Water Research (Spanish: Instituto de Diagnóstico Ambiental y Estudios del Agua, IDAEA; 41.3873° N, 2.1156° E, 77 m a.s.l.), in Barcelona, northeastern Spain. The station is integrated into the atmospheric pollution monitoring and forecasting network of the Government of Catalonia (XVPCA; Barcelona – Palau Reial station). The site lies 200 m from one of the busiest streets in the city, thus it is significantly influenced by traffic emissions. Continuous observations at the current location started in 2012. For the publications presented in this thesis, BC, particle size distributions, NOx, O_3, SO_2 and CO were measured with a MAAP, an SMPS and chemiluminescence, photometry, fluorescence and gas filter correlation analyzers, respectively.

2.3.3 Montseny

Observations made at Montseny (41.77928° N, 2.35800° E, 720 m a.s.l.) were used for **Papers II** and **III**. It is a regional background station located 48 NE of Barcelona, in a forested area restricted to traffic in the Montseny Natural Park. The station is integrated into the European Aerosols, Clouds and Trace gases Research InfraStructure (ACTRIS) and XVPCA networks. Although the station was established in 2002, continuous aerosol size distribution measurements are available only since 2013. Instrumentation used for the studies presented in this thesis include a MAAP, an SMPS and chemiluminescence, photometry, fluorescence and gas filter correlation analyzers.

Additionally, during an intensive campaign in June and July 2017, a PSM and an AIS were deployed 250 m from the station and the balloon sounding system was set for a week during the campaign.

2.4 Data Analysis

2.4.1 Identification of NPF

The identification and classification of NPF events was originally proposed by Dal Maso et al. (2005). This method relies on the visual identification of different patterns in the daily plots of particle size distributions. With this method, each day is classified under only one of the following categories: event, non-event, or undefined if the distribution is unclear. A day is classified as an event if there is a new nucleation mode that grows in size for at least an hour and grows to larger sizes throughout the day. Events are further classified into two categories: Class I or Class II if the distribution presents fluctuations in concentration or mode diameter. Using this scheme, a substantial number of days fall under the undefined classification because of the definition of the categories and the inherent personal subjectivity of the visual identification. Moreover, the method only considers NPF events occurring in a vast region (regional event) and/or during very stable conditions. Transported events that would only appear for a short time in the distribution are not classified as events.

Other methods derived from the original classification scheme (Buenrostro Mazon et al., 2009; Dada et al., 2018; Hirsikko et al., 2007; Vana et al., 2008) improve the classification of events by using ion size distribution measurements, which are not widely available. More recently, the automatic detection of events, first introduced by Kulmala et al. (2012), is being explored by a few authors that make use of artificial intelligence algorithms (e. g., Joutsensaari et al., 2018; Zaidan et al., 2018). These methods would reduce the subjectivity of human classification, while being

also less time-consuming. However, to this day, these techniques are not as reliable as the classical visual methods.

In **Papers I** and **II**, NPF events were classified following the original method proposed by Dal Maso et al. (2005) using the particle size distributions measured by the SMPS spectrometers. In **Paper II**, the size distribution provided by the AIS was used when available to improve the classification. In **Paper II** an additional category was considered to include observed burst events that would have been classified as non-events. These events last about an hour and stop rapidly due to a change of air masses or sudden dilution after sunrise.

In **Paper III**, NPF was explored by applying a Positive Matrix Factorization (PMF) receptor model (Paatero, 1997) to the particle size distribution. With this method, instead of identifying and classifying whole days, the hourly contribution of NPF processes to the total and mode-segregated particle concentration is calculated.

The PMF model is based on the principle of mass conservation: the concentration of a given species x_j in a sample i can be expressed as the sum of the contributions g_{ik} from p independent sources f_{jk} (Hopke, 2016):

$$x_{ij} = \sum_{k=1}^{p} g_{ik} \cdot f_{jk} + e_{ij} \,, \tag{2.7}$$

where e_{ij} accounts for the part of the concentration that the model cannot fit. The model allows solving (2.7) without knowing the number or characteristics of the sources. This is accomplished by using a weighted least squares approach, weighting by error estimates (uncertainties matrix).

In **Paper III**, the particle number concentrations of each size bin measured with the SMPS spectrometers were used as x_j in (2.7). The hourly averages of the particle size distributions measured with the SMPS spectrometers, gaseous pollutant concentrations (NO, NO_2, O_3, SO_2 and CO) and meteorological variables (temperature, wind speed, relative humidity and solar radiation) were used to identify and apportion the sources contributing to the observed particle size distributions. Further information on the PMF model, details of its implementation and the calculation of uncertainties are given in Rivas et al. (2020) and in **Paper III**.

2.4.2 Calculation of particle sinks

Aerosols grow in size by taking up a range of vapors, including sulfuric acid (H_2SO_4), nitric acid, water, ammonia and organic vapors. This process, called condensational growth, is most effective for particles smaller than 100 nm. The condensation sink (*CS*) is a measure of the rate at which

molecules condense onto the surface of pre-existing aerosols. In **Papers I, II** and **III**, CSs were calculated using the expression derived by Pirjola et al. (1999):

$$CS = 2\pi D \sum_i \beta_i \, D_{p,i} \, N_i \,, \tag{2.8}$$

where D is the diffusion coefficient of H_2SO_4, assumed to be the condensing vapor, β_i is the transitional correction factor (Fuchs and Sutugin, 1971), $D_{p,i}$ is the particle diameter and N_i is the concentration of particles in the size range i.

Small atmospheric particles can also be depleted by coagulating with pre-existing larger particles. Coagulation occurs when two particles collide, mainly due to their Brownian movement, and the smallest particle is absorbed by the larger particle to form a single, bigger particle (coalescence). Thus, the number of particles in the aerosol population is reduced. Coagulation is most effective to particles smaller than 10 nm. To quantify coagulation processes, the coagulation sink of particles with diameter D_p ($CoagS_{Dp}$) is calculated in **Paper I** following the formula proposed by Kulmala et al. (2001):

$$CoagS_{D_p} = \sum_{D_p'} K(D_p, D_p') \, N_{D_p'} \,, \tag{2.9}$$

where K is the coagulation coefficient in the transitional regime (Fuchs et al., 1965).

2.4.3 Calculation of NPF parameters

In order to calculate NPF parameters related with the particle diameters, log-normal modes were fitted to the particle size distribution using the algorithm proposed by Hussein et al. (2005). With this, up to three different modes are identified for each time step, which represent the most probable sizes of the aerosol population. This method was applied to all NPF events identified in **Papers I** and **II**.

The growth rate (*GR*) of particles, defined as the increase in particle diameter per unit of time during a NPF event, was calculated in **Papers I** and **II**. *GRs* were calculated for two different size ranges: from 9 to 25 nm when using SMPS data, and the measuring size range of the instrument when using PSM data. Analogous to the *GR*, the shrinking rate (*SR*)[1] was calculated in **Paper I** when a sustained decrease in particle diameters was observed in NPF events.

[1] In **Papers II** and **III**, in which the shrinking rate is not calculated, the abbreviation SR is used for solar radiation.

The formation rate of particles with diameters in the size range ΔD_p formed by nucleation ($J_{\Delta Dp}$), also called nucleation rate, was calculated in **Paper I** using the equation proposed by Kulmala et al. (2012):

$$J_{\Delta D_p} = \frac{dN_{\Delta D_p}}{dt} + N_{\Delta D_p} \cdot CoagS_{\Delta D_p} + N_{\Delta D_p} \frac{GR}{\Delta D_p} \quad (2.10)$$

$N_{\Delta Dp}$ is the concentration of particles in the size range ΔD_p, measured with the PSMs in this case. The measuring range of each model of PSM determined the range of ΔD_p used in each case. $CoagS_{\Delta Dp}$ is calculated following (2.9).

3 RESULTS

3.1 Review of publications and author's contributions

Paper I explores the vertical and horizontal distribution of NPF events in different environments in Madrid by measuring particle size distributions at ground level in urban, urban background and suburban sites within a two-week field campaign. The evolution of particle size distributions, condensation and coagulation sinks, growth rates and formation rates were compared and discussed to elucidate differences during the episodes in the different environments. Occurrences of particle shrinkage and nocturnal nucleation-mode bursts were also reported. The dynamics of UFPs and NPF events were further studied by measuring the particle size distributions throughout the planet boundary layer by performing vertical balloon soundings in a suburban location. Episodes with formation of new particles were identified and the respective growth rates were calculated. The results were discussed taking into consideration the vertical structure of the boundary layer. The NPF events identified in the soundings were compared with the measurements taken simultaneously at the ground level locations. The results suggested that, on days with regional NPF events affecting a vast area in the Madrid metropolitan area, NPF has a greater contribution to UFPs concentrations than traffic emissions. Nonetheless, traffic is the major contributor to UFPs concentrations when considering annual averages. The NPF events occur inside the mixing layer, with homogeneous concentrations and growth rates throughout the layer. For this publication, I performed the analysis of the ground level and vertical measurements and wrote most of the manuscript.

In **Paper II**, 4 years of data collected at the Montseny regional background station and data measured during an intensive field campaign, including vertical balloon soundings, were analyzed to assess whether and how high O_3 episodes, high UFPs episodes and NPF events are interconnected in the warm season (April–September). The results show that, in this period, conditions leading to simultaneous high O_3 and UFPs concentrations inhibit NPF, whereas NPF events occur together with the lowest O_3 and UFPs concentrations and register the lowest concentration of particles in the nucleation mode. For this paper, I designed the methodology of the data analysis, analyzed the 4-year dataset, participated in the field campaign, contributed to the analysis of the field campaign data and wrote the manuscript.

Paper III describes how the contribution of various sources to the particle size distribution and mode-segregated primary and secondary particle number concentrations have changed at an urban background station in Barcelona and at the Montseny regional background station over 7 years. The study reports a general decrease in primary particles and an increase in NPF at both stations. The total number of particles decreases only in the urban background station, whereas it increases in the regional background station. An increase in VOCs and H_2SO_4 may have been an important factor in increasing NPF, which could be contributing enough to compensate the loss in aerosol loads due to decreasing primary particles. In this publication, I contributed to the conceptualization of the idea and design of the methodology, analyzed the Barcelona and Montseny datasets with the exception of the PMF model implementation, calculated the trends and wrote the manuscript.

3.2 Paper I

Vertical and horizontal distribution of regional new particle formation events in Madrid

Carnerero, C., Pérez, N., Reche, C., Ealo, M., Titos, G., Lee, H.-K., Eun, H.-R., Park, Y.-H., Dada, L., Paasonen, P., Kerminen, V.-M., Mantilla, E., Escudero, M., Gómez-Moreno, F. J., Alonso-Blanco, E., Coz, E., Saiz-Lopez, A., Temime-Roussel, B., Marchand, N., Beddows, D. C. S., Harrison, R. M., Petäjä, T., Kulmala, M., Ahn, K.-H., Alastuey, A. and Querol, X.

Published in *Atmospheric Chemistry and Physics* on November 22, 2018

https://doi.org/10.5194/acp-18-16601-2018

Atmos. Chem. Phys., 18, 16601–16618, 2018
https://doi.org/10.5194/acp-18-16601-2018

Atmospheric Chemistry and Physics Open Access EGU

Vertical and horizontal distribution of regional new particle formation events in Madrid

Cristina Carnerero[1,2], Noemí Pérez[1], Cristina Reche[1], Marina Ealo[1], Gloria Titos[1], Hong-Ku Lee[3], Hee-Ram Eun[3], Yong-Hee Park[3], Lubna Dada[4], Pauli Paasonen[4], Veli-Matti Kerminen[4], Enrique Mantilla[5], Miguel Escudero[6], Francisco J. Gómez-Moreno[7], Elisabeth Alonso-Blanco[7], Esther Coz[7], Alfonso Saiz-Lopez[8], Brice Temime-Roussel[9], Nicolas Marchand[9], David C. S. Beddows[10], Roy M. Harrison[10,11], Tuukka Petäjä[4], Markku Kulmala[4], Kang-Ho Ahn[3], Andrés Alastuey[1], and Xavier Querol[1]

[1]Institute of Environmental Assessment and Water Research (IDAEA-CSIC), Barcelona, 08034, Spain
[2]Department of Civil and Environmental Engineering, Universitat Politècnica de Catalunya, Barcelona, 08034, Spain
[3]Department of Mechanical Engineering, Hanyang University, Seoul, Republic of Korea
[4]Department of Physics, University of Helsinki, Helsinki, 00560, Finland
[5]Centro de Estudios Ambientales del Mediterráneo, CEAM, Paterna, 46980, Spain
[6]Centro Universitario de la Defensa de Zaragoza, Academia General Militar, Zaragoza, 50090, Spain
[7]Department of Environment, Joint Research Unit Atmospheric Pollution, CIEMAT, Madrid, 28040, Spain
[8]Department of Atmospheric Chemistry and Climate, Institute of Physical Chemistry Rocasolano (IQFR-CSIC), Madrid, 28006, Spain
[9]Aix Marseille Univ, CNRS, LCE, Marseille, 13003, France
[10]National Centre for Atmospheric Science, University of Birmingham, Birmingham, B15 2TT, UK
[11]Department of Environmental Sciences, Centre for Excellence in Environmental Studies, King Abdulaziz University, Jeddah, 21589, Saudi Arabia

Correspondence: Cristina Carnerero (cristina.carnerero@idaea.csic.es)

Received: 15 February 2018 – Discussion started: 27 March 2018
Revised: 29 October 2018 – Accepted: 10 November 2018 – Published: 22 November 2018

Abstract. The vertical profile of new particle formation (NPF) events was studied by comparing the aerosol size number distributions measured aloft and at surface level in a suburban environment in Madrid, Spain, using airborne instruments. The horizontal distribution and regional impact of the NPF events was investigated with data from three urban, urban background, and suburban stations in the Madrid metropolitan area. Intensive regional NPF episodes followed by particle growth were simultaneously recorded at three stations in and around Madrid during a field campaign in July 2016. The urban stations presented larger formation rates compared to the suburban station. Condensation and coagulation sinks followed a similar evolution at all stations, with higher values at urban stations. However, the total number concentration of particles larger than 2.5 nm was lower at the urban station and peaked around noon, when black carbon (BC) levels are at a minimum. The vertical soundings demonstrated that ultrafine particles (UFPs) are formed exclusively inside the mixed layer. As convection becomes more effective and the mixed layer grows, UFPs are detected at higher levels. The morning soundings revealed the presence of a residual layer in the upper levels in which aged particles (nucleated and grown on previous days) prevail. The particles in this layer also grow in size, with growth rates significantly smaller than those inside the mixed layer. Under conditions with strong enough convection, the soundings revealed homogeneous number size distributions and growth rates at all altitudes, which follow the same evolution at the other stations considered in this study. This indicates that UFPs are detected quasi-homogenously in an area spanning at least 17 km horizontally. The NPF events extend over the full vertical extension of the mixed layer, which can reach as high as 3000 m in the area, according to previous studies. On some days a marked decline in particle size (shrinkage)

was observed in the afternoon, associated with a change in air masses. Additionally, a few nocturnal nucleation-mode bursts were observed at the urban stations, for which further research is needed to elucidate their origin.

1 Introduction

In urban areas, traffic emissions are a major source of ultrafine particles (UFPs; Kumar et al., 2014; Ma and Birmili, 2015; Pey et al., 2008, 2009; Dall'Osto et al., 2012; Salma et al., 2014; Paasonen et al., 2016). These emissions include primary UFP exhaust emissions (Shi and Harrison, 1999; Shi et al., 2000; Charron and Harrison, 2003; Uhrner et al., 2007), the cooling of engine exhaust emissions, and the condensation of a semi-volatile-phase vapor species that creates new UFPs during dilution (Charron and Harrison, 2003; Kittelson et al., 2006; Robinson et al., 2007; Rönkkö et al., 2017). These are also considered primary particles, since they are formed near the source. Other relevant UFP sources include industrial emissions (Keuken et al., 2015; El Haddad et al., 2013), city waste incineration (Buonanno and Morawska, 2015), shipping (Kecorius et al., 2016; Johnson et al., 2014), airports (Cheung et al., 2011; Hudda et al., 2014; Keuken et al., 2015), and construction (Kumar and Morawska, 2014).

New particle formation (NPF) from gaseous precursors has been shown to cause high UFP episodes in relatively clean atmospheres due to low condensation sinks (CSs) originating from low pre-existing particle concentrations (e.g., Kulmala et al., 2000, 2004; Boy and Kulmala, 2002; Wiedensohler et al., 2002; Wehner et al., 2007; O'Dowd et al., 2010; Sellegri et al., 2010; Vakkari et al., 2011; Cusack et al., 2013a, b; Tröstl et al., 2016; Kontkanen et al., 2017). However, at mountain sites, precursors' availability seems to be the most influential parameter in NPF events, with higher values of CSs during NPF events than during non-NPF events (Boy et al., 2008; Boulon et al., 2010; García et al., 2014; Nie et al., 2014; among others). Tröstl et al. (2016) reported experimental results on nucleation driven by the oxidation of volatile organic compounds (VOCs), and Kirkby et al. (2016) reported pure biogenic nucleation.

NPF events also contribute significantly to ambient UFP concentrations in urban environments (Costabile et al., 2009; Wegner et al., 2012; von Bismarck-Osten et al., 2013, 2014; Ma and Birmili, 2015; Hofman et al., 2016; Kontkanen et al., 2017). Common features enhancing urban NPF are high insolation, low relative humidity, the availability of SO_2 and organic condensable vapors, and low condensation and coagulation sinks (Kulmala et al., 2004; Kulmala and Kerminen, 2008; Sipilä et al., 2010; Salma et al., 2016). Urban NPF episodes can be driven either regionally or locally and may or may not impact regional background areas (Dall'Osto et al., 2013; Brines et al., 2015; Salma et al., 2016). Cheung et al. (2011) and Brines et al. (2015) reported that, in urban areas, nucleation bursts without growth of particles are common, whereas the frequently occurring "banana-like" nucleation bursts at regional background sites are scarcely detected at urban sites, probably because the high CS during traffic rush hours limits the duration of the particle growth. These processes seem to prevail in summer and spring in southern European urban areas (Dall'Osto et al., 2013; Brines et al., 2014, 2015). Brines et al. (2015) also reported that, in urban environments, the highest O_3 levels occur simultaneously with NPF events, the highest SO_2 concentrations and insolation, and the lowest relative humidity and NO and NO_2 levels. This close association between O_3 and UFPs may be due to ambient conditions that favor two different, but simultaneous, processes or to the fact that they are both products of photochemical reactions in the same overall process.

Reche et al. (2011) evaluated the prevalence of primary versus newly formed UFPs in several European cities and found a different daily pattern for the southern European cities, in which the newly formed particles contributed substantially to the annual average concentrations, probably because of high insolation and possible site-specific chemical precursors. Brines et al. (2015) determined that NPF events lasting for 2 h or more occurred on 55 % of the days, and those extending to 4 h occurred on 28 % of the days, with NPF being the main contributor 14 %–19 % of the time in Mediterranean and subtropical climates (Barcelona, Madrid, Rome, Los Angeles, and Brisbane). The latter percentages reached 2 % and 24 %–28 % in Helsinki and Budapest, respectively (Wegner et al., 2012; Salma et al., 2016). Furthermore, Brines et al. (2015) calculated that 22 % of the annual average UFP number concentration recorded at an urban background site in Barcelona originated from NPF. Ma and Birmili (2015) reported that the annual contribution of traffic to the UFP number concentration was 7 %, 14 %, and 30 % at roadside, urban background, and rural sites, respectively, in and around Leipzig, Germany. On the other hand, traffic emissions contributed to 44 %–69 % of UFP concentrations in Barcelona (Pey et al., 2009; Dall'Osto et al., 2012; Brines et al., 2015), 65 % in London (Harrison et al., 2011; Beddows et al., 2015), and 69 % in Helsinki (Wegner et al., 2012).

Minguillón et al. (2015) and Querol et al. (2017) demonstrated that intensive NPF episodes take place inside the planetary boundary layer (PBL) in Barcelona, occurring around midday at surface level, when insolation and dilution of pollution are at their maxima. Earlier in the morning, NPF can only take place at upper atmospheric levels, at an altitude where pollutants are diluted, since at surface level, a high CS prevents particle formation.

While many studies have investigated NPF around the world, only a few have focused on the vertical distribution of these events (Stratmann et al., 2003; Wehner et al., 2010). In view of this, we devised a campaign with the aim to study photochemical episodes, including high O_3 levels and NPF in

the Madrid metropolitan area. In a twin article (Querol et al., 2018), the study of the temporal and spatial variability of O_3 is presented. In this work we will focus exclusively on the phenomenology of the NPF events, comparing the aerosol size distribution at surface level at urban, urban background, and suburban stations in Madrid and the outskirts of a residential village 17 km from Madrid. We also study the vertical distribution of the events using airborne instrumentation carried by tethered balloons.

2 Methodology

2.1 The study area

The Madrid metropolitan area (MMA) lies in the center of the Iberian Peninsula at an elevation of 667 m a.s.l. (meters above sea level). It is surrounded by mountain ranges and river basins that channel the winds in a NE–SW direction. Having an inland Mediterranean climate, winters are cool and summers are hot, and precipitation occurs mainly in autumn and spring. Road traffic and residential heating in winter are the main sources of air pollutants, with small contributions made by industrial and aircraft emissions (Salvador et al., 2015).

In summer, the area is characterized by strong convection, which results in PBL heights as high as 3000 m a.g.l. (above ground level) and mesoscale recirculation caused by anabatic and katabatic winds in the surrounding mountain ranges (Plaza et al., 1997; Crespí et al., 1995), which can lead to the accumulation of pollutants if the recirculation persists for several days.

The cold and warm advection of air masses associated with the passage of upper-level troughs and ridges over the area gives rise to a sequence of accumulation and venting periods, respectively. During accumulation periods, pollutants accumulate in the area, and concentrations increase for 2–6 days, until a trough aloft brings a cold advection and a venting period starts. For a detailed description of the meteorological context during the campaign, see Querol et al. (2018).

A few studies have focused on NPF events in the area. For instance, Gómez-Moreno et al. (2011) reported NPF episodes in Madrid to be "not a frequent phenomenon", since only 63 events per year were detected, with 17 % of the total days occurring mostly in spring and summer. However, Brines et al. (2015) reported both intensive summer and winter NPF episodes at the same station, which accounted for 58 % of the time as an annual average, considering the prevalence of nucleation bursts for 2 h or more. Alonso-Blanco et al. (2017) described the phenomenology of particle-shrinking events, i.e., a decline in particle size caused by particle-to-gas conversion, at an urban background station in Madrid (CIEMAT), stating that they occur mainly between May and August in the afternoon, due to either a change in wind direction or the reduction of photochemical processes. Particle shrinkage following their growth is not a common phenomenon but has been observed in a few areas around the world. Yao et al. (2010), Cusack et al. (2013a, b), Young et al. (2013), Skrabalova et al. (2015), and Alonso-Blanco et al. (2017) and references therein, reported shrinkage rates ranging from -1.0 to $-11.1\,\mathrm{nm\,h^{-1}}$.

2.2 Instrumentation

The data used in this study were collected during a summer campaign in and around Madrid in July 2016. Three air quality supersites were used, namely, an urban station, an urban background station, and a suburban station, in addition to a setting in a suburban environment with two tethered balloons that allowed for the study of the vertical distribution of aerosols and air pollutants. All stations are located within a range of 17 km. A map displaying all locations is shown in Fig. 1.

The CSIC (Consejo Superior de Investigaciones Científicas, the Spanish national research council) urban station, operative from 9 to 20 July, was located in the Institute of Agricultural Sciences (40°26′25″ N, 03°41′17″ W, 713 m a.s.l.) in central Madrid. The instrumentation at this station was installed on the sixth floor of the building, with instruments sampling through a window. NO_x and equivalent black carbon (BC) concentrations were measured with a chemiluminescence-based analyzer (Teledyne API, 200EU) and an Aethalometer (AE33, Magee Scientific, $5\,\mathrm{L\,min^{-1}}$), respectively. The aerosol number size distribution in the size range 8–120 nm was measured with a Scanning Mobility Particle Spectrometer (SMPS; TSI, 3082) equipped with a Nano-Differential Mobility Analyzer (DMA; TSI 3085) and a condensation particle counter (CPC; TSI 3772, $1\,\mathrm{L\,min^{-1}}$). A particle size magnifier (PSM, Airmodus A10) combined with a CPC (TSI 3775) were used to measure size distributions in the size range 1.2–2.5 nm. This system was operated in scanning mode using Airmodus software ($2.5\,\mathrm{L\,min^{-1}}$). PSM data were post-processed and corrected for diffusion losses by using tailored software provided by Airmodus.

The CIEMAT (Centro de Investigaciones Energéticas, Medioambientales y Tecnológicas, Research center for energy, environment, and technology) urban background station, operative from 4 to 20 July, was located on the outskirts of Madrid, 4 km from the CSIC station (40°27′23″ N, 03°43′32″ W, 669 m a.s.l.). NO_x, O_3, and BC concentrations were measured with a chemiluminescence-based analyzer (THERMO 17i), an ultraviolet photometry analyzer (THERMO 49i), and an Aethalometer (AE33 Magee Scientific, $5\,\mathrm{L\,min^{-1}}$), respectively. The aerosol number size distribution in the size range 15–660 nm was measured with an SMPS (TSI 3080) combined with a CPC (TSI 3775, $1.5\,\mathrm{L\,min^{-1}}$) and in the size range 1–30 nm was measured with a 1 nm SMPS (TSI 3938E77, $2.5\,\mathrm{L\,min^{-1}}$). All data were processed and corrected for multiple charge and diffusion losses by using the TSI Aerosol Instrument Manager

the Madrid metropolitan area. In a twin article (Querol et al., 2018), the study of the temporal and spatial variability of O_3 is presented. In this work we will focus exclusively on the phenomenology of the NPF events, comparing the aerosol size distribution at surface level at urban, urban background, and suburban stations in Madrid and the outskirts of a residential village 17 km from Madrid. We also study the vertical distribution of the events using airborne instrumentation carried by tethered balloons.

2 Methodology

2.1 The study area

The Madrid metropolitan area (MMA) lies in the center of the Iberian Peninsula at an elevation of 667 m a.s.l. (meters above sea level). It is surrounded by mountain ranges and river basins that channel the winds in a NE–SW direction. Having an inland Mediterranean climate, winters are cool and summers are hot, and precipitation occurs mainly in autumn and spring. Road traffic and residential heating in winter are the main sources of air pollutants, with small contributions made by industrial and aircraft emissions (Salvador et al., 2015).

In summer, the area is characterized by strong convection, which results in PBL heights as high as 3000 m a.g.l. (above ground level) and mesoscale recirculation caused by anabatic and katabatic winds in the surrounding mountain ranges (Plaza et al., 1997; Crespí et al., 1995), which can lead to the accumulation of pollutants if the recirculation persists for several days.

The cold and warm advection of air masses associated with the passage of upper-level troughs and ridges over the area gives rise to a sequence of accumulation and venting periods, respectively. During accumulation periods, pollutants accumulate in the area, and concentrations increase for 2–6 days, until a trough aloft brings a cold advection and a venting period starts. For a detailed description of the meteorological context during the campaign, see Querol et al. (2018).

A few studies have focused on NPF events in the area. For instance, Gómez-Moreno et al. (2011) reported NPF episodes in Madrid to be "not a frequent phenomenon", since only 63 events per year were detected, with 17 % of the total days occurring mostly in spring and summer. However, Brines et al. (2015) reported both intensive summer and winter NPF episodes at the same station, which accounted for 58 % of the time as an annual average, considering the prevalence of nucleation bursts for 2 h or more. Alonso-Blanco et al. (2017) described the phenomenology of particle-shrinking events, i.e., a decline in particle size caused by particle-to-gas conversion, at an urban background station in Madrid (CIEMAT), stating that they occur mainly between May and August in the afternoon, due to either a change in wind direction or the reduction of photochemical processes. Particle shrinkage following their growth is not a common phenomenon but has been observed in a few areas around the world. Yao et al. (2010), Cusack et al. (2013a, b), Young et al. (2013), Skrabalova et al. (2015), and Alonso-Blanco et al. (2017) and references therein, reported shrinkage rates ranging from -1.0 to $-11.1\,\mathrm{nm\,h^{-1}}$.

2.2 Instrumentation

The data used in this study were collected during a summer campaign in and around Madrid in July 2016. Three air quality supersites were used, namely, an urban station, an urban background station, and a suburban station, in addition to a setting in a suburban environment with two tethered balloons that allowed for the study of the vertical distribution of aerosols and air pollutants. All stations are located within a range of 17 km. A map displaying all locations is shown in Fig. 1.

The CSIC (Consejo Superior de Investigaciones Científicas, the Spanish national research council) urban station, operative from 9 to 20 July, was located in the Institute of Agricultural Sciences (40°26′25″ N, 03°41′17″ W, 713 m a.s.l.) in central Madrid. The instrumentation at this station was installed on the sixth floor of the building, with instruments sampling through a window. NO_x and equivalent black carbon (BC) concentrations were measured with a chemiluminescence-based analyzer (Teledyne API, 200EU) and an Aethalometer (AE33, Magee Scientific, $5\,\mathrm{L\,min^{-1}}$), respectively. The aerosol number size distribution in the size range 8–120 nm was measured with a Scanning Mobility Particle Spectrometer (SMPS; TSI, 3082) equipped with a Nano-Differential Mobility Analyzer (DMA; TSI 3085) and a condensation particle counter (CPC; TSI 3772, $1\,\mathrm{L\,min^{-1}}$). A particle size magnifier (PSM, Airmodus A10) combined with a CPC (TSI 3775) were used to measure size distributions in the size range 1.2–2.5 nm. This system was operated in scanning mode using Airmodus software ($2.5\,\mathrm{L\,min^{-1}}$). PSM data were post-processed and corrected for diffusion losses by using tailored software provided by Airmodus.

The CIEMAT (Centro de Investigaciones Energéticas, Medioambientales y Tecnológicas, Research center for energy, environment, and technology) urban background station, operative from 4 to 20 July, was located on the outskirts of Madrid, 4 km from the CSIC station (40°27′23″ N, 03°43′32″ W, 669 m a.s.l.). NO_x, O_3, and BC concentrations were measured with a chemiluminescence-based analyzer (THERMO 17i), an ultraviolet photometry analyzer (THERMO 49i), and an Aethalometer (AE33 Magee Scientific, $5\,\mathrm{L\,min^{-1}}$), respectively. The aerosol number size distribution in the size range 15–660 nm was measured with an SMPS (TSI 3080) combined with a CPC (TSI 3775, $1.5\,\mathrm{L\,min^{-1}}$) and in the size range 1–30 nm was measured with a 1 nm SMPS (TSI 3938E77, $2.5\,\mathrm{L\,min^{-1}}$). All data were processed and corrected for multiple charge and diffusion losses by using the TSI Aerosol Instrument Manager

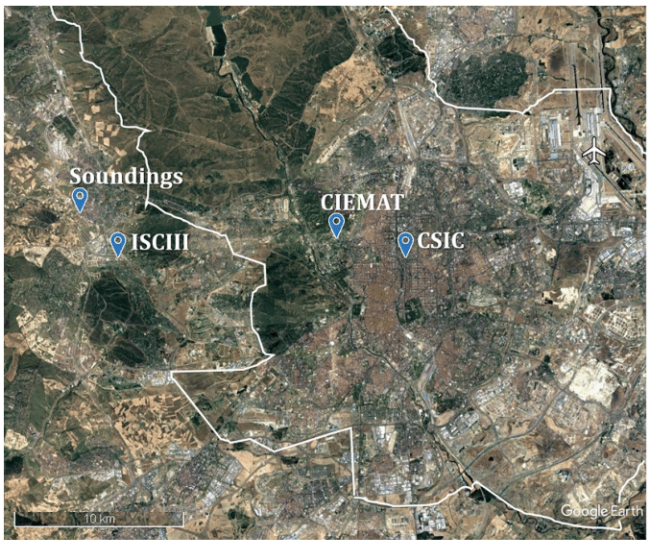

Figure 1. Location of the stations and sounding setting used in the campaign. The location of the airport is also shown. A white solid line marks the city limits of Madrid.

(AIM) software. In the overlapping range (15–30 nm), the nano-SMPS yielded slightly higher concentration values. In order to correct these higher values and obtain a continuous size distribution, the daily nano-SMPS values were corrected to adapt to those of the SMPS. We compared the resulting merged particle size distribution with CPC measurements (CPC TSI 3776, > 2.5 nm) to check that there was good agreement in total particle concentration. Temperature (4 m a.g.l.), relative humidity (4 m a.g.l.), solar radiation (35 m a.g.l.), and wind speed and direction (55 m a.g.l.) were measured at a meteorological tower at the station.

The ISCIII (Instituto de Salud Carlos III, Carlos III Institute of Health) suburban station was located at the Carlos III Institute of Health in Majadahonda, 15 km from the CSIC station (40°27′27″ N, 03°51′54″ W, 739 m a.s.l.), and was operative from 4 to 20 July. An SMPS (TSI 3080) equipped with a CPC (TSI 3775, 1.5 L min^{-1}) measured the aerosol number size distribution in the size range 9–360 nm. Data were processed and corrected for multiple charge and diffusion losses by using the TSI AIM software. Size distributions in the range 1.2–4.0 nm were measured with a PSM (Airmodus, A11, 2.5 L min^{-1}) in combination with a CPC (Airmodus, A20) working in scanning mode. Data were post-processed and corrected for diffusion losses by using the Scilab code provided by Airmodus. A proton-transfer-reaction time-of-flight mass spectrometer (PTR-ToF-MS; Ionicon Analytik, PTR-TOF 8000) operating in H3O+ mode was used to measure VOC concentrations. A detailed description of the instrument can be found in Graus et al. (2010). The operational procedure for the PTR-ToF-MS is fully described in Querol et al. (2018). Results regarding these measurements are briefly presented in Sect. S1 in the Supplement.

UFP instrument calibration was performed by the manufacturers: TSI in the case of SMPS and CPCs and Airmodus for PSM. Particle sizing and counting instrumentation at all stations were collocated next to windows or walls where holes were available for inlets and equipped with individual 1/4 inch, 20 cm long conductive silicone tubing inlets for PSM. SMPS and CPC also had individual 30 cm conductive silicone tubing inlets. Each instrument had its own flow rate since there were individual inlets. TSI instrument data were corrected for diffusion losses and multiple charge losses using the instruments' own software.

Regarding the vertical measurements, two tethered balloons carrying miniaturized instrumentation were based at the Majadahonda (MJDH) rugby field (40°28′29.9″ N 3°52′54.6″ W, 728 m a.s.l.), 17 km from CSIC. Twenty-eight flights up to 1200 m a.g.l. were carried out from 11 to 14 July. A miniaturized SMPS (Hy-SMPS, an SMPS designed by the University of Hanyang) measured the particle size distribution in the range 8–245 nm with a time resolution of 45 s and flow of 0.125 L min^{-1} (Lee et al., 2015). However, only particles larger than 10 nm could be detected due to lower efficiency for finer particles. The instrument was inter-compared with an SMPS (TSI, Standard DMA with 3776 CPC) for 50 nm monodispersed NaCl particles and polydispersed aerosols (Fig. S1). The number concentration of particles larger than 3 nm was measured with a miniaturized butanol-based CPC (Hy-CPC, designed by the University of Hanyang). The time resolution was 1 s, and sample flow was 0.125 L min^{-1} (Lee et al., 2014). Temperature, relative humidity, pressure, wind speed, and wind direction were also measured. The instrumentation was also equipped with a global positioning system (GPS). An additional set of miniaturized instrumentation was placed at surface level for comparison.

2.3 Data analysis techniques

Identification of NPF events was made via the method proposed by Dal Maso et al. (2005). After the examination of the daily particle size distribution, if the day was classified as an event day, we proceeded to calculate growth rates (GRs), shrinking rates (SRs), condensation and coagulation sinks (CSs and CoagSs), and formation rates (J_{D_p}).

The algorithm proposed by Hussein et al. (2005) was used to fit log-normal modes to the particle size distribution, from which GRs were calculated by following Eq. (1):

$$\mathrm{GR} = \frac{\mathrm{d}D_\mathrm{p}}{\mathrm{d}t}, \quad (1)$$

where D_p is the selected geometric mean diameter corresponding to the growing particle mode. Unless stated otherwise, in this work, GRs are calculated for particles growing from 9 to 25 nm. When calculating GRs with PSM data, the

range was selected according to the measuring range of each instrument (see Sect. 2.2). SRs were calculated analogously when a decrease in the diameter of the fitted modes was observed.

The CS, a measure of the removal rate of condensable vapor molecules due to their condensation onto pre-existing particles (Kulmala et al., 2012), is calculated using Eq. (2):

$$\mathrm{CS} = 2\pi D \sum_i \beta_i D_{\mathrm{p},i} N_i, \quad (2)$$

where D is the diffusion coefficient of the condensing vapor (here we use H_2SO_4), $D_{\mathrm{p},i}$ and N_i are the particle diameter and particle concentration, respectively, for the size class i, and β_i is the transitional correction factor:

$$\beta_i = \frac{1 + K_i}{1 + \left(\frac{4}{3\alpha} + 0.337\right) K_i + \frac{4}{3\alpha} K_i^2}, \quad (3)$$

where the Knudsen number $K_i = 2\lambda / D_{\mathrm{p},i}$, with λ representing the mean free path of the condensing vapor in air and α representing the sticking coefficient, here assumed to be equal to 1.

The formation rates of particles were calculated as 30 min averages, following Eq. (4):

$$J_{D_\mathrm{p}} = \frac{\mathrm{d}N_{D_\mathrm{p}}}{\mathrm{d}t} + \mathrm{CoagS}_{D_\mathrm{p}} \cdot N_{D_\mathrm{p}} + \frac{\mathrm{GR}}{\Delta D_\mathrm{p}} N_{D_\mathrm{p}}, \quad (4)$$

where we use the PSM measuring range for N_{D_p}, and CoagS is a quantification of the ability of the preexisting aerosols to scavenge newly formed particles. For its calculation we take the geometric mean diameter of the size ranges 1–25 nm, using a merged PSM and SMPS particle size distribution. The CoagS can be calculated using Eq. (5):

$$\mathrm{CoagS}_{D_\mathrm{p}} = \sum_{D'_\mathrm{p}} K\left(D_\mathrm{p}, D'_\mathrm{p}\right) N_{D'_\mathrm{p}}, \quad (5)$$

where K is the coagulation coefficient. For a detailed description of the parameters and their derivation, see Kulmala et al. (2012).

A rough estimation of the mixed layer height was determined using Hy-CPC measurements. The top of the mixed layer was considered to be at an altitude at which particle concentration decreases an order of magnitude quasi-instantaneously and remains constant above this altitude. All UFP profiles are included in Querol et al. (2018).

Additionally, bivariate polar plots of concentration have been used to relate wind speed and direction with total particle concentration using PSM data by means of the R package "openair" (Carslaw and Ropkins, 2012).

3 Results and discussion

3.1 Meteorological context

Figure S2 shows the evolution of the temperature, relative humidity, wind speed, and wind direction measured at CIEMAT from 5 to 20 July 2016. The evolution of temperatures during this period evidences a succession of accumulation and venting episodes. Rain gauges collected significant precipitation only on 6 July at midnight (not shown).

The balloon field campaign, held from 11 to 14 July, coincided with the start of a venting period, the passage of an upper-level trough, and the transition to an accumulation period when the trough moved to the east of the Iberian Peninsula and a ridge passed over the area of study (see Fig. S3). Maxima and minima temperatures dropped, while strong westerly winds predominated until they veered to the NE on 12 July 18:00 UTC. High nocturnal wind speed peaks were recorded in this period and were often accompanied by a change in wind direction. For detailed information on the meteorological parameters during this campaign, see Querol et al. (2018).

3.2 Comparison of NPF events at urban and suburban surface stations

In the following discussions, we group CSIC (urban) and CIEMAT (urban background) as urban stations and compare them to ISCIII (suburban). This grouping is done because of the availability of data during the period of interest. However, it has to be noted that CSIC is more influenced by traffic than CIEMAT, therefore it is more representative of urban environments, and, for this reason, CSIC data are chosen when possible. Eighteen NPF episodes have been identified on a total of 7 days throughout the campaign. A summary of these events is presented in Table 1. Out of these, a total of 14 events on 6 days had simultaneous data available for at least one of the urban stations (CSIC, CIEMAT) and the suburban station (ISCIII). These episodes, marked with an asterisk in Table 1, are selected for further analysis in this section. Figure 2 represents the aerosol number particle size distributions for the selected episodes (12–18 July 2016).

3.2.1 Episode characteristics

In the selected episodes, intensive daytime nucleation and subsequent condensational growth processes took place simultaneously at urban and suburban stations, located 17 km apart, and, accordingly, we classify these as regional NPF episodes. If the episodes were caused by primary emissions, then we would observe different size distributions at all stations, because each one of them is differently influenced by traffic. The urban station is largely influenced by traffic emissions, whereas the suburban station is much less affected by these emissions. Since we observe the same size distribution at both stations, we can say that traffic emissions are not the

Table 1. Summary of new particle formation events recorded during the campaign, showing the starting time, considered as the moment of first detection of the nucleation mode, the final time, considered as the time when the mode reaches 25 nm, the growth rate calculated in that period using SMPS and PSM data, and formation rates at the starting time. An asterisk marks the events that are detected simultaneously at all stations and were chosen for further analysis in this work.

	Date (dd/mm/yyyy)	Starting time (UTC)	Final time (UTC)	GR ($nm\,h^{-1}$)	GR_{PSM} ($nm\,h^{-1}$)	J_1 ($cm^{-3}\,s^{-1}$)
CSIC	12/07/2016 (*)	06:20	10:39	3.9	1.9	2.4
	13/07/2016 (*)	08:30	12:49	2.0	1.1	8.5
	14/07/2016 (*)	08:45	11:53	1.4	6.75	15.7
ISCIII	12/07/2016 (*)	05:30	09:44	3.0	0.7	1.9
	13/07/2016 (*)	08:50	11:54	4.6	4.3	8.1
	14/07/2016 (*)	09:20	10:39	7.6	6.8	6.5
	16/07/2016 (*)	–	–	–	4.3	–
	17/07/2016 (*)	–	–	–	4.4	3.2
	18/07/2016 (*)	10:44	12:20	2.9	1.38	6.8
CIEMAT	13/07/2016 (*)	08:15	13:45	2.5	–	–
	14/07/2016 (*)	09:00	13:10	4.1	–	–
	15/07/2016	08:34	13:08	4.0	–	–
	18/07/2016 (*)	09:09	11:49	2.6	–	–
MJDH Sounding	12/07/2016	07:27	08:08	3.5	–	–
	13/07/2016	08:39	09:56	5.3	–	–
	14/07/2016	09:00	10:34	6.2	–	–

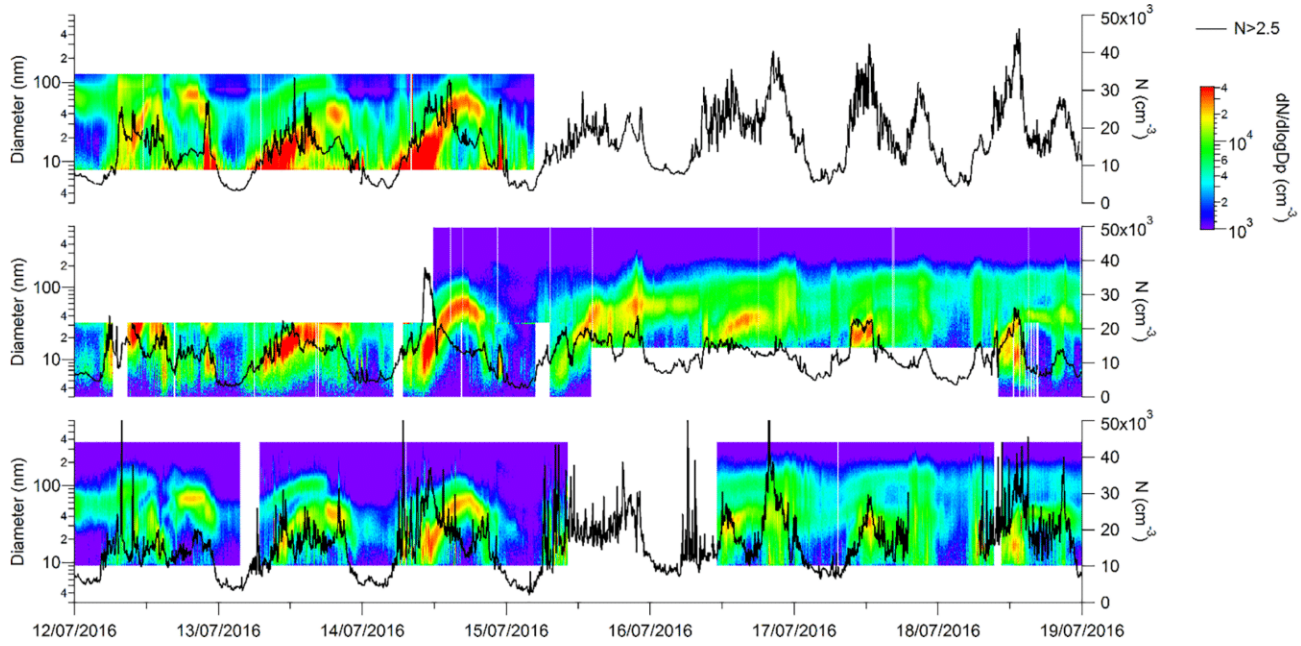

Figure 2. Particle size distribution at CSIC, CIEMAT, and ISCIII (top to bottom), from 4 to 20 July 2016. Total particle concentration of particles with diameter greater than 2.5 nm is also shown.

origin of the observed distributions. Additional arguments include the fact that number concentrations of sub-25 nm particles peak at noon, when BC levels are at their minimum, as well as the concentration of particles measured by PSM being higher at the suburban station compared to the urban station, implying that the particles did not originate from traffic sources.

At urban stations, particles of the order of 10 nm are detected throughout the day, even during the night. Conversely, at the suburban station, such small particles are only detected

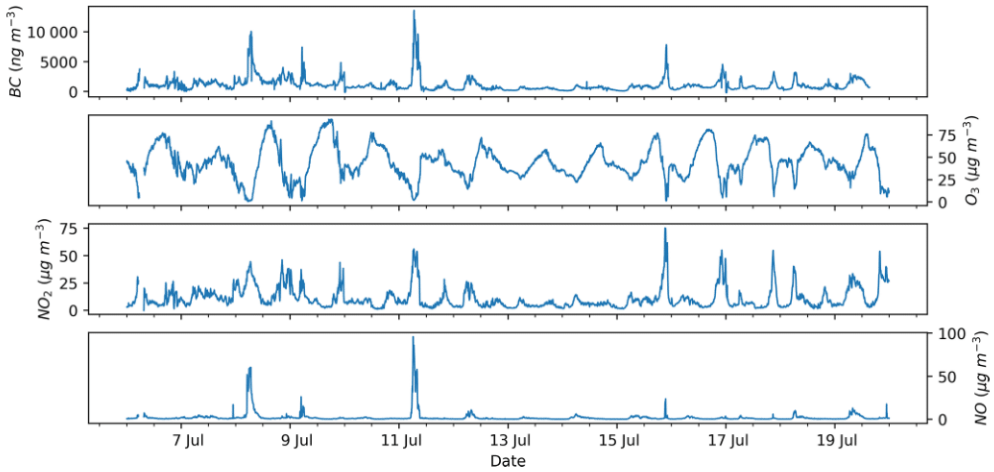

Figure 3. Concentrations of BC, O_3, NO, and NO_2 measured from 6 to 20 July 2016 at CIEMAT.

during daytime. Additionally, during some days, a very intense short nucleation burst is registered at around midnight local time at urban stations, but nothing of this nature is detected at the suburban station. This phenomenon is analyzed in Sect. 3.4.2.

Despite the detection of sub-10 nm particles as early as 04:00 UTC (06:00 LT – local time) at the urban stations, only after around 09:00 UTC is the growth of the particles observed, occurring roughly at the same time in both urban and suburban stations. Newly formed particles grow until they have reached sizes of up to 50 nm, usually around 13:00 UTC (15:00 LT). After this, shrinkage is observed on 10 days, corresponding to 71 % of the days with available data. Consequently, the evolution of the particle size distribution is arc-shaped in these cases.

It should be noted that nucleation episodes coincide in time with the early increases in O_3 concentrations in the morning, whereas the occurrence of maximum O_3 concentration (120 to 150 $\mu g\,m^{-3}$ hourly daily maxima between 14:00 and 16:00 UTC; see Fig. 3) takes place during the UFP growth stage, since oxidation of VOCs and inorganic gases is also accelerated with photochemistry and the presence of O_3 and OH radicals, among others (Coleman et al., 2008; Wang et al., 2017; Saiz-Lopez et al., 2017).

3.2.2 Comparison of GR, J_1, CS, and CoagS

For the observed daily regional NPF events, GRs for the nucleation mode, J_1, CSs, and CoagSs have been determined using PSM and SMPS aerosol size distribution measurements. Here, the GR is calculated from the time of detection of the smallest mode until either the particle reaches 25 nm or it stops growing before reaching that size. We considered only the events that are observed simultaneously at the suburban station and at least at one urban station (highlighted in Table 1). GRs regarding the vertical measurements are discussed in the following section due to differing sampling periods.

The calculated GR for the surface stations are shown in Table 1. GRs ranged from 2.9 to 7.6 $nm\,h^{-1}$ at the suburban site, with a mean value of $4.5 \pm 2.1\,nm\,h^{-1}$, and from 1.4 to 4.0 $nm\,h^{-1}$ at the urban stations, with a mean value of $2.8 \pm 1.0\,nm\,h^{-1}$. We cannot affirm that the mean value of the suburban station is higher than that of the urban stations, because the mean value of the GR at urban stations is included in the confidence interval of the GR at the suburban station. It also has to be considered that only 7 days of measurements are available for these calculations, hence further studies would be needed to confirm the observed differences between urban and suburban stations. Nevertheless, the GRs calculated are consistent with those observed by Alonso-Blanco et al. (2017), ranging 1.4–10.6 $nm\,h^{-1}$ at CIEMAT.

The GRs calculated in this study are also consistent with those observed in other urban and suburban areas. Kulmala et al. (2004) concluded that typical GRs are 1–20 $nm\,h^{-1}$ in midlatitudes. In particular, Stolzenburg et al. (2005) observed GRs ranging from 2.4 to 8.5 $nm\,h^{-1}$ in regional events in an urban environment in Atlanta, GA, US. Qian et al. (2007) reported regional events with a median GR of 5.1 $nm\,h^{-1}$ in an urban environment in St. Louis, MO, US. Ahlm et al. (2012) reported an average GR of 7.3 $nm\,h^{-1}$ in Bakersfield, CA, US. Manninen et al. (2010) characterized NPF events at 12 European sites. Cabauw (the Netherlands) and San Pietro Capofiume (Italy) are stations located in environments comparable to that in our suburban station, ISCIII. For these stations, the observed median GRs were 7–8 $nm\,h^{-1}$, corresponding well with our calculated GR for the suburban station.

Figure 4 shows the average daily cycles of particle concentrations in the size ranges 9–25 nm ($N_{9–25}$) and 1.2–2.5 nm ($N_{1.2–2.5}$), where the total particle concentration was measured by the PSM ($N_{>2.5}$), CS, and CoagS during the re-

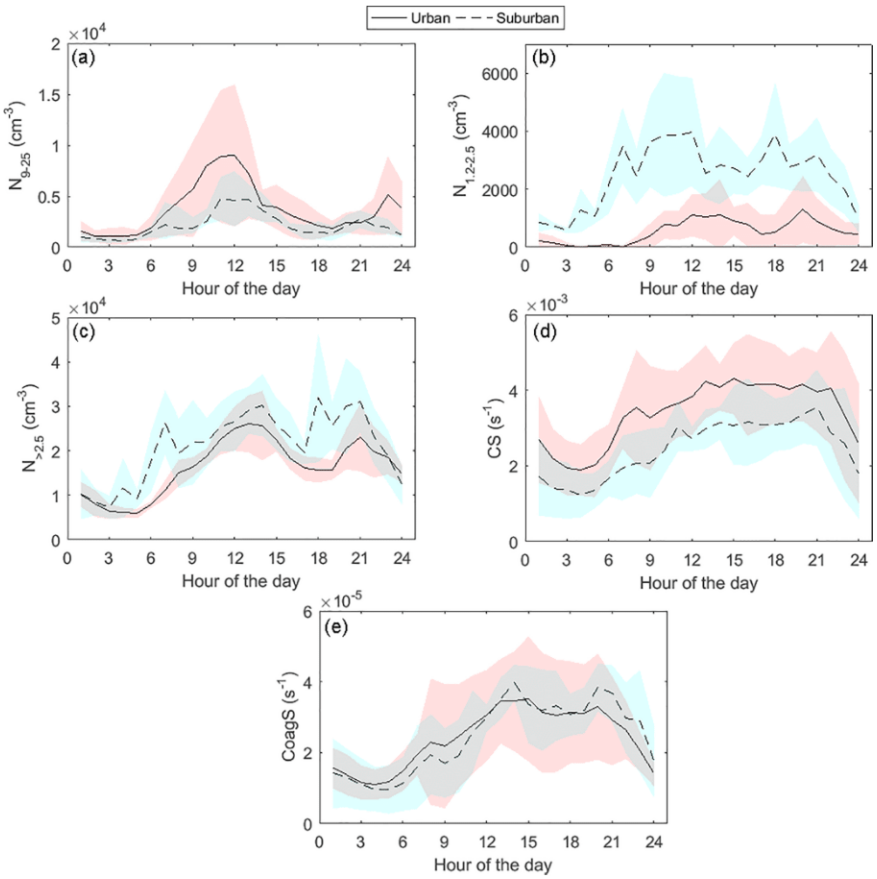

Figure 4. Mean daily cycles of **(a)** total particle concentration in the size range 9–25 nm, **(b)** total particle concentration in the size range 1.2–2.5 nm measured with PSM at CSIC and ISCIII, **(c)** total concentration of particles > 2.5 nm measured with PSM at CSIC and ISCIII, **(d)** condensation sink (CS), and **(e)** coagulation sink (CoagS) during regional new particle formation events at urban (CSIC and CIEMAT, solid line) and suburban (ISCIII, dashed line) stations. Red (urban) and blue (suburban) shaded shapes show 95 % confidence intervals. The hour of the day is given in UTC. Local time is UTC + 2 h.

gional NPF events at the urban and suburban stations. Average $N_{9–25}$ daily mean values are 3.7×10^3 and 2.2×10^3 cm^{-3} at the urban and suburban stations, respectively. $N_{>2.5}$ has average daily mean values of 1.6×10^4 and 2.1×10^4 cm^{-3} at the urban and suburban stations, respectively. It has to be highlighted that $N_{1.2–2.5}$ is considerably larger at the suburban station throughout the day, with mean values of 2.5×10^3 cm^{-3}, compared to 0.5×10^3 cm^{-3} at the urban stations. CSs and CoagSs have average daily mean values of 3.4×10^{-3} s^{-1} (2.5×10^{-3} s^{-1} at the suburban station) and 2.4×10^{-5} s^{-1}, respectively. After dawn, anthropogenic activities start, and $N_{9–25}$, $N_{1.2–2.5}$, $N_{>2.5}$, CSs, and CoagSs start to increase at the same time, both in the urban and suburban environments. Around 07:00 UTC, once the morning traffic rush diminishes, $N_{9–25}$, $N_{>2.5}$ and the sinks increase more slowly; moreover, total particle concentration decreases in the suburban station, indicating that, in this environment, the impact of the traffic emissions on total particle concentration is smaller than near the city center, as expected. Shortly afterwards, at 09:00 UTC, the photochemical processes are strong enough to start NPF, as suggested by the increase in particle concentrations, while the sinks achieve relative minimums. $N_{9–25}$ reaches its maximum at midday (9×10^3 and 5×10^3 cm^{-3} at the urban and suburban stations, respectively) and then decreases because the particles start growing to diameters greater than 25 nm, adding to the sinks, which increase gradually until the evening. NPF leads to maximal UFP concentrations around midday at all stations, as suggested by the peak in $N_{>2.5}$, which is recorded simultaneously with very low BC levels (see Figs. 3 and S4). Around 19:00 UTC, the effect of the afternoon traffic rush is evident, as the variables evolve in a manner similar to that in the morning. Finally, at 23:00 UTC, a sharp and short increase in $N_{9–25}$ is observed, associated with the aircraft emissions discussed in Sect. 3.4.2.

Growth rates (GR_{PSM}) and total formation rates of 1.2–4.0 nm particles (J_1) were calculated from PSM data at CSIC and ISCIII stations. GR_{PSM} were calculated from 11 to 18 July 2016, averaging 4.3 nm h^{-1} at the urban station and 3.7 nm h^{-1} at the suburban station. J_1 were calculated only

for the days in which NPF is identified. The results for these days are included in Table 1. Average J_1 values are higher at the urban station (8.9 cm^{-3} s^{-1}) compared to the suburban station (5.3 cm^{-3} s^{-1}). Concentrations of 1.2–4.0 nm particles are lower at the urban station (Fig. S4), which could lead to lower formation rates. However, the coagulation sink is greater at the urban station, as discussed before, which contributes to the second factor in Eq. (4). It has to be noted that only 3 days of overlapping between PSM and SMPS data were available for NPF events at the urban station and 6 days at the suburban station. A larger dataset would be needed to confirm these results.

The average values of the formation rates agree with those reported at similar stations around the world. For instance, Woo et al. (2001) reported J_3 ranging from 10 to 15 cm^{-3} s^{-1} in Atlanta, GA, US. Wehner and Wiedensohler (2003) reported an average J_3 of 13 cm^{-3} s^{-1} in Leipzig, Germany. Hussein et al. (2008) reported nucleation rates ($D_p < 25$ nm) ranging from 2.1 to 3.0 cm^{-3} s^{-1} in summer in Helsinki, Finland.

3.3 Vertical distribution of NPF events

3.3.1 UFP concentrations

Querol et al. (2018) studied the vertical profiles of UFP and O_3 concentrations measured during the campaign using the balloon soundings at Majadahonda. UFP concentrations are homogeneous throughout the mixing layer and present a sharp decrease at the top. As the day progresses, convection is more effective, and high UFP levels reach higher altitudes as the mixing layer heightens. Moreover, the concentrations tend to increase until midday. Afterwards, they remain constant or decrease slightly, always showing homogeneous levels from surface levels to the top of the PBL. Concentrations of UFPs increased markedly from 11 to 14 July, both at the surface and upper levels. This is consistent with the observed decrease in the convective activity during that period, evidenced by a decrease in temperatures, but also with an increase in the formation rates calculated in this study. Therefore, the increase in particle concentration is probably the result of both a decline in PBL height and more intense nucleation episodes.

3.3.2 Particle size distribution and NPF episodes

The NPF events described in Sect. 3.2 that took place between 12 and 14 July were not only detected at surface level, but also in the upper layers with the balloons soundings in Majadahonda. However, the measurements were not continuous, since the balloons could not be operated safely if the wind speed was above 8 $m\,s^{-1}$ at any vertical level.

Figure 5 shows the fitted modes to the particle size distribution measured in the soundings on 12 July. The fact that sub-40 nm particles are not detected at the higher levels of the first flights suggests that convection is not very effective yet, and the sounding goes through different atmospheric layers, most likely the mixed layer and the residual layer. In the residual layer, Aitken-mode particles formed on previous days prevail (Stull, 1988). The interphase between the mixed layer and the residual layer, i.e., the mixed layer height, has been derived using the UFP vertical profiles (see Querol et al., 2018). From 10:00 UTC onwards, once convection has fully developed, the mixed layer covers all the sounding, and we see a homogeneous distribution at all levels, which is also comparable to those recorded with the instrumentation measuring at the surface. This agrees with the fact that UFPs are homogeneously distributed in the mixed layer and are detected at higher altitudes as the mixed layer rises.

In the early morning the size distribution is dominated by a 60 nm mode at all altitudes, which grows to 100 nm at 11:00 UTC. Even though it is detected at all levels, the mode decreases slightly in size when the sounding ascends above the mixed layer limit, which is more clearly visible on the second flight at around 09:00 UTC. This result suggests that there are lower vapor concentrations in the residual layer, which inhibits particle growth, whereas the mixed layer is more polluted, spurring faster particle growth. The GRs calculated for this mode were 1.8 $nm\,h^{-1}$ in the residual layer and 7.3 $nm\,h^{-1}$ in the mixed layer. The concentration and size of the Aitken mode decrease after midday, which might be related to an increase in wind speed, entailing dilution and evaporation; this leads to the shrinking of the particles. Because of the increase in wind speed, the balloons could not be operated safely, and no additional flights were made on that day.

Moreover, during the morning, we observed particles growing inside the mixing layer, from 10 nm at 07:00 UTC to 30 nm at midday. This mode is observed simultaneously at ISCIII; therefore, we consider it for calculation. The GR obtained is 3.5 $nm\,h^{-1}$. The fact that the GR is the same throughout the mixing layer, even though we expect VOCs to be higher near the surface, upholds the assumption that the convection is very efficient and the entire layer is well-mixed. After 13:00 UTC, due to the increase in wind speed, particles start to shrink. While concentrations were not as high as they were during other episodes, the evolution is remarkably similar to the NPF event measured at the same time at ISCIII, which had a GR of 3.0 $nm\,h^{-1}$.

The size distribution and the corresponding fitted modes for the soundings made on 13 July are presented in Fig. 6. Although the balloons could not fly until 10:30 UTC for safety reasons, at least two modes are detected from early morning at the sounding location. A mode starting roughly at 40 nm at 07:00 UTC grows to 100 nm at 15:00 UTC. With a GR of 8.5 $nm\,h^{-1}$, this mode was detected at all altitudes once the soundings started, indicating that the convection was already effective by 10:30 UTC and all the measured altitudes were completely mixed, leading to a homogeneous particle distribution throughout the soundings. This mode is the prolon-

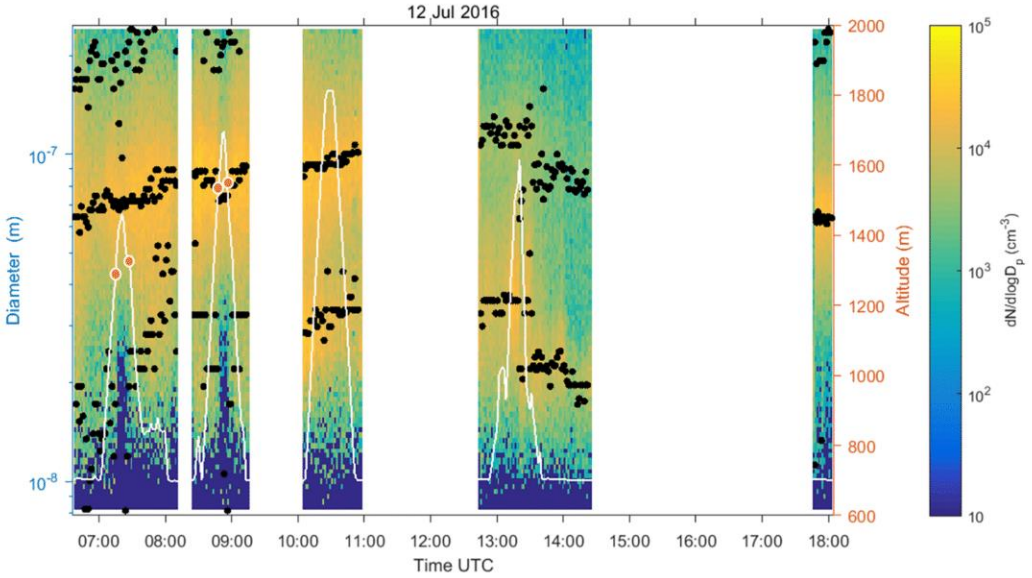

Figure 5. Particle size distribution with fitted log-normal modes (black dots) measured during the balloon soundings at Majadahonda on 12 July 2016. An estimation of the mixing layer height is represented with orange dots. The altitude of the instrumentation is represented with a white line. Surface level is 630 m above sea level. Time is UTC. Local time is UTC + 2 h.

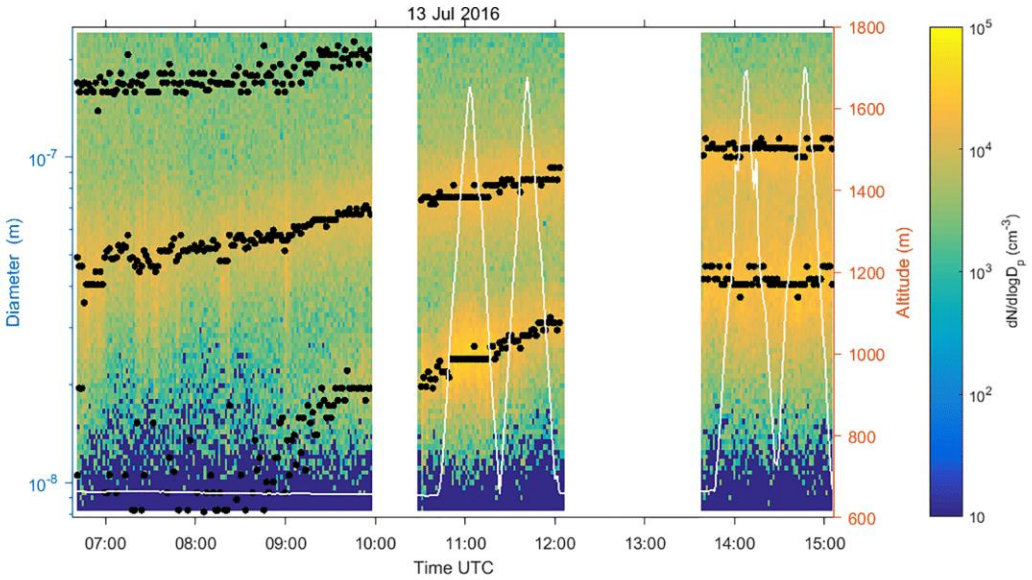

Figure 6. Particle size distribution with fitted log-normal modes (black dots) measured during the balloon soundings at Majadahonda on 13 July 2016. The altitude of the instrumentation is represented with a white line. Surface level is 630 m a.s.l. Time is UTC. Local time is UTC + 2 h.

gation of the Aitken mode detected the day before, which shrank from midday until the following morning. It is also detected at ISCIII and CSIC, with GRs of 7.5 and 6.9 nm h^{-1}, respectively. A nucleation mode also grew from the detection limit of the instrument, from around 10 nm at 08:30 UTC to 40 nm at 15:00 UTC. Comparing with other stations, we considered this mode only after 09:00 UTC and calculated the GR from that time. We consider this a regional NPF event, since the start of the particle growth is registered simultaneously at all the stations. The GRs at the sounding location, ISCIII and CSIC are 5.3, 4.6, and 2.0 nm h^{-1}, respectively.

Figure 7 shows the particle size distribution and fitted modes for the soundings made on 14 July. Correspondingly, in Fig. 8, the vertical distribution of particles for some of the soundings is presented. The earliest soundings revealed the existence of a residual layer aloft. In order to verify this

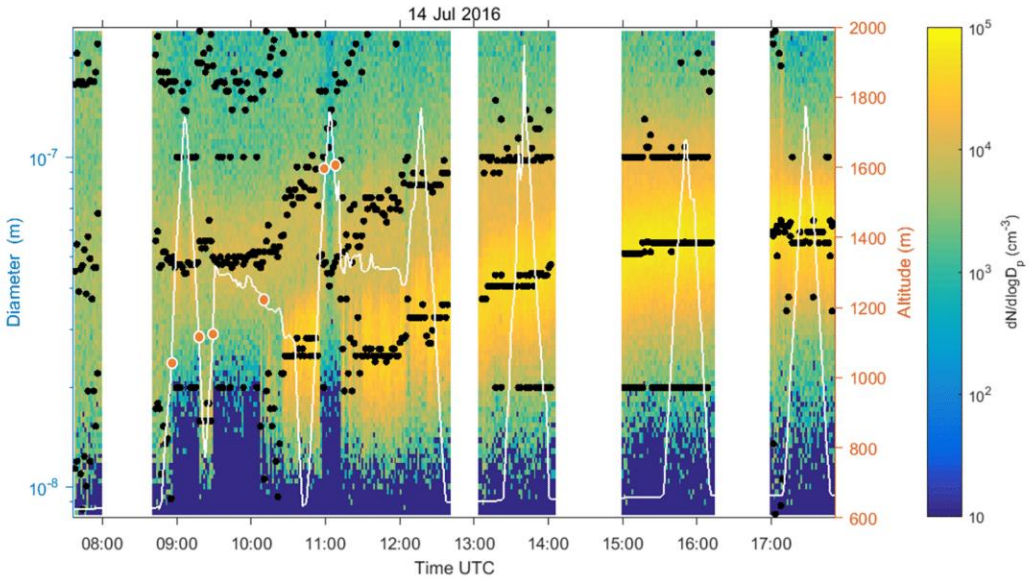

Figure 7. Particle size distribution with fitted log-normal modes (black dots) measured during the balloon soundings at Majadahonda on 14 July 2016. The altitude of the instrumentation is represented with a white line. An estimation of the mixing layer height is represented with orange dots. Surface level is 630 m above sea level. Time is UTC. Local time is UTC + 2 h.

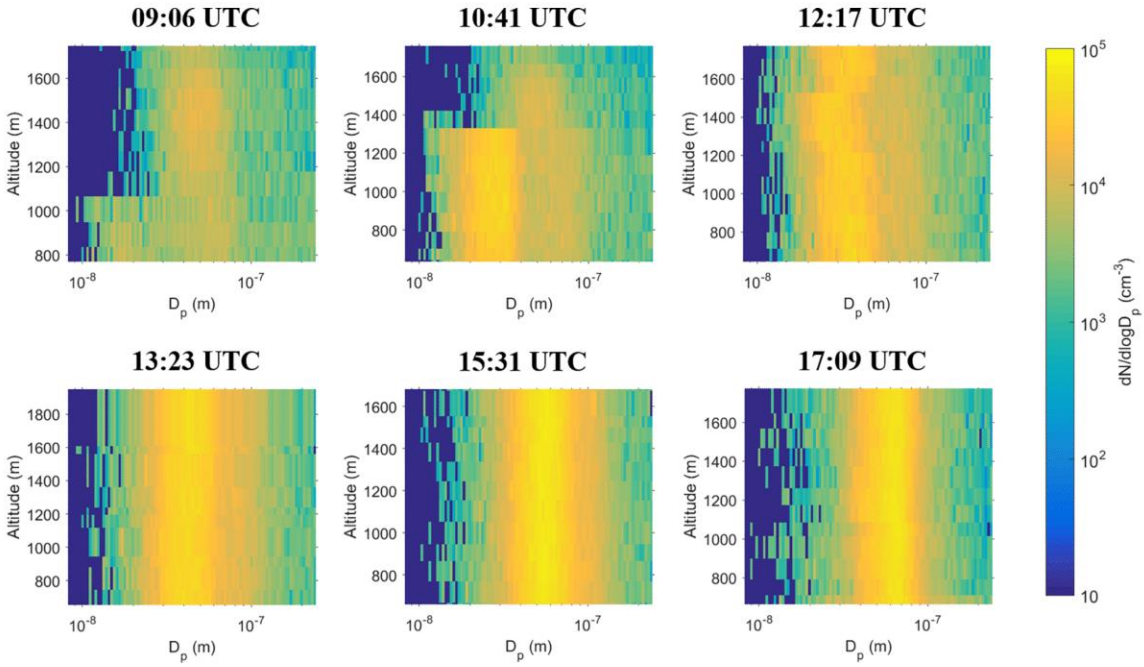

Figure 8. Vertical particle size distribution measured on 14 July during selected soundings.

result, two constant altitude flights were made during the morning. The extension of the wire was not modified during these flights. However, changing wind conditions varied the altitude of the instruments slightly. The altitude was chosen so that the instruments initially remained outside the mixing layer, i.e., inside the residual layer. As the insolation increased, so did the altitude of the mixing layer, until it reached the altitude at which the balloons were positioned. As the mixing layer reached the balloons, total particle concentration increased sharply from 4×10^3 to 2×10^4 cm^{-3}, demonstrating that newly formed particles remain inside the mixing layer.

According to the abrupt decline in particle concentration, the boundary between the mixing and residual layers was lo-

cated at 1000 m at 09:00 UTC, 1200 m at 10:00 UTC, 1350 m at 11:00 UTC, and beyond 1800 m after 12:00 UTC. This can be taken as an indicator of the effectiveness of convection, meaning that after 12:00 UTC, the whole measured particle population was well mixed throughout the sounding range. Inside the residual layer, particles had a slower GR ($0.5\,nm\,h^{-1}$ compared to $8.45\,nm\,h^{-1}$ for the 40 nm mode – note that due to the use of a log scale, this might be unnoticeable visually), and no particles smaller than 20 nm were observed.

Nucleation mode particles were detected exclusively inside the mixing layer from 08:00 to 12:00 UTC, whereas growth was only observed from 09:00 to 11:00 UTC and from 12:00 UTC onwards. The time spacing between both growth periods coincides with a marked decrease in wind speed. During the first period, GRs at the sounding station, ISCIII, and CSIC were 6.2, 5.4, and $1.4\,nm\,h^{-1}$, respectively. However, during the second stage, particles grew faster at the urban station ($8.6\,nm\,h^{-1}$) than at the sounding location ($4.5\,nm\,h^{-1}$). As the latter is a suburban environment, this contrasts with the results obtained in Sect. 3.2.2. This fact could be explained by the veer of NE winds to weaker southerly winds in Madrid, which was not observed in Majadahonda.

Overall, the soundings revealed that there is simultaneous growth and shrinking of nucleation and Aitken modes and that both of them grow and shrink at different rates. This was also observed in the surface measurements when comparing urban and suburban stations (see Sect. 3.2.2).

3.4 Other observations

3.4.1 Prevalence of particles and shrinkage

A further interesting feature is the presence of the Aitken mode on most days. Usually in the size range between 50–100 nm, reaching 110 nm in some cases, this mode does not correspond to newly formed particles, but it follows a parallel evolution (condensational growth and potential shrinkage). When looking at the evolution of aerosol size distributions on consecutive days, it is possible to see a connection between this 50–100 nm mode and the distribution of the previous days. The nucleated and grown mode from one day is still present the following day, and it continues to grow until it eventually fades away or grows beyond the detection limits of the instruments. On some occasions, the Aitken mode can be tracked for 2 or more consecutive days, alternating between the stages of growth and shrinkage.

The start of the shrinking phase coincides with a marked increase in wind speed (Fig. S5); therefore, it is associated with dilution, which favors the evaporation of semi-volatile vapors, resulting in a decline in particle diameter and concentrations, as observed in most cases. The calculated shrinkage rates are shown in Table S1. SRs for particles with a starting diameter below 40 nm range from -1.1 to $-8.0\,nm\,h^{-1}$. For particles in the Aitken mode above 40 nm, the values fall between -4.9 and $-20.5\,nm\,h^{-1}$. The results seem to indicate that, the larger the starting diameter, the faster the particles shrink. Since shrinkage is observed simultaneously at urban and suburban stations, shrinkage seems to be a regional phenomenon in the Madrid area, as already suggested by Alonso-Blanco et al. (2017). However, we could only identify a limited number of simultaneous shrinking episodes, and further research would be needed to confirm these results.

3.4.2 Nocturnal UFP peaks

Although outside of the major focus of this study (photochemical nucleation), other interesting events were detected which took place at night. From 6 to 11 and 17 to 19 July, high concentrations of 1.2–4 nm particles are registered shortly after sunset for several hours, simultaneously at urban and suburban stations (see Fig. 2). BC, NO, and NO_2 concentrations also increase during that time (see Fig. 3). Therefore, these processes are probably related to local traffic emissions and the decrease of the mixing layer after sunset. On the other hand, from 12 to 14 July, high concentrations of sub-25 nm particles are also detected, but they only registered at the urban stations at around 23:00 UTC. These are sudden, shorter, and more intense, with concentrations greater than $10^5\,cm^{-3}$. They appear as intense bursts that last 1 h or less, with no subsequent growth. They are not accompanied by simultaneously high BC or NO concentrations; thus, they are not linked to traffic emissions, although NO_2 levels are significant. Furthermore, these episodes occur outside local traffic rush hours and are registered together with strong NE winds, which suggests that they might be transported from a stationary source and not formed locally. To better support this hypothesis, Fig. S6 shows PSM data together with wind direction and wind speed, showing that the episodes coincide with strong NE winds.

In order to determine the origin of these sub-25 nm particles, bivariate polar plots of concentration have been used to relate wind speed and direction measured at CIEMAT with total particle concentration of 1.2–2.5 nm particles, BC, NO_2, and NO measured at CSIC, analyzing daylight and nighttime periods separately (Fig. 9). These plots must be interpreted carefully, since the color scale only represents the average value for a given wind speed and direction. The results are consistent with what we previously stated; the highest nocturnal 1.2–2.5 nm particle concentrations are linked with strong winds from the NE direction. Air masses transported from this direction have the lowest BC levels and moderate NO_2 concentrations. NO concentrations are insignificant during the nighttime considering any direction, probably because of titration due to the high concentrations of O_3 observed during the daytime.

In the discussion paper, we pointed out the airport Adolfo Suárez Madrid–Barajas, located NE of the city, as a possible

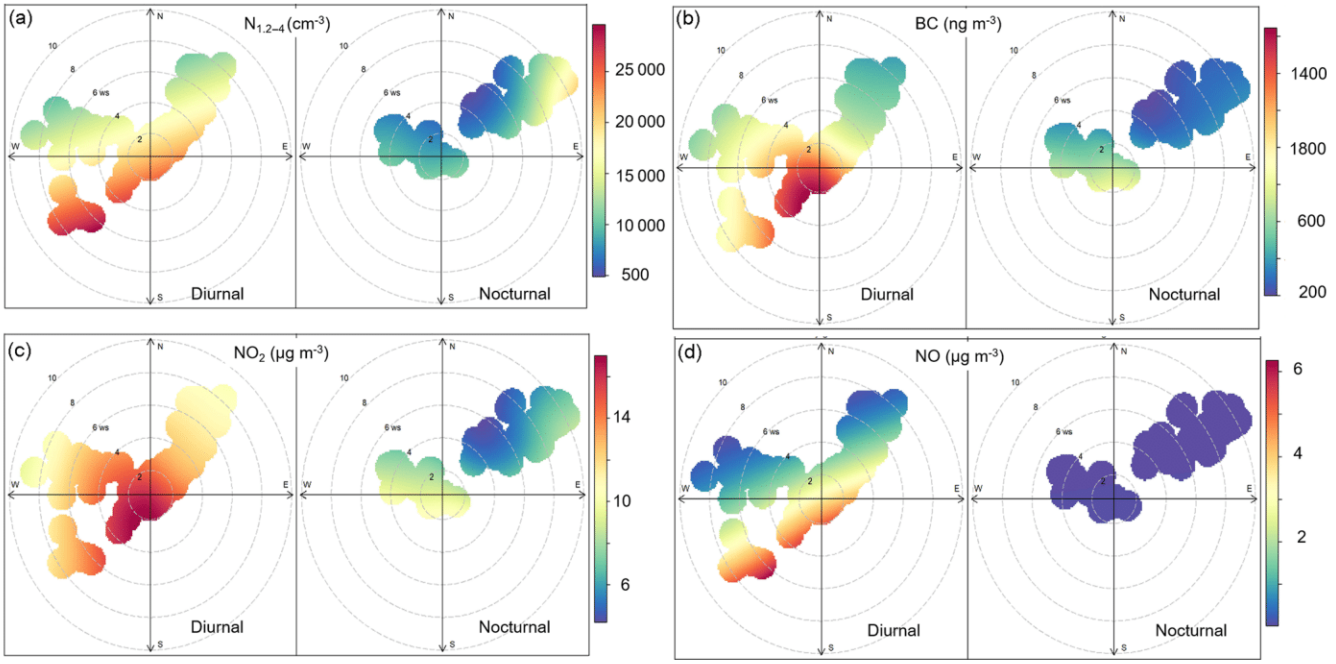

Figure 9. Bipolar plot of **(a)** total particle concentration in the size range 1.2–4 nm measured with the PSM, **(b)** black carbon (BC), **(c)** NO_2, and **(d)** NO concentrations at CSIC urban station using the wind data registered at CIEMAT. Daylight and nighttime hours are separated according to sunrise (05:00 UTC) and sunset (20:00 UTC). The data correspond to the period 11–15 July 2016.

source of these high UFP concentrations. However, the UFP peaks lasted for about 1 h on all days, whereas strong NE winds prevailed for a few hours. Moreover, the airport has flights all night; therefore, a longer period with high UFPs should be observed. Although other studies have linked aircraft emissions with nucleation bursts without growth (Cheung et al., 2011; Masiol et al., 2017), in this study we cannot affirm that the airport is the origin of these bursts. As mentioned before, these episodes were unexpected and were not the main focus of this study. To elucidate the origin of these UFP bursts, further research will be required.

4 Conclusions

We investigated the phenomenology of regional and secondary new particle formation (NPF) episodes in central Spain. To this end, we set up three supersites (an urban, an urban background, and a suburban site) 17 km apart in and around Madrid. We were able to characterize six NPF events, and, in all cases, the evolution of the particle size distribution (PSD) was very similar at all stations; around sunrise, nucleation-mode particles appear and start growing, and in the afternoon, a decline in particle sizes, i.e., shrinkage, is observed. The regional origin of the NPF is supported by the simultaneous variation in PSD in the nucleation mode, particle number concentrations, and growth and shrinkage rates. Furthermore, temporal evolutions of condensation and coagulation sinks were similar at all stations, having minimum values shortly before sunrise and increasing after dawn towards the maximum value after midday in the early afternoon. In spite of the 17 km scale and the simultaneous processes affecting particle number concentrations, the following relevant differences between urban and suburban stations were observed: (i) the urban stations presented larger formation rates as compared to the suburban stations, and (ii) in general, the sinks were higher at the urban stations.

Regarding the vertical soundings of the NPF events, we observed that, in the early morning, the vertical distribution of newly formed particles is differentiated into two layers. The lower layer (mixed layer – ML), in which convection is effective, is well-mixed and has a homogeneous PSD. This ML heightens throughout the day, as insolation is more pronounced, extending beyond the sounding limits around midday. NPF occurs throughout this ML, and GRs and concentrations are homogeneous. The upper layer is a stable residual layer (RL), in which particles formed or transported during the previous days prevail. In the RL, growth is inhibited or even completely restrained, compared with the growth of the same particles in the ML. Overall, the soundings demonstrate that particles are formed inside the ML, but they can prevail and be displaced and stored at upper levels and continue to evolve on following days.

In this campaign we could not measure during the earliest stages of NPF due to the safety requirements imposed on the balloon flights early in the morning. We think it is important for future work to carry out soundings during the

nucleation phase of the episodes. However, miniaturized instruments able to measure smaller particles would be needed and are not available at the present time. Carrying out these soundings would allow us to determine whether secondary NPF takes place throughout the ML or occurs at the surface and is transported upwards afterwards by convection. If the former is true, then locations with high ML could produce more secondary particles than we have considered, and they could affect a larger population or influence climate to a greater extent.

Additionally, a few nocturnal bursts of nucleation-mode particles were observed in the urban stations, and further research is needed to elucidate their origin.

We cannot determine whether the NPF episodes were triggered by the pollution generated in the city that extended to the region or caused by a broader phenomenon. Either way, it can be concluded that, in summer, the particle number concentrations are dominated by NPF in a wide area. The impact of traffic emissions on concentrations of UFPs is much smaller than that of NPF, even near the city center, where the pollution load is at the highest. This result is in line with other studies performed in cities from high-insolation regions (e.g., Kulmala et al., 2016). Given the extent of the episodes, the health effects of NPF can affect a vast number of people, considering that the Madrid metropolitan area, with more than 6 million inhabitants, is the most populated area in Spain and one of the most populated in Europe (UN, 2008). For this reason, we believe that the study of health effects related to newly formed particle inhalation is crucial.

Data availability. All data used in this study can be accessed here: https://doi.org/10.17632/x5gw4stjyb.1 (Pérez et al., 2018).

Supplement. The supplement related to this article is available online at: https://doi.org/10.5194/acp-18-16601-2018-supplement.

Author contributions. Data analysis was done by CC, NP and LD. CC, NP, LD, PP, VK, BT, NM, DB, RH, TP, MK, AA and XQ contributed to the discussion and interpretation of the results. CC and XQ wrote the manuscript. NP, CR, MEa, GT, HL, HE, YP, EM, MEs, FG, EA, EC, AS, BT, NM, DB, RH, KA, AA and XQ carried out the measurements. All the authors commented on the manuscript.

Competing interests. The authors declare that they have no conflict of interest.

Acknowledgements. This work was supported by the Spanish Ministry of Agriculture, Fishing, Food and Environment; the Ministry of Economy, Industry and Competitiveness; the Madrid City Council and Regional Government; FEDER funds under the project HOUSE (CGL2016-78594-R); the CUD of Zaragoza (project CUD 2016-05); the Government of Catalonia (AGAUR 2017 SGR44); and the Korean Ministry of Environment through "The Eco-Innovation project". The funding received by ERA-PLANET (http://www.era-planet.eu, last access: 16 November 2018), the trans-national project SMURBS (http://www.smurbs.eu, last access: 16 November 2018) (Grant agreement No. 689443), and the support of the Academy of Finland via the Center of Excellence in Atmospheric Sciences are acknowledged. These results are part of a project (ATM-GTP/ERC) that has received funding from the European Research Council (ERC) under the European Union's Horizon 2020 research and innovation program (Grant agreement No. 742206). The authors also acknowledge the Doctoral program of Atmospheric Sciences at the University of Helsinki (ATM-DP). Markku Kulmala acknowledges the support of the Academy of Finland via his Academy Professorship (no. 302958). We also thank the City Council of Majadahonda for logistic assistance, and the Instituto de Ciencias Agrarias, Instituto de Salud Carlos III, Alava Ingenieros, TSI, Solma Environmental Solutions, and Airmodus for their support.

Edited by: Paul Zieger
Reviewed by: two anonymous referees

References

Ahlm, L., Liu, S., Day, D. A., Russell, L. M., Weber, R., Gentner, D. R., Goldstein, A. H., Digangi, J. P., Henry, S. B., Keutsch, F. N., Vandenboer, T. C., Markovic, M. Z., Murphy, J. G., Ren, X., and Scheller, S.: Formation and growth of ultrafine particles from secondary sources in Bakersfield, California, J. Geophys. Res.-Atmos., 117, D00V08, https://doi.org/10.1029/2011JD017144, 2012.

Alonso-Blanco, E., Gómez-Moreno, F. J., Núñez, L., Pujadas, M., Cusack, M., and Artíñano, B.: Aerosol particle shrinkage event phenomenology in a South European suburban area during 2009–2015, Atmos. Environ., 160, 154–164, 2017.

Beddows, D. C. S., Harrison, R. M., Green, D. C., and Fuller, G. W.: Receptor modelling of both particle composition and size distribution from a background site in London, UK, Atmos. Chem. Phys., 15, 10107–10125, https://doi.org/10.5194/acp-15-10107-2015, 2015.

Boulon, J., Sellegri, K., Venzac, H., Picard, D., Weingartner, E., Wehrle, G., Collaud Coen, M., Bütikofer, R., Flückiger, E., Baltensperger, U., and Laj, P.: New particle formation and ultrafine charged aerosol climatology at a high altitude site in the Alps (Jungfraujoch, 3580 m a.s.l., Switzerland), Atmos. Chem. Phys., 10, 9333–9349, https://doi.org/10.5194/acp-10-9333-2010, 2010.

Boy, M. and Kulmala, M.: Nucleation events in the continental boundary layer: Influence of physical and meteorological parameters, Atmos. Chem. Phys., 2, 1–16, https://doi.org/10.5194/acp-2-1-2002, 2002.

Boy, M., Karl, T., Turnipseed, A., Mauldin, R. L., Kosciuch, E., Greenberg, J., Rathbone, J., Smith, J., Held, A., Barsanti, K., Wehner, B., Bauer, S., Wiedensohler, A., Bonn, B., Kulmala, M., and Guenther, A.: New particle formation in the Front Range of

the Colorado Rocky Mountains, Atmos. Chem. Phys., 8, 1577–1590, https://doi.org/10.5194/acp-8-1577-2008, 2008.

Brines, M., Dall'Osto, M., Beddows, D. C. S., Harrison, R. M., and Querol, X.: Simplifying aerosol size distributions modes simultaneously detected at four monitoring sites during SAPUSS, Atmos. Chem. Phys., 14, 2973–2986, https://doi.org/10.5194/acp-14-2973-2014, 2014.

Brines, M., Dall'Osto, M., Beddows, D. C. S., Harrison, R. M., Gómez-Moreno, F., Núñez, L., Artíñano, B., Costabile, F., Gobbi, G. P., Salimi, F., Morawska, L., Sioutas, C., and Querol, X.: Traffic and nucleation events as main sources of ultrafine particles in high-insolation developed world cities, Atmos. Chem. Phys., 15, 5929–5945, https://doi.org/10.5194/acp-15-5929-2015, 2015.

Buonanno, G. and Morawska, L.: Ultrafine particle emission of waste incinerators and comparison to the exposure of urban citizens, Waste Manage., 37, 75–81, 2015.

Carslaw, D. C. and Ropkins, K.: openair – an R package for air quality data analysis, Environ. Modell. Softw., 27–28, 52–61, 2012.

Charron, A. and Harrison, R. M.: Primary particle formation from vehicle emissions during exhaust dilution in the roadside atmosphere, Atmos. Environ., 37, 4109–4119, 2003.

Cheung, H. C., Morawska, L., and Ristovski, Z. D.: Observation of new particle formation in subtropical urban environment, Atmos. Chem. Phys., 11, 3823–3833, https://doi.org/10.5194/acp-11-3823-2011, 2011.

Coleman, B. K., Lunden, M. M., Destaillats, H., and Nazaroff, W. W.: Secondary organic aerosol from ozone-initiated reactions with terpene-rich household products, Atmos. Environ., 42, 8234–8245, 2008.

Costabile, F., Birmili, W., Klose, S., Tuch, T., Wehner, B., Wiedensohler, A., Franck, U., König, K., and Sonntag, A.: Spatio-temporal variability and principal components of the particle number size distribution in an urban atmosphere, Atmos. Chem. Phys., 9, 3163–3195, https://doi.org/10.5194/acp-9-3163-2009, 2009.

Crespí, S. N., Artíñano, B., and Cabal, H.: Synoptic classification of the mixed-layer height evolution, J. Appl. Meteorol., 34, 1668–1677, 1995.

Cusack, M., Pérez, N., Pey, J., Alastuey, A., and Querol, X.: Variability of submicrometer particle number size distributions in the western Mediterranean regional background, Tellus B, 65, 19243, https://doi.org/10.3402/tellusb.v65i0.19243, 2013a.

Cusack, M., Alastuey, A., and Querol, X.: Case studies of new particle formation and evaporation processes in the western Mediterranean regional background, Atmos. Environ., 81, 651–659, 2013b.

Dall'Osto, M., Beddows, D. C. S., Pey, J., Rodriguez, S., Alastuey, A., Harrison, R. M., and Querol, X.: Urban aerosol size distributions over the Mediterranean city of Barcelona, NE Spain, Atmos. Chem. Phys., 12, 10693–10707, https://doi.org/10.5194/acp-12-10693-2012, 2012.

Dall'Osto, M., Querol, X., Alastuey, A., O'Dowd, C., Harrison, R. M., Wenger, J., and Gómez-Moreno, F. J.: On the spatial distribution and evolution of ultrafine particles in Barcelona, Atmos. Chem. Phys., 13, 741–759, https://doi.org/10.5194/acp-13-741-2013, 2013.

Dal Maso, M., Kulmala, M., Riipinen, I., Wagner, R., Hussein, T., Aalto, P. P., and Lehtinen, K. E. J.: Formation and growth of fresh atmospheric aerosols: eight years of aerosol size distribution data from SMEAR II, Hyytiälä, Finland, Boreal Environ. Res., 10, 323–336, 2005.

El Haddad, I., D'Anna, B., Temime-Roussel, B., Nicolas, M., Boreave, A., Favez, O., Voisin, D., Sciare, J., George, C., Jaffrezo, J.-L., Wortham, H., and Marchand, N.: Towards a better understanding of the origins, chemical composition and aging of oxygenated organic aerosols: case study of a Mediterranean industrialized environment, Marseille, Atmos. Chem. Phys., 13, 7875–7894, https://doi.org/10.5194/acp-13-7875-2013, 2013.

García, M. I., Rodríguez, S., González, Y., and García, R. D.: Climatology of new particle formation at Izaña mountain GAW observatory in the subtropical North Atlantic, Atmos. Chem. Phys., 14, 3865–3881, https://doi.org/10.5194/acp-14-3865-2014, 2014.

Gómez-Moreno, F. J., Pujadas, M., Plaza, J., Rodríguez-Maroto, J. J., Martínez-Lozano, P., and Artíñano, B.: Influence of seasonal factors on the atmospheric particle number concentration and size distribution in Madrid, Atmos. Environ., 45, 3199–3180, 2011.

Graus, M., Muller, M., and Hansel, A.: High Resolution PTR-TOF: Quantification and Formula Confirmation of VOC in Real Time, J. Am. Soc. Mass Spectr., 21, 1037–1044, 2010.

Hofman, J., Staelensa, J., Cordell, R., Stroobants, C., Zikova, N., Hama, S. M. L., Wyche, K. P., Kosf, G. P. A., Van Der Zeeg, S., Smallbone, K. L., Weijers, E. P., and Monks, P. S.: Ultrafine particles in four European urban environments: Results from a new continuous long-term monitoring network, Atmos. Environ., 136, 68–81, 2016.

Hudda, N., Gould, T., Hartin, K., Larson, T. V., and Fruin, S. A.: Emissions from an International Airport Increase Particle Number Concentrations 4-fold at 10 km Downwind, Environ. Sci. Technol., 48, 6628–6635, 2014.

Hussein, T., Dal Maso, M., Petäjä, T., Koponen, I., Paatero, P., Aalto, P., Hämeri, K., and Kulmala, M.: Evaluation of an automatic algorithm for fitting the particle number size distributions, Boreal Environ. Res., 10, 337–355, 2005.

Hussein, T., Martikainen, J., Junninen, H., Sogacheva, L., Wagner, R., Dal Maso, M., Riipinen, I., Aalto, P. P., and Kulmala, M.: Observation of regional new particle formation in the urban atmosphere, Tellus B, 60, 509–521, https://doi.org/10.1111/j.1600-0889.2008.00365.x, 2008.

Johnson, G. R., Juwono, A. M., Friend, A. J., Cheung, H.-C., Stelcer, E., Cohen, D., Ayoko, G. A., and Morawska, L.: Relating urban airborne particle concentrations to shipping using carbon based elemental emission ratios, Atmos. Environ., 95, 525–536, 2014.

Kecorius, S., Kivekäs, N., Kristenssond, A., Tuch, T., Covert, D. S., Birmili, W. Lihavainen, H., Hyvärinen, A.-P., Martinsson, J., Sporre, M. K., Swietlicki, E., Wiedensohler, A., and Ulevicius, V.: Significant increase of aerosol number concentrations in air masses crossing a densely trafficked sea area, Oceanologia, 58, 1–12, 2016.

Keuken, M. P., Moerman, M., Zandveld, P., Henzing, J. S., and Hoek, G.: Total and size-resolved particle number and black carbon concentrations in urban areas near Schiphol airport (the Netherlands), Atmos. Environ., 104, 132–142, 2015.

Kirkby, J., Duplissy, J., Sengupta, K., Frege, C., Gordon, H., Williamson, C., Heinritzi, M., Simon, M., Yan, C., Almeida, J., Trostl, J., Nieminen, T., Ortega, I. K., Wagner, R., Adamov, A.,

Amorim, A., Bernhammer, A. K., Bianchi, F., Breitenlechner, M., Brilke, S., Chen, X., Craven, J., Dias, A., Ehrhart, S., Flagan, R. C., Franchin, A., Fuchs, C., Guida, R., Hakala, J., Hoyle, C. R., Jokinen, T., Junninen, H., Kangasluoma, J., Kim, J., Krapf, M., Kurten, A., Laaksonen, A., Lehtipalo, K., Makhmutov, V., Mathot, S., Molteni, U., Onnela, A., Perakyla, O., Piel, F., Petaja, T., Praplan, A. P., Pringle, K., Rap, A., Richards, N. A. D., Riipinen, I., Rissanen, M. P., Rondo, L., Sarnela, N., Schobesberger, S., Scott, C. E., Seinfeld, J. H., Sipila, M., Steiner, G., Stozhkov, Y., Stratmann, F., Tomé, A., Virtanen, A., Vogel, A. L., Wagner, A. C., Wagner, P. E., Weingartner, E., Wimmer, D., Winkler, P. M., Ye, P., Zhang, X., Hansel, A., Dommen, J., Donahue, N. M., Worsnop, D. R., Baltensperger, U., Kulmala, M., Carslaw, K. S., and Curtius, J.: Ion-induced nucleation of pure biogenic particles, Nature, 533, 521–526, https://doi.org/10.1038/nature17953, 2016.

Kittelson, D. B., Watts, W. F., and Johnson, J. P.: On-road and laboratory evaluation of combustion aerosols – Part 1: Summary of diesel engine results, J. Aerosol Sci., 37, 913–930, 2006.

Kontkanen, J., Lehtipalo, K., Ahonen, L., Kangasluoma, J., Manninen, H. E., Hakala, J., Rose, C., Sellegri, K., Xiao, S., Wang, L., Qi, X., Nie, W., Ding, A., Yu, H., Lee, S., Kerminen, V.-M., Petäjä, T., and Kulmala, M.: Measurements of sub-3 nm particles using a particle size magnifier in different environments: from clean mountain top to polluted megacities, Atmos. Chem. Phys., 17, 2163–2187, https://doi.org/10.5194/acp-17-2163-2017, 2017.

Kulmala, M. and Kerminen, V.-M.: On the formation and growth of atmospheric nanoparticles, Atmos. Res., 90, 132–150, 2008.

Kulmala, M., Pirjola, L., and Mäkelä, J. M.: Stable Sulphate Clusters as a Source of New Atmospheric Particles, Nature, 404, 66–69, 2000.

Kulmala, M., Vehkamehk, H., Pet, P. T., Dal Maso, M., Lauri, A., Kerminen, V.-M., Birmili, W., and McMurry, P.: Formation and growth rates of ultrafine atmospheric particles: a review of observations, J. Aerosol Sci., 35, 143–176, 2004.

Kulmala, M., Petäjä, T., Nieminen, T., Sipilä, M., Manninen, H. E., Lehtipalo, K., Dal Maso, M., Aalto, P. P., Junninen, H., Paasonen, P., Riipinen, I., Lehtinen, K. E. J., Laaksonen, A., and Kerminen, V.-M.: Measurement of the nucleation of atmospheric aerosol particles, Nat. Protoc., 7, 1651–1667, 2012.

Kulmala, M., Luoma, K., Virkkula, A., Petäjä, T., Paasonen, P., Kerminen, V.M., Nie, W., Qi, X., Shen, Y., Chi, X., and Ding, A.: On the mode-segregated aerosol particle number concentration load: Contributions of primary and secondary particles in Hyytiälä and Nanjing, Boreal Environ. Res., 21, 319–331, 2016.

Kumar, P. and Morawska, L.: Recycling Concrete: An Undiscovered Source of Ultrafine Particles, Atmos. Environ, 90, 51–58, 2014.

Kumar, P., Morawska, L., Birmili, W., Paasonen, P., Hu, M., Kulmala, M., Harrison, R. M., Norford, L., and Britter, R.: Ultrafine particles in cities, Environ. Int., 66, 1–10, 2014.

Lee, H.-K., Hwang, I.-K., and Ahn, K.-H.: Development and Evaluation of Hy-CPC, Particle and Aerosol Research, 10, 93–97, 2014.

Lee, H.-K., Eun, H.-R., Lee, G.-H., and Ahn, K.-H.: Development and evaluation of Hy-SMPS, Particle and Aerosol Research, 11, 57–61, 2015.

Ma, N. and Birmili, W.: Estimating the contribution of photochemical particle formation to ultrafine particle number averages in an urban atmosphere, Sci. Total Environ., 512–513, 154–166, 2015.

Manninen, H. E., Nieminen, T., Asmi, E., Gagné, S., Häkkinen, S., Lehtipalo, K., Aalto, P., Vana, M., Mirme, A., Mirme, S., Hõrrak, U., Plass-Dülmer, C., Stange, G., Kiss, G., Hoffer, A., Töro, N., Moerman, M., Henzing, B., de Leeuw, G., Brinkenberg, M., Kouvarakis, G. N., Bougiatioti, A., Mihalopoulos, N., O'Dowd, C., Ceburnis, D., Arneth, A., Svenningsson, B., Swietlicki, E., Tarozzi, L., Decesari, S., Facchini, M. C., Birmili, W., Sonntag, A., Wiedensohler, A., Boulon, J., Sellegri, K., Laj, P., Gysel, M., Bukowiecki, N., Weingartner, E., Wehrle, G., Laaksonen, A., Hamed, A., Joutsensaari, J., Petäjä, T., Kerminen, V.-M., and Kulmala, M.: EUCAARI ion spectrometer measurements at 12 European sites – analysis of new particle formation events, Atmos. Chem. Phys., 10, 7907–7927, https://doi.org/10.5194/acp-10-7907-2010, 2010.

Masiol, M., Harrison, R. M., Vu, T. V., and Beddows, D. C. S.: Sources of sub-micrometre particles near a major international airport, Atmos. Chem. Phys., 17, 12379–12403, https://doi.org/10.5194/acp-17-12379-2017, 2017.

Minguillón, M. C., Brines, M., Pérez, N., Reche, C., Pandolfi, M., Fonseca, A. S., Amato, F., Alastuey, A., Lyasota, A., Codina, B., Lee, H.-K., Eun, H.-R., Ahn, K.-H., and Querol, X.: New particle formation at ground level and in the vertical column over the Barcelona area, Atmos. Res., 164–165, 118–130, 2015.

Nie, W., Ding, A. J., Wang, T., Kerminen, V.-M., George, C., Xue, L. K., Wang, W. X., Zhang, Q. Z., Petäjä, T., Qi, X. M., Gao, X. M., Wang, X. F., Yang, X. Q., Fu, C. B., and Kulmala, M.: Polluted dust promotes new particle formation and growth, Sci. Rep.-UK, 4, 6634, https://doi.org/10.1038/srep06634, 2014.

O'Dowd, C., Monahan, C., and Dall'Osto, M.: On the occurrence of open ocean particle production and growth events, Geophys. Res. Lett., 37, L19805, https://doi.org/10.1029/2010GL044679, 2010.

Paasonen, P., Kupiainen, K., Klimont, Z., Visschedijk, A., Denier van der Gon, H. A. C., and Amann, M.: Continental anthropogenic primary particle number emissions, Atmos. Chem. Phys., 16, 6823–6840, https://doi.org/10.5194/acp-16-6823-2016, 2016.

Pérez, N., Reche, C., Ealo, M., Titos, G., Lee, H. K., Eun, H.-R., Park, Y.-H., Mantilla, E., Escudero, M., Gómez-Moreno, F. J., Alonso-Blanco, E., Coz, E., Saiz-Lopez, A., Beddows, D., Harrison, R. M., Ahn, K.-H., Alastuey, A., and Querol, X.: O3, UFP and VOCs field campaign in Madrid, July 2016, Mendeley Data, v1 https://doi.org/10.17632/x5gw4stjyb.1, 2018.

Pey, J., Rodríguez, S., Querol, X., Alastuey, A., Moreno, T., Putaud, J. P., and Van Dingenen, R.: Variations of urban aerosols in the western Mediterranean, Atmos. Environ., 42, 9052–9062, 2008.

Pey, J., Querol, X., Alastuey, A., Rodríguez, S., Putaud, J. P., and Van Dingenen, R.: Source Apportionment of urban fine and ultrafine particle number concentration in a Western Mediterranean city, Atmos. Environ., 43, 4407–4415, 2009.

Plaza, J., Pujadas, M., and Artíñano, B.: Formation and Transport of the Madrid Ozone Plume, J. Air Waste Manage., 47, 766–774, 1997.

Qian, S., Sakurai, H., and McMurry, P. H.: Characteristics of regional nucleation events in urban East St. Louis, Atmos. Environ., 41, 4119–4127, 2007.

Querol, X., Gangoiti, G., Mantilla, E., Alastuey, A., Minguillón, M. C., Amato, F., Reche, C., Viana, M., Moreno, T., Karanasiou, A., Rivas, I., Pérez, N., Ripoll, A., Brines, M., Ealo, M., Pandolfi, M., Lee, H.-K., Eun, H.-R., Park, Y.-H., Escudero, M., Beddows, D., Harrison, R. M., Bertrand, A., Marchand, N., Lyasota, A., Codina, B., Olid, M., Udina, M., Jiménez-Esteve, B., Soler, M. R., Alonso, L., Millán, M., and Ahn, K.-H.: Phenomenology of high-ozone episodes in NE Spain, Atmos. Chem. Phys., 17, 2817–2838, https://doi.org/10.5194/acp-17-2817-2017, 2017.

Querol, X., Alastuey, A., Gangoiti, G., Perez, N., Lee, H. K., Eun, H. R., Park, Y., Mantilla, E., Escudero, M., Titos, G., Alonso, L., Temime-Roussel, B., Marchand, N., Moreta, J. R., Revuelta, M. A., Salvador, P., Artíñano, B., García dos Santos, S., Anguas, M., Notario, A., Saiz-Lopez, A., Harrison, R. M., Millán, M., and Ahn, K.-H.: Phenomenology of summer ozone episodes over the Madrid Metropolitan Area, central Spain, Atmos. Chem. Phys., 18, 6511–6533, https://doi.org/10.5194/acp-18-6511-2018, 2018.

Reche, C., Querol, X., Alastuey, A., Viana, M., Pey, J., Moreno, T., Rodríguez, S., González, Y., Fernández-Camacho, R., de la Rosa, J., Dall'Osto, M., Prévôt, A. S. H., Hueglin, C., Harrison, R. M., and Quincey, P.: New considerations for PM, Black Carbon and particle number concentration for air quality monitoring across different European cities, Atmos. Chem. Phys., 11, 6207–6227, https://doi.org/10.5194/acp-11-6207-2011, 2011.

Robinson, A. L., Donahue, N. M., Shrivastava, M. K., Weitkamp, E. A., Sage, A. M., Grieshop, A. P., Lane, T. E., Pierce, J. R., and Pandis, S. N.: Rethinking organic aerosols: semivolatile emissions and photochemical aging, Science 31, 1259–1262, 2007.

Rönkkö, T., Kuuluvainen, H., Karjalainen, P., Keskinen, J., Hillamo, R., Niemi, J. V, Pirjola, L., Timonen, H.J., Saarikoski, S., Saukko, E., Järvinen, A., Silvennoinen, H., Rostedt, A., Olin, M., Yli-Ojanperä, J., Nousiainen, P., Kousa, A., and Dal Maso, M.: Traffic is a major source of atmospheric nanocluster aerosol, P. Natl. Acad. Sci. USA, 114, 7549–7554, https://doi.org/10.1073/pnas.1700830114, 2017.

Saiz-Lopez, A., Borge, R., Notario, A., Adame, J. A., De la Paz, D., Querol, X., Artíñano, B., Gomez-Moreno, F. J., and Cuevas, C. A.: Unexpected increase in the oxidation capacity of the urban atmosphere of Madrid, Spain, Sci. Rep., 7, 45956, https://doi.org/10.1038/srep45956, 2017.

Salma, I., Borsos T., Nemeth Z., Weidiger T., Aalto P., and Kulmala M.: Comparative study of ultrafine atmospheric aerosol within a city, Atmos. Environ., 92, 154–161, 2014.

Salma, I., Németh, Z., Kerminen, V.-M., Aalto, P., Nieminen, T., Weidinger, T., Molnár, Á., Imre, K., and Kulmala, M.: Regional effect on urban atmospheric nucleation, Atmos. Chem. Phys., 16, 8715–8728, https://doi.org/10.5194/acp-16-8715-2016, 2016.

Salvador, P., Artíñano, B., Viana, M., Alastuey, A., and Querol, X.: Multicriteria approach to interpret the variability of the levels of particulate matter and gaseous pollutants in the Madrid metropolitan area, during the 1999–2012 period, Atmos. Environ., 109, 205–216, 2015.

Sellegri, K., Laj, P., Venzac, H., Boulon, J., Picard, D., Villani, P., Bonasoni, P., Marinoni, A., Cristofanelli, P., and Vuillermoz, E.: Seasonal variations of aerosol size distributions based on long-term measurements at the high altitude Himalayan site of Nepal Climate Observatory-Pyramid (5079 m), Nepal, Atmos. Chem. Phys., 10, 10679–10690, https://doi.org/10.5194/acp-10-10679-2010, 2010.

Sipilä, M., Berndt, T., Petaja, T., Brus, D., Vanhanen, J., Stratmann, F., Patokoski, J., Mauldin, R. L., Hyvärinen, A. P., Lihavainen, H., and Kulmala, M.: The role of sulfuric acid in atmospheric nucleation, Science, 327, 1243–1246, https://doi.org/10.1126/science.1180315, 2010.

Shi, J. P. and Harrison, R. M.: Investigation of ultrafine particle formation during diesel exhaust dilution, Environ. Sci. Technol., 33, 3730–3736, 1999.

Shi, J. P., Mark, D., and Harrison, R. M.: Characterization of particles from a current technology heavy-duty diesel engine, Environ. Sci. Technol., 34, 748–755, 2000.

Skrabalova, L., Zikova, N., and Zdimal, V.: Shrinkage of newly formed particles in an urban environment, Aerosol Air Qual. Res., 15, 1313–1324, 2015.

Stolzenburg, M. R., McMurry, P. H., Sakurai, H., Smith, J. N., Lee, M. R., Eisele, F. L., and Clement, C. F.: Growth rates of freshly nucleated atmospheric particles in Atlanta, J. Geophys. Res., 110, D22S05, https://doi.org/10.1029/2005JD005935, 2005.

Stratmann, F., Siebert, H., Spindler, G., Wehner, B., Althausen, D., Heintzenberg, J., Hellmuth, O., Rinke, R., Schmieder, U., Seidel, C., Tuch, T., Uhrner, U., Wiedensohler, A., Wandinger, U., Wendisch, M., Schell, D., and Stohl, A.: New-particle formation events in a continental boundary layer: first results from the SATURN experiment, Atmos. Chem. Phys., 3, 1445–1459, https://doi.org/10.5194/acp-3-1445-2003, 2003.

Stull, R. B.: An introduction to boundary layer meteorology, Kluwer Academic Publishers, Dordrecht, the Netherlands, Boston, USA and London, UK, 1988.

Tröstl, J., Chuang, W. K., Gordon, H., Heinritzi, M., Yan, C., Molteni, U., Ahlm, L., Frege, C., Bianchi, F., Wagner, R., Simon, M., Lehtipalo, K., Williamson, C., Craven, J. S., Duplissy, J., Adamov, A., Almeida, J., Bernhammer, A. K., Breitenlechner, M., Brilke, S., Dias, A., Ehrhart, S., Flagan, R. C., Franchin, A., Fuchs, C., Guida, R., Gysel, M., Hansel, A., Hoyle, C. R., Jokinen, T., Junninen, H., Kangasluoma, J., Keskinen, H., Kim, J., Krapf, M., Kürten, A., Laaksonen, A., Lawler, M., Leiminger, M., Mathot, S., Möhler, O., Nieminen, T., Onnela, A., Petäjä, T., Piel, F. M., Miettinen, P., Rissanen, M. P., Rondo, L., Sarnela, N., Schobesberger, S., Sengupta, K., Sipilä, M., Smith, J. N., Steiner, G., Tomè, A., Virtanen, A., Wagner, A. C., Weingartner, E., Wimmer, D., Winkler, P. M., Ye, P., Carslaw, K. S., Curtius, J., Dommen, J., Kirkby, J., Kulmala, M., Riipinen, I., Worsnop, D. R., Donahue, N. M., and Baltensperger, U.: The role of low-volatility organic compounds in initial particle growth in the atmosphere, Nature, 533, 527–531, https://doi.org/10.1038/nature18271, 2016.

Uhrner, U., von Lowis, S., Vehkamaki, H., Wehner, B., Brasel, S., Hermann, M., Stratmann, F., Kulmala, M., and Wiedensohler, A.: Dilution and aerosol dynamics within a diesel car exhaust plume – CFD simulations of on-road conditions, Atmos. Environ., 41, 7440–7461, 2007.

United Nations: World Urbanization Prospects (2007 revision), Department of Economic and Social Affairs, available at: https://www.un.org/esa/population/publications/wup2007/2007WUP_Highlights_web.pdf (last access: 16 November 2018), 2008.

Vakkari, V., Laakso, H., Kulmala, M., Laaksonen, A., Mabaso, D., Molefe, M., Kgabi, N., and Laakso, L.: New particle formation events in semi-clean South African savannah, Atmos. Chem. Phys., 11, 3333–3346, https://doi.org/10.5194/acp-11-3333-2011, 2011.

von Bismarck-Osten, C., Birmili, W., Ketzel, M., Massling, A., Petäjä, T., and Weber, S.: Characterization of parameters influencing the spatio-temporal variability of urban particle number size distributions in four European cities, Atmos. Environ., 77, 415–429, 2013.

Wang, N., Sun, X., Chen, J., and Li, X.: Sci. Heterogeneous Nucleation of Trichloroethylene Ozonation Products in the Formation of New Fine Particles, Sci. Rep.-UK, 7, 42600, https://doi.org/10.1038/srep42600, 2017.

Wegner, T., Hussein, T., Hämeri, K., Vesala, T., Kulmala, M., and Weber, S.: Properties of aerosol signature size distributions in the urban environment as derived by cluster analysis, Atmos. Environ., 61, 350–360, 2012.

Wehner, B. and Wiedensohler, A.: Long term measurements of submicrometer urban aerosols: statistical analysis for correlations with meteorological conditions and trace gases, Atmos. Chem. Phys., 3, 867–879, https://doi.org/10.5194/acp-3-867-2003, 2003.

Wehner, B., Siebert, H., Stratmann, F., Tuch, T., Wiedensohler, A., Petäjä, T., Dal Maso, M., and Kulmala, M.: Horizontal homogeneity and vertical extent of new particle formation events, Tellus, 59B, 362–371, 2007.

Wehner, B., Siebert, H., Ansmann, A., Ditas, F., Seifert, P., Stratmann, F., Wiedensohler, A., Apituley, A., Shaw, R. A., Manninen, H. E., and Kulmala, M.: Observations of turbulence-induced new particle formation in the residual layer, Atmos. Chem. Phys., 10, 4319–4330, https://doi.org/10.5194/acp-10-4319-2010, 2010.

Wiedensohler, A., Wehner, B., and Birmili, W.: Aerosol number concentrations and size distributions at mountain-rural, urban-influenced rural, and urban-background sites in Germany, J. Aerosol Med., 15, 237–243, 2002.

Woo, K. S., Chen, D. R., Pui, D. Y. H., and McMurry, P. H.: Measurement of Atlanta aerosol size distributions: observations of ultrafine particle events, Aerosol Sci. Tech., 34, 75–87, 2001.

Yao, X., Choi, M. Y., Lau, N. T., Lau, A. P. S., Chan, C. K., and Fang, M.: Growth and shrinkage of new particles in the atmosphere in Hong Kong, Aerosol Sci. Tech., 44, 639–650, 2010.

Young, L.-H., Lee, S.-H., Kanawade, V. P., Hsiao, T.-C., Lee, Y. L., Hwang, B.-F., Liou, Y.-J., Hsu, H.-T., and Tsai, P.-J.: New particle growth and shrinkage observed in subtropical environments, Atmos. Chem. Phys., 13, 547–564, https://doi.org/10.5194/acp-13-547-2013, 2013.

Supplement of

Vertical and horizontal distribution of regional new particle formation events in Madrid

Carnerero et al. (2018)

S1 PTR-ToF-MS measurements

Among the 152 ions identified with the PTR-ToF-MS, only 3 exhibit temporal trends that might be relevant in the growth processes of NPF (Fig. S7). Two highly-oxygenated ions, $C_4H_4O_3H^+$ (m/z 101.023) and $C_2H_4O_3H^+$ (m/z 77.023), and NO_2^+ (m/z 45.9924) presented evolutions parallel to those of the particle diameter, i.e. the concentration of these ions increased simultaneously with the increase of particle diameter, and growth stopped when the concentration of the ions decreased (Fig. S9). This is observed also on days in which there is no particle formation but there is particle growth. Thus, the parent molecules of these ions are not linked to particle formation, but they would most probably contribute to particle growth. The fragment $C_4H_4O_3H^+$ has, to the best of our knowledge, only been reported once over an orange grove in California (Park et al., 2013) and is most probably from secondary origin considering both its diurnal variation and oxidation state. It contains sufficient carbon atoms and oxygen functional groups to likely partition into the condensed phase. NO_2^+ and $C_2H_4O_3^+$ are known fragments of peroxyacetyl nitrate (PAN) (de Gouw et al., 2003), but NO_2^+ can also arise from the fragmentation of a wide range of peroxynitrates ($ROONO_2$) or alkyl and multifunctional nitrates ($RONO_2$) (Aoki et al., 2017; Duncianu et al., 2017). While the uptake of PAN on particles can be considered as negligible (Roberts, 2005), higher molecular weight organonitrates are more likely to partition onto the particle phase. Thus, the particles growth appears to be driven by the uptake of secondary organic compounds. More precisely, in an urban atmosphere such as Madrid characterized by high NO_2 concentrations, the formation of organonitrates and/or peroxynitrates could play an important role in the particle growth processes. We cannot prove this assumption using the PTR-ToF-MS measurements. We cannot check if the growth rates can be explained by sulfuric acid alone, since SO_2 levels were below the detection limit of the standard air quality UV spectrometry instruments during all the period.

References

Aoki, N., Inomata, S., and Tanimoto, H.: Detection of C1-C5 alkyl nitrates by proton transfer reaction time-of-flight mass spectrometry, Int. J. Mass Spectrom., 263, 12–21, 2007.

de Gouw, J.A., Goldan, P.D., Warneke, C., Kuster, W.C., Roberts, J.M., Marchewka, M., Bertman, S.B., Pszenny, A.A.P., Keene, W.C: Validation of proton transfer reaction-mass spectrometry (PTR-MS) measurements of gas-phase organic compounds in the atmosphere during the New England air quality study (NEAQS) in 2002, J. Geophys. Res. Atmos. 108 (D21), 2003.

Duncianu, M., David, M., Kartigueyane, S., Cirtog, M., Doussin, J-F., Picquet-Varrault, B.: Measurement of alkyl and multifunctional organic nitrates by proton-transfer-reaction mass spectrometry, Atmospheric Measurement Techniques, 10 (4), 1445-1463, 2017.

Table S1: Summary of shrinkage events showing the starting time, considered as the moment of first detection of a decrease in size, the final time, shrinking rate (SR) and geometric mean diameters at the beginning and end of the process. It is noted that on some days more than one shrinkage process is observed and all SR are shown.

	$SR_{Dp<40\ nm}$ (nm h^{-1})			$SR_{Aitk,\ Dp>40\ nm}$ (nm h^{-1})		
Date	CSIC	CIEMAT	ISCIII	CSIC	CIEMAT	ISCIII
03/07/2016						-1.7
12/07/2016	-8.3		-5.4	-7		-9
13/07/2016	-7.9, -5.5					-4.9
14/07/2016				-20.5, -6.3		-11.9
15/07/2016		-1.9				
16/07/2016		-1.9				
17/07/2016			-1.5			
18/07/2016		-2.2	-3.6			
19/07/2016						

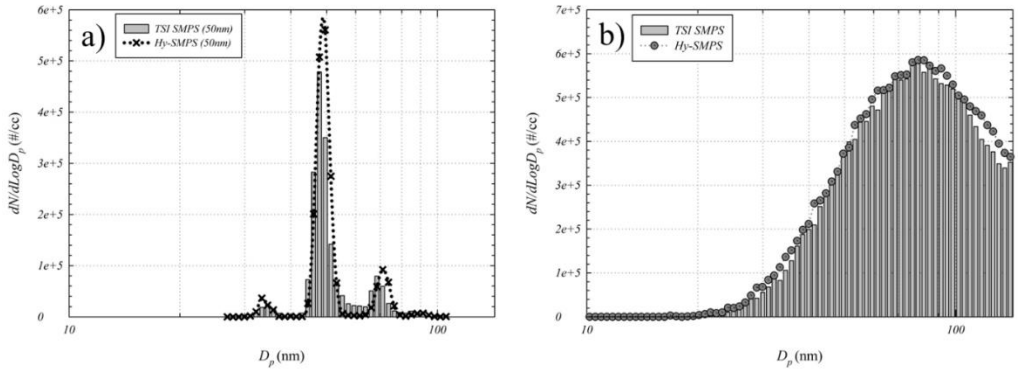

Figure S1: a) Intercomparison between TSI-SMPS and Hy-SMPS for 50 nm monodisperse NaCl particles. The major peak shows 50 nm particle and the 2 minor peaks are the doubly charged particles. b) Poly-disperse aerosol size distribution intercomparison between TSI-SMPS and Hy-SMPS.

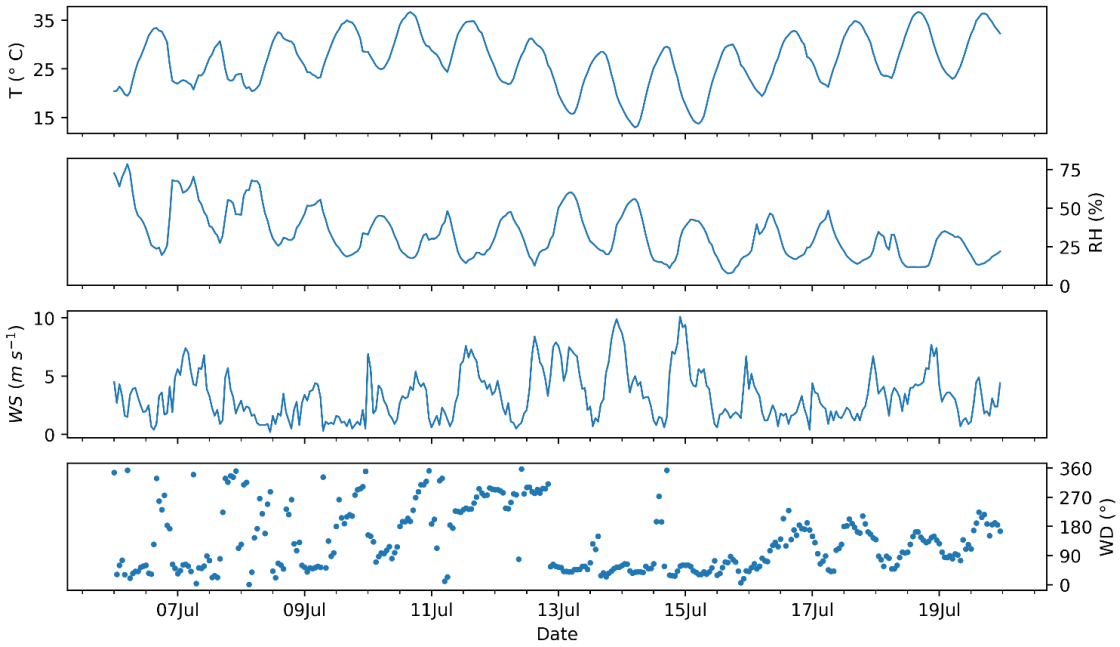

Figure S2: Temperature, relative humidity, wind speed and wind direction measured at the CIEMAT meteorological tower from 6 to 20 July 2016. Temperature and relative humidity are measured at 4 m, and the anemometer is located at 55 m. Time is UTC, local time is UTC+2.

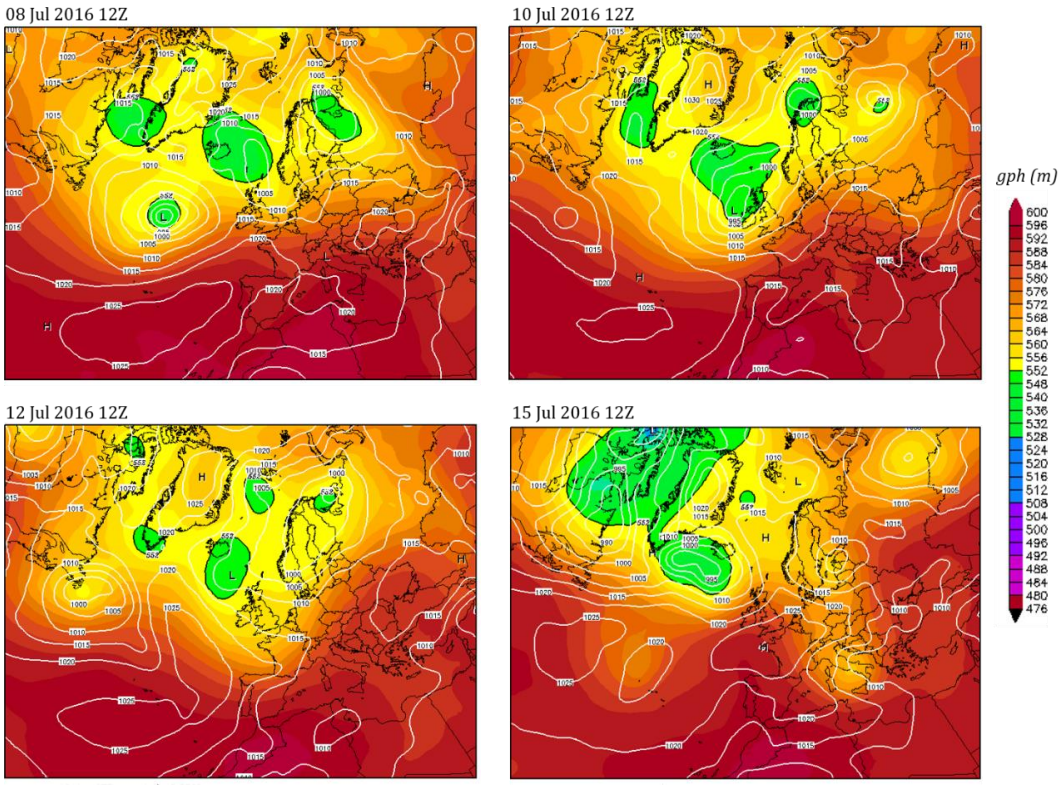

Figure S3: 500 hPa geopotential height, in m, and mean sea level pressure in hPa obtained from the Climate Forecast System reanalysis. The maps correspond to 8, 10, 12 and 15 July 2016, at 12:00 UTC.

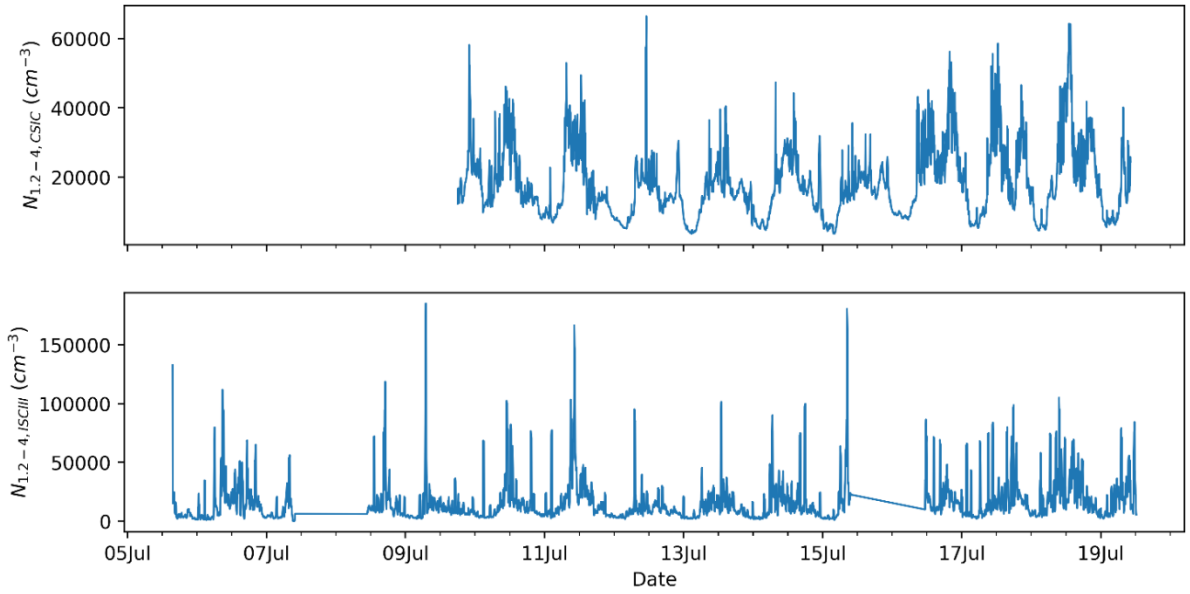

Figure S4: Concentrations of 1.2-4 nm particles measured from 6 to 20 July at CSIC and ISCIII.

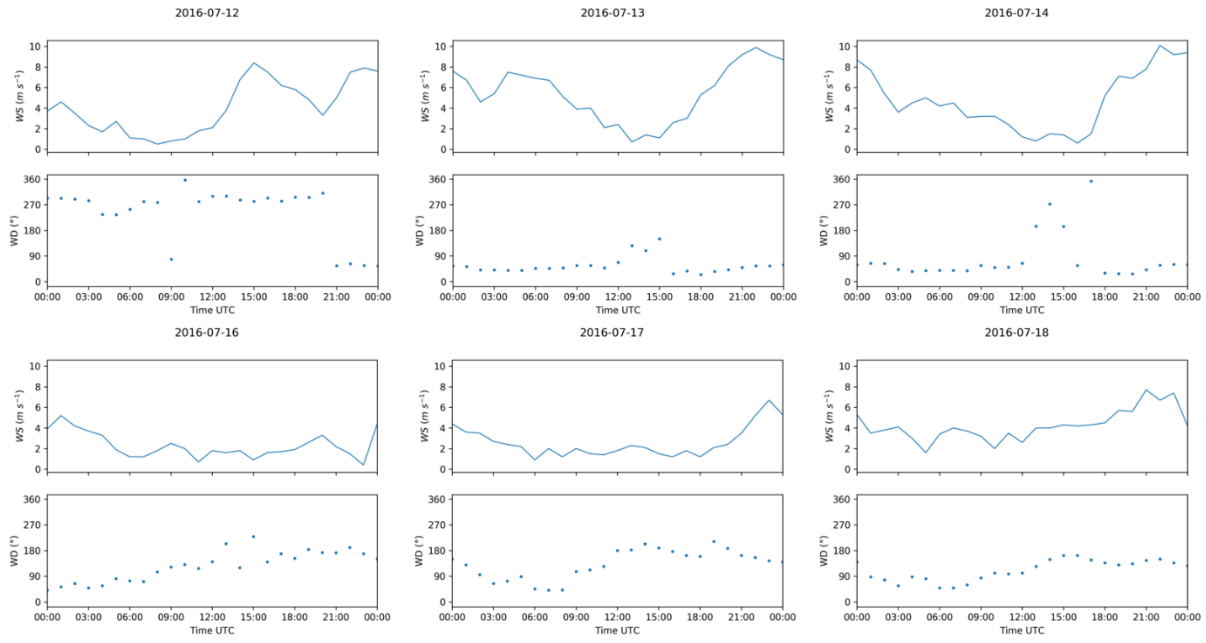

Figure S5: Daily plots of wind speed and wind direction for the days in which shrinkage is observed.

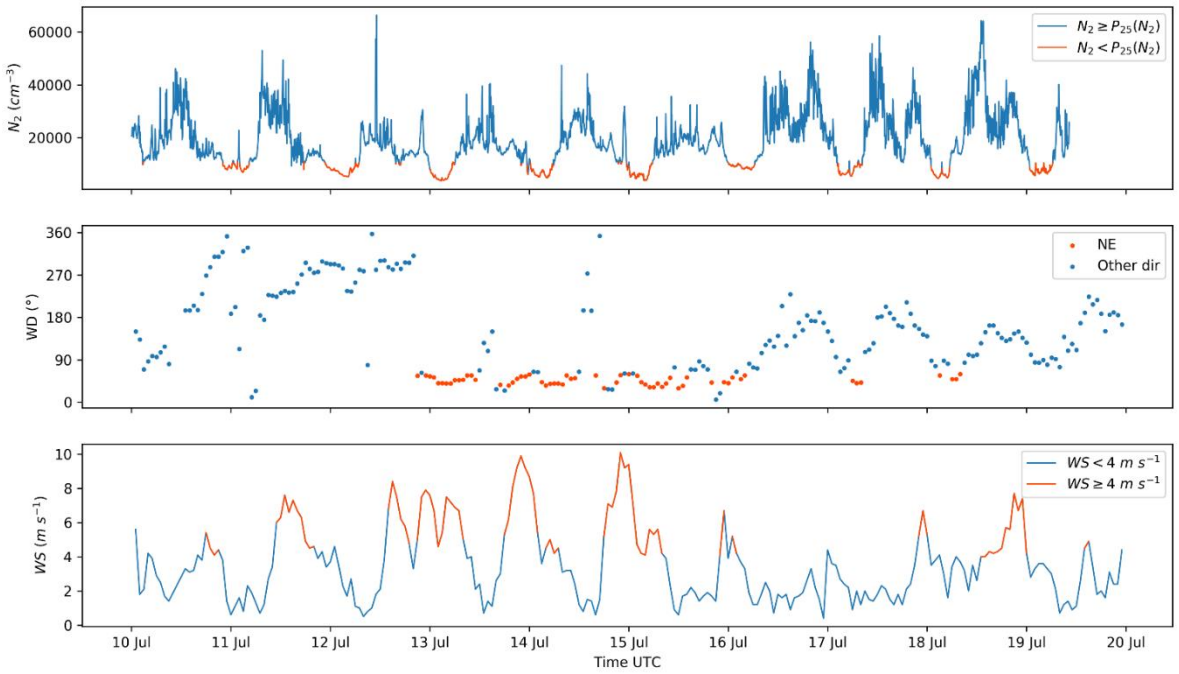

Figure S6: Concentration of particles >2 nm measured with PSM at CSIC station, wind direction and wind speed from 10 to 20 July 2016. N_2 lower than 25th percentile has been highlighted, as well as NE directions and wind speeds higher than 4 m/s.

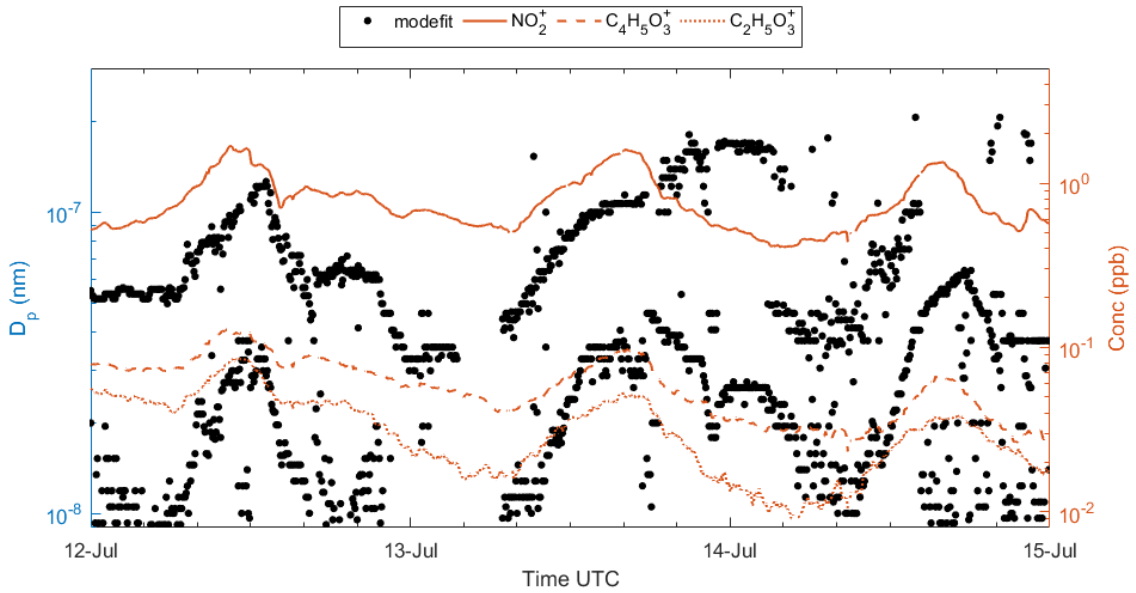

Figure S7: Temporal evolution of the log-normal fitted modes to the particle size distributions from 12 to 14 July 2016 at ISCIII and measured concentrations of three relevant VOCs.

3.3 Paper II

Relating high ozone, ultrafine particles, and new particle formation episodes using cluster analysis

Carnerero, C., Pérez, N., Petäjä, T., Laurila, T. M., Ahonen, L. R., Kontkanen, J., Ahn, K.-H., Alastuey, A. and Querol, X.

Published in *Atmospheric Environment: X* on October 17, 2019

https://doi.org/10.1016/j.aeaoa.2019.100051

ATMOSPHERIC ENVIRONMENT: X 4 (2019) 100051

Contents lists available at ScienceDirect

Atmospheric Environment: X

journal homepage: http://www.journals.elsevier.com/atmospheric-environment-x

Relating high ozone, ultrafine particles, and new particle formation episodes using cluster analysis

Cristina Carnerero [a,b,*], Noemí Pérez [a], Tuukka Petäjä [c], Tiia M. Laurila [c], Lauri R. Ahonen [c], Jenni Kontkanen [c], Kang-Ho Ahn [d], Andrés Alastuey [a], Xavier Querol [a]

[a] Institute of Environmental Assessment and Water Research (IDAEA-CSIC), Barcelona, 08034, Spain
[b] Department of Civil and Environmental Engineering, Universitat Politècnica de Catalunya, Barcelona, 08034, Spain
[c] Institute for Atmospheric and Earth System Research (INAR) / Physics, Faculty of Science, University of Helsinki, 00014, Finland
[d] Department of Mechanical Engineering, Hanyang University, Seoul, Republic of Korea

ARTICLE INFO

Keywords:
Tropospheric ozone
Ultrafine particles
Photochemical pollutants
Cluster analysis
Rural station
Urban influence
Balloon soundings
Vertical distribution

ABSTRACT

We studied the simultaneity of tropospheric ozone (O_3) episodes, high ultrafine particle (UFP; diameter < 100 nm) concentrations, and the occurrence of new particle formation at a regional background station in the Western Mediterranean (northeast Spain), which is affected considerably by the transport of pollutants emitted in the Barcelona metropolitan area and nearby populated and industrial areas. Using cluster analysis, we categorized summer and spring days between 2014 and 2018 according to their daily cycles of O_3 concentrations, and then studied the evolution of the particle number size distribution, meteorological variables, and black carbon and sulfur dioxide concentrations. The analysis revealed that, in spring and summer, the highest UFP concentrations coincided with the highest O_3 episodes, but new particle formation was largely inhibited during these episodes, probably due to the high aerosol pollution load transported from the Barcelona metropolitan area to the station. In contrast, new particle formation episodes were concurrent with the lowest concentrations of O_3 and UFPs, including the number of particles in the 9–25 nm size range. Measurements carried out in an intensive field study, using an air ion spectrometer and a particle size magnifier, support these results. In addition, measurements obtained onboard tethered balloons revealed that sea and land breezes transported regional pollutants vertically up to about 400 m above ground level. This coincided with episodes of vertical recirculation of air masses that lasted for several days, which resulted in high O_3 and high UFP episodes, while new particle formation was inhibited.

1. Introduction

Ultrafine particles (UFPs; particles less than 100 nm in diameter) are not included in air quality regulations, but they have considerable potential for affecting health (Atkinson et al., 2010; Lanzinger et al., 2016; Stafoggia et al., 2017; Tobías et al., 2018). In urban areas, the main source of primary UFPs is road traffic (Pey et al., 2009; Dall'Osto et al., 2012; Kumar et al., 2014; Salma et al., 2014; Ma and Birmili, 2015; Paasonen et al., 2016). Industrial emissions (Keuken et al., 2015b), airports (Keuken et al., 2015a), harbors (Kecorius et al., 2016), and biomass burning (Pöschl, 2005) also contribute significantly to the increase in UFP concentrations. Furthermore, photochemical formation of new particles may also exert a large influence on ambient levels of UFPs in urban and regional environments (Dall'Osto et al., 2013; Salma et al., 2016; Kerminen et al., 2018; Chu et al., 2019), and even dominate the total particle number concentrations at a global scale (Gordon et al., 2017). Here, we use the term UFP episodes to designate the periods when number concentration (not necessarily particulate matter mass) markedly increases over the (usually low) regional background particle number concentration (2000–3000 cm^{-3}). These episodes may be caused by new particle formation bursts or by regional transport of air masses and plumes polluted with UFP particles.

Tropospheric ozone (O_3) is a secondary pollutant originating from the chemical reaction of precursors, such as volatile organic compounds (VOCs), carbon monoxide (CO), and nitrogen dioxide (NO_2). It is estimated that 95–98% of the population is exposed to O_3 levels exceeding the World Health Organization (WHO) guidelines for the protection of human health (100 $\mu g\, m^{-3}$ as an 8-h moving average; WHO, 2006),

* Corresponding author. Institute of Environmental Assessment and Water Research (IDAEA-CSIC), Barcelona, 08034, Spain.
E-mail address: cristina.carnerero@idaea.csic.es (C. Carnerero).

https://doi.org/10.1016/j.aeaoa.2019.100051
Received 8 May 2019; Received in revised form 10 October 2019; Accepted 15 October 2019
Available online 17 October 2019

while according to the European Union (EU) target value (120 μg m^{-3} as an 8-h moving average; human health target value), 7–30% of the population is exposed EEA, 2018). The EU specifies two additional target values for tropospheric O_3: a public information threshold of 180 μg m^{-3} h^{-1} and an alert threshold of 240 μg m^{-3} h^{-1}.

Given their largely secondary origin, characterization of O_3 and photochemical UFP pollution episodes is highly complex, creating challenges for defining effective strategies to abate the ambient concentrations of the pollutants. The Western Mediterranean is particularly exposed to photochemical O_3 and UFP episodes due to its climate of high insolation and low precipitation. Furthermore, its complex topography, with steep valleys oriented in the same direction as the diurnal sea breeze, allows pollution emitted in the densely populated coastal areas to be channeled inland, especially in the summer (Millán et al., 1991). In addition to urban and industrial emissions, high levels of nitrogen oxide (NOx) and sulfur dioxide (SO_2) emissions are associated with shipping in the Mediterranean. The area is also characterized by relatively high biogenic VOC emissions in the summer, compared to other Mediterranean forests and mixed forests in Europe and the US (Seco et al., 2011). Therefore, the atmospheric and geographic patterns of this area create conditions that allow for the production of high O_3 concentrations and UFP regional episodes, the latter due to new particle formation (NPF) and/or transported UFP-polluted air masses.

Previous studies on particle number size distribution (PNSD) time series in high insolation urban areas revealed the frequent simultaneous occurrence of photochemical NPF and O_3 episodes in the spring and summer (Minoura and Takekawa, 2005; Park et al., 2008; Pey et al., 2009; Fernández-Camacho et al., 2010; Wonaschütz et al., 2015; Wang et al., 2016). In a cluster analysis, Brines et al. (2015) reported that average O_3 concentrations reached their highest levels in the NPF cluster in most of the cities studied during periods of high solar insolation, temperatures, and wind speeds, and when humidity was low and the concentrations of other pollutants (e.g., CO, NOx, particulate matter mass, and black carbon [BC]) were at background levels. It should be noted that these studies usually covered the whole year, and, therefore, the simultaneous seasonal peaking of O_3 and UFPs may be due to either similarities in seasonal patterns of these photochemically driven pollutants or the same atmospheric processes causing both pollution episodes. However, O_3 formation peaks under the presence of high concentrations of precursors (Monks et al., 2015), whereas NPF depends on the balance between the rates of formation of clusters and the rates of loss to pre-existing surfaces. In areas with low precursor concentrations, thus low formation rates, NPF requires clean atmospheres, so that loss rates do not outweigh formation rates (Boy and Kulmala, 2002).

Carnerero et al. (2018) and Querol et al. (2018) studied NPF and O_3 in Madrid in July 2016, and found that even though O_3 concentrations were high throughout the period, NPF only occurred with relatively low O_3 episodes. According to this analysis, NPF and O_3 peaks were out of phase, i.e., relative minimum concentrations of O_3 coincided with periods with NPF, and relative maximum concentrations of O_3 corresponded to periods without NPF. To understand the interconnections at a deeper level, in this study we focus on the warm seasons in the period 2014–2018 to investigate the relationship between episodes of O_3, UFPs, and NPF in the northern region of the Barcelona Province (northeast Spain), where these episodes occurred with a relatively high frequency. In the last decade, the O_3 threshold for health protection of the European Air Quality Directive (120 μg m^{-3} for the maximum 8 h moving daily averages in less than 25 days as an average for 3 years) was consistently exceeded in the study area. In 2015–2018, 34 to 40 days of exceedance per year, mostly concentrated in June and July, were recorded in the monitoring site of this study. Data on episode frequency for UFP and NPF are not available for the regional background. For the nearest urban background, the frequency of NPF bursts has been estimated to reach 15% of the time on an annual basis, mainly in spring and summer (Brines et al., 2015).

As stated above, previous studies have found a clear relationship between NPF episodes and high O_3 levels. Given that these studies covered annual periods, the O_3–NPF correlation may be due merely to the fact that both are maximized in spring and summer or that the occurrence of episodes of high O_3 and NPF are interrelated. O_3 levels may, directly or indirectly, play a key role in NPF by increasing OH radicals; however, our focus here is to determine the relationships between the most intense O_3 and NPF episodes, rather than all episodes. Thus, the main objectives of this study are to identify the highest episodes of NPF, UFP, and O_3 using long time series of O_3 and size-segregated UFP obtained during the warm season, and to investigate commonalities and differences in the patterns of these events. Furthermore, we use data from a field study that provide information on vertical profiles of O_3 and UFP during 10–14 July 2017 to support the interpretations of the relationship between UFP and O_3 in these photochemical pollution episodes.

2. Methodology

2.1. The study area

The data presented in this study were obtained at Montseny (MSY; 41°46′45.63″N, 02°21′28.92″E, 720 m a.s.l.), a regional background monitoring station established in 2002. The station is included in the European Aerosols, Clouds and Trace gases Research InfraStructure network (ACTRIS), the Global Atmosphere Watch network (GAW), and the atmospheric pollution monitoring and forecasting network of the Government of Catalonia (XVPCA). Montseny is considered a good representation of regional environments in the Western Mediterranean Basin (Pérez et al., 2008).

Montseny is located in a rural environment in a valley oriented in a northwest–southeast direction. It lies in the Montseny Natural Park, 40 km northeast of Barcelona and 30 km northwest of the Mediterranean coastline. The site is densely forested, the prominent vegetation being holm oak (*Quercus ilex* L.). The area around Montseny is restricted to traffic; the closest road is located 3 km from the station. The main sources of pollutants from the nearby Barcelona metropolitan area (BMA) are road traffic and industries, with additional contributions from aircraft, shipping, biomass burning, power generation, and livestock.

In the absence of strong synoptic winds, sea and mountain breezes are the main factors that determine the atmospheric dynamics at Montseny, which in turn regulate the daily evolution of pollutant concentrations. For this reason, the station is frequently affected by anthropogenic emissions originating from the valley and the BMA, channeled northward due to the complex orography. Previous studies have demonstrated that, without dominant synoptic winds, the sea breeze may transport polluted air masses up to the Pyrenees (>3000 m) and inject them at high altitudes, from where they are transported by mesoscale winds toward the Mediterranean Sea and sink due to subsidence. The following day, the sea and land breezes can transport the aged polluted air mass inland, closing the recirculation and causing high O_3 (Millán et al., 1997, 2000; Toll and Baldasano, 2000; Gonçalves et al., 2009; Valverde et al., 2016; Querol et al., 2017) and particulate matter episodes (Rodríguez et al., 2003) in the Western Mediterranean. This phenomenon is most favored in the spring and summer, when synoptic winds are frequently absent in the area, and the sea and land breezes are stronger as a consequence of maximal solar radiation. Hemispheric transport and stratospheric intrusions also contribute, to a lesser extent, to O_3 concentrations (Kalabokas et al., 2007, 2017; Querol et al., 2017, 2018).

2.2. Instrumentation

From April to September 2014–2018, part of the permanent instrumentation at Montseny was used. Particle number size distribution in the size range 9–856 nm (N) was measured continuously every 5 min

Table 1
Occurrences of new particle formation (NPF) events in absolute numbers and percentages according to ozone (O3) clusters (see Table 2 for characteristics of the clusters). The sum of values for the categories for each cluster may not total 100% due to rounding. The total number of days in each cluster is also shown.

NPF category	Extreme O_3	High O_3	Mild O_3	Low O_3
No data	7 (11.9%)	31 (14.2%)	57 (16.2%)	51 (21.8%)
Nonevent	43 (72.9%)	144 (66.1%)	214 (60.8%)	132 (56.4%)
Undefined	2 (3.4%)	6 (2.8%)	10 (2.8%)	3 (1.3%)
Burst	6 (10.2%)	22 (10.1%)	31 (8.8%)	20 (8.5%)
Class II	1 (1.7%)	7 (3.2%)	10 (2.8%)	8 (3.4%)
Class I	0 (0.0%)	8 (3.7%)	30 (8.5%)	20 (8.6%)
Total number of days	59	218	352	234

with a scanning mobility particle spectrometer (SMPS; TROPOS) connected to a condensation particle counter (CPC; TSI 3772). O_3 was measured with a photometry-based analyzer (MCV 48AV); SO_2 was measured with a UV fluorescence analyzer (Teledyne T100); BC was determined with a multi-angle absorption photometer (MAAP; Thermo Scientific). All the inlets were located at 3.5 m above ground level. The station was also equipped with an automatic meteorological station placed at 10 m above ground level (Vantage Pro Plus; Davis Instruments).

In addition, an intensive field study was carried out from 12 June to 31 July 2017 at a location 250 m east of the station. During the study, an air ion spectrometer (AIS; AIREL Ltd; Mirme et al., 2007) measured the mobility distribution of ambient ions in the size range 0.8–40 nm. A particle size magnifier (PSM; Airmodus Ltd., Vanhanen et al., 2011) was used to measure the number size distributions of charged and neutral particles in the size range 1.15–2.6 nm and total number concentration above 1.15 nm. The PSM was installed together with an inlet system, comparable to one described in Kangasluoma et al. (2016), incorporating an automatic zero measurement and a core sampling (an inlet system with a bypass flow, on/off ion filter, and a flow system to automate background measurement) to minimize sampling losses. Prior to the field study, the PSM was calibrated with tungsten oxide particles produced with a hot wire generator (e.g., Kangasluoma et al., 2015).

In addition, from 10 to 14 July, the vertical distribution of pollutants up to 2 km was measured using miniaturized instrumentation suspended from two tethered balloons. A miniaturized butanol-based CPC (Hy-CPC; Hanyang University; Lee et al., 2014) measured the number concentration of particles with diameters > 3 nm (N_3). The measurements had a time resolution of 1 s and a sample flow of 0.125 L min^{-1}. O_3 concentrations were measured with a photometry-based personal ozone monitor (POM; 2B Technologies). The balloons were also equipped with a global positioning system (GPS), a thermometer, hygrometer, barometer, anemometer, and wind vane. Each profile took approximately 15 min from the surface to the maximum altitude. When there were high horizontal winds during the sounding, the balloons were dragged horizontally instead of ascending, and the sounding time increased.

2.3. Data analysis

For the cluster analysis, we considered the period 2014–2018. We only used data between April and September to focus on periods of high photochemical activity and high insolation, and, therefore, high concentrations of the pollutants of interest. All times are expressed in local time (UTC + 2 h), unless otherwise stated.

K-means clustering was applied to the daily O_3 hourly concentration averages. The K-means algorithm divides a set of n samples into K clusters $C = \{C_1, C_2, \ldots, C_K\}$ of equal variance, minimizing the sum of squared distances of the samples to their closest cluster center, described by the mean of the samples μ_j:

$$\sum_{i=0}^{n} \min_{\mu_j \in C} |x_i - \mu_j|^2$$

We used the Python module *Scikit-learn* (Pedregosa et al., 2011) to implement the K-means algorithm. The number of clusters K has to be decided by the user. K was chosen so that only one cluster contained all the days registering an exceedance of the "information value" (180 μg m^{-3} h^{-1}) fixed by the EU 2008/50/CE Directive, using the minimum number of clusters. This was achieved by using $K = 10$ clusters. Despite being statistically different, some of these initial 10 clusters represented similar atmospheric conditions. For this reason, we reduced the number of clusters by grouping similar clusters, i.e., clusters that shared similar patterns in all or most of the variables considered. To that end, for each set of days corresponding to the same cluster, we studied the average values of all the other variables available in order to characterize every cluster (Fig. S1 and Table S1). With this information, we were able to detect similar clusters and group them. Note that the original cluster containing all the O_3 information value exceedances was not grouped with any other cluster. More information on the original clusters and grouping can be found in the supplementary material. Eventually, four different situations leading to distinct O_3 daily patterns were identified with four cluster groups: days with an exceedance of the information value ("extreme" cluster), days with high O_3 levels without

Table 2
Qualitative summary of the days in each ozone (O_3) cluster (see also Fig. 1).

	Extreme O_3	High O_3	Mild O_3	Low O_3
Number of days	59	218	352	234
Temporal distribution	June and July	Mainly in summer	Mainly in spring and autumn	Spring and autumn
Days with exceedances of the EU information value[a]	8	0	0	0
Days with exceedances of the EU target value[b]	59	104	12	0
Temperature	Highest	Intermediate	Intermediate	Lowest
Relative Humidity	Lowest	Low	High	Highest
Wind speed	Highest	High	Intermediate	Lowest
Solar radiation	Highest	High	High	Lowest
$N_{9\text{-}855}$	Highest	Intermediate	Intermediate	Lowest
$N_{9\text{-}25}$	Highest	High	Intermediate	Lowest
CS	Highest	Intermediate	Intermediate	Lowest
BC	Highest	Intermediate	Intermediate	Lowest
SO_2	Highest	Intermediate	Low	Low
Comments	Very hot and dry summer days, strong breezes cause transport of pollutants	Warm and dry days, breezes cause transport of pollutants	Mild temperature and humidity, light breezes may transport pollutants	Cool and humid days with no transport of pollutants

[a] European Union (EU) information value: hourly O_3 concentration average exceeds 180 μg m^{-3}.
[b] EU target value: O_3 concentrations exceed 120 μg m^{-3} for the maximum 8 h moving daily averages in at least 25 days as an average for 3 years.

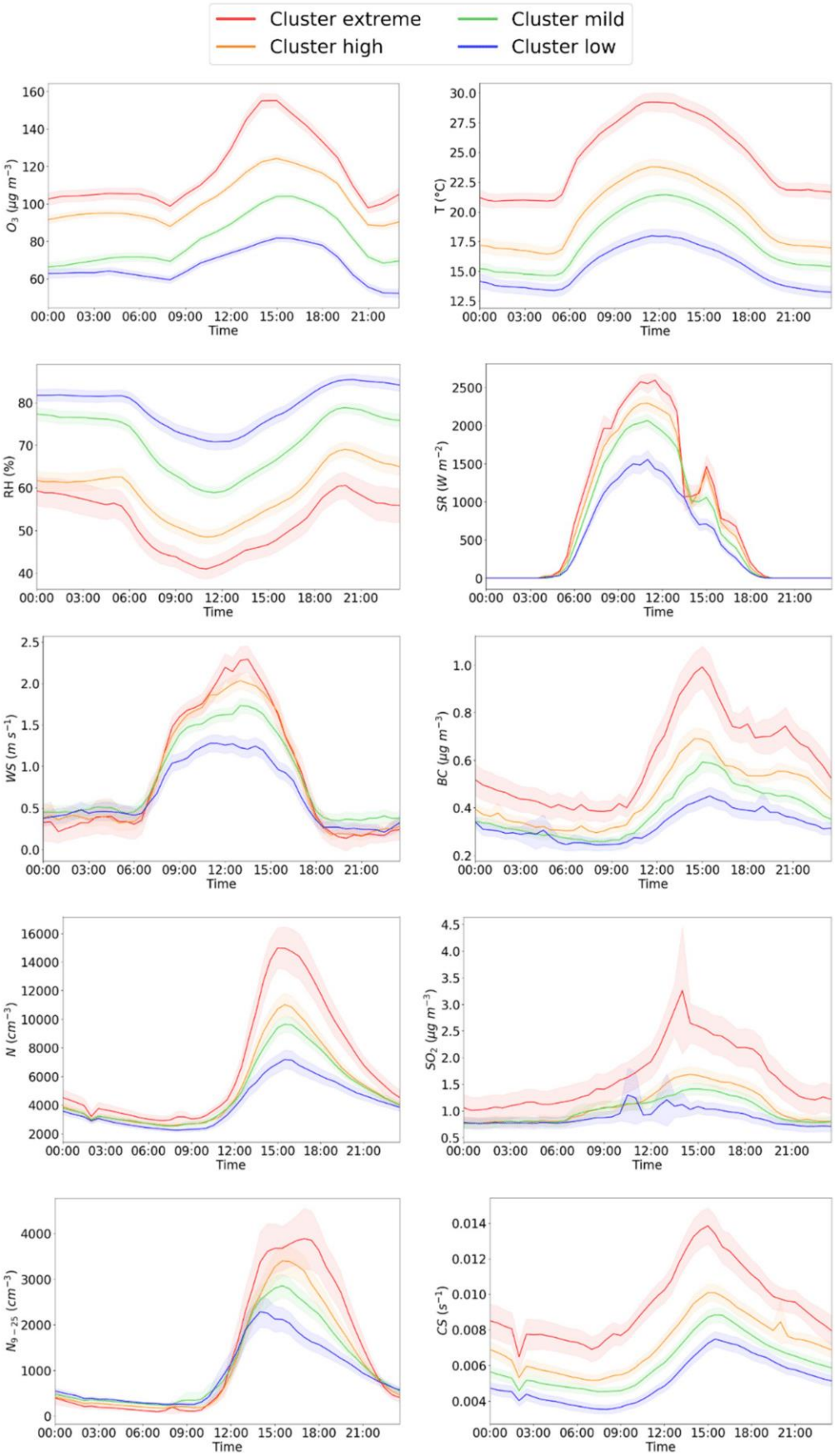

Fig. 1. Average daily evolutions of ozone (O_3), temperature (T), relative humidity (RH), solar radiation (SR), wind speed (WS), black carbon (BC), particle number concentration (N), sulfur dioxide (SO_2), particle number concentration of the nucleation mode ($N_{9\text{-}25}$), and the condensation sink (CS) at Montseny between April and September 2014–2018. Data are shown separately for the clusters determined from K-means cluster analysis (cluster characteristics are shown in Table 2). Shaded areas represent 95% confidence intervals.

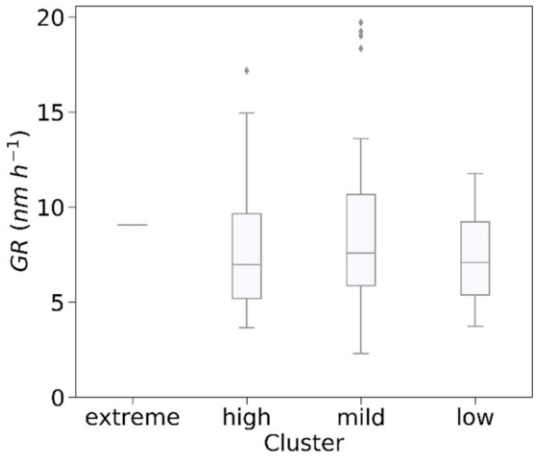

Fig. 2. Boxplot of particle growth rates (GRs) of Class I and Class II new particle formation (NPF) events according to their corresponding cluster classification for the period between April and September 2014–2018. The boxes show the three quartiles of the distribution, while the whiskers extend to 1.5 times the interquartile ranges. Values outside this range are shown as outliers. For the "extreme" cluster, only one value is shown because only one NPF episode was identified. Cluster characteristics are given in Table 2.

exceedances ("high" cluster), days with moderate O_3 concentrations ("mild" cluster), and days with low O_3 levels ("low" cluster).

Using the PNSD, we calculated the total number concentration of particles in the size range 9–855 nm (N), the number concentration of UFP ($N_{9\text{-}100}$), the nucleation-mode concentration, here considered as the concentration of particles in the size range 9–25 nm ($N_{9\text{-}25}$), and the condensation sink (CS, the frequency with which condensable vapor molecules condense on existing particles; Kulmala et al., 2012).

NPF episodes were manually classified according to a scheme adapted from that of Dal Maso et al. (2005). Days with clear particle formation and growth were classified as Class I. If the mode, concentration, or diameter fluctuated strongly during NPF, the day was classified as Class II. Days without a nucleation mode (<25 nm) lasting for at least 1 h were classified as nonevent. Days with a nucleation mode that did not grow with time were classified as undefined. In addition to this classification, we considered an extra NPF category for burst-like events. Burst events are similar to short Class I events lasting for about 1 h, in which there is clear NPF that stops rapidly (see example in Fig. S2). This may be due to either a change of air mass after particles have formed locally (the air mass is coming from a region where NPF has not occurred, and the newly formed particles are transported elsewhere) or the sudden dilution of the particles after sunrise. These bursts were not registered with increases in BC, and, therefore, cannot be associated with local emissions such as those from nearby vehicles. Burst events would be considered nonevents according to the scheme proposed by Dal Maso et al. (2005) if they lasted for less than 1 h. However, we regarded them as a separate category because they were observed about three times per month on average during the period of study. Finally, days that could not be clearly categorized were classified as undefined.

Log-normal modes were fit to the daily PNSD using the algorithm proposed by Hussein et al. (2005). The modes were used to calculate growth rates (GR) for all Class I and Class II NPF events.

3. Results

3.1. Data clustering

In classifying NPF events, a total of 717 daily PNSDs were classified, out of which 533 were categorized as non-NPF events (74% of the days for which data were available). Only 84 days (12%) were classified as Class I or Class II events, and 79 days were classified as burst events (11%). The rest (3%) were classified as undefined NPF events. The number of days in each NPF event category and the percentages according to each cluster are shown in Table 1. These results are in agreement with those reported in other European studies (see e.g., Manninen et al., 2010; Németh et al., 2018; Nieminen et al., 2018; Pikridas et al., 2012; Wonaschütz et al., 2015), with NPF ranging from 10 to 57% of the days for which data were available. However, a direct comparison with these studies is not possible, because most give annual or seasonal data, whereas in this study we considered data for only

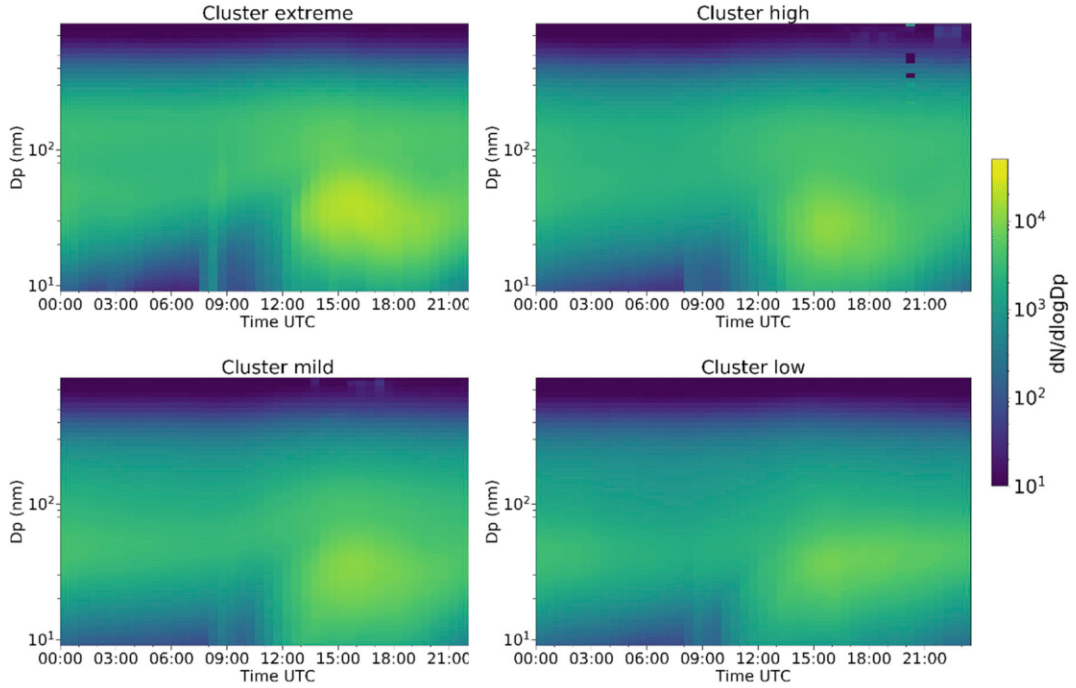

Fig. 3. Average particle number size distribution for the days in each cluster at Montseny between April and September 2014–2018. Cluster characteristics are given in Table 2.

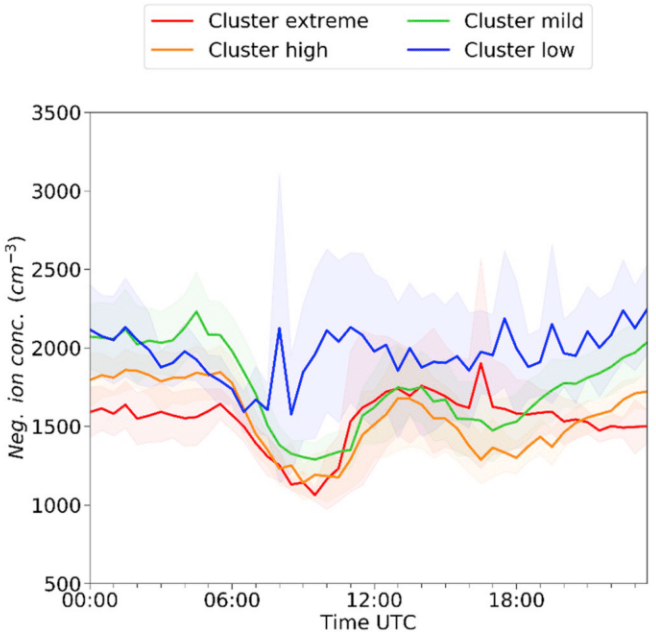

Fig. 4. Average daily cycles of the concentration of negative ions in the size range 0.8–40 nm, measured with an air ion spectrometer and shown by cluster classification, during an intensive field study from 12 June to 31 July 2017. Shaded areas represent 95% confidence intervals. Cluster characteristics are given in Table 2.

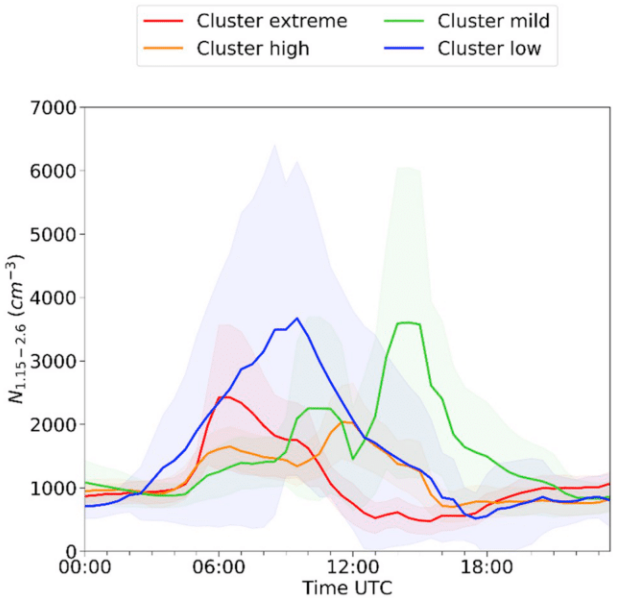

Fig. 5. Average daily cycles of particle number concentration in the size range 1.15–2.6 nm (N1.15-2.6), measured with a particle size magnifier shown by cluster classification, during an intensive field study from 12 June to 31 July 2017. Shaded areas represent 95% confidence intervals. Cluster characteristics are given in Table 2.

April–September. Moreover, we considered burst events as a separate category, which would have been classified as events or non-events in other studies (see Table 1).

The results of the O_3 cluster analysis are presented in Fig. 1, showing the average daily cycles of O_3, temperature, relative humidity, wind speed, solar radiation, BC, SO_2, CS, N, and $N_{9\text{-}25}$. A qualitative summary of the results shown in this figure can be found in Table 2. Fig. 2 shows the particle growth rates for the days that registered Class I or Class II NPF, according to their corresponding cluster. Fig. 3 represents the average 30 min PNSD calculated for each cluster separately.

The O_3 daily pattern in the "extreme" cluster was found only in June and July in a total of 59 days (7% of the period). This is the only cluster registering O_3 exceedances of the hourly information threshold (180 μg m^{-3}), a total of 10 h registered in 8 days. In addition, all days in this cluster registered at least one 8 h moving average greater than 120 μg O_3 m^{-3}. The majority of the days in this cluster were categorized as non-NPF events (72.9% of the days), and only one Class II NPF event was detected (1.7% of the days). However, burst-like events occurred at a higher rate in this cluster compared to the others (see the sharp increase in concentration at 08:00 in Fig. 3). This cluster was characterized by the highest N, $N_{9\text{-}25}$, CS, solar radiation, and temperature, and the lowest relative humidity. Transported pollution made an important contribution to the cluster, as suggested by the highest wind speed (with peaks around 13:00 that point to the arrival of the BMA plume), as well as the highest BC and SO_2, both increasing simultaneously from 09:00 and peaking after midday with the wind speed (Table 2). N peaked at 15:00, simultaneously with BC; thus, we may interpret that the high UFP concentrations of this cluster – the highest of all clusters – were not attributable to NPF, but to the transport of highly polluted air masses from the BMA. In addition, $N_{9\text{-}25}$ exhibited two peaks (Fig. 1), the earliest one coinciding in time with the main $N_{9\text{-}25}$ peak associated with the "low" cluster and with the highest SO_2 peak for the "high" cluster. This suggests that during this early peak, the high SO_2 (and O_3) might have given rise to NPF, in spite of a relatively large CS.

The O_3 pattern in the "high" cluster occurred mostly in the summer, with a few events in April, and 218 days (25% of the period) were assigned to this cluster. Almost half the days in this cluster (104 days) registered 8 h moving averages greater than 120 μg O_3 m^{-3}. These days had high solar radiation and temperature, low relative humidity, and an important contribution from transported pollutants and precursors, as suggested by the high peaks for wind speed around 13:00. High levels of BC, SO_2, N, and $N_{9\text{-}25}$ were registered in this cluster (Table 2). NPF occurred only in 6.9% of the days in this cluster; therefore, transported UFP emissions were accountable for the majority of the high UFP concentrations. When NPF occurred, the range of values for GRs was high within this cluster, indicating that the transported precursors also contributed to rapidly growing newly formed particles.

The O_3 pattern in the "mild" cluster was found mainly in the spring and late summer, and 352 days (41% of the period) were assigned to this cluster. Only 12 days in this cluster (3% of the days) register 8 h moving averages greater than 120 μg O_3 m^{-3}. The cluster was mainly characterized by mild temperature, high relative humidity, and a moderate contribution of pollutants from regional transport (Table 2). NPF was relatively frequent (11.3% of the days within the cluster), although N and $N_{9\text{-}25}$ levels were relatively low. This cluster also had the highest values and range for GRs. Thus, the cluster included days with high concentrations of condensable vapors that caused high particle growth rates, as well as days when the concentration of these vapors was very low and particles grew slowly.

The O_3 daily pattern in the "low" cluster was found mainly in the spring and September, and this cluster consisted of 234 days (27% of the period). There were no exceedances of the hourly or 8 h O_3 thresholds within this cluster. NPF was detected in 12% of the days, the highest fraction of all clusters. CS, N, and $N_{9\text{-}25}$ were lower than in the other clusters. These days were characterized by the lowest solar radiation, temperature, and wind speed and the highest relative humidity (Table 2). The low concentrations of BC and SO_2 also suggest that pollutants were not transported to the station. According to Fig. 3, this cluster had the lowest average number particle concentrations of all diameters, but especially those larger than 100 nm. For days registering NPF, the growth rates in this cluster had the lowest range and the lowest 3rd quartile. This suggests that despite NPF being frequent during these days, there were less condensable vapors that caused particle growth, and, therefore, the particles grew more slowly than in days in other

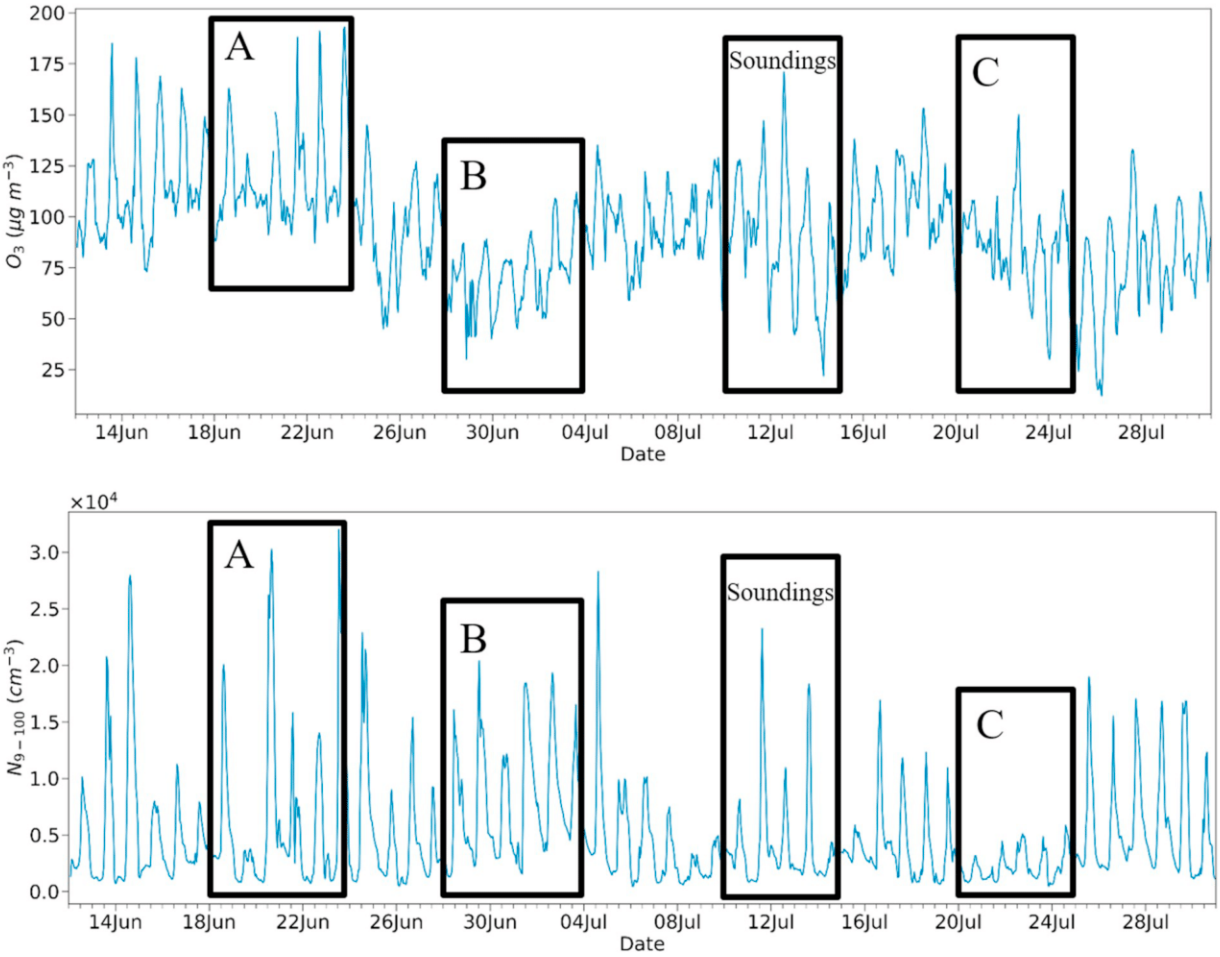

Fig. 6. Hourly concentrations of ozone (O_3) and ultrafine particles (UFPs, in the size range 9–100 nm) at Montseny during the field study between 12 June and 31 July 2017. Three cases are highlighted: A is an example of a period of extreme O_3 concentrations; B is an example of low O_3 levels; and C is an example of low UFP concentrations. The period when the balloon soundings were made is also highlighted.

clusters.

In summary, clustering based on O_3 concentrations revealed an apparent time correlation between O_3 concentrations and aerosol number concentrations, but different time patterns between high O_3 concentrations and NPF events with a marked impact on total N. We explore this connection in the following subsections.

3.2. Intensive field measurements

During the intensive field study from 12 June 2017 to 31 July 2017 at Montseny, a total of 49 days could be classified according to the cluster analysis described in section 3.1. Of these, 10 days were classified as falling within the "extreme" cluster, 17 within "high", 15 within "mild", and 7 within "low". For each cluster, the average cycles of the concentration of negative ions measured with the AIS, and the concentration of particles in the size range 1.15–2.6 nm ($N_{1.15\text{-}2.6}$) measured with the PSM are presented in Figs. 4 and 5, respectively. Fig. 6 shows the evolution of O_3 and UFP concentrations during the field study.

Days recording the most NPF events (days assigned to the "low" cluster) had the highest negative ion concentration, with relatively stable concentrations throughout the day with a peak at 2100 cm^{-3} at 11:00 UTC. All the other clusters registered their minimum at that time (around 1000 cm^{-3}), while the maximums were recorded at 13:30 UTC (around 1700 cm^{-3}). $N_{1.15\text{-}2.6}$ was also highest for clusters registering the most NPF episodes ("low" and "mild"). However, due to technical issues, several days of PSM data were missing, and only 30 days were used to calculate the daily cycles, resulting in the high uncertainties shown in Fig. 5.

From 10 to 14 July 2017, balloon soundings were made at the station. During this period, the middle levels of the troposphere were dominated by westerly winds, with low pressure systems located in northern Europe, and an anticyclonic ridge affecting the Southern Mediterranean, which caused stagnation of air masses over this area (see synoptic maps in Fig. S3). O_3 concentrations were very high, with maximum hourly values exceeding 170 μg O_3 m^{-3}. Three days, 10–12 July, were assigned to the "high" cluster, and two days, 13 and 14 July, to the "mild" cluster. No NPF events were observed in this period, although the aerosol loads were high. These observations were consistent with the cluster analysis summary presented in Table 2 for clusters "high" and "mild".

Fig. 7 shows the most representative vertical measurements obtained with the balloon soundings on 10 and 12 July. Both days were assigned to the "high" classified as cluster; therefore "high", hence, according to Table 2, it is expected to observe sea or land breezes are suggested to that transport pollutants to the station. On 10 July, O_3 and N_3 concentrations were relatively low all day and at all levels. Concentrations were constant with altitude, excluding the lowest part of the sounding, due to deposition of O_3 at the surface and consumption by NO. The potential temperature (θ) and water vapor mixing ratio (r) profiles corresponding to the first sounding (09:57 UTC) suggested the presence of a stable layer near the surface level (up to about 50 m) that was diluted by the sounding at 16:35 UTC. The wind speed profile was consistent with a sea or land breeze at both soundings, as expected. The morning and afternoon soundings were very similar suggesting that pollutants and

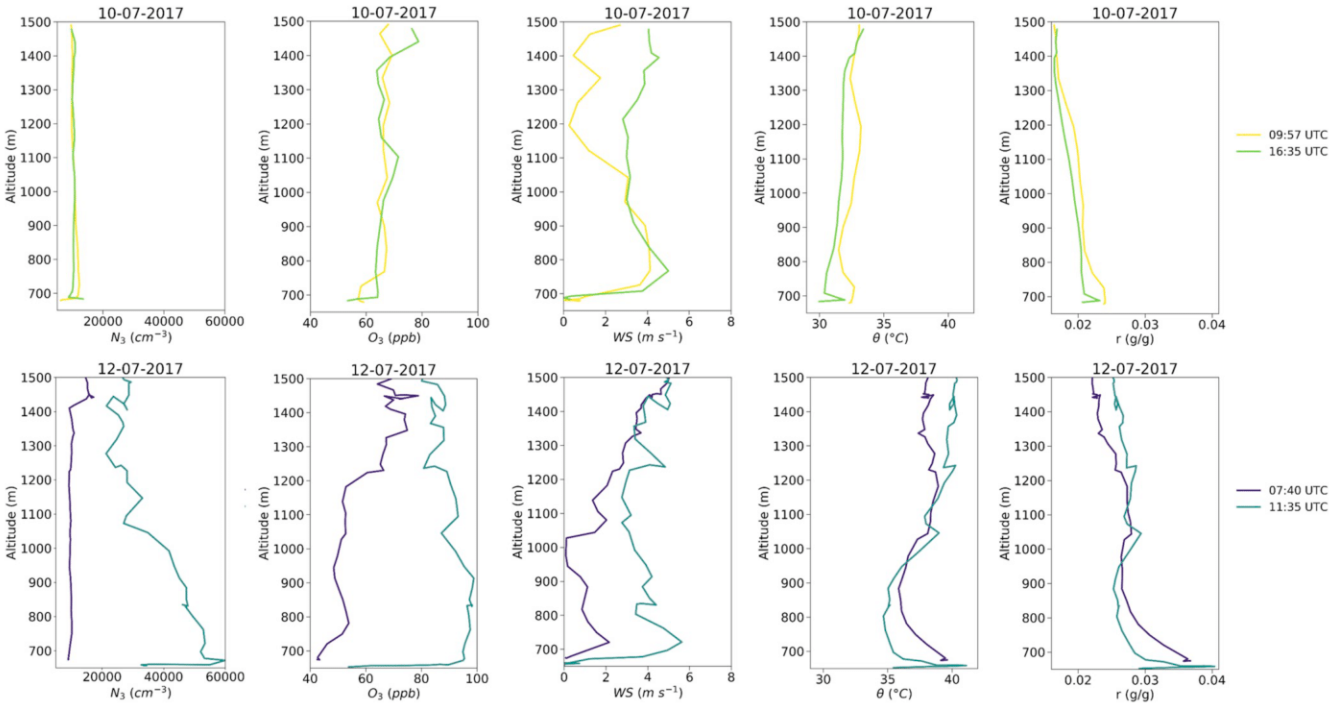

Fig. 7. Vertical soundings of the total number of particles with diameter >3 nm (N_3), ozone (O_3) concentration, wind speed (WS), potential temperature (θ), and water vapor mixing ratio (r) at Montseny on 10 July 2017 (top row) and 12 July 2017 (bottom row). Note that the balloon flight times are different on the two days. The profiles at 09:57 UTC on 10 July and 07:40 UTC on 12 July correspond to ascending flights; the profiles at 16:35 UTC on 10 July and 11:35 UTC on 12 July correspond to descending flights.

precursors were not transported into the station, contrary to the results shown in Table 2.

On 12 July, O_3 and N_3 concentrations at 07:40 UTC were similar to those recorded on 10 July. At 10:40, O_3 and N_3 concentrations were notably higher, especially in a vertical extension of 200 m above ground level; maximum concentrations of 194 μg O_3 m^{-3} and 6×10^4 particles cm^{-3} were recorded. It is important to highlight that N_3 and O_3 concentrations showed a similar pattern at midday, when the mixing layer was the highest (sounding at 10:44 UTC, 12 July); concentrations were the lowest at ground level (around 650 m a.s.l.) and maximum at about 900 m a.s.l. The differences in the profiles at morning and midday and the wind speed profiles were consistent with a sea breeze that transported a polluted air mass from the Mediterranean, which had been recirculating for one or more days. This is associated with an increase in pollutant and UFP concentrations, and, therefore, high CS, which inhibited NPF. This is consistent with the summary presented in Table 2 for the "high" cluster. Similar observations were also reported by Carnerero et al. (2018) and Querol et al. (2018) during an intensive balloon soundings study in Madrid.

3.3. Case studies of O_3, UFP and NPF episodes

For an in-depth analysis of the different time patterns of O_3 and major NPF episodes, we selected as case studies observations for three different episodes (Cases A to C) during the field study performed at Montseny from 12 June to 31 July 2017, which are discussed in detail below. The hourly concentrations of O_3 and $N_{9–100}$ at Montseny throughout the study are shown in Fig. 6. The corresponding PNSD, combining AIS size spectra of negative ions in the size range 0.8–20 nm and SMPS data in the size range 20–855 nm, are shown in Fig. 8. Note that the lower half of the figure only accounts for the negative ions measured with the AIS, while the upper half represents the concentration of all charged particles (negative and positive) measured with the SMPS. Therefore, the concentrations at the boundary between the two distributions differ. Further information about these differences and a comparison between AIS and other instruments, including a differential mobility particle sizer, are found in Gagné et al. (2011). Fig. 9 shows the averages of 30 min $N_{1.15–2.6}$ (PSM) and $N_{9–100}$ (SMPS), and Fig. 10 shows the 30 min averages of the CS. In addition, Figs. S4, S5, and S6 show the daily synoptic conditions (geopotential height at 500 hPa and mean sea level pressure at 12:00 UTC) for each case study.

Case A (18–23 June 2017) comprises a period of very high O_3 concentrations. A heatwave affected the area during this period, as a consequence of an anticyclonic ridge over the Iberian Peninsula and the presence of a very warm air mass transported from North Africa. Maximum temperatures over 30 °C and minimum temperatures over 20 °C were registered during the episode. Maximum O_3 hourly concentrations exceeded 180 μg m^{-3} on three consecutive days (21–23 June), and a maximum hourly concentration of 193 μg O_3 m^{-3} was registered, the most severe episode at Montseny since O_3 measurements started in 2008. All the days in this period were assigned to the "extreme" cluster, which agrees with the description for this cluster presented in Table 2.

The PNSD reveals only two weak NPF episodes on 19 and 20 June, coinciding with the lowest O_3 concentrations for this case (Fig. 8). The size distribution of these two events (classic "banana" events) suggests that NPF occurred over a vast area (Manninen et al., 2010). During the remaining days, fluctuations in the concentration of the finest particles detected with the AIS were observed around 06:00 UTC, although this was not necessarily related to NPF (Manninen et al., 2010). This was consistent with the concentration of particles measured with the PSM and SMPS (Fig. 9): around 06:30 UTC, the concentration of total UFPs and the CS (6×10^{-3} s^{-1}; Fig. 10) were at their minimum, while a maximum for $N_{1.15-2.6}$ concentration was registered simultaneously. This may be related to the initial stages of NPF, although growth above 10 nm was not observed. Later, the breeze transported regionally generated pollutants to the station, which was reflected by an increase in CS (18×10^{-3} s^{-1}) and N_{9-100}, both peaking at midday. It is plausible that the increased CS subsequently stopped the NPF process and the particles formed in the morning hours never reached sizes above 10 nm.

Case B (28 June–3 July 2017) was a period with relatively low

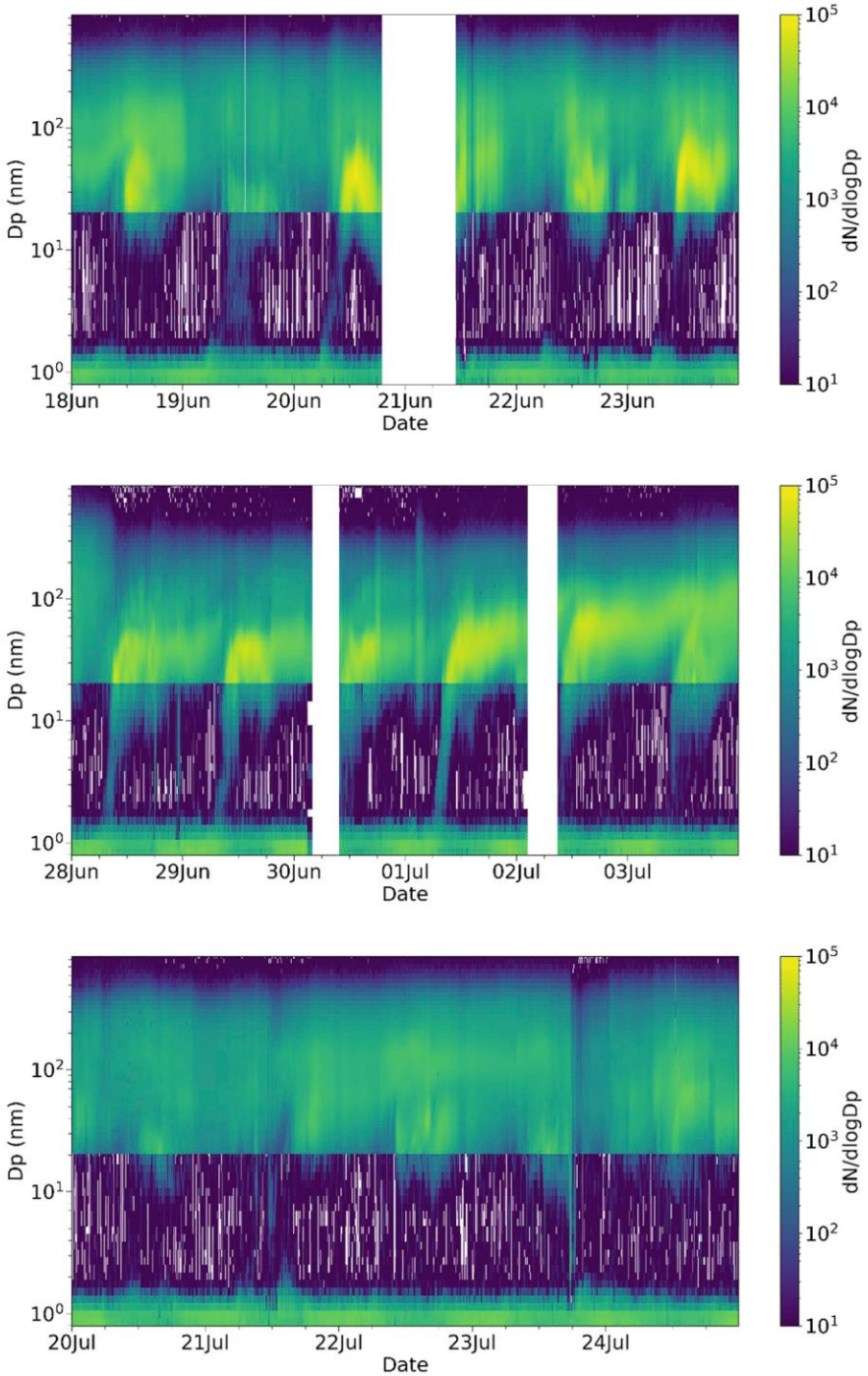

Fig. 8. Size distribution spectra combining air ion spectrometer (negative ions, 0.8–20.0 nm) and scanning mobility particle spectrometer (20–856 nm) readings for the case studies A, B, and C (from top to bottom). Case study A is an example of a period of extreme ozone (O_3) concentrations, B an example of low O_3 levels, and C an example of low ultrafine particle concentrations. Missing data and values below the detection limit of the instruments are represented in white.

concentrations of O_3. The lowest temperatures (both maxima and minima) of the summer were recorded during this period. From 28 to 30 June, there were frequent and intense storms in the area as a consequence of the passage of a front and the associated entrance of a cold air mass. During this period, there were intense regional NPF Class I events starting around 11:00 UTC every day (Fig. 8), coinciding with relatively low O_3 concentrations (days between 28 June and 2 July were assigned to the "low" cluster; 3 July was assigned to the "mild" cluster). The low temperatures and O_3 concentrations agreed with the description for clusters "low" and "mild" clusters in Table 2.

Fig. 9 shows data consistent with the occurrence of the events: $N_{1.15\text{-}2.6}$ concentration increased until 10:30 UTC, after $N_{9\text{-}100}$ started increasing but before it peaked at midday. The influence of pollution from the BMA was limited during these days, as shown also by lower CS (ranging from 3×10^{-3} s^{-1} at 07:00 UTC to 8×10^{-3} s^{-1} at 15:30 UTC) and $N_{9\text{-}100}$ compared to those in Case A. Nevertheless, the area probably received a moderate concentration of NPF precursors in a relatively clean atmosphere with low CS and high levels of biogenic VOCs and NH_3. According to Van Damme et al. (2018), the area of study is one of the NH_3 hotspots worldwide. These are ideal ambient conditions for NPF episodes (Lehtipalo et al., 2018).

Case C (20–24 July 2017) was a period with low UFPs, during which

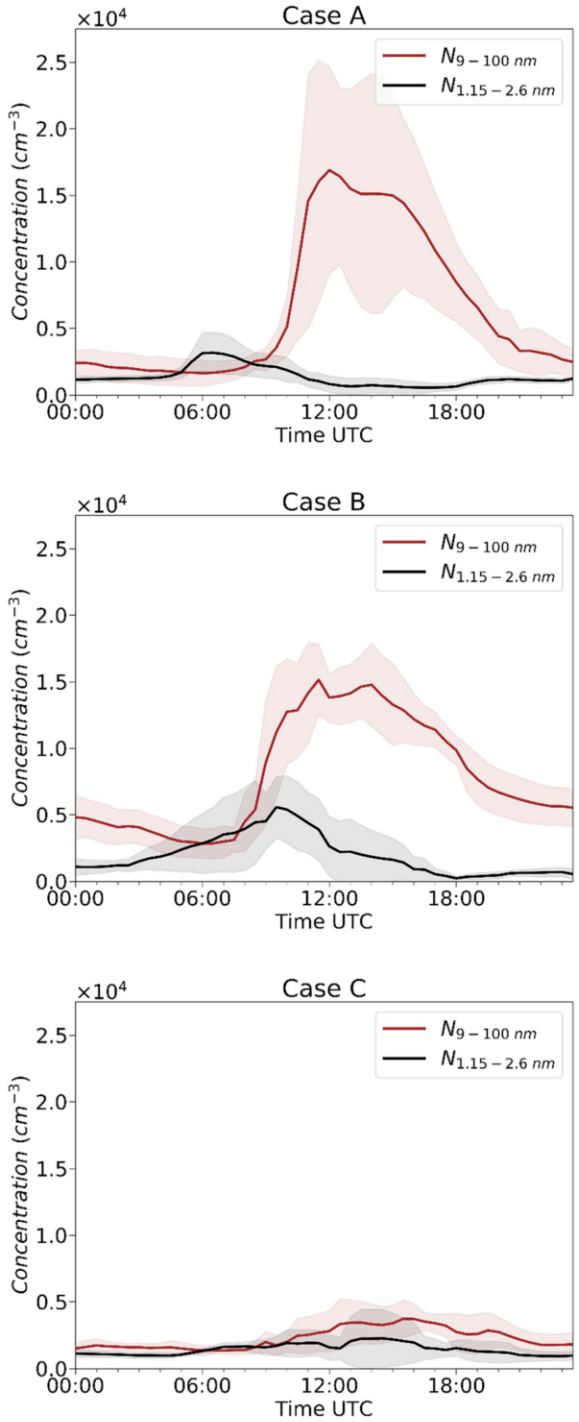

Fig. 9. Thirty-minute average concentrations of particles in size ranges 1.15–2.6 nm (measured with a particle size magnifier) and 9–100 nm (measured with a scanning mobility particle spectrometer), during case study (A, B, and C) periods. Case study A is an example of a period of extreme ozone (O_3) concentrations, B an example of low O_3 levels, and C an example of low ultrafine particle concentrations. Shaded areas represent 95% confidence intervals.

the combination of an anticyclonic ridge in the Mediterranean and a low-pressure system in the North Sea caused the passage of a trough over the Iberian Peninsula, with cold air in its center. At the surface, a stationary high-pressure system caused the stagnation of warm air in the area of study. The warm air at the surface in combination with the cold air aloft favored strong thunderstorms, especially in the afternoons.

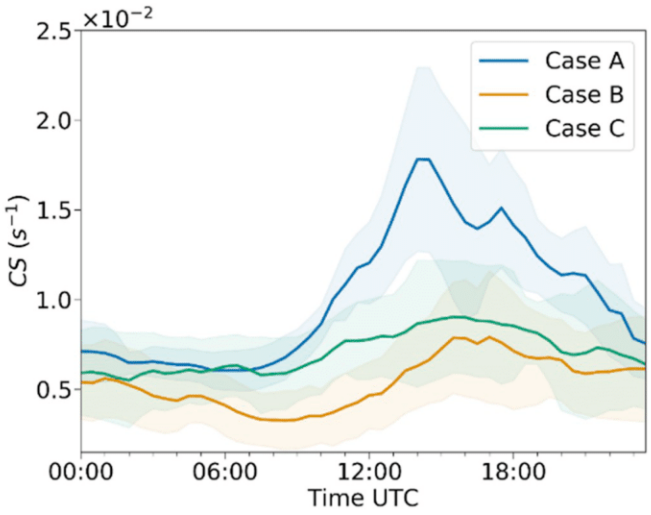

Fig. 10. Thirty-minute averages of the condensation sink (CS) at Montseny for cases A, B and C. Case study A is an example of a period of extreme ozone (O_3) concentrations, B an example of low O_3 levels, and C an example of low ultrafine particle concentrations. Shaded areas represent 95% confidence intervals.

During this period, UFP concentrations were very low, suggesting a low pollution load, but no NPF events were observed. This agreed with the average evolution of CS, which was higher than in Case B, when NPF was observed every day. O_3 concentrations were moderate, but the daily formation was low, i.e., there was no large difference in the concentrations throughout the day. In addition, the background concentration decreased during this period. For this reason, the days in this case were not assigned to a single cluster, but to "high" (22 July), "mild" (20, 21, and 24 July), and "low" (23 July) clusters. In this case, the conditions for inhibiting O_3 formation also inhibited NPF.

4. Conclusions

We studied the simultaneity of the occurrence of peak episodes of O_3, UFPs, and NPF in a regional background station located 40 km often downwind of the BMA in northeast Spain in the Western Mediterranean, between April and September in 2014–2018. In addition, the concentrations of negative ions and particles <3 nm were measured during a field study from 12 June to 31 July 2017. The vertical distribution of pollutants up to 1500 m above ground level was determined from 10 to 14 July 2017.

During these warm periods, the results indicate that the highest UFP concentrations coincided with the highest O_3 episodes. However, the probability of NPF with particles growing to >25 nm (according to the definition of an NPF episode) was the lowest during these days, even though the nucleation-mode number concentration was the highest due to the contribution of traffic emissions and growth rates were high due to high concentrations of condensable vapors. In this period, temperature, solar radiation, and wind speed were at their highest, and relative humidity at its lowest. The CS and concentrations of BC and SO_2 were also at a maximum. This suggests that pollutants are recirculated and/or transported from the BMA and other populated and industrial areas to the station during warm periods. Conversely, when the transported air mass is relatively clean and there is no recirculation, especially during and after the passage of weather fronts, UFP and O_3 concentrations are at their lowest, and NPF is most favored, although growth rates are at their lowest. This may be because high O_3 episodes at Montseny require polluted air masses (with high levels of particles, and accordingly CS) being transported from the valleys and the BMA. On the other hand, NPF requires either high precursor concentrations or clean atmospheres when precursor concentrations are low. However, when the atmosphere

is too clean, for example during the passage of a cold front causing strong convection and instability, the concentrations of NPF precursors are too low, and loss rates are greater than formation rates, thus the formation of particles is not detected. In addition, the concentration of newly formed particles in this case is low compared to the background particle number concentration. Thus, it is important to be aware of the scales of background and episode concentrations at the location of study. For example, NPF has been described in the Artic with much lower concentrations of precursors (Nieminen et al., 2018).

In essence, summertime vertical recirculation of Wester Mediterranean air masses is a major cause of regional O_3 pollution episodes, and it is also responsible for enrichment of aerosol particles and particle precursors, which results in high levels of UFPs associated with higher O_3. This increases the CS to the point that NPF is inhibited. On the other hand, in the absence of recirculation and during its initial stages, humid air masses with NPF precursors are transported inland by the diurnal local-scale circulations (Millán et al., 1997). These are diluted into dryer and warmer rural air masses, enriched with biogenic volatile organic compounds and NH_3. This is the optimum scenario for NPF in air masses with relatively low O_3 background concentrations (Lehtipalo et al., 2018). However, the dynamics of O_3, UFP, and NPF episodes are very complex, and we cannot conclude that these episodes are either simultaneous or mutually excluding. Further studies are needed to better understand these intense episodes.

With regard to implications for air quality, the occurrence of the highest O_3 episodes with the highest UFP levels may magnify the health impacts of the episodes. The transported UFPs consist of both primary and secondary particles. During the lowest (but still high in absolute concentration) spring–summer O_3 episodes (days in the "low" cluster), the contribution of primary UFPs is very low, with UFPs being mainly secondary resulting from NPF. The health impact of UFPs in these two distinct types of episodes is probably different, as reported by Tobías et al. (2018) when evaluating the health outcomes of traffic-related and bulk UFP concentrations in Barcelona. They reported that NPF-dominated days were associated with low premature mortality risk, because these episodes were linked with less polluted days. During these days, the total number of particles is the lowest, as we have demonstrated in this study.

Declaration of competing interest

The authors declare that they have no known competing financial interests or personal relationships that could have appeared to influence the work reported in this paper.

Acknowledgments

The present work was supported by the Spanish State Research Agency – integrated in the Spanish Ministry of Science, Innovation and Universities –, FEDER funds under the project HOUSE (CGL2016-78594-R), and by the Government of Catalonia (AGAUR 2017 SGR41). The work was supported by Academy of Finland via Center of Excellence in Atmospheric Sciences (project 272041), via Biofuture2025 project "Nano BioMass, 304347" European Commission via ACTRIS2 (project 654109). The authors thank the Department of Territory of the Government of Catalonia for maintaining the XVPC air quality network and providing the data for O_3, NOx and SO_2. The authors also acknowledge the valuable contributions of Miguel Escudero, Enrique Mantilla, Hong-Ku Lee, Hee-Ram Eun and Yong-Hee Park during the tethered balloons measurements. C. Carnerero thanks the Spanish Ministry of Science, Innovation and Universities for her FPI grant (BES-2017-080027).

Appendix A. Supplementary data

Supplementary data to this article can be found online at https://doi.org/10.1016/j.aeaoa.2019.100051.

References

Atkinson, R.W., Fuller, G.W., Anderson, H.R., Harrison, R.M., Armstrong, B., 2010. Urban ambient particle metrics and health. Epidemiology 21 (4), 501–511. https://doi.org/10.1097/EDE.0b013e3181debc88.

Boy, M., Kulmala, M., 2002. Nucleation events in the continental boundary layer: influence of physical and meteorological parameters. Atmos. Chem. Phys. https://doi.org/10.5194/acp-2-1-2002.

Brines, M., Dall'Osto, M., Beddows, D.C.S., Harrison, R.M., Gómez-Moreno, F., Núñez, L., Artíñano, B., Costabile, F., Gobbi, G.P., Salimi, F., Morawska, L., Sioutas, C., Querol, X., 2015. Traffic and nucleation events as main sources of ultrafine particles in high-insolation developed world cities. Atmos. Chem. Phys. https://doi.org/10.5194/acp-15-5929-2015.

Carnerero, C., Pérez, N., Reche, C., Ealo, M., Titos, G., Lee, H.-K., Eun, H.-R., Park, Y.-H., Dada, L., Paasonen, P., Kerminen, V.-M., Mantilla, E., Escudero, M., Gómez-Moreno, F.J., Alonso-Blanco, E., Coz, E., Saiz-Lopez, A., Temime-Roussel, B., Marchand, N., Beddows, D.C.S., Harrison, R.M., Petäjä, T., Kulmala, M., Ahn, K.-H., Alastuey, A., Querol, X., 2018. Vertical and horizontal distribution of regional new particle formation events in Madrid. Atmos. Chem. Phys. 18 (22), 16601–16618. https://doi.org/10.5194/acp-18-16601-2018.

Chu, B., Kerminen, V.-M., Bianchi, F., Yan, C., Petäjä, T., Kulmala, M., 2019. Atmospheric new particle formation in China. Atmos. Chem. Phys. 19, 115–138. https://doi.org/10.5194/acp-19-115-2019.

Dal Maso, M., Kulmala, M., Riipinen, I., Wagner, R., Hussein, T., Aalto, P.P., Lehtinen, K. E.J., Maso, D., Kulmala, M., Riipinen, M., Wagner, I., Hussein, R., Aalto, T., Lehtinen, P.P., 2005. Formation and growth of fresh atmospheric aerosols: eight years of aerosol size distribution data from SMEAR II, Hyytiälä, Finland. Boreal Environ. Res. 10, 323–336.

Dall'Osto, M., Beddows, D.C.S., Pey, J., Rodriguez, S., Alastuey, A., Harrison, R.M., Querol, X., 2012. Urban aerosol size distributions over the Mediterranean city of Barcelona, NE Spain. Atmos. Chem. Phys. 12 (22), 10693–10707. https://doi.org/10.5194/acp-12-10693-2012.

Dall'Osto, M., Querol, X., Alastuey, A., O&apos, Dowd, C., Harrison, R.M., Wenger, J., Gómez-Moreno, F.J., 2013. On the spatial distribution and evolution of ultrafine particles in Barcelona. Atmos. Chem. Phys. 13 (2), 741–759. https://doi.org/10.5194/acp-13-741-2013.

Van Damme, M., Clarisse, L., Whitburn, S., Hadji-Lazaro, J., Hurtmans, D., Clerbaux, C., Coheur, P.-F., 2018. Industrial and agricultural ammonia point sources exposed. Nature 564 (7734), 99–103. https://doi.org/10.1038/s41586-018-0747-1.

EC Directive 2008/50/EC of 21 May 2008, 2008. On ambient air quality and cleaner air for Europe [online] Available from: https://eur-lex.europa.eu/legal-content/EN/TXT/HTML/?uri=CELEX:32008L0050&from=ES. (Accessed 31 January 2019).

EEA, 2018. Air Quality in Europe — 2018 Report.

Fernández-Camacho, R., Rodríguez, S., De La Rosa, J., Sánchez De La Campa, A.M., Viana, M., Alastuey, A., Querol, X., 2010. Ultrafine particle formation in the inland sea breeze airflow in Southwest Europe. Atmos. Chem. Phys. 10, 9615–9630. https://doi.org/10.5194/acp-10-9615-2010.

Gagné, S., Lehtipalo, K., Manninen, H.E., Nieminen, T., Schobesberger, S., Franchin, A., Yli-Juuti, T., Boulon, J., Sonntag, A., Mirme, S., Mirme, A., Hõrrak, U., Petäjä, T., Asmi, E., Kulmala, M., 2011. Atmospheric Measurement Techniques Intercomparison of air ion spectrometers: an evaluation of results in varying conditions. Atmos. Meas. Tech. 4, 805–822. https://doi.org/10.5194/amt-4-805-2011.

Gonçalves, M., Jiménez-Guerrero, P., Baldasano, J.M., 2009. Contribution of atmospheric processes affecting the dynamics of air pollution in South-Western Europe during a typical summertime photochemical episode. Atmos. Chem. Phys. 9 (3), 849–864. https://doi.org/10.5194/acp-9-849-2009.

Gordon, H., Kirkby, J., Baltensperger, U., Bianchi, F., Breitenlechner, M., Curtius, J., Dias, A., Dommen, J., Donahue, N.M., Dunne, E.M., Duplissy, J., Ehrhart, S., Flagan, R.C., Frege, C., Fuchs, C., Hansel, A., Hoyle, C.R., Kulmala, M., Kürten, A., Lehtipalo, K., Makhmutov, V., Molteni, U., Rissanen, M.P., Stozkhov, Y., Tröstl, J., Tsagkogeorgas, G., Wagner, R., Williamson, C., Wimmer, D., Winkler, P.M., Yan, C., Carslaw, K.S., 2017. Causes and importance of new particle formation in the present-day and preindustrial atmospheres. J. Geophys. Res. Atmos. 122 (16), 8739–8760. https://doi.org/10.1002/2017JD026844.

Hussein, T., Dal Maso, M., Petaja, T., Koponen, I.K., Paatero, P., Aalto, P.P., Hameri, K., Kulmala, M., 2005. Evaluation of an automatic algorithm for fitting the particle number size distributions. Boreal Environ. Res. 10 (5), 337–355.

Kalabokas, P., Hjorth, J., Foret, G., Dufour, G., Eremenko, M., Siour, G., Cuesta, J., Beekmann, M., 2017. An investigation on the origin of regional springtime ozone episodes in the Western Mediterranean. Atmos. Chem. Phys. 17 (6), 3905–3928. https://doi.org/10.5194/acp-17-3905-2017.

Kalabokas, P.D., Volz-Thomas, A., Brioude, J., Thouret, V., Cammas, J.-P., Repapis, C.C., 2007. Vertical ozone measurements in the troposphere over the Eastern Mediterranean and comparison with central Europe. Atmos. Chem. Phys. 7 (14), 3783–3790. https://doi.org/10.5194/acp-7-3783-2007.

Kangasluoma, J., Attoui, M., Junninen, H., Lehtipalo, K., Samodurov, A., Korhonen, F., Sarnela, N., Schmidt-Ott, A., Worsnop, D., Kulmala, M., Petäjä, T., 2015. Sizing of neutral sub 3 nm tungsten oxide clusters using airmodus particle size magnifier. J. Aerosol Sci. 87, 53–62. https://doi.org/10.1016/J.JAEROSCI.2015.05.007.

Kangasluoma, J., Franchin, A., Duplissy, J., Ahonen, L., Korhonen, F., Attoui, M., Mikkilä, J., Lehtipalo, K., Vanhanen, J., Kulmala, M., Petäjä, T., 2016. Operation of the Airmodus A11 nano Condensation Nucleus Counter at various inlet pressures and various operation temperatures, and design of a new inlet system. Atmos. Meas. Tech. 9, 2977–2988. https://doi.org/10.5194/amt-9-2977-2016.

Kecorius, S., Kivekäs, N., Kristensson, A., Tuch, T., Covert, D.S., Birmili, W., Lihavainen, H., Hyvärinen, A.-P., Martinsson, J., Sporre, M.K., Swietlicki, E., Wiedensohler, A., Ulevicius, V., 2016. Significant increase of aerosol number concentrations in air masses crossing a densely trafficked sea area. Oceanologia 58 (1), 1–12. https://doi.org/10.1016/J.OCEANO.2015.08.001.

Kerminen, V.-M., Chen, X., Vakkari, V., Petäjä, T., Kulmala, M., Bianchi, F., 2018. Atmospheric new particle formation and growth: review of field observations. Environ. Res. Lett. 13 (10), 103003. https://doi.org/10.1088/1748-9326/aadf3c.

Keuken, M.P., Moerman, M., Zandveld, P., Henzing, J.S., Hoek, G., 2015. Total and size-resolved particle number and black carbon concentrations in urban areas near Schiphol airport (The Netherlands). Atmos. Environ. 104, 132–142. https://doi.org/10.1016/J.ATMOSENV.2015.01.015.

Keuken, M.P., Moerman, M., Zandveld, P., Henzing, J.S., 2015. Total and size-resolved particle number and black carbon concentrations near an industrial area. Atmos. Environ. 122, 196–205. https://doi.org/10.1016/J.ATMOSENV.2015.09.047.

Kulmala, M., Petäjä, T., Nieminen, T., Sipilä, M., Manninen, H.E., Lehtipalo, K., Dal Maso, M., Aalto, P.P., Junninen, H., Paasonen, P., Riipinen, I., Lehtinen, K.E.J., Laaksonen, A., Kerminen, V.-M., 2012. Measurement of the nucleation of atmospheric aerosol particles. Nat. Protoc. 7 (9), 1651–1667. https://doi.org/10.1038/nprot.2012.091.

Kumar, P., Morawska, L., Birmili, W., Paasonen, P., Hu, M., Kulmala, M., Harrison, R.M., Norford, L., Britter, R., 2014. Ultrafine particles in cities. Environ. Int. 66, 1–10. https://doi.org/10.1016/J.ENVINT.2014.01.013.

Lanzinger, S., Schneider, A., Breitner, S., Stafoggia, M., Erzen, I., Dostal, M., Pastorkova, A., Bastian, S., Cyrys, J., Zscheppang, A., Kolodnitska, T., Peters, A., 2016. Associations between ultrafine and fine particles and mortality in five central European cities — results from the UFIREG study. Environ. Int. 88, 44–52. https://doi.org/10.1016/J.ENVINT.2015.12.006.

Lee, H.-K., Hwang, I.-K., Ahn, K.-H., 2014. Development and evaluation of Hy-CPC, part. Aerosol Res. 10 (93–97).

Lehtipalo, K., Yan, C., Dada, L., Bianchi, F., Xiao, M., Wagner, R., Stolzenburg, D., Ahonen, L.R., Amorim, A., Baccarini, A., Bauer, P.S., Baumgartner, B., Bergen, A., Bernhammer, A.-K., Breitenlechner, M., Brilke, S., Buchholz, A., Mazon, S.B., Chen, D., Chen, X., Dias, A., Dommen, J., Draper, D.C., Duplissy, J., Ehn, M., Finkenzeller, H., Fischer, L., Frege, C., Fuchs, C., Garmash, O., Gordon, H., Hakala, J., He, X., Heikkinen, L., Heinritzi, M., Helm, J.C., Hofbauer, V., Hoyle, C.R., Jokinen, T., Kangasluoma, J., Kerminen, V.-M., Kim, C., Kirkby, J., Kontkanen, J., Kürten, A., Lawler, M.J., Mai, H., Mathot, S., Mauldin, R.L., Molteni, U., Nichman, L., Nie, W., Nieminen, T., Ojdanic, A., Onnela, A., Passananti, M., Petäjä, T., Piel, F., Pospisilova, V., Quéléver, L.L.J., Rissanen, M.P., Rose, C., Sarnela, N., Schallhart, S., Schuchmann, S., Sengupta, K., Simon, M., Sipilä, M., Tauber, C., Tomé, A., Tröstl, J., Väisänen, O., Vogel, A.L., Volkamer, R., Wagner, A.C., Wang, M., Weitz, L., Wimmer, D., Ye, P., Ylisirniö, A., Zha, Q., Carslaw, K.S., Curtius, J., Donahue, N.M., Flagan, R.C., Hansel, A., Riipinen, I., Virtanen, A., Winkler, P.M., Baltensperger, U., Kulmala, M., Worsnop, D.R., 2018. Multicomponent new particle formation from sulfuric acid, ammonia, and biogenic vapors. Sci. Adv. 4 (12), eaau5363. https://doi.org/10.1126/sciadv.aau5363.

Ma, N., Birmili, W., 2015. Estimating the contribution of photochemical particle formation to ultrafine particle number averages in an urban atmosphere. Sci. Total Environ. 512–513, 154–166. https://doi.org/10.1016/J.SCITOTENV.2015.01.009.

Manninen, H.E., Nieminen, T., Asmi, E., Gagné, S., Häkkinen, S., Lehtipalo, K., Aalto, P., Vana, M., Mirme, A., Mirme, S., Hõrrak, U., Plass-Dülmer, C., Stange, G., Kiss, G., Hoffer, A., Törő, N., Moerman, M., Henzing, B., de Leeuw, G., Brinkenberg, M., Kouvarakis, G.N., Bougiatioti, A., Mihalopoulos, N., O'Dowd, C., Ceburnis, D., Arneth, A., Svenningsson, B., Swietlicki, E., Tarozzi, L., Decesari, S., Facchini, M.C., Birmili, W., Sonntag, A., Wiedensohler, A., Boulon, J., Sellegri, K., Laj, P., Gysel, M., Bukowiecki, N., Weingartner, E., Wehrle, G., Laaksonen, A., Hamed, A., Joutsensaari, J., Petäjä, T., Kerminen, V.-M., Kulmala, M., 2010. EUCAARI ion spectrometer measurements at 12 European sites – analysis of new particle formation events. Atmos. Chem. Phys. 10 (16), 7907–7927. https://doi.org/10.5194/acp-10-7907-2010.

Millán, M.M., Artíñano, B., Alonso, L., Navazo, M., Castro, M., 1991. The effect of meso-scale flows on regional and long-range atmospheric transport in the Western Mediterranean area. Atmos. Environ. Part A. Gen. Top. 25 (5–6), 949–963. https://doi.org/10.1016/0960-1686(91)90137-V.

Millán, M.M., Salvador, R., Mantilla, E., Kallos, G., 1997. Photooxidant dynamics in the Mediterranean basin in summer: results from European research projects. J. Geophys. Res. Atmos. 102 (D7), 8811–8823. https://doi.org/10.1029/96JD03610.

Millán, M.M., Mantilla, E., Salvador, R., Carratalá, A., Sanz, M.J., Alonso, L., Gangoiti, G., Navazo, M., Millán, M.M., Mantilla, E., Salvador, R., Carratalá, A., Sanz, M.J., Alonso, L., Gangoiti, G., Navazo, M., 2000. Ozone cycles in the Western Mediterranean basin: interpretation of monitoring data in complex coastal terrain. J. Appl. Meteorol. 39 (4), 487–508. https://doi.org/10.1175/1520-0450(2000)039<0487:OCITWM>2.0.CO;2.

Minoura, H., Takekawa, H., 2005. Observation of number concentrations of atmospheric aerosols and analysis of nanoparticle behavior at an urban background area in Japan. Atmos. Environ. 39 (32), 5806–5816. https://doi.org/10.1016/J.ATMOSENV.2005.06.033.

Mirme, A., Tamm, E., Mordas, G., Vana, M., Uin, J., Mirme, S., Bernotas, T., Laakso, L., Hirsikko, A., Kulmala, M., 2007. A wide-range multi-channel air ion spectrometer. Boreal Environ. Res. 12 (3), 247–264 [online] Available from: https://pdfs.semanticscholar.org/01fa/9a8eb45aafee02a4d4c20d3230a7fa7554e0.pdf. (Accessed 11 April 2019).

Monks, P.S., Archibald, A.T., Colette, A., Cooper, O., Coyle, M., Derwent, R., Fowler, D., Granier, C., Law, K.S., Mills, G.E., Stevenson, D.S., Tarasova, O., Thouret, V., Von Schneidemesser, E., Sommariva, R., Wild, O., Williams, M.L., 2015. Tropospheric ozone and its precursors from the urban to the global scale from air quality to short-lived climate forcer. Atmos. Chem. Phys. https://doi.org/10.5194/acp-15-8889-2015.

Németh, Z., Rosati, B., Zíková, N., Salma, I., Bozó, L., Dameto de España, C., Schwarz, J., Ždímal, V., Wonaschütz, A., 2018. Comparison of atmospheric new particle formation events in three Central European cities. Atmos. Environ. 178, 191–197. https://doi.org/10.1016/J.ATMOSENV.2018.01.035.

Nieminen, T., Kerminen, V.-M., Petäjä, T., Aalto, P.P., Arshinov, M., Asmi, E., Baltensperger, U., Beddows, D.C.S., Beukes, J.P., Collins, D., Ding, A., Harrison, R. M., Henzing, B., Hooda, R., Hu, M., Hõrrak, U., Kivekäs, N., Komsaare, K., Krejci, R., Kristensson, A., Laakso, L., Laaksonen, A., Leaitch, W.R., Lihavainen, H., Mihalopoulos, N., Németh, Z., Nie, W., O'dowd, C., Salma, I., Sellegri, K., Svenningsson, B., Swietlicki, E., Tunved, P., Ulevicius, V., Vakkari, V., Vana, M., Wiedensohler, A., Wu, Z., Virtanen, A., Kulmala, M., 2018. Global analysis of continental boundary layer new particle formation based on long-term measurements. Atmos. Chem. Phys. 18, 14737–14756. https://doi.org/10.5194/acp-18-14737-2018.

Paasonen, P., Kupiainen, K., Klimont, Z., Visschedijk, A., Denier van der Gon, H.A.C., Amann, M., 2016. Continental anthropogenic primary particle number emissions. Atmos. Chem. Phys. 16 (11), 6823–6840. https://doi.org/10.5194/acp-16-6823-2016.

Park, K., Park, J.Y., Kwak, J.-H., Cho, G.N., Kim, J.-S., 2008. Seasonal and diurnal variations of ultrafine particle concentration in urban Gwangju, Korea: observation of ultrafine particle events. Atmos. Environ. 42 (4), 788–799. https://doi.org/10.1016/J.ATMOSENV.2007.09.068.

Pedregosa, F., Varoquaux, G., Gramfort, A., Michel, V., Thirion, B., Grisel, O., Blondel, M., Prettenhofer, P., Weiss, R., Dubourg, V., Vanderplas, J., Passos, A., Cournapeau, D., Brucher, M., Perrot, M., Duchesnay, É., 2011. Scikit-learn: machine learning in Python. Oct J. Mach. Learn. Res. 12, 2825–2830 [online] Available from: http://jmlr.csail.mit.edu/papers/v12/pedregosa11a.html.

Pérez, N., Pey, J., Castillo, S., Viana, M., Alastuey, A., Querol, X., 2008. Interpretation of the variability of levels of regional background aerosols in the Western Mediterranean. Sci. Total Environ. 407 (1), 527–540. https://doi.org/10.1016/J.SCITOTENV.2008.09.006.

Pey, J., Querol, X., Alastuey, A., Rodríguez, S., Putaud, J.P., Van Dingenen, R., 2009. Source apportionment of urban fine and ultra-fine particle number concentration in a Western Mediterranean city. Atmos. Environ. Times 43 (29), 4407–4415. https://doi.org/10.1016/J.ATMOSENV.2009.05.024.

Pikridas, M., Riipinen, I., Hildebrandt, L., Kostenidou, E., Manninen, H., Mihalopoulos, N., Kalivitis, N., Burkhart, J.F., Stohl, A., Kulmala, M., Pandis, S.N., 2012. New particle formation at a remote site in the Eastern Mediterranean. J. Geophys. Res. Atmos. 117 (D12) https://doi.org/10.1029/2012JD017570 n/a-n/a.

Pöschl, U., 2005. Atmospheric aerosols: composition, transformation, climate and health effects. Angew. Chem. Int. Ed. 44 (46), 7520–7540. https://doi.org/10.1002/anie.200501122.

Querol, X., Gangoiti, G., Mantilla, E., Alastuey, A., Minguillón, M.C., Amato, F., Reche, C., Viana, M., Moreno, T., Karanasiou, A., Rivas, I., Pérez, N., Ripoll, A., Brines, M., Ealo, M., Pandolfi, M., Lee, H.-K., Eun, H.-R., Park, Y.-H., Escudero, M., Beddows, D., Harrison, R.M., Bertrand, A., Marchand, N., Lyasota, A., Codina, B., Olid, M., Udina, M., Jiménez-Esteve, B., Soler, M.R., Alonso, L., Millán, M., Ahn, K.-H., 2017. Phenomenology of high-ozone episodes in NE Spain. Atmos. Chem. Phys. 17 (4), 2817–2838. https://doi.org/10.5194/acp-17-2817-2017.

Querol, X., Alastuey, A., Gangoiti, G., Perez, N., Lee, H.K., Eun, H.R., Park, Y., Mantilla, E., Escudero, M., Titos, G., Alonso, L., Temime-Roussel, B., Marchand, N., Moreta, J.R., Revuelta, M.A., Salvador, P., Artíñano, B., García dos Santos, S., Anguas, M., Notario, A., Saiz-Lopez, A., Harrison, R.M., Millán, M., Ahn, K.-H., 2018. Phenomenology of summer ozone episodes over the Madrid metropolitan area, central Spain. Atmos. Chem. Phys. 18 (9), 6511–6533. https://doi.org/10.5194/acp-18-6511-2018.

Rodríguez, S., Querol, X., Alastuey, A., Viana, M.-M., Mantilla, E., 2003. Events Affecting Levels and Seasonal Evolution of Airborne Particulate Matter Concentrations in the Western Mediterranean. https://doi.org/10.1021/ES020106P.

Salma, I., Borsós, T., Németh, Z., Weidinger, T., Aalto, P., Kulmala, M., 2014. Comparative study of ultrafine atmospheric aerosol within a city. Atmos. Environ. 92, 154–161. https://doi.org/10.1016/J.ATMOSENV.2014.04.020.

Salma, I., Németh, Z., Kerminen, V.-M., Aalto, P., Nieminen, T., Weidinger, T., Molnár, Á., Imre, K., Kulmala, M., 2016. Regional effect on urban atmospheric nucleation. Atmos. Chem. Phys. 16 (14), 8715–8728. https://doi.org/10.5194/acp-16-8715-2016.

Seco, R., Peñuelas, J., Filella, I., Llusià, J., Molowny-Horas, R., Schallhart, S., Metzger, A., Müller, M., Hansel, A., 2011. Contrasting winter and summer VOC mixing ratios at a forest site in the Western Mediterranean basin: the effect of local biogenic emissions. Atmos. Chem. Phys. 11 (24), 13161–13179. https://doi.org/10.5194/acp-11-13161-2011.

Stafoggia, M., Schneider, A., Cyrys, J., Samoli, E., Andersen, Z.J., Bedada, G.B., Bellander, T., Cattani, G., Eleftheriadis, K., Faustini, A., Hoffmann, B., Jacquemin, B., Katsouyanni, K., Massling, A., Pekkanen, J., Perez, N., Peters, A., Quass, U., Yli-Tuomi, T., Forastiere, F., 2017. Association between short-term exposure to ultrafine particles and mortality in eight European urban areas. Epidemiology 28 (2), 172–180. https://doi.org/10.1097/EDE.0000000000000599.

Tobías, A., Rivas, I., Reche, C., Alastuey, A., Rodríguez, S., Fernández-Camacho, R., Sánchez de la Campa, A.M., de la Rosa, J., Sunyer, J., Querol, X., 2018. Short-term effects of ultrafine particles on daily mortality by primary vehicle exhaust versus

secondary origin in three Spanish cities. Environ. Int. 111, 144–151. https://doi.org/10.1016/J.ENVINT.2017.11.015.

Toll, I., Baldasano, J.M., 2000. Modeling of photochemical air pollution in the Barcelona area with highly disaggregated anthropogenic and biogenic emissions. Atmos. Environ. 34 (19), 3069–3084. https://doi.org/10.1016/S1352-2310(99)00498-7.

Valverde, V., Pay, M.T., Baldasano, J.M., 2016. Ozone attributed to Madrid and Barcelona on-road transport emissions: characterization of plume dynamics over the iberian Peninsula. Sci. Total Environ. 543, 670–682. https://doi.org/10.1016/J.SCITOTENV.2015.11.070.

Vanhanen, J., Mikkilä, J., Lehtipalo, K., Sipilä, M., Manninen, H.E., Siivola, E., Petäjä, T., Kulmala, M., 2011. Particle size magnifier for nano-CN detection. Aerosol Sci. Technol. 45 (4), 533–542. https://doi.org/10.1080/02786826.2010.547889.

Wang, D., Zhou, B., Fu, Q., Zhao, Q., Zhang, Q., Chen, J., Yang, X., Duan, Y., Li, J., 2016. Intense secondary aerosol formation due to strong atmospheric photochemical reactions in summer: observations at a rural site in eastern Yangtze River Delta of China. Sci. Total Environ. 571, 1454–1466. https://doi.org/10.1016/J.SCITOTENV.2016.06.212.

WHO, 2006. WHO Air Quality Guidelines for Particulate Matter, Ozone, Nitrogen Dioxide and Sulfur Dioxide.

Wonaschütz, A., Demattio, A., Wagner, R., Burkart, J., Zíková, N., Vodička, P., Ludwig, W., Steiner, G., Schwarz, J., Hitzenberger, R., 2015. Seasonality of new particle formation in Vienna, Austria – influence of air mass origin and aerosol chemical composition. Atmos. Environ. 118, 118–126. https://doi.org/10.1016/J.ATMOSENV.2015.07.035.

Supplement of

Relating high ozone, ultrafine particles, and new particle formation episodes using cluster analysis

Carnerero et al (2019)

Table S1: Qualitative summary of the days in each O_3 cluster before grouping (see also Figure S1). * EU information value: hourly O_3 concentration average exceeds 180 µg m^{-3}. ** EU target value: O_3 concentrations exceed 120 µg m^{-3} for the maximum 8-h moving daily averages in at least 25 days as an average for 3 years. Cluster 2 was identified as cluster "extreme". Clusters 9 and 3 were grouped into cluster "high". Clusters 0, 1, 7 and 8 were grouped into cluster "mild". Clusters 4, 5 and 6 were grouped into cluster "low".

Clusters	**0**	**1**	**2**	**3**	**4**	**5**	**6**	**7**	**8**	**9**
Number of days	97	112	59	122	58	128	48	58	85	96
Temporal distribution	Early spring and late summer	Whole period	June and July	May, June and July	Early and late summer	Early spring and late summer	Early spring and late summer	Whole period	Early spring and late summer	Whole period
Days exceeding information value *	0	0	8	0	0	0	0	0	0	0
Days exceeding EU target value **	7	0	59	51	0	0	0	5	0	53
Temperature	High	Intermediate	Highest	High	Lowest	Low	Low	Intermediate	Intermediate	High
Relative humidity	Intermediate	Intermediate	Lowest	Low	Highest	High	Very high	High	High	Low
Wind speed	Intermediate	High	Highest	High	Lowest	Low	Very low	Intermediate	Low	High
Solar radiation	Intermediate	Intermediate	Highest	Very high	Lowest	Low	Lowest	Intermediate	Low	Intermediate
$N_{9\text{-}855}$	High	Intermediate	Highest	High	Low	Intermediate	Lowest	Intermediate	Intermediate	Intermediate
$N_{9\text{-}25}$	Intermediate	High	Highest	High	Lowest	Intermediate	Lowest	Intermediate	Low	High
CS	High	Very low	Highest	High	Very low	Very low	Lowest	Intermediate	Intermediate	Intermediate
BC	High	Intermediate	Highest	High	Lowest	Intermediate	Very low	High	Intermediate	High
SO_2	High	Low	Highest	High	Very low	Very low	Very low	High	Intermediate	Intermediate
Comments	Intermediate temperature and humidity, pollutants and precursors are transported	Low temperature, intermediate humidity, low transport	Very hot and dry summer days, strong transport of pollutants and precursors	Hot and dry summer days, pollutants and precursors are transported	Cool and humid days, no pollutants or precursors are transported	Cool and humid days with low transport of pollutants and precursors	Cool and humid days, no pollutants or precursors are transported	Intermediate temperature, humid afternoons, with moderate transport	Intermediate temperature, high humidity, low transport of pollutants and precursors	Intermediate temperature, low humidity, moderate transport

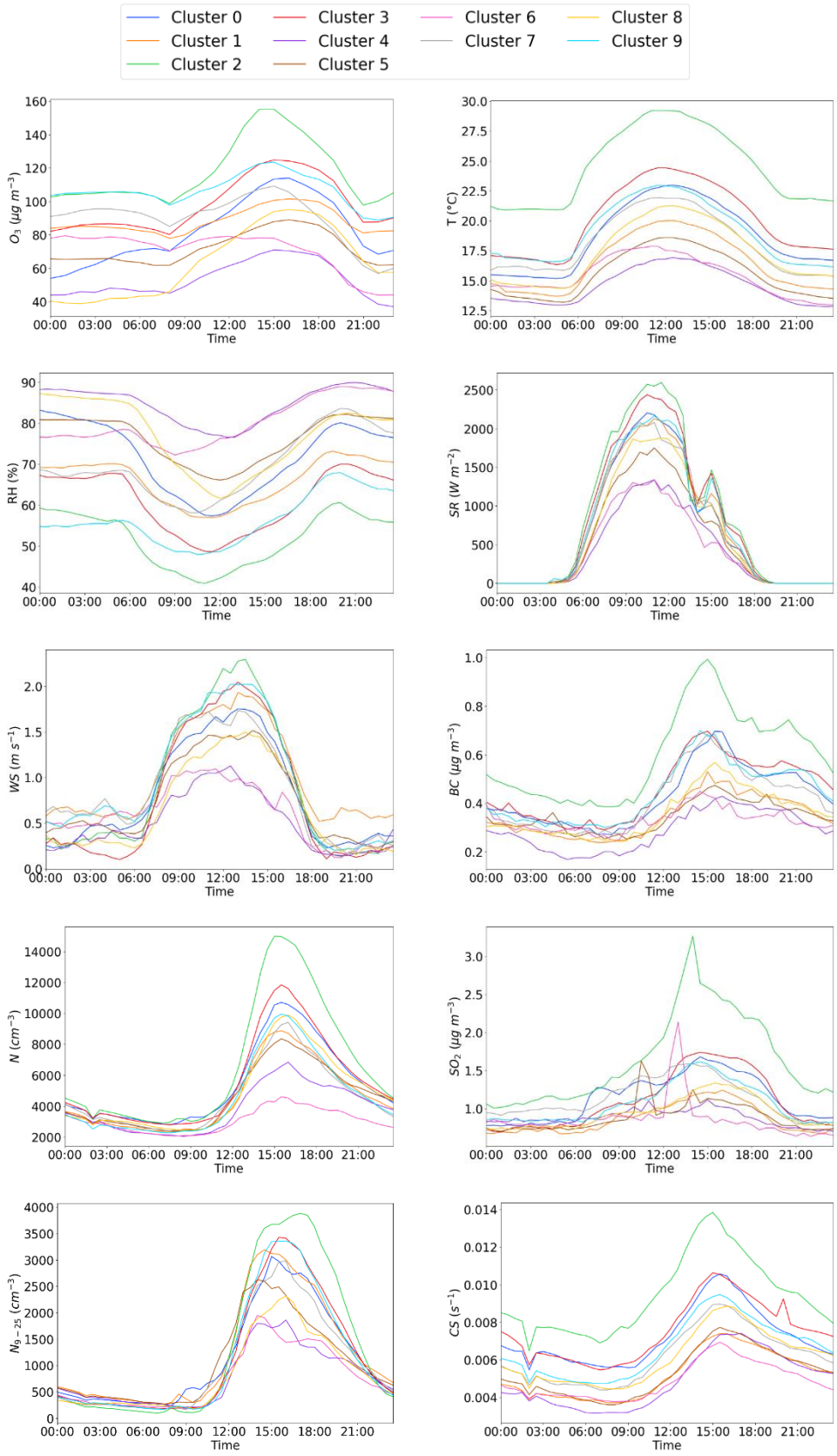

Figure S1: Results of the average O_3 daily cycles after the first level of clustering analysis at Montseny for the time period 01/04/2014 – 30/09/2018.

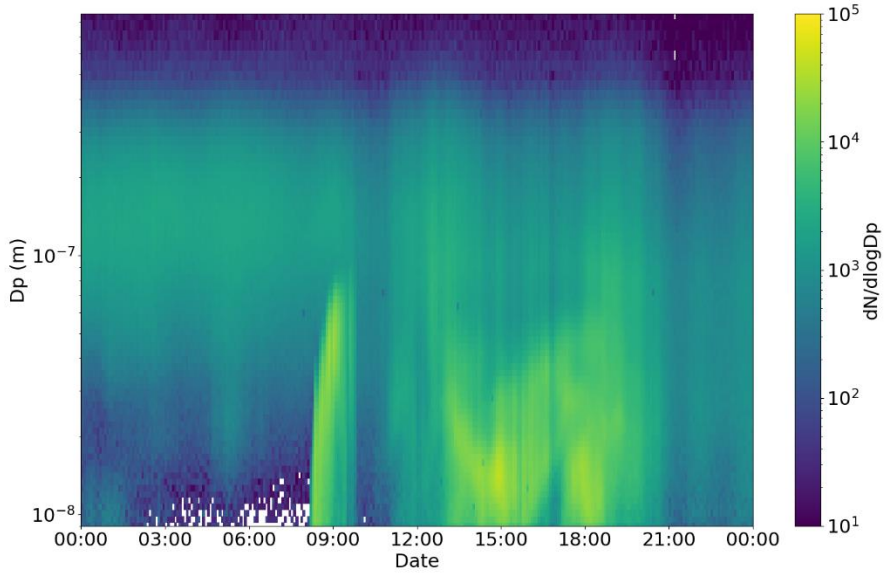

Figure S2: Example of a burst-like new particle formation event at Montseny on 29 August 2017 06:00 UTC.

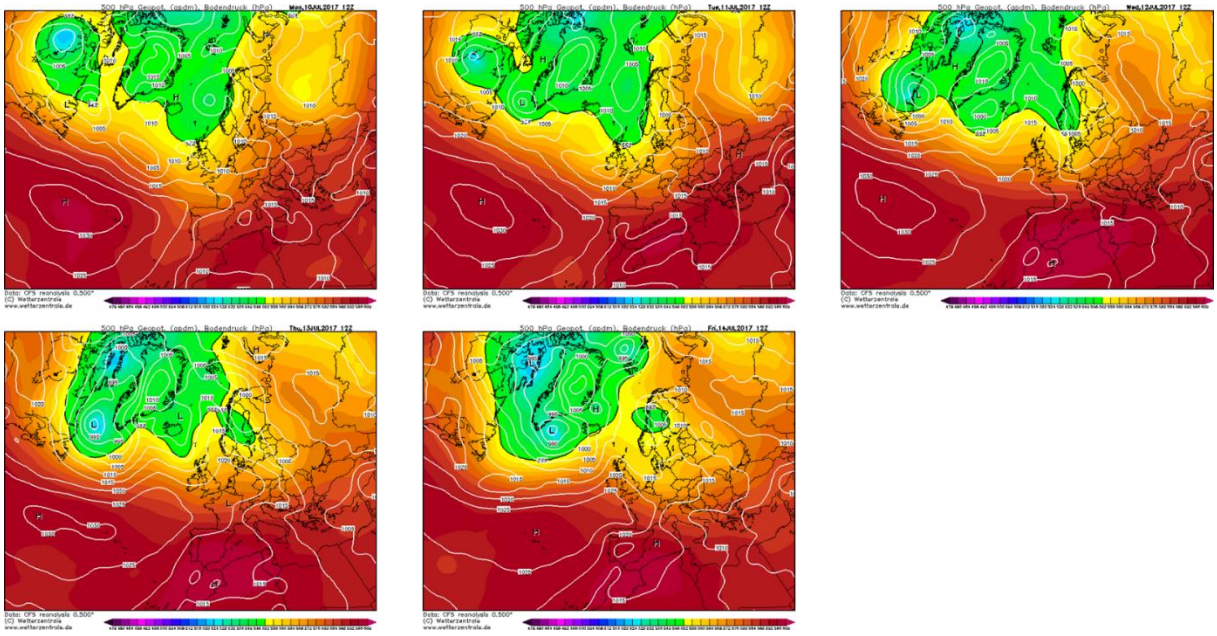

Figure S3: Geopotential height at 500 hPa and mean sea level pressure at 12:00 UTC for Case C (10 – 14 July 2017).

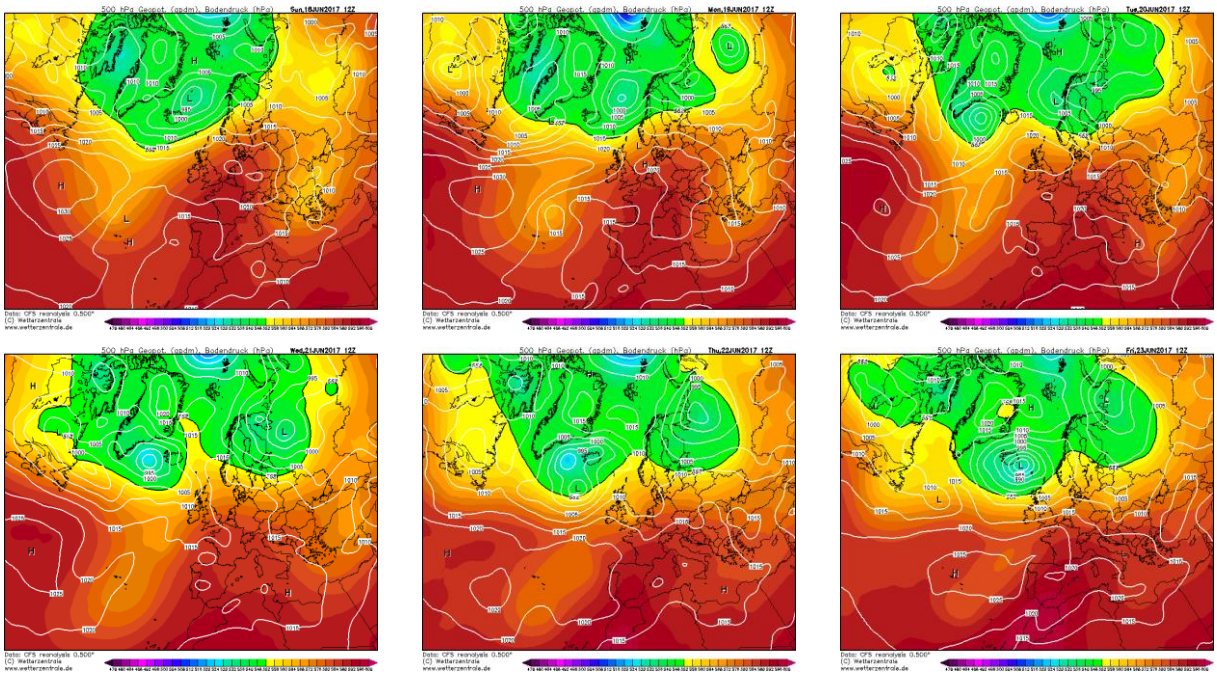

Figure S4: Geopotential height at 500 hPa and mean sea level pressure at 12:00 UTC for Case A (18 – 23 June 2017).

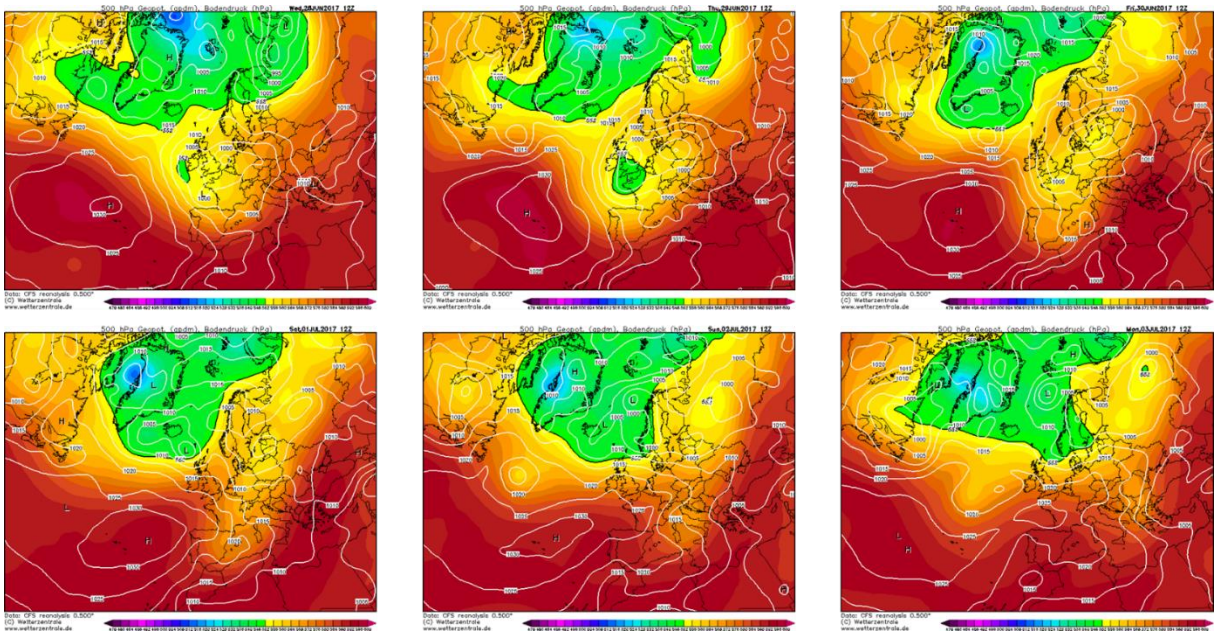

Figure S5: Geopotential height at 500 hPa and mean sea level pressure at 12:00 UTC for Case B (28 June – 3 July 2017).

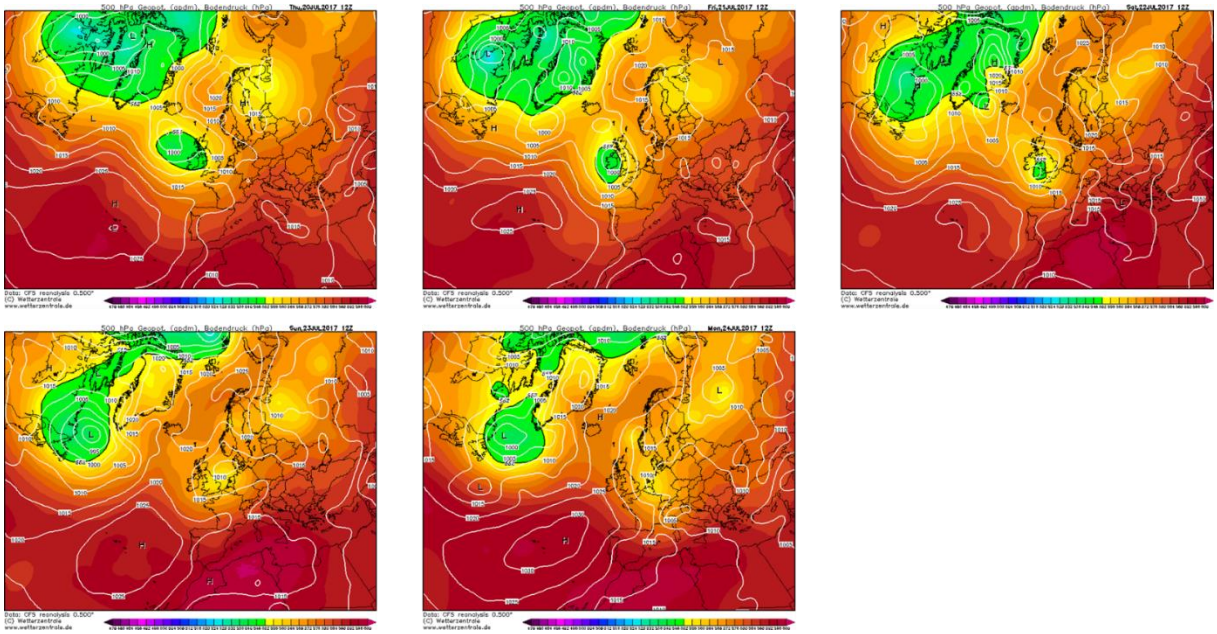

Figure S6: Geopotential height at 500 hPa and mean sea level pressure at 12:00 UTC for Case C (20 – 24 July 2017).

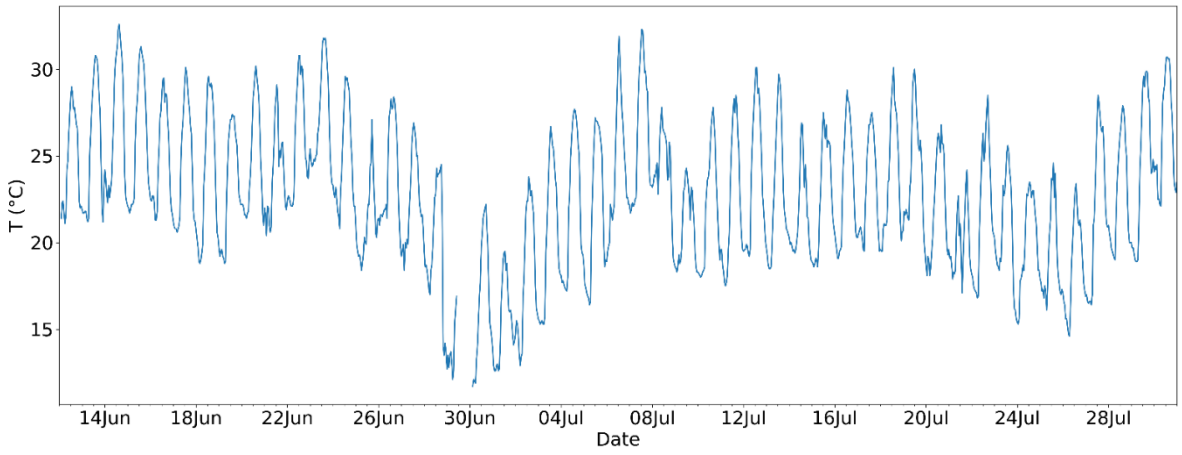

Figure S7: Temperature registered at Montseny from 12 June - 31 July 2017.

3.4 Paper III

Trends in primary and secondary particle number concentrations in urban and regional environments in NE Spain

Carnerero, C., Rivas, I., Reche, C., Pérez, N., Alastuey, A. and Querol, X.

Published in *Atmospheric Environment* on October 6, 2020

https://doi.org/10.1016/j.atmosenv.2020.117982

Atmospheric Environment 244 (2021) 117982

Contents lists available at ScienceDirect

Atmospheric Environment

journal homepage: http://www.elsevier.com/locate/atmosenv

Trends in primary and secondary particle number concentrations in urban and regional environments in NE Spain

Cristina Carnerero [a,b,*], Ioar Rivas [c], Cristina Reche [a], Noemí Pérez [a], Andrés Alastuey [a], Xavier Querol [a]

[a] Institute of Environmental Assessment and Water Research (IDAEA-CSIC), Barcelona, 08034, Spain
[b] Dept. of Civil and Environmental Engineering, Universitat Politècnica de Catalunya, Barcelona, 08034, Spain
[c] ISGlobal, Barcelona Institute for Global Health, Barcelona, 08036, Spain

HIGHLIGHTS

- Decreasing traffic emissions in cities could favour photonucleation in high-insolated rural areas.
- We measured gaseous pollutants, black carbon and particle size distributions.
- We statistically analysed trends and applied positive matrix factorisation receptor modelling.
- Reducing emissions in cities increases the number of particles in nearby rural areas.
- Policies aimed at improving air quality in cities may negatively affect nearby rural regions.

ARTICLE INFO

Keywords:
Ultrafine particles
New particle formation
Trend analysis
Photonucleation
Positive matrix factorisation receptor model

ABSTRACT

We analysed long-term datasets of ambient air concentrations of gaseous pollutants, black carbon (BC) and particle size distributions at an urban background air quality station (Barcelona, Spain; 2013–2019) and a regional background station (Montseny, Spain; 2014–2019). Using BC as a tracer of primary emissions, we segregated the aerosol load in modes and analysed their trends, considering all-year data and seasons separately. We also applied the positive matrix factorisation (PMF) receptor model to the particle size distributions to identify different sources that contribute to the particle number concentration. Our results show that the number concentration of primary particles decreased at the urban and regional background stations (−4.1 and −4.7% per year, respectively) along the period of study. This decrease was also observed for primary particles in the nucleation, Aitken and accumulation modes separately. This change leads to a decrease in condensation sinks (CS, −3.1 and −5.6% per year), that, together with an increase in temperatures (+1.5% per year in the urban background; +1.4% per year in the regional background), results in a markedly increasing trend in the contribution of new particle formation to the total number particle concentration (+17.7% and +11.9% per year). The total particle number concentration decreased in the urban background (−2.5% per year), whereas the trend increased for the regional background (+3.0% per year). The latter result is in contrast to most literature reports and is most likely due to higher insolation and increased biogenic VOC (BVOC) emissions that would enhance photonucleation, along with a marked decrease in the CS. An increasing trend in H_2SO_4 concentrations driven by increasing SO_2 concentrations (+11.1% per year) could also be favouring the formation of new particles in the regional background, but it is not clear that the increasing trend in SO_2 is real or it is related to a faulty maintenance of the instrumentation.

Overall, we conclude that decreasing primary emissions results in a decrease in the total number concentrations of urban aerosols, despite the increase in the formation of new particles by photonucleation. Moreover, the total particle number concentration of regions downwind of the urban areas increases because new particle formation is more favoured and compensates for the primary particles' number concentration decrease.

* Corresponding author. Institute of Environmental Assessment and Water Research (IDAEA-CSIC), Barcelona, 08034, Spain.
E-mail address: cristina.carnerero@idaea.csic.es (C. Carnerero).

https://doi.org/10.1016/j.atmosenv.2020.117982
Received 7 August 2020; Received in revised form 2 October 2020; Accepted 5 October 2020
Available online 6 October 2020

1. Introduction

Nitrogen oxides (NOx) and black carbon (BC) emissions, tracers of road traffic emissions in urban environments, have decreased in high-income cities around the world in the past decades (Colette et al., 2011; Font and Fuller, 2016; Geddes et al., 2016; Guerreiro et al., 2014; Krecl et al., 2017; Olstrup et al., 2018; Querol et al., 2014). This decrease is a consequence of the implementation of emission abatement policies, including the reduction in vehicle fleet emissions, regardless of trends in urban traffic intensity.

Despite the clear health benefits from reducing primary emissions, cleaner environments might increase the formation or decrease the consumption of secondary pollutants, such as tropospheric ozone (O_3, due to a decreased titration by NO), and the production of newly generated secondary particles, due to a decline in condensation sinks (CS) favouring nucleation (Kerminen et al., 2018 and references therein). Thus, particle number concentrations may increase despite a decrease in primary pollutant emissions (Wichmann et al., 2000).

Ultrafine particles (UFPs; particles less than 100 nm in diameter) might have serious adverse health effects, including oxidative stress with DNA damage, which can lead to carcinogenic mutations and pulmonary diseases (Bräuner et al., 2007; Lanzinger et al., 2016). Furthermore, their health impact is enhanced because, when inhaled, a proportion of these particles might translocate to the lung and reach different body organs (Cassee et al., 2011). In spite of this, UFPs are not regulated in air quality standards and, therefore, no efforts are being made to reduce their ambient concentrations. In urban environments, road traffic is the main source of directly emitted UFPs (Paasonen et al., 2016), followed by non-road transport and domestic fuel burning (Kumar et al., 2014). Furthermore, UFPs may be newly formed in the atmosphere as a result of the reaction of gaseous precursors in favourable conditions. Atmospheric new particle formation (NPF) dominates the total particle concentration in the global troposphere (Gordon et al., 2017), but its contribution varies in different environments (Kerminen et al., 2018; Ma and Birmili, 2015; Nieminen et al., 2018).

In regional environments located near polluted cities, NPF may be favoured under low UFP concentrations (Carnerero et al., 2019). Transported air masses with high UFP concentrations, although enriched with precursors, increase CS levels and inhibit NPF (Wichmann et al., 2000). Thus, a decrease in urban emissions could lead to an increase in NPF in nearby regional environments. If, on the other hand, the aerosol load decreases, a decreased radiative forcing would potentially produce rapid warming rates (Kloster et al., 2008; Makkonen et al., 2012).

Here, we aim to evaluate and compare trends in the contribution of primary and secondary sources and NPF to the total particle number concentration (N) and the mode-segregated N in urban and regional background environments in the area of Barcelona (NE Spain) using a long time series (2013–2019 and 2014–2019, respectively). We use BC as an indicator of primary combustion-related emissions, and positive matrix factorisation (PMF) receptor modelling applied to the particle size distribution (PSD) to apportion primary and secondary contributions to the aerosol population.

2. Methodology

2.1. Monitoring stations

In this study, we use data collected at two air quality research supersites located in NE Spain: Barcelona, an urban background site into the city, and Montseny, a regional background site located into the Montseny Natural Park, 48 km NE of Barcelona (see Fig. S1 for the detailed location of the stations). Both stations are integrated into the European Aerosols, Clouds and Trace gases Research InfraStructure network (ACTRIS), and the atmospheric pollution monitoring and forecasting network of the Government of Catalonia (XVPCA).

2.1.1. Barcelona (urban background)

The station is located in the Institute of Environmental Assessment and Water Research (IDAEA; 41° 23′14.28″N, 2°6′56.34″E, 77 m a.s.l.). The site is located 200 m from one of the busiest streets in Barcelona. The data presented here correspond to the period 2013–2019.

Black carbon (BC) concentrations were measured with a multi-angle absorption photometer (MAAP; Thermo Scientific). Levels of O_3 were determined with a UV photometry based analyser (MCV 48AV); SO_2 concentrations were measured with a UV fluorescence analyser (Teledyne T100 EU); NO_2 levels were registered with a chemiluminescence analyser (Model 42i-TL; Thermo Scientific), and CO was measured with a gas filter correlation analyser (Teledyne T300 EU). Particle number size distributions (PNSD) were measured with a scanning mobility particle spectrometer (SMPS; TSI 3080) connected to a condensation particle counter (CPC; TSI 3772). We discarded the lower range (10–15 nm) of the distribution due to an instrument malfunction during a considerable length of the time series considered in this study. The distribution used in this study includes size ranges from 15 to 478 nm. Using the PNSD, we calculated the total particle number (N; 15–478 nm), nucleation-mode number concentration (N_{nuc}; 15–25 nm), Aitken-mode number concentration (N_{Ait}; 25–100 nm) and accumulation-mode number concentration (N_{acc}; 100–478 nm).

Meteorological parameters were measured at the rooftop of the University of Barcelona, Faculty of Physics, located 350 m from the urban background station.

2.1.2. Montseny (regional background)

The station is located in a natural environment in the Montseny Natural Park (41°46′45.63″N, 02°21′28.92″E, 720 m a.s.l.). It lies in a forested valley oriented in a northwest-southwest direction, 48 km NE of Barcelona. When sea and mountain breezes are sufficiently strong—mostly in spring and summer, when solar irradiance is high—emissions originated in industrial and urban areas nearby are channelled inland and reach the station because of the complex orography in the area. In these cases, high UFP and O_3 concentrations are registered, whereas NPF is less favoured due to an increased CS (Carnerero et al., 2019). The data presented here correspond to the period 2014–2019. Note that the data series begins one year later than in Barcelona because of substantial data gaps in 2013.

Particle number size distribution in the size range 9–856 nm was measured with a mobility particle size spectrometer (MPSS; TROPOS) connected to a condensation particle counter (CPC; TSI 3772). Levels of BC, O_3, SO_2, NO_2 and CO were measured with the same instruments used at the urban site. Meteorological data were obtained using an automatic station (Davis Vantage Pro Plus).

Analogously to the urban background station, we calculated the total particle number (N; 9–856 nm), N_{nuc} (9–25 nm), N_{Ait} (25–100 nm) and N_{acc} (100–856 nm). Despite having different size ranges, we consider that N_{acc} is comparable at both sites, given that particles larger than 478 nm (the maximum diameter detected by the SMPS at the urban background) do not contribute significantly to the number concentration. However, N_{nuc} may not be directly comparable between stations, given that we do not consider particles between 9 and 15 mm at the urban background, and this will be taken into account when discussing the results.

2.2. Data analysis

We averaged all measured variables to hourly values in order to carry out a homogeneous data analysis. All times are expressed in coordinated universal time (UTC), unless otherwise stated. Local time is UTC +2 h in summer and UTC +1 h in winter.

2.2.1. Contributions of primary and secondary particles

Following the methodology proposed by Rodríguez and Cuevas (2007) and later improved by Kulmala et al. (2016), we used BC as a

tracer for primary particles to distinguish primary (N_1) and secondary (N_2) contributions to N, N_{nuc}, N_{Ait} and N_{acc}. According to this method, the minimum emission of primary particles, N_1, is estimated using the following expression:

$$N_1 = s_1\ BC, \tag{1}$$

where s_1 (particles per unit of BC) is a scaling factor determined with observations of particle number and BC. Throughout this study, we calculated s_1 as the 1st percentile of the ratio N/BC. In other words, in the N vs BC scatter-plot, 1% of the data points are located below a line with a slope equal to s_1.

Considering that the total particle number is the sum of primary and secondary particles, the number concentration of secondary particles that may occur during the dilution of the vehicle exhaust or in ambient air, N_2, is estimated using:

$$N_2 = N - N_1. \tag{2}$$

It has to be noted that only particles containing BC are considered as primary particles; therefore, there might be non-BC-related particles that fall into N_2 when using this method.

Equations *1* and *2* have been used analogously for the mode-segregated particle numbers N_{nuc}, N_{Ait}, and N_{acc}, as in (Kulmala et al., 2016) to calculate $N1_{nuc}$, $N1_{Ait}$, $N1_{acc}$, $N2_{nuc}$, $N2_{Ait}$ and $N1_{acc}$.

2.2.2. Mann-Kendall tests

All trends presented here were obtained using *pymannkendall*, a Python package for Mann-Kendall tests (Hussain and Mahmud, 2019). The Mann-Kendall test is a non-parametric trend test used to evaluate monotonic trends. The Mann Kendall test statistic is calculated as follows:

$$\mathrm{S} = \sum_{k=1}^{n-1} \sum_{j=k+1}^{n} sgn\left(X_j - X_k\right), \tag{3}$$

where *sgn* (x) is the sign function.

If S is positive (negative), the variable X has a monotonically increasing (decreasing) trend, provided that the p-value indicates statistical significance ($p < 0.05$).

Through this work, we present two types of tendencies. Firstly, we calculated Mann-Kendall tests for all data. Separately, we subsetted 3-month data corresponding to winter (DJF; December-January-February), spring (MAM; March-April-May), summer (JJA; June-July-August) or autumn (SON; September-October-November) and computed independent Mann-Kendall tests. In all cases, the data used are the daily averages of the variable, considering only days with at least 75% of data availability.

When the Mann-Kendall test suggests a significant trend, the Theil-Sen method is applied to quantify the magnitude of the trend by means of the Sen's slope estimator (Sen, 1968; Theil, 1992), calculated as the median slope of all data pairs in X (Eq. (4)). Using the estimator, we calculated the average percent change per year for each variable, considering all year data and seasons separately.

$$\mathrm{m} = median\left\{\frac{x_j - x_i}{j - i}\right\} \tag{4}$$

2.2.3. Positive matrix factorisation (PMF)

The positive matrix factorisation receptor model (PMF; Paatero, 1997) was used to identify and quantify the sources of the PNSD at each station. The model was conducted with Multilinear Engine 2 (ME-2; Paatero (1999)), using R (version 3.6.1; R Development Core Team (2017)), following the methodology described in Rivas et al. (2020). PMF is a multivariate least-squares method that presumes that the observed aerosol size distribution, *X*, considered as a matrix with dimensions *n* observations x *m* size bins, can be determined by means of a source matrix, *F*, and a contribution matrix, *G*:

$$x_{ij} = \sum_{k=1}^{p} g_{ik} f_{jk} + e_{ij}, \tag{5}$$

where *p* is the number of independent sources, F_{jk} is the concentration of the component emitted by the *k*th source in the *j*th size bin, G_{ik} is the contribution of the *k*th source to the *i*th sample, and *E* is a residual matrix.

To identify and apportion the sources of PNSD, hourly averages of the PNSD were used in combination with hourly concentrations of gaseous pollutants (NO, NO_2, O_3, SO_2 and CO), and meteorological variables (temperature, wind speed and relative humidity). Solar radiation measurements were also used for Montseny, but not for Barcelona, because the residuals did not meet the normality condition.

The uncertainty matrix is calculated as follows:

$$s_{ij} = \alpha_j \cdot \left(N_{ij} + \overline{N_j}\right) + C_3 \cdot N_{ij}, \tag{6}$$

where α and C_3 are constants, N_{ij} is the concentration of sample *i* for the size bin or pollutant *j*, and $\overline{N_j}$ is the average concentration of the size bin or pollutant *j*. Values for α and C_3 were empirically determined (0.01 and 0.1 for the urban background dataset, and 0.04 and 0.12 for the regional background dataset). We assigned higher uncertainties to the lower and higher ends of the particle size distribution (2α for the first and last 3% size bins, and 1.5α for the following 3% bins). Moreover, we used a scaling factor of 5α for the gaseous pollutants, which was empirically determined so that the residuals were randomly distributed around zero. For detailed information on the methodology used for PMF, see Rivas et al. (2020).

3. Results

3.1. Urban background

Fig. 1 shows daily cycles of BC, O_3, SO_2, N and CS. Table 1 provides all-year and season-separated average annual trends for all variables discussed in this subsection.

BC concentrations peak at 7 UTC and 19 UTC in Barcelona, coinciding with the typical morning and afternoon traffic rush hours. Monotonically decreasing BC concentrations over all the period (−4.2% per year) and in all seasons, suggest a decrease in primary emissions, particularly those coming from road traffic.

The daily evolution of O_3 concentrations follows that of solar radiation, with marked decreases around the traffic rush hours due to titration by NO, and is maximal in summer. Overall, O_3 decreases when using all-year data (−2.7% per year). Considering seasons separately, O_3 decreases all seasons except in spring.

SO_2 concentrations follow a typical sea breeze pattern, peaking at noon. The main source of SO_2 in Barcelona is shipping emissions that are transported inland from the harbour and the Mediterranean Sea to the urban background station with the sea breeze. During the period considered in this study, SO_2 concentrations had a monotonic decrease (−2.0% per year). Moreover, concentrations have radically decreased since 2009 (not shown here) pointing to a decrease in the SO_2 emissions emitted by freight ships and cruises, as reported by (Schembari et al., 2012) in Western Mediterranean harbours after the European directive 2005/33/EC, implemented in 2010.

The number of particles in the size range 15–478 nm (N) peaks at 7 UTC and 19 UTC, and has a secondary peak at 12 UTC, especially marked in summer and spring, when the high insolation favours NPF. N decreases throughout all the period (−2.5% per year), and in spring and autumn, although there is no significant trend in winter and summer.

CS has a similar evolution to BC and N, peaking later (8 UTC and 21 UTC). Moreover, in between the peaks at midday—when NPF is more likely—CS levels do not decrease as much as they do during the night. When considering all-year trends, CS decreases in Barcelona (−3.1% per

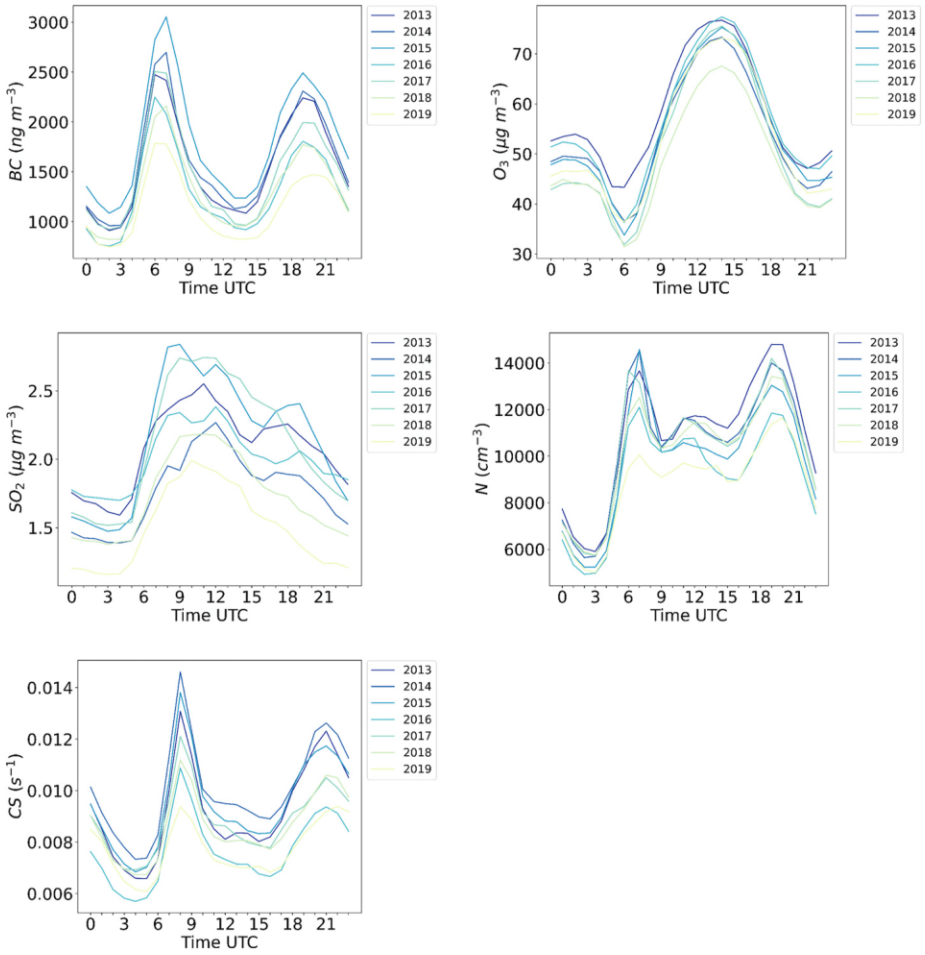

Fig. 1. Daily cycles of black carbon (BC), ozone (O_3), sulphur dioxide (SO_2), number of particles in the size range 15–478 nm (N) and condensation sink (CS), separated by annual averages from 2013 to 2019 at Barcelona (urban background).

year). Calculating the trends separately for seasons, CS decreases only in spring and autumn.

Temperature has an increasing trend when considering all-year data (+1.5% per year). When considering seasons separately, the trend is increasing for all seasons except in autumn, with a slight decreasing trend (−0.5% per year).

N_{nuc} has a clear seasonal evolution. In general, N_{nuc} peaks at noon and has two minor peaks at 7 UTC and 19 UTC. However, in winter, the noon peak is unnoticeable, whereas in summer, the midday peak is twice as high as the morning and afternoon peaks (not shown here). N_{nuc} does not follow a significant monotonic trend in the period of study. Taking into account that the size range 15–25 nm includes both primary and secondary emissions, this may suggest that the decrease in primary emissions might compensate for any possible increases in NPF favoured by the decrease in CS and the increase in temperature. This will be further analysed in more depth in this section by separating primary and secondary contributions to N, and PMF modelling in sections 3.1.1 and 3.1.2. It should be noted that ignoring the SMPS size bins from 10 to 15 nm (see Sect. 2.1.1) most likely has an increased effect on the NPF than on the primary particles in the size range 15–25 nm.

N_{Ait} has a similar evolution to that of N, with a lower contribution at midday. However, there is clearly a slight increase at midday from spring to autumn, corresponding to newly formed particles that have increased to 25 nm. Throughout the study period, N_{Ait} decreases when considering all-year data (−4.1% per year) and in all seasons separately.

The daily evolution of N_{acc} is similar to that of BC, peaking at 7 and 20 UTC. This agrees with a decreasing trend overall (−3.8% per year), and in all seasons except in summer, when the trend is not statistically significant.

3.1.1. *Primary and secondary particle number concentrations*

The primary contribution to the total number of particles (N1), as well as to the different modes considered ($N1_{nuc}$, $N1_{Ait}$, $N1_{acc}$), have a clear traffic pattern, with morning and afternoon peaks (Fig. 2). $N1_{Ait}$ contributes the most to N1, followed by $N1_{acc}$. They all decrease over the entire period (−4.1% per year for N1 and -4.2% per year the mode-segregated N1) and in all seasons, agreeing with the trend in BC.

The secondary contribution to the total number of particles (N2), $N2_{nuc}$ and $N2_{Ait}$ have a similar evolution throughout the day (Fig. 2): these peak with the morning and afternoon rush hours, but also at midday, pointing to a formation of particles by photonucleation generating new particles that later grow to over 25 nm. The midday peak is more pronounced in spring and summer in all cases. $N2_{nuc}$ and $N2_{Ait}$ contribute by a similar amount to N2 (Fig. 2). $N2_{acc}$ is mostly constant throughout the day and has no trend for the entire period except for an increase in winter and a decrease in autumn. Its contribution to N2 is smaller than that of the other modes. N2 only has a significant increasing trend in winter. $N2_{nuc}$ increases over all of the period (+2.4% per year) and in winter and autumn. $N2_{Ait}$ decreases when considering all-year data (−2.4% per year) and in autumn.

3.1.2. *PMF barcelona*

The PMF solution that made the most physical sense had four factors (Fig. 3): *NPF* (diameter mode 15 nm), *Fresh traffic* (diameter mode 32 nm), *Aged Traffic* (diameter mode 88 nm) and *Regional Secondary* (diameter modes 16 and 224 nm). This solution is comparable to that

Table 1
Sen's slope of 2013–2019 data at Barcelona (urban background), expressed as an average annual percent change. All year (January–December) and season-separated data are presented. Slopes for variables with non-significant monotonic trends are not shown (indicated with a hyphen).

Variable	All year (% $year^{-1}$)	DJF (% $year^{-1}$)	MAM (% $year^{-1}$)	JJA (% $year^{-1}$)	SON (% $year^{-1}$)
BC	−4.2	−1.5	−1.3	−1.0	−2.2
T	1.5	0.5	0.6	0.5	−0.5
O_3	−2.7	−1.0	–	−1.1	−0.7
SO_2	−2.0	−0.4	−0.5	−2.0	−0.3
CS	−3.1	–	−0.9	–	−3.6
$N_{15\text{-}478}$	−2.5	–	−0.8	–	−1.1
N1 (primary)	−4.1	−1.4	−1.3	−1.0	−2.2
N1 in Nuc. mode	−4.2	−1.5	−1.3	−1.0	−2.2
N1 in Aitk. mode	−4.2	−1.5	−1.3	−1.0	−2.2
N1 in Acc. mode	−4.2	−1.5	−1.3	−1.0	−2.2
N2 (secondary)	–	2.1	–	–	–
N2 in Nuc. mode	2.4	2.1	–	–	1.3
N2 in Aitk. mode	−2.4	–	–	–	−1.3
N2 in Acc. mode	–	1.3	–	–	−3.4
N_{nuc}	–	–	–	–	–
N_{Ait}	−4.1	−1.4	−1.0	−1.2	−1.7
N_{acc}	−3.8	−1.1	−0.8	–	−3.3
Photonucleation (PMF)	17.7	10.7	–	–	15.4
Fresh traffic (PMF)	−4.0	–	−1.4	−1.5	−1.3
Aged traffic (PMF)	−5.3	−1.6	–	−1.4	−3.3
Regional secondary (PMF)	–	–	–	1.8	−2.4

obtained in Rivas et al. (2020) for Barcelona when considering the period 2013–2016. The daily cycles of each factor are presented in Fig. 4. In addition, Fig. S2 shows the average weekly and monthly cycles of each factor.

NPF has a daily distribution similar to that of solar radiation, peaking at 12 UTC. The solution chosen here makes this factor fluctuate around zero before sunrise, with negative contributions to the N that make no physical sense. This is probably due to a compensation in one or more of the other factors. Given that in this study we are assessing trends, and we are interested in the factors' temporal distributions and the changes with time rather than obtaining quantitative data of contributions, we acknowledge this inaccuracy; however, we strongly believe that the conclusions resulting from this section on trends are sound. *NPF* has the highest average daily contribution on 7% of the days considered (Fig. 5) and has a median contribution of 11% to N. The highest dominance (number of days with a higher daily contribution than the other factors) and the highest contribution to N occur in summer (June-July-August; Fig. S3), with 15% of the days and 18% contribution to N, respectively. On days when *NPF* dominates the total number concentration, BC and NO_2 concentrations are at their lowest, as is the relative humidity. Insolation, temperature and O_3 are intermediate. Both the contribution and dominance of this factor increase throughout the period considered here (2013–2019). The Mann-Kendall tests reveal monotonically statistically significant increasing trends when considering the entire period (+17.7% per year; note that for this quantification, only the positive values have been considered; therefore, the quantification of the trend might be inaccurate) and also winter and autumn.

Fresh traffic has a typical traffic daily distribution, with peaks at 7 and 20 UTC (8 and 21 LT in winter, and 9 and 22 LT in summer). The contribution of this factor is higher in the colder seasons (Fig. S4). Overall, *Fresh traffic* has the highest average daily contribution on most days (91% of the days with data availability, Fig. 5). On these days, BC

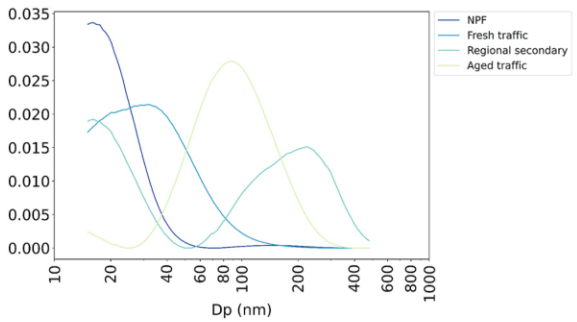

Fig. 3. Normalised factors for the selected solution of the positive matrix factorisation (PMF) for Barcelona (urban background).

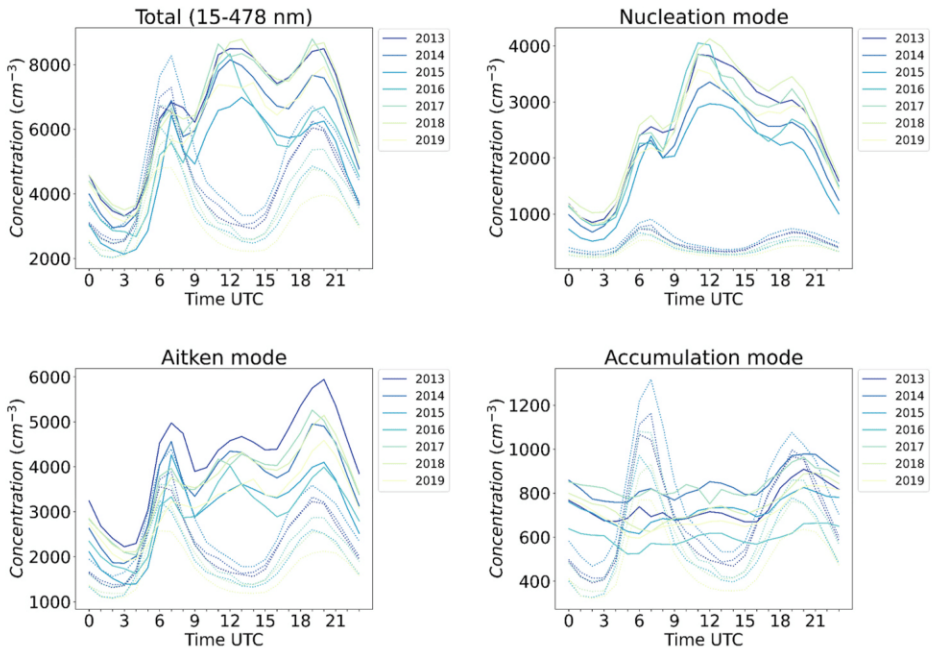

Fig. 2. Daily cycles of primary (dashed) and secondary particles (solid) contributions to the total and mode-segregated aerosol load, separated by annual averages from 2013 to 2019 at Barcelona (urban background).

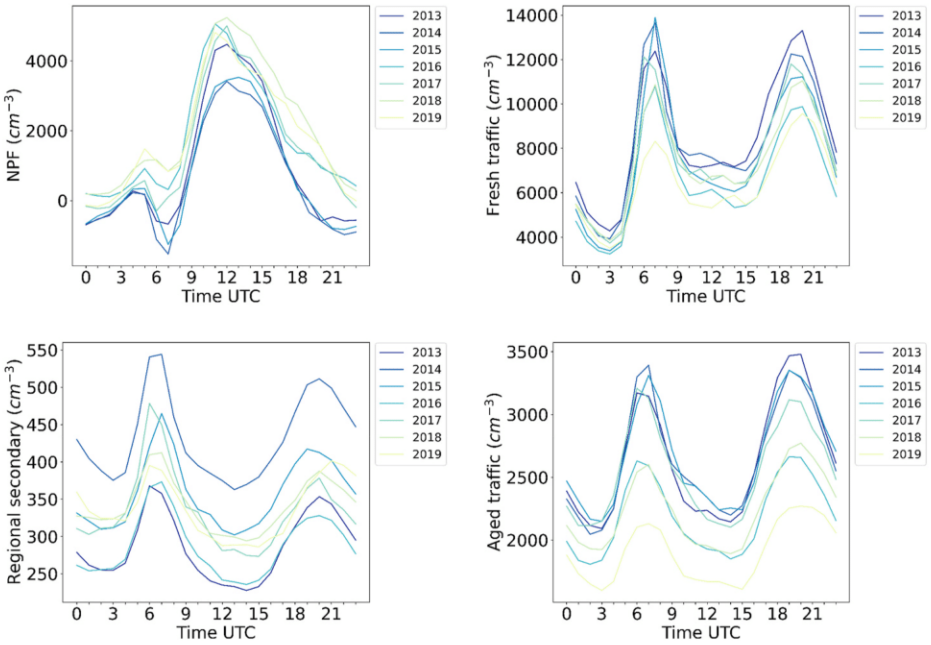

Fig. 4. Daily cycles of the contribution of PMF factors, separated by annual averages from 2013 to 2019 at Barcelona (urban background).

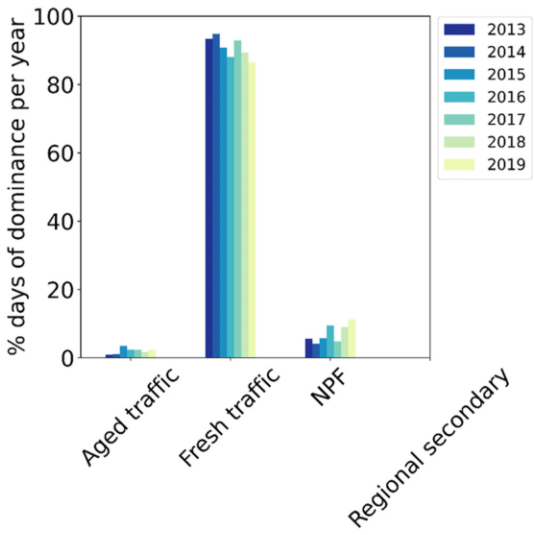

Fig. 5. Percentage of days in which the contribution of each PMF factor dominates the total particle number concentration at Barcelona (urban background), separated by years from 2013 to 2019.

and NO_2 concentrations are at their highest, whereas insolation, temperature and O_3 levels are the lowest. *Fresh traffic* is also the factor that contributes the most to the total number of particles, with a median contribution of 63% to N. The number of days of dominance, the contribution to N and the annual (−4.0% per year) and seasonal tendencies (except in winter) decrease throughout the period considered, agreeing with the decrease in BC concentrations that suggested a reduction in traffic from 2013 to 2019 in Barcelona (Sect. 3.1).

Aged traffic describes the same daily distribution as *Fresh traffic*, but it has a much lower contribution to N. The average contribution of this factor to N is homogeneous throughout the year (Fig. S5). *Aged traffic* dominates only on 2% of the days (Fig. 5) and contributes to a median of 20% of the hourly average of N. Both indicators have a decreasing trend, agreeing with the trends in *Fresh traffic*. On days dominated by *Aged Traffic*, insolation, temperature and O_3 concentrations are higher than days in which other factors dominate. The Mann-Kendall tests also reveal decreasing trends throughout the period (−5.3% per year) and in all seasons except in spring.

The distribution of *Regional Secondary* also peaks at 7 and 20 UTC, suggesting sources related to traffic. There is no significant variation in the contribution of *Regional Secondary* to N along the period of study (Fig. S6). This factor is not to be confused with N2 (particles with a secondary origin; see Sect. 2.2.1). The contribution of *Regional Secondary* to N is the smallest of all factors (2%), and there are no days in which this factor dominates. The trend tests only reveal significant trends in summer (increasing) and autumn (decreasing).

3.2. Regional background

As might be expected, the daily evolution of the concentrations of most pollutants and N at the regional background station in Montseny are markedly different from those at the urban background of Barcelona. As in most mountain sites, patterns affected by sea or mountain breezes are recorded for most variables, instead of typical rush hour patterns: concentrations begin to increase smoothly after sunrise and peak around midday (Fig. 6). Table 2 shows all-year and season-separated average annual percent changes derived from Sen's slopes of all variables discussed in this subsection.

BC concentrations peak around 13 UTC and have a similar daily evolution and magnitude in all seasons. BC decreases monotonically when considering the period 2014–2019 (−4.5% per year) and in spring and autumn. However, when considering winter and summer separately, BC concentrations have no trend. This could be related to biomass burning for household heating in the area during the colder months, and from agriculture, which we expect to be widespread in the rural area.

Temperature increases when considering all-year data (+1.4% per year). When considering seasons separately, up to an increase in +2.6% per year is recorded in winter and spring, whereas the trend is decreasing in autumn.

The evolution of O_3 concentrations is clearly seasonal. Not only are the concentrations higher in summer and spring, but the influence of solar radiation is also markedly higher in the warm period, when the difference in minimum and maximum O_3 levels is around 40 μg m^{-3} as an average, peaking at 13 UTC, whereas in winter, the concentrations are constant throughout the day. O_3 concentrations slightly decrease

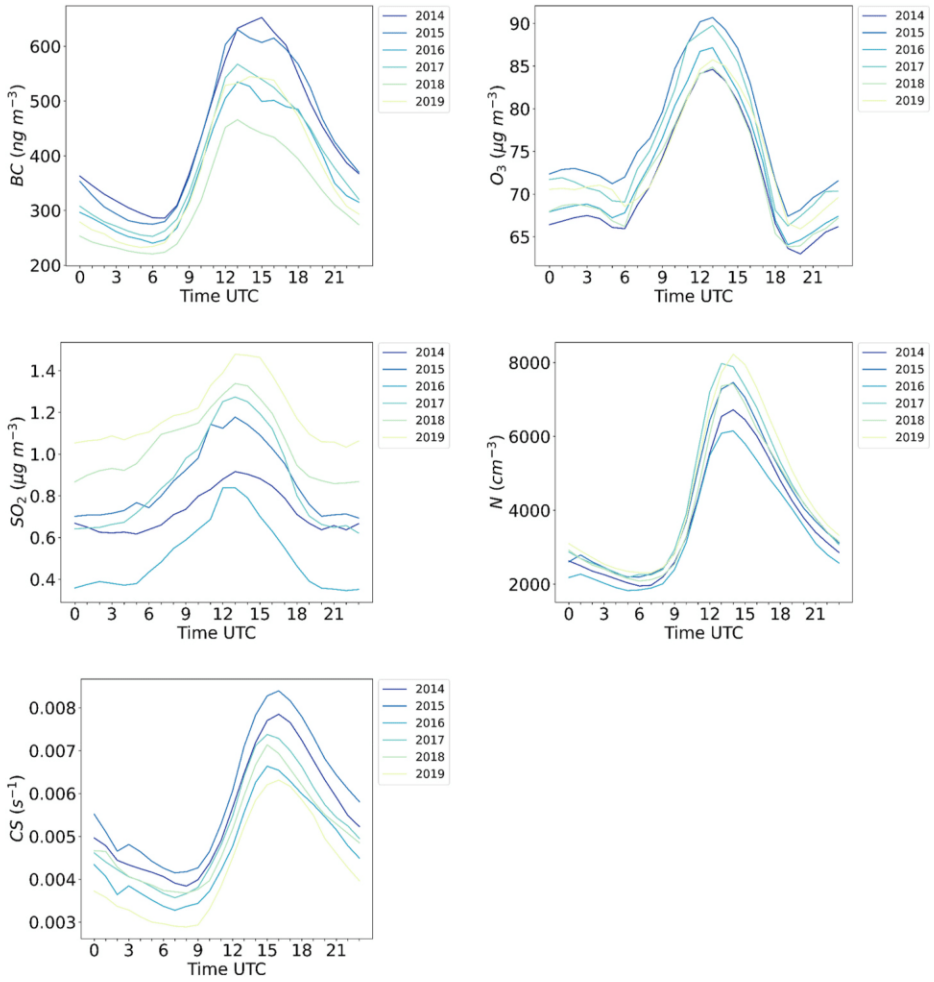

Fig. 6. Daily cycles of black carbon (BC), ozone (O_3), sulphur dioxide (SO_2), number of particles in the size range 9–856 nm (N) and condensation sink (CS), separated by annual averages from 2014 to 2019 at Montseny (regional background).

Table 2
Sen's slope of 2014–2019 data at Montseny (regional background), expressed as an average annual percent change. All year (January–December) and season-separated data are presented. Slopes for variables with non-significant monotonic trends are not shown (indicated with a hyphen).

Variable	All year (% year^{-1})	DJF (% year^{-1})	MAM (% year^{-1})	JJA (% year^{-1})	SON (% year^{-1})
BC	−4.5	–	−5.2	–	−10.4
T	1.4	2.6	2.6	1.9	−2.0
O_3	−0.7	−1.0	–	–	−1.5
SO_2	11.1	7.7	9.4	14.6	9.9
CS	−5.6	–	−4.6	−4.1	−10.8
$N_{9\text{-}8\ 56}$	3.0	4.7	3.9	–	3.3
N1 (primary)	−4.7	–	−5.2	−2.2	−10.4
N1 in Nuc. mode	−4.6	–	−5.2	–	−10.4
N1 in Aitk. mode	−4.1	–	−5.2	–	−10.4
N1 in Acc. mode	−4.6	–	−5.2	–	−10.4
N2 (secondary)	8.0	7.9	10.0	–	9.1
N2 in Nuc. mode	12.7	10.2	14.9	5.1	16.1
N2 in Aitk. mode	−1.1	–	7.5	–	–
N2 in Acc. mode	−4.3	–	–	−6.3	−11.8
N_{nuc}	9.7	8.6	10.2	6.5	15.3
N_{Ait}	–	–	2.9	–	–
N_{acc}	−5.3	–	–	−3.8	−11.8
Photonucleation (PMF)	11.9	10.4	11.4	7.5	19.9
Aged aerosol (PMF)	3.6	5.4	5.4	–	–
Regional (PMF)	−9.4	–	−10.4	−8.5	−16.8

when considering all year (−0.7% per year), and in winter and autumn, but have no significant trends in the warmer period of the year, as opposed to the urban background station.

SO_2 is also transported with sea breezes, similar to many other pollutants in this station, peaking at 13 UTC. SO_2 concentrations increase throughout all of the period (+11.1% per year) and all seasons. This high increase is probably related to inaccuracies in the corrections of the zero baseline during the instrumentation maintenance and changes in the data retrieving system since 2019 (see Fig. S7), although it might also point to different sources of SO_2 in the regional and urban backgrounds because we found no trend for SO_2 in Barcelona.

The number of particles in the size range 9–856 nm (N), as well as N_{nuc} and N_{Ait}, peak at 14 UTC and has a marked seasonal influence, with twice as many particles in summer as in winter. Conversely, N_{acc} also peaks at 14 UTC but does not show significant seasonal differences. N increases throughout the period (+3.0% per year). When considering seasons separately, N shows no trend in summer and increases during the rest of the year. N_{nuc} increases throughout the period (+9.7% per year), also when considering seasons separately. N_{Ait} increases only in spring. N_{acc} decreases throughout the entire period (−5.3% per year) and in summer and autumn.

CS levels also describe a pattern similar to a breeze, but they peak at 16 UTC, later than any other variable considered here. This is associated with particles being formed locally or transported to the station. The fact that CS has clear seasonal variations (maximum in summer) agrees with NPF occurring locally and contributing to an increase CS in the warmer periods and around midday, when the irradiance is higher. The trend

analysis reveals that CS levels decrease throughout all of the period (−5.6% per year), except in winter, when the trend is not statistically significant.

3.2.1. Primary and secondary particle concentrations

N1 is consistently low throughout the year. $N1_{nuc}$ and $N1_{Ait}$ are very low, and the main contribution to N1 is $N1_{acc}$, which peaks around 13 UTC (Fig. 7). The trend analysis reveals that N1, as well as the mode-segregated N1, decrease when considering the entire period (−4.7% per year) and in all seasons except in winter. The mode-segregated N1 decrease when considering all year data (−4.6% per year for nucleation and accumulation modes and −4.1% per year for Aitken mode) and when considering spring and autumn separately, similarly to BC.

N2 has a clear seasonal pattern, comparable to that of N. The contribution to the mode-segregated particle numbers is also parallel to that of N_{nuc}, N_{Ait} and N_{acc}. Regarding period and seasonal trends, N2 increases when considering the whole period (+8.0% per year) and in all seasons except in summer (no significant trend). $N2_{nuc}$ markedly increases during all of the period (+12.7% per year) and seasons. $N2_{Ait}$ decreases during the entire period (−1.1% per year), but only has a significant trend in spring when separating seasons. Finally, $N2_{acc}$ decreases when considering the whole period (−4.3% per year) and in summer and autumn.

3.2.2. PMF montseny

The PMF solution that made the most physical sense had three factors (Fig. 8): *NPF* (diameter mode 18 nm), *Aged aerosol* (diameter mode 41 nm) and *Regional* (diameter mode 123 nm). The average daily cycles of each factor are presented in Fig. 9. In addition, Fig. S8 shows the average weekly and monthly cycles of each factor.

NPF begins increasing at 7 UTC and peaks at 14 UTC (Fig. 9). The absolute concentration of this factor is higher during weekdays, compared to weekends, and in summer and spring (Figs. S8 and S9). *NPF* dominates an average of 14% of the days (Fig. 10), and the median contribution of this factor to N reaches 20%. The highest contribution to N occurs in spring (median contribution of 23%), with summer and autumn registering the lowest contribution (18%). Winter registers the highest occurrence of days with NPF dominating N (21% of the days), whereas the lowest occurrence of NPF-dominated days takes place in summer (only 5% of the days). On days when NPF dominates N, the relative humidity is lower, the wind speed is constant throughout the day (in contrast to the typical breeze pattern), and the concentration of BC is the lowest of all factors. The contribution of the *NPF* increases monotonically in the period considered in this study (+11.9% per year), including when considering seasons separately.

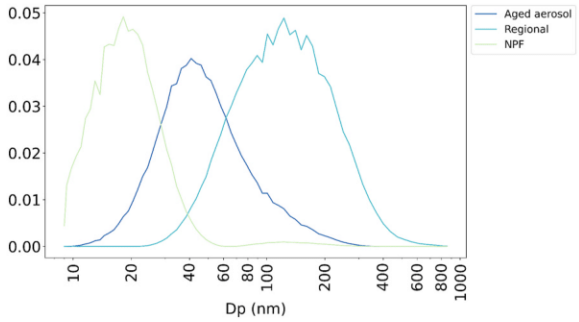

Fig. 8. Normalised factors for the selected solution of the positive matrix factorisation (PMF) for Montseny (regional background).

Aged aerosol increases rapidly from 8 to 14 UTC, and declines at a slower pace (Fig. 9). Similar to *NPF*, this factor is higher during weekdays and in summer (Figs. S8 and S10). The highest absolute contribution of *Aged aerosol* is registered in summer. The relative contribution to N and the dominance of *Aged aerosol* are approximately constant throughout the year, with slightly higher percentages in spring (53% and 70%, respectively). The contribution of *Aged aerosol* to N increases monotonically in the period considered (+3.6% per year) for all seasons except in summer and autumn, with no significant trends.

The contribution of the *Regional* factor increases from 5 to 13 UTC (Fig. 9). The absolute contribution is relatively homogeneous throughout the week and higher in summer (Figs. S8 and S11). The relative contribution of *Regional* to N, as well as the number of days with dominance of this factor, are similar from autumn to spring (averages of 28% and 26%, respectively), but markedly lower in summer (18% and 16%, respectively). The Mann-Kendall tests reveal a decreasing trend of this factor, when considering the entire period (−9.4% per year) and when separating trends, except in winter, with no significant trend.

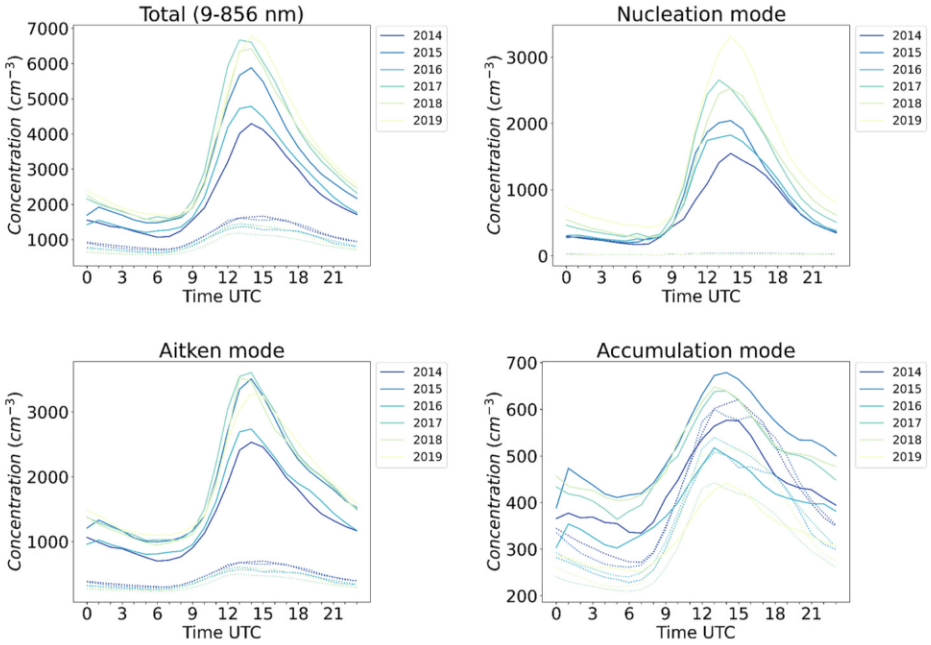

Fig. 7. Daily cycles of primary (dashed) and secondary particles (solid) contributions to the total and mode-segregated aerosol load, separated by annual averages from 2014 to 2019 at Montseny (regional background).

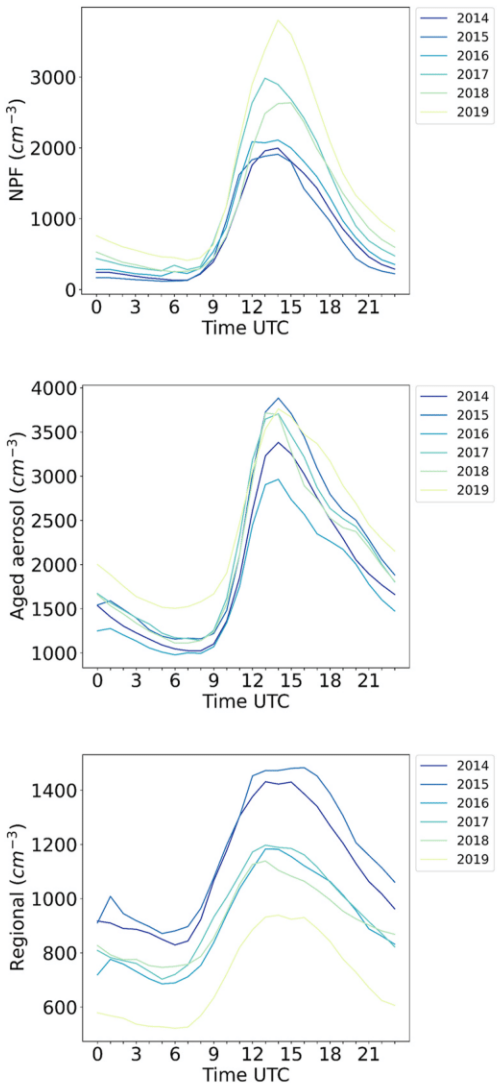

Fig. 9. Daily cycles of the contribution of PMF factors, separated by annual averages from 2014 to 2019 at Montseny (regional background).

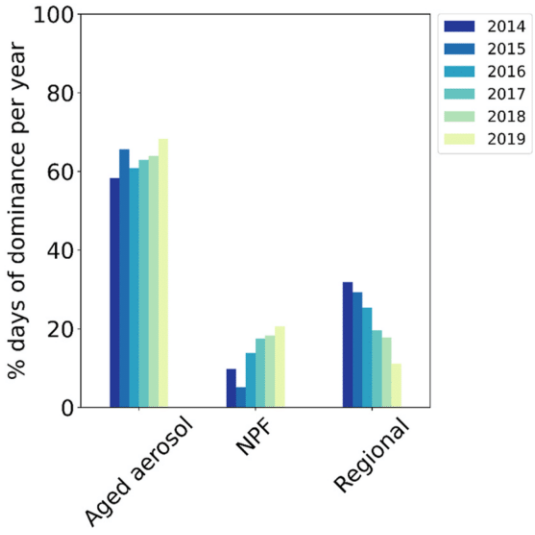

Fig. 10. Percentage of days in which the contribution of each PMF factor dominates the total particle number concentration at Montseny (regional background), separated by years from 2014 to 2019.

4. Discussion

At both stations considered in this study, our analysis reveals a reduction of primary particles (N1), and consequently a decline in CS levels, as well as an increase in temperature, all of which could favour photonucleation. Moreover, according to our PMF results, the absolute and relative contribution of NPF to N increases at both the urban and rural stations throughout the period considered here. This is also supported with an increasing trend in N2 and N_{nuc} (the latter only in the regional background). However, N decreases at the urban station, whereas it increases at the rural station. This difference may imply that either (i) the impact of policies on decreasing primary emissions is lower at the regional station, compared to the urban station, because of different ratios of primary and secondary particles at each station; (ii) the increase of NPF at the regional background is more significant, compared to the urban station, despite having a lower percentage of increase per year; or (iii) the increase in temperature plays a crucial role at the rural station (e.g., increasing BVOC emissions that could enhance photonucleation and particle growth in the rural environment). The difference in the lowest particle size ranges considered at each station (15 nm at the urban station; 9 nm at the regional station) may also contribute to some extent to the difference in trends. This could also play a role in the similarity of the trends for $N2_{nuc}$ and NPF at the regional background, whereas they differ at the urban station.

We found a general increasing trend for temperatures at both environments. Rising temperatures increase the saturation vapour pressure of nucleating species, thus decreasing nucleation rates. This, in turn, leads to decreasing N (Yu et al., 2012). However, increasing temperatures generally lead to increasing emissions of BVOCs. The increasing CO_2 concentrations registered around the world enhance photosynthesis and the gross primary production of the forests, which in turn increases BVOC emissions (Nieminen et al., 2014). The increase in BVOCs can have two opposing consequences. On the one hand, it may contribute to increased nucleation via oxidation of biogenic vapors and, therefore, enhanced nucleation (Lehtipalo et al., 2018) and increased aerosol load. On the other hand, increasing biogenic emissions may increase the coagulation sink and decrease N (Kulmala et al., 2004). In our regional background with large and dense forests, N increases. Therefore, it seems that the contribution of oxidised BVOCs is more important than the contribution to the coagulation sink or the increase in the saturation vapour pressure.

There are no observations of a direct link between increasing temperatures and decreasing BC concentrations in the literature. However, increasing temperatures most likely lead to a decrease in emissions related to household heating during colder seasons (Sun et al., 2020). This is not the case at either of our stations: BC concentrations have no trend in winter, whereas they decrease during the rest of the year.

The decrease in N_{Ait} at the urban station agrees with the decreasing trend for the *Aged traffic* factor. N_{Ait} has no trend at the regional background. However, given that $N1_{Ait}$ (primary Aitken-mode particles) decreases significantly more than $N2_{Ait}$, the *Aged aerosol* factor is more representative of primary emissions transported to the station by land and sea breezes, given that the regional station is located in a natural park restricted to traffic and with no local emissions. This agrees with the reported decrease in the contribution of 30–100 nm particles at locations around Paris (France) when the stations were downwind of the city (Pikridas et al., 2015), evidencing a direct link between the urban plume and primary Aitken particles. Considering that emissions have decreased at our urban background station, $N1_{Ait}$ were expected to decrease at the regional background station.

Average O_3 concentrations decrease during summer at the urban station. This does not agree with the general increasing trends for most of the urban air quality sites in the same area reported by Massagué et al. (2019), which were attributed to the decrease in NO/NO_2 ratios (and the consequent decline in O_3 titration) or to a VOCs-limited regime of O_3 formation in the urban environment (Massagué et al., 2019). On the

other hand, no significant trend is recorded at the regional station during the warmer seasons, agreeing with the constant average concentration patterns reported by (Massagué et al., 2019) during the last decade.

Our findings regarding the decreasing trend in primary emissions agree with previous studies in the same area. Querol et al. (2016) and Massagué et al. (2019) reported a decrease in urban NO and NO_2 concentrations in Spain from 2000 to 2015, and in Barcelona from 2005 to 2017, respectively. Decreasing NO and NO_2 concentrations at the urban background station could lead to increasing new particle formation from organic vapors (Yan et al., 2020), agreeing with the increasing *NPF* factor contribution at this station. However, this is not the cause of increasing NPF at the regional background station, where NOx concentrations have no trend in the period considered in this study.

Previous studies around the world describe decreasing trends in anthropogenic emissions over the last decades. Asmi et al. (2013) reported decreasing trends for the N and N_{acc} in many stations in the Northern Hemisphere from 2001 to 2010, particularly in winter. They attributed this trend to a general decrease in anthropogenic emissions on a global scale. Similarly, Nieminen et al. (2014) reported N_{nuc} and N_{acc} decreasing trends at Hyytiälä (Finland) in all seasons from 1997 to 2013. This was also described by Riuttanen et al. (2013) at the same station from 1998 to 2008, especially in air masses that were more influenced by anthropogenic emissions.

Sabaliauskas et al. (2012) reported a decrease in the number of particles less than 50 nm in diameter, as well as N, at a roadside station in Toronto from 2006 to 2011. This was attributed to changes in the vehicle fleet. Squizzato et al. (2019) reported decreasing concentrations of NOx, SO_2, CO and UFPs in Rochester (Northeastern US) in the period 2002–2016. The authors attributed these decreases to the implementation of emission controls and economic changes. Sun et al. (2020) noted a decreasing trend in BC concentrations at 16 urban background and regional background stations in Germany from 2009 to 2018. This was attributed to decreasing anthropogenic emissions, which lead to a decrease in N at all stations.

Most of these studies describe decreases in N as a result of decreasing anthropogenic emissions, which agrees with our observations at the urban background station, but is in contrast to the increasing trend in N at the regional background station. Considering that the area of Barcelona receives more insolation than most of the stations reported in the locations where the studies referred here were carried out, we believe that the increasing trend of the aerosol number load at our regional background station is due to enhanced NPF favoured by the intense insolation, and increasing BVOCs emissions that would contribute to photonucleation and particle growth more than in the urban environment. Increasing local VOCs emissions could also be enhancing local NPF events in the regional background area, as reported by (Dai et al., 2017) in the Yangtze River Delta region (China). Unfortunately, VOC measurements were not available for this study. The increasing trend in SO_2 could also lead to increasing H_2SO_4 concentrations, which would be favoring NPF, thus increasing Nnuc. However, as we mentioned in section 3.2, the increase in SO_2 concentrations might not be real, as it could be related with faulty instrumentation maintenance.

The fact that NPF contributes the most in summer at the urban background, whereas the regional background has the maximum contribution of NPF in spring, points to the relevance of BVOCs in the formation and growth of new particles in the regional background. This agrees with the observations reported by Kalivitis et al. (2019) at Finokalia, a marine background station in the eastern Mediterranean, from 2008 to 2018; they found NPF to be more frequent in spring due to increased biogenic emissions, monoterpenes being the main contributor, and summer the season with the least frequency of NPF, despite having the highest solar radiation.

The occurrences of the different PMF factors identified in Barcelona also agree with those reported in previous studies in Barcelona. Using a cluster analysis, Brines et al. (2015) found that traffic was the source that contributed the most (dominated 63% of the days), whereas nucleation dominated only on 15% of the days. Our study revealed that the urban fresh traffic contribution dominated 91% of the days, whereas NPF dominated only on 7% of the days. Despite the difference in the relative contributions, due to the different methodology applied in both studies, as well as the different time periods, the results are consistent. Other studies in Barcelona concluded that the majority of UFPs (65–69%) correspond to traffic emissions, and photonucleation events contribute substantially to the annual N average (Dall'Osto et al., 2012; Pey et al., 2008, 2009). The results of our study reveal that traffic emissions contribute to 63% of N as an hourly average, whereas NPF contributes to 11%. Taking into the account that in summer the contribution of photonucleation is higher, we agree that NPF can contribute remarkably to the annual particle number.

5. Conclusions

We analysed and compared time trends in levels of gaseous pollutants and the mode-segregated particle number concentrations, distinguishing between primary and secondary particle contributions based on BC concentrations, in an urban background (2013–2019) and a regional background station (2014–2019) in the area of Barcelona (NE Spain, W Mediterranean). We have also applied positive matrix factorisation receptor modelling (PMF) to the particle number size distributions in order to identify sources and analyse the trends of their contributions.

Primary particles and condensation sinks (CS) have decreased in both environments, whereas temperature has an increasing trend. In this scenario, the contribution of NPF to the total number of particles has increased significantly at the urban and regional background stations. The time trend of the total particle number concentrations differs at both stations. At the urban background station, the decreasing trend in primary emissions forces a decreasing trend in the total particle number concentrations, whereas the increase in the new particle formation (NPF) at the regional background station leads to an increasing trend in the total particle number concentration.

The decrease in primary emissions impacts the number of accumulation-mode particles, which have decreased at both stations. Moreover, the *Regional* factor at the regional background station (mainly consisting on accumulation-mode particles) has a decreasing trend as well.

Our results agree with the generalised decreasing trend in anthropogenic emissions around the world over recent years. However, this leads to different consequences regarding the total particle number at our stations. At the urban background station, the decreasing trend agrees with most of the literature reports. However, the increasing trend at the regional background is in contrast to those reported in most studies. We believe that this is related to the more intense insolation in this area, compared to most of the locations in those studies. The difference between the urban and regional stations could be explained by the effect of the increasing biogenic emissions, favoured by increasing temperatures, which would enhance photonucleation in the rural area, which would, in turn, increase the total number of particles. The increasing trend in SO_2 could also lead to increasing H_2SO_4 concentrations, which would be favoring new particle formation. However, as we mentioned in section 3.2, the increase in SO_2 concentrations might not be real, as it could be related with faulty instrumentation maintenance. The lower primary emissions from urban areas could also favour new particle formation events in the regional environment.

From our results, we may infer that applying local measures aimed at the reduction of urban emissions of pollutants decreased UFPs concentrations at urban locations, but the particle number concentration of aerosols finer than 25 nm in diameter increased because climate patterns favour NPF in the study area. Moreover, the reduction of urban traffic would cause an increase in UFP concentrations at nearby regional locations affected by urban plumes. The increase in the regional particle

number concentration is driven by both nucleation and Aitken mode particles, whereas in the urban locations, only the number of nucleation-mode particles increases.

Overall, we conclude that decreasing primary emissions results in a decrease in the total number concentrations of urban aerosols, despite the increase in the formation of new particles by photonucleation. Moreover, the aerosol load of regions enriched with BVOCs downwind of urban areas increases because photonucleation is more favoured, and the decrease in number concentration of primary particles is compensated for by the newly formed particles.

CRediT authorship contribution statement

Cristina Carnerero: Conceptualization, Methodology, Software, Formal analysis, Writing - original draft, Writing - review & editing, Visualization. **Ioar Rivas:** Methodology, Software, Writing - review & editing. **Cristina Reche:** Data curation, Writing - review & editing. **Noemí Pérez:** Data curation, Writing - review & editing. **Andrés Alastuey:** Conceptualization, Writing - review & editing, Supervision, Project administration, Funding acquisition. **Xavier Querol:** Conceptualization, Writing - review & editing, Supervision, Project administration, Funding acquisition.

Declaration of competing interest

The authors declare that they have no known competing financial interests or personal relationships that could have appeared to influence the work reported in this paper.

Acknowledgements

The authors thank Jesús Yus-Díez for his contribution in the Montseny dataset, and the Meteorology research group (Faculty of Physics, Universitat de Barcelona) for providing meteorological data from Barcelona. This work was supported by FEDER funds and projects HOUSE (CGL2016-78594-R) and CAIAC (PID2019-108990RB-I00), the Government of Catalonia (AGAUR 2017 SGR41), and the European Commission via ACTRIS2 (project 654109). Cristina Carnerero thanks the Spanish Ministry of Science and Innovation for her FPI grant (BES-2017-080027).

Appendix A. Supplementary data

Supplementary data to this article can be found online at https://doi.org/10.1016/j.atmosenv.2020.117982.

References

Asmi, A., Collaud Coen, M., Ogren, J.A., Andrews, E., Sheridan, P., Jefferson, A., Weingartner, E., Baltensperger, U., Bukowiecki, N., Lihavainen, H., Kivekäs, N., Asmi, E., Aalto, P.P., Kulmala, M., Wiedensohler, A., Birmili, W., Hamed, A., O&apos, Dowd, C., G Jennings, S., Weller, R., Flentje, H., Fjaeraa, A.M., Fiebig, M., Myhre, C.L., Hallar, A.G., Swietlicki, E., Kristensson, A., Laj, P., 2013. Aerosol decadal trends – Part 2: in-situ aerosol particle number concentrations at GAW and ACTRIS stations. Atmos. Chem. Phys. 13 (2), 895–916. https://doi.org/10.5194/acp-13-895-2013.

Bräuner, E.V., Forchhammer, L., Møller, P., Simonsen, J., Glasius, M., Wåhlin, P., Raaschou-Nielsen, O., Loft, S., 2007. Exposure to ultrafine particles from ambient air and oxidative stress-induced DNA damage. Environ. Health Perspect. 115 (8), 1177–1182. https://doi.org/10.1289/ehp.9984.

Brines, M., Dall'Osto, M., Beddows, D.C.S., Harrison, R.M., Gómez-Moreno, F., Núñez, L., Artíñano, B., Costabile, F., Gobbi, G.P., Salimi, F., Morawska, L., Sioutas, C., Querol, X., 2015. Traffic and nucleation events as main sources of ultrafine particles in high-insolation developed world cities. Atmos. Chem. Phys. https://doi.org/10.5194/acp-15-5929-2015.

Carnerero, C., Pérez, N., Petäjä, T., Laurila, T.M., Ahonen, L.R., Kontkanen, J., Ahn, K.-H., Alastuey, A., Querol, X., 2019. Relating high ozone, ultrafine particles, and new particle formation episodes using cluster analysis. Atmos. Environ. X, 100051. https://doi.org/10.1016/j.aeaoa.2019.100051.

Cassee, F.R., Mills, N.L., Newby, D., 2011. Cardiovascular Effects of Inhaled Ultrafine and Nanosized Particles. John Wiley & Sons, Inc., Hoboken, NJ, USA.

Colette, A., Granier, C., Hodnebrog, Jakobs, H., Maurizi, A., Nyiri, A., Bessagnet, B., D'Angiola, A., D'Isidoro, M., Gauss, M., Meleux, F., Memmesheimer, M., Mieville, A., Roüil, L., Russo, F., Solberg, S., Stordal, F., Tampieri, F., 2011. Air quality trends in Europe over the past decade: a first multi-model assessment. Atmos. Chem. Phys. 11 (22), 11657–11678. https://doi.org/10.5194/acp-11-11657-2011.

Dai, L., Wang, H., Zhou, L., An, J., Tang, L., Lu, C., Yan, W., Liu, R., Kong, S., Chen, M., Lee, S., Yu, H., 2017. Regional and local new particle formation events observed in the Yangtze River Delta region, China. J. Geophys. Res. https://doi.org/10.1002/2016JD026030.

Dall'Osto, M., Beddows, D.C.S., Pey, J., Rodriguez, S., Alastuey, A., Harrison, R.M., Querol, X., 2012. Urban aerosol size distributions over the Mediterranean city of Barcelona, NE Spain. Atmos. Chem. Phys. 12 (22), 10693–10707. https://doi.org/10.5194/acp-12-10693-2012.

Font, A., Fuller, G.W., 2016. Did policies to abate atmospheric emissions from traffic have a positive effect in London? Environ. Pollut. 218, 463–474. https://doi.org/10.1016/j.envpol.2016.07.026.

Geddes, J.A., Martin, R.V., Boys, B.L., van Donkelaar, A., 2016. Long-term trends worldwide in ambient NO_2 concentrations inferred from satellite observations. Environ. Health Perspect. 124 (3), 281–289. https://doi.org/10.1289/ehp.1409567.

Gordon, H., Kirkby, J., Baltensperger, U., Bianchi, F., Breitenlechner, M., Curtius, J., Dias, A., Dommen, J., Donahue, N.M., Dunne, E.M., Duplissy, J., Ehrhart, S., Flagan, R.C., Frege, C., Fuchs, C., Hansel, A., Hoyle, C.R., Kulmala, M., Kürten, A., Lehtipalo, K., Makhmutov, V., Molteni, U., Rissanen, M.P., Stozkhov, Y., Tröstl, J., Tsagkogeorgas, G., Wagner, R., Williamson, C., Wimmer, D., Winkler, P.M., Yan, C., Carslaw, K.S., 2017. Causes and importance of new particle formation in the present-day and preindustrial atmospheres. J. Geophys. Res. Atmos. 122 (16), 8739–8760. https://doi.org/10.1002/2017JD026844.

Guerreiro, C.B.B., Foltescu, V., de Leeuw, F., 2014. Air quality status and trends in Europe. Atmos. Environ. 98, 376–384. https://doi.org/10.1016/j.atmosenv.2014.09.017.

Hussain, M.M., Mahmud, I., 2019. pyMannKendall: a python package for non parametric Mann Kendall family of trend tests. J. Open Source Softw. 4 (39), 1556. https://doi.org/10.21105/joss.01556.

Kalivitis, N., Kerminen, V.-M., Kouvarakis, G., Stavroulas, I., Tzitzikalaki, E., Kalkavouras, P., Daskalakis, N., Myriokefalitakis, S., Bougiatioti, A., Manninen, H.E., Roldin, P., Petäjä, T., Boy, M., Kulmala, M., Kanakidou, M., Mihalopoulos, N., 2019. Formation and growth of atmospheric nanoparticles in the eastern Mediterranean: results from long-term measurements and process simulations. Atmos. Chem. Phys. 19 (4), 2671–2686. https://doi.org/10.5194/acp-19-2671-2019.

Kerminen, V.-M., Chen, X., Vakkari, V., Petäjä, T., Kulmala, M., Bianchi, F., 2018. Atmospheric new particle formation and growth: review of field observations. Environ. Res. Lett. 13 (10), 103003. https://doi.org/10.1088/1748-9326/aadf3c.

Kloster, S., Dentener, F., Feichter, J., Raes, F., van Aardenne, J., Roeckner, E., Lohmann, U., Stier, P., Swart, R., 2008. Influence of future air pollution mitigation strategies on total aerosol radiative forcing. Atmos. Chem. Phys. 8 (21), 6405–6437. https://doi.org/10.5194/acp-8-6405-2008.

Krecl, P., Johansson, C., Targino, A.C., Ström, J., Burman, L., 2017. Trends in black carbon and size-resolved particle number concentrations and vehicle emission factors under real-world conditions. Atmos. Environ. 165, 155–168. https://doi.org/10.1016/j.atmosenv.2017.06.036.

Kulmala, M., Suni, T., Lehtinen, K.E.J., Dal Maso, M., Boy, M., Reissell, A., Rannik, Ü, Aalto, P., Keronen, P., Hakola, H., Bäck, J., Hoffmann, T., Vesala, T., Hari, P., 2004. Atmospheric Chemistry and Physics A new feedback mechanism linking forests, aerosols, and climate [online] Available from: www.atmos-chem-phys.org/acp/4/557/. (Accessed 26 June 2020).

Kulmala, M., Luoma, K., Virkkula, A., Petäjä, T., Paasonen, P., Kerminen, V.M., Nie, W., Qi, X., Shen, Y., Chi, X., Ding, A., 2016. On the mode-segregated aerosol particle number concentration load: contributions of primary and secondary particles in Hyytiälä and Nanjing. Boreal Environ. Res. 21 (3–4), 319–331.

Kumar, P., Morawska, L., Birmili, W., Paasonen, P., Hu, M., Kulmala, M., Harrison, R.M., Norford, L., Britter, R., 2014. Ultrafine particles in cities. Environ. Int. 66, 1–10. https://doi.org/10.1016/J.ENVINT.2014.01.013.

Lanzinger, S., Schneider, A., Breitner, S., Stafoggia, M., Erzen, I., Dostal, M., Pastorkova, A., Bastian, S., Cyrys, J., Zscheppang, A., Kolodnitska, T., Peters, A., 2016. Associations between ultrafine and fine particles and mortality in five central European cities — results from the UFIREG study. Environ. Int. 88, 44–52. https://doi.org/10.1016/j.envint.2015.12.006.

Lehtipalo, K., Yan, C., Dada, L., Bianchi, F., Xiao, M., Wagner, R., Stolzenburg, D., Ahonen, L.R., Amorim, A., Baccarini, A., Bauer, P.S., Baumgartner, B., Bergen, A., Bernhammer, A.-K., Breitenlechner, M., Brilke, S., Buchholz, A., Mazon, S.B., Chen, D., Chen, X., Dias, A., Dommen, J., Draper, D.C., Duplissy, J., Ehn, M., Finkenzeller, H., Fischer, L., Frege, C., Fuchs, C., Garmash, O., Gordon, H., Hakala, J., He, X., Heikkinen, L., Heinritzi, M., Helm, J.C., Hofbauer, V., Hoyle, C.R., Jokinen, T., Kangasluoma, J., Kerminen, V.-M., Kim, C., Kirkby, J., Kontkanen, J., Kürten, A., Lawler, M.J., Mai, H., Mathot, S., Mauldin, R.L., Molteni, U., Nichman, L., Nie, W., Nieminen, T., Ojdanic, A., Onnela, A., Passananti, M., Petäjä, T., Piel, F., Pospisilova, V., Quéléver, L.L.J., Rissanen, M.P., Rose, C., Sarnela, N., Schallhart, S., Schuchmann, S., Sengupta, K., Simon, M., Sipilä, M., Tauber, C., Tomé, A., Tröstl, J., Väisänen, O., Vogel, A.L., Volkamer, R., Wagner, A.C., Wang, M., Weitz, L., Wimmer, D., Ye, P., Ylisirniö, A., Zha, Q., Carslaw, K.S., Curtius, J., Donahue, N.M., Flagan, R.C., Hansel, A., Riipinen, I., Virtanen, A., Winkler, P.M., Baltensperger, U., Kulmala, M., Worsnop, D.R., 2018. Multicomponent new particle formation from sulfuric acid, ammonia, and biogenic vapors. Sci. Adv. 4 (12), eaau5363. https://doi.org/10.1126/sciadv.aau5363.

Ma, N., Birmili, W., 2015. Estimating the contribution of photochemical particle formation to ultrafine particle number averages in an urban atmosphere. Sci. Total Environ. 512–513, 154–166. https://doi.org/10.1016/J.SCITOTENV.2015.01.009.

Makkonen, R., Asmi, A., Kerminen, V.-M., Boy, M., Arneth, A., Hari, P., Kulmala, M., 2012. Air pollution control and decreasing new particle formation lead to strong climate warming. Atmos. Chem. Phys. 12 (3), 1515–1524. https://doi.org/10.5194/acp-12-1515-2012.

Massagué, J., Carnerero, C., Escudero, M., Baldasano, J.M., Alastuey, A., Querol, X., 2019. 2005–2017 ozone trends and potential benefits of local measures as deduced from air quality measurements in the north of the Barcelona metropolitan area. Atmos. Chem. Phys. 19 (11), 7445–7465. https://doi.org/10.5194/acp-19-7445-2019.

Nieminen, T., Asmi, A., Aalto, P.P., Keronen, P., Petäjä, T., Kulmala, M., Kerminen, V.M., Nieminen, T., Dal Maso, M., 2014. Trends in atmospheric new-particle formation: 16 years of observations in a boreal-forest environment. Boreal Environ. Res. 19, 191–214.

Nieminen, T., Kerminen, V.M., Petäjä, T., Aalto, P.P., Arshinov, M., Asmi, E., Baltensperger, U., Beddows, D.C.S., Paul Beukes, J., Collins, D., Ding, A., Harrison, R. M., Henzing, B., Hooda, R., Hu, M., Hõrrak, U., Kivekäs, N., Komsaare, K., Krejci, R., Kristensson, A., Laakso, L., Laaksonen, A., Richard Leaitch, W., Lihavainen, H., Mihalopoulos, N., Németh, Z., Nie, W., O'Dowd, C., Salma, I., Sellegri, K., Svenningsson, B., Swietlicki, E., Tunved, P., Ulevicius, V., Vakkari, V., Vana, M., Wiedensohler, A., Wu, Z., Virtanen, A., Kulmala, M., 2018. Global analysis of continental boundary layer new particle formation based on long-term measurements. Atmos. Chem. Phys. 18 (19), 14737–14756. https://doi.org/10.5194/acp-18-14737-2018.

Olstrup, H., Forsberg, B., Orru, H., Spanne, M., Nguyen, H., Molnár, P., Johansson, C., 2018. Trends in air pollutants and health impacts in three Swedish cities over the past three decades. Atmos. Chem. Phys. 18 (21), 15705–15723. https://doi.org/10.5194/acp-18-15705-2018.

Paasonen, P., Kupiainen, K., Klimont, Z., Visschedijk, A., Denier van der Gon, H.A.C., Amann, M., 2016. Continental anthropogenic primary particle number emissions. Atmos. Chem. Phys. 16 (11), 6823–6840. https://doi.org/10.5194/acp-16-6823-2016.

Paatero, P., 1997. Least squares formulation of robust non-negative factor analysis. In: Chemometrics and Intelligent Laboratory Systems, 37. Elsevier., pp. 23–35

Paatero, P., 1999. The multilinear engine—a table-driven, least squares program for solving multilinear problems, including the n-way parallel factor Analysis model. J. Comput. Graph Stat. https://doi.org/10.1080/10618600.1999.10474853.

Pey, J., Rodríguez, S., Querol, X., Alastuey, A., Moreno, T., Putaud, J.P., Van Dingenen, R., 2008. Variations of urban aerosols in the western Mediterranean. Atmos. Environ. 42 (40), 9052–9062. https://doi.org/10.1016/j.atmosenv.2008.09.049.

Pey, J., Querol, X., Alastuey, A., Rodríguez, S., Putaud, J.P., Van Dingenen, R., 2009. Source apportionment of urban fine and ultra-fine particle number concentration in a Western Mediterranean city. Atmos. Environ. 43 (29), 4407–4415. https://doi.org/10.1016/J.ATMOSENV.2009.05.024.

Pikridas, M., Sciare, J., Freutel, F., Crumeyrolle, S., Von Der Weiden-Reinmüller, S.L., Borbon, A., Schwarzenboeck, A., Merkel, M., Crippa, M., Kostenidou, E., Psichoudaki, M., Hildebrandt, L., Engelhart, G.J., Petäjä, T., Prévôt, A.S.H., Drewnick, F., Baltensperger, U., Wiedensohler, A., Kulmala, M., Beekmann, M., Pandis, S.N., 2015. In situ formation and spatial variability of particle number concentration in a European megacity. Atmos. Chem. Phys. https://doi.org/10.5194/acp-15-10219-2015.

Querol, X., Alastuey, A., Pandolfi, M., Reche, C., Pérez, N., Minguillón, M.C., Moreno, T., Viana, M., Escudero, M., Orio, A., Pallarés, M., Reina, F., 2014. 2001–2012 trends on air quality in Spain. Sci. Total Environ. 490, 957–969. https://doi.org/10.1016/j.scitotenv.2014.05.074.

Querol, X., Alastuey, A., Reche, C., Orio, A., Pallares, M., Reina, F., Dieguez, J.J., Mantilla, E., Escudero, M., Alonso, L., Gangoiti, G., Millán, M., 2016. On the origin of the highest ozone episodes in Spain. Sci. Total Environ. 572, 379–389. https://doi.org/10.1016/j.scitotenv.2016.07.193.

R Development Core Team, 2017. R: a language and environment for statistical computing., Vienna, Austria. R Foundation for Statistical Computing, Vienna, Austria, ISBN 3-900051-07-0. https://www.R-project.org.

Riuttanen, L., Hulkkonen, M., Dal Maso, M., Junninen, H., Kulmala, M., 2013. Trajectory analysis of atmospheric transport of fine particles, SO2, NOx and O3 to the SMEAR II station in Finland in 1996-2008. Atmos. Chem. Phys. 13 (4), 2153–2164. https://doi.org/10.5194/acp-13-2153-2013.

Rivas, I., Beddows, D.C.S., Amato, F., Green, D.C., Järvi, L., Hueglin, C., Reche, C., Timonen, H., Fuller, G.W., Niemi, J.V., Pérez, N., Aurela, M., Hopke, P.K., Alastuey, A., Kulmala, M., Harrison, R.M., Querol, X., Kelly, F.J., 2020. Source apportionment of particle number size distribution in urban background and traffic stations in four European cities. Environ. Int. 135, 105345. https://doi.org/10.1016/j.envint.2019.105345.

Rodríguez, S., Cuevas, E., 2007. The contributions of "minimum primary emissions" and "new particle formation enhancements" to the particle number concentration in urban air. J. Aerosol Sci. 38 (12), 1207–1219. https://doi.org/10.1016/j.jaerosci.2007.09.001.

Sabaliauskas, K., Jeong, C.H., Yao, X., Jun, Y.S., Jadidian, P., Evans, G.J., 2012. Five-year roadside measurements of ultrafine particles in a major Canadian city. Atmos. Environ. 49, 245–256. https://doi.org/10.1016/j.atmosenv.2011.11.052.

Schembari, C., Cavalli, F., Cuccia, E., Hjorth, J., Calzolai, G., Pérez, N., Pey, J., Prati, P., Raes, F., 2012. Impact of a European directive on ship emissions on air quality in Mediterranean harbours. Atmos. Environ. 61, 661–669. https://doi.org/10.1016/j.atmosenv.2012.06.047.

Sen, P.K., 1968. Estimates of the regression coefficient based on kendall's tau. J. Am. Stat. Assoc. 63 (324), 1379–1389. https://doi.org/10.1080/01621459.1968.10480934.

Squizzato, S., Masiol, M., Emami, F., Chalupa, D., Utell, M., Rich, D., Hopke, P., 2019. Long-term changes of source apportioned particle number concentrations in a metropolitan area of the northeastern United States. Atmosphere (Basel) 10 (1), 27. https://doi.org/10.3390/atmos10010027.

Sun, J., Birmili, W., Hermann, M., Tuch, T., Weinhold, K., Merkel, M., Rasch, F., Müller, T., Schladitz, A., Bastian, S., Löschau, G., Cyrys, J., Gu, J., Flentje, H., Briel, B., Asbach, C., Kaminski, H., Ries, L., Sohmer, R., Gerwig, H., Wirtz, K., Meinhardt, F., Schwerin, A., Bath, O., Ma, N., Wiedensohler, A., 2020. Decreasing trends of particle number and black carbon mass concentrations at 16 observational sites in Germany from 2009 to 2018. Atmos. Chem. Phys. 20 (11), 7049–7068. https://doi.org/10.5194/acp-20-7049-2020.

Theil, H., 1992. A Rank-Invariant Method of Linear and Polynomial Regression Analysis. Springer, Dordrecht., pp. 345–381

Wichmann, H.E., Spix, C., Tuch, T., Wölke, G., Peters, A., Heinrich, J., Kreyling, W.G., Heyder, J., 2000. Daily mortality and fine and ultrafine particles in Erfurt, Germany part I: role of particle number and particle mass. Res. Rep. Health Eff. Inst. (98).

Yan, C., Nie, W., Vogel, A.L., Dada, L., Lehtipalo, K., Stolzenburg, D., Wagner, R., Rissanen, M.P., Xiao, M., Ahonen, L., Fischer, L., Rose, C., Bianchi, F., Gordon, H., Simon, M., Heinritzi, M., Garmash, O., Roldin, P., Dias, A., Ye, P., Hofbauer, V., Amorim, A., Bauer, P.S., Bergen, A., Bernhammer, A.K., Breitenlechner, M., Brilke, S., Buchholz, A., Mazon, S.B., Canagaratna, M.R., Chen, X., Ding, A., Dommen, J., Draper, D.C., Duplissy, J., Frege, C., Heyn, C., Guida, R., Hakala, J., Heikkinen, L., Hoyle, C.R., Jokinen, T., Kangasluoma, J., Kirkby, J., Kontkanen, J., Kürten, A., Lawler, M.J., Mai, H., Mathot, S., Mauldin, R.L., Molteni, U., Nichman, L., Nieminen, T., Nowak, J., Ojdanic, A., Onnela, A., Pajunoja, A., Petäjä, T., Piel, F., Quéléver, L.L.J., Sarnela, N., Schallhart, S., Sengupta, K., Sipilä, M., Tomé, A., Tröstl, J., Väisänen, O., Wagner, A.C., Ylisirniö, A., Zha, Q., Baltensperger, U., Carslaw, K.S., Curtius, J., Flagan, R.C., Hansel, A., Riipinen, I., Smith, J.N., Virtanen, A., Winkler, P.M., Donahue, N.M., Kerminen, V.M., Kulmala, M., Ehn, M., Worsnop, D.R., 2020. Size-dependent influence of NOx on the growth rates of organic aerosol particles. Sci. Adv. https://doi.org/10.1126/sciadv.aay4945.

Yu, F., Luo, G., Turco, R.P., Ogren, J.A., Yantosca, R.M., 2012. Decreasing particle number concentrations in a warming atmosphere and implications. Atmos. Chem. Phys. 12 (5), 2399–2408. https://doi.org/10.5194/acp-12-2399-2012.

Supplement of

Trends in primary and secondary particle number concentrations in urban and regional environments in NE Spain

Carnerero et al. (2021)

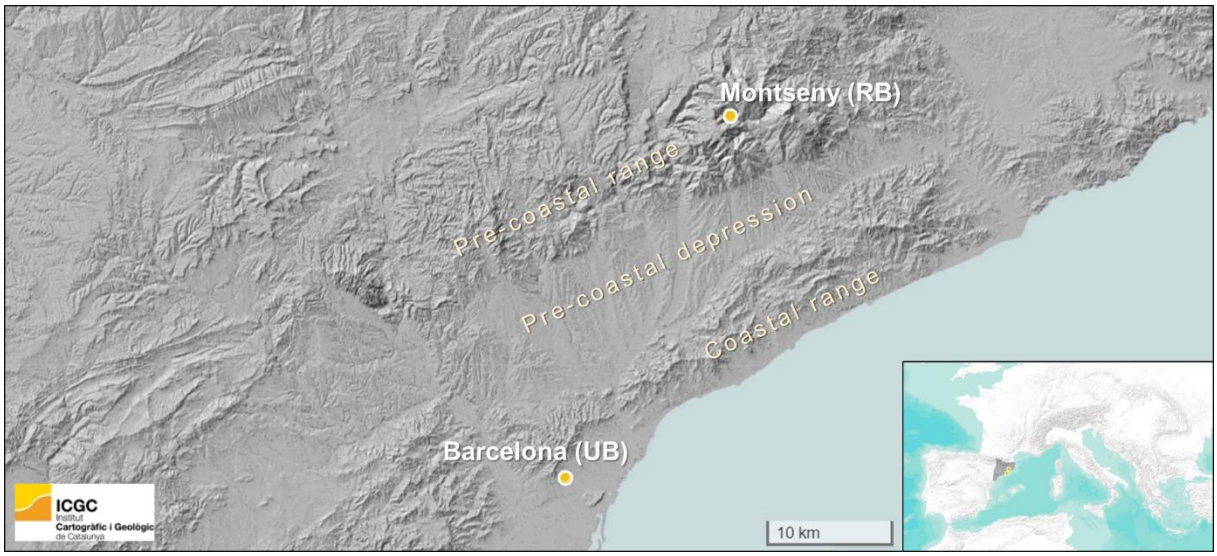

Figure S1: Detailed location of the urban background (Barcelona) and the regional background station (Montseny).

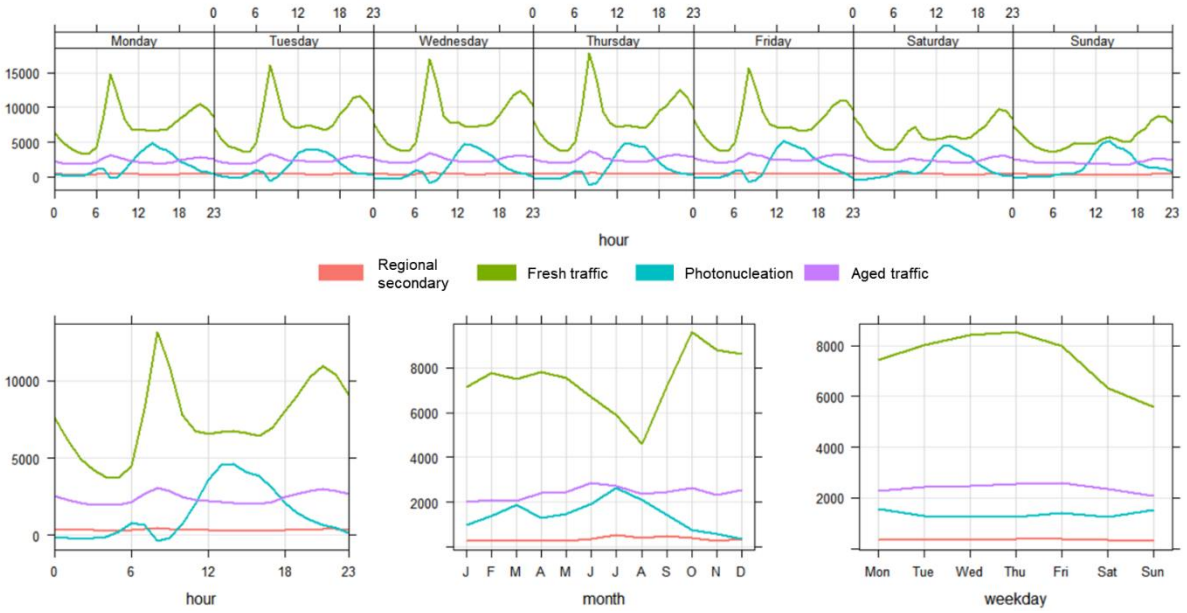

Figure S2: Average daily, weekly and monthly cycles of the contributions of each PMF factor to the total particle number at Barcelona (urban background station) from 2013 to 2019.

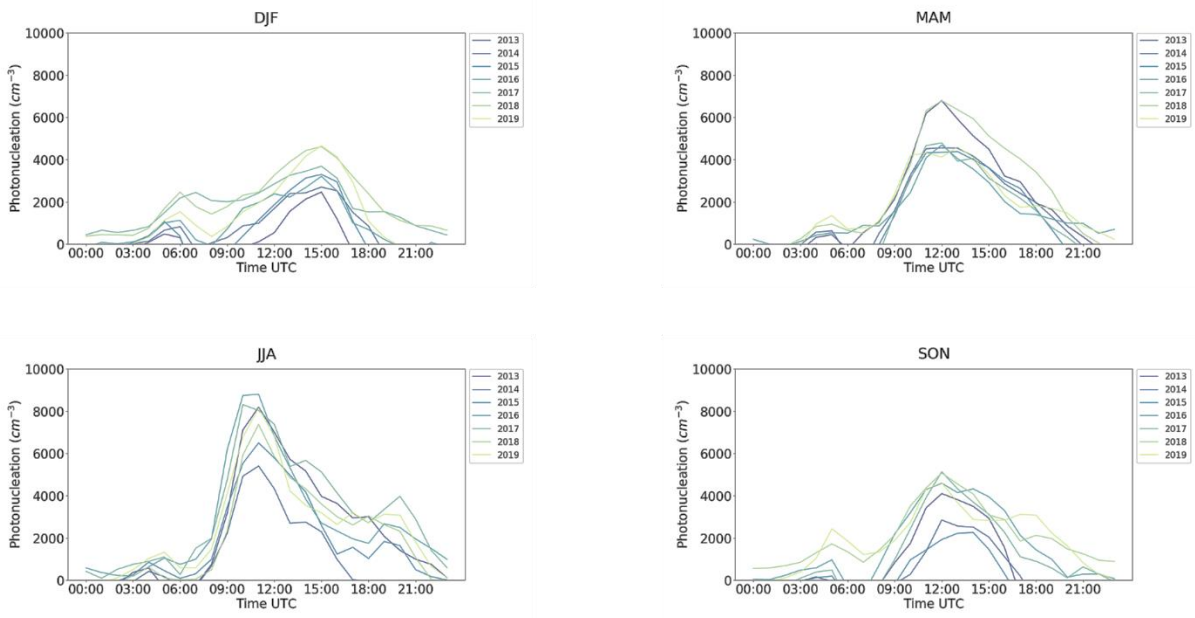

Figure S3: Seasonal average daily cycles for the "Photonucleation" factor contribution to the total particle number at Barcelona (urban background station), separating annual averages from 2013 to 2019.

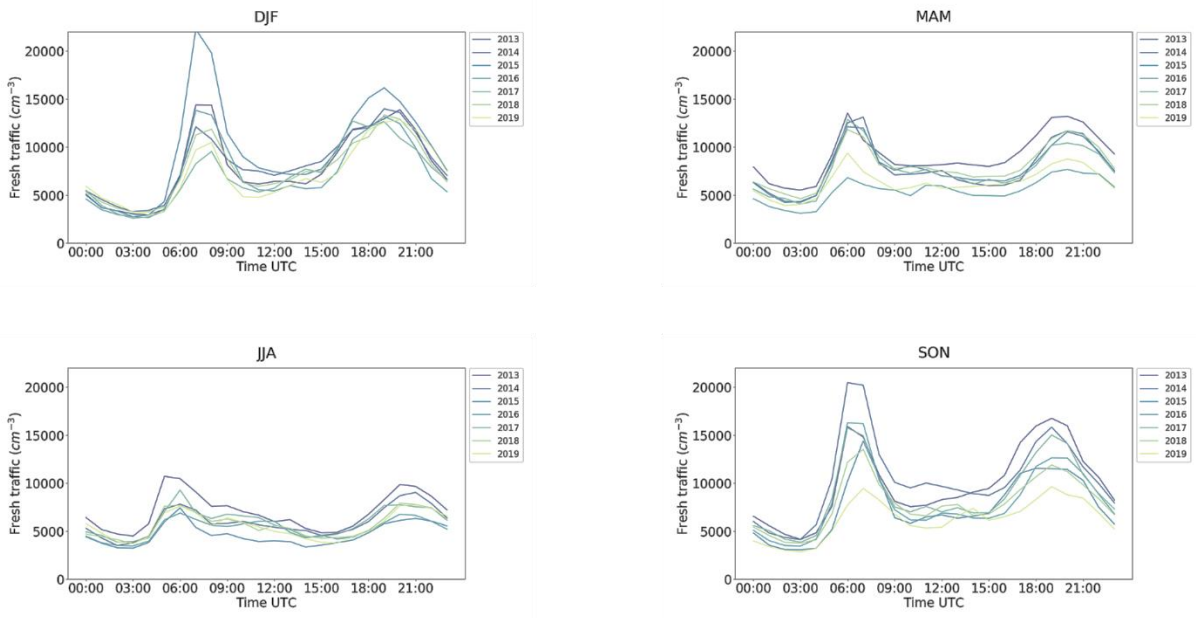

Figure S4: Seasonal average daily cycles for the "Fresh traffic" factor contribution to the total particle number at Barcelona (urban background station), separating annual averages from 2013 to 2019.

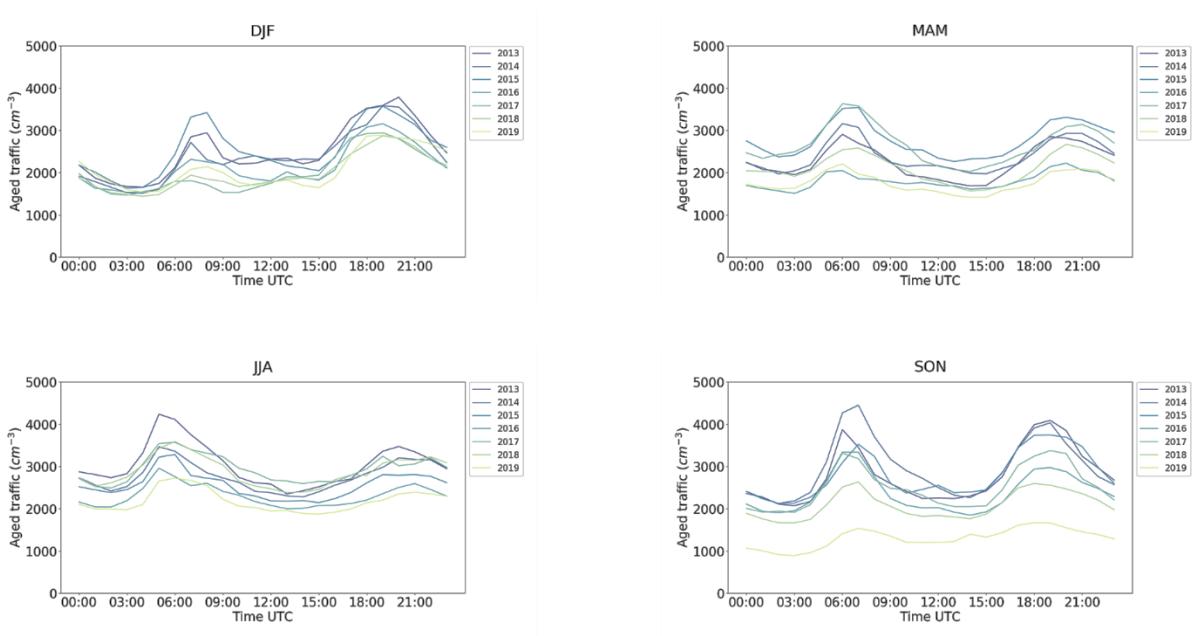

Figure S5: Seasonal average daily cycles for the "Aged traffic" factor contribution to the total particle number at Barcelona (urban background station), separating annual averages from 2013 to 2019.

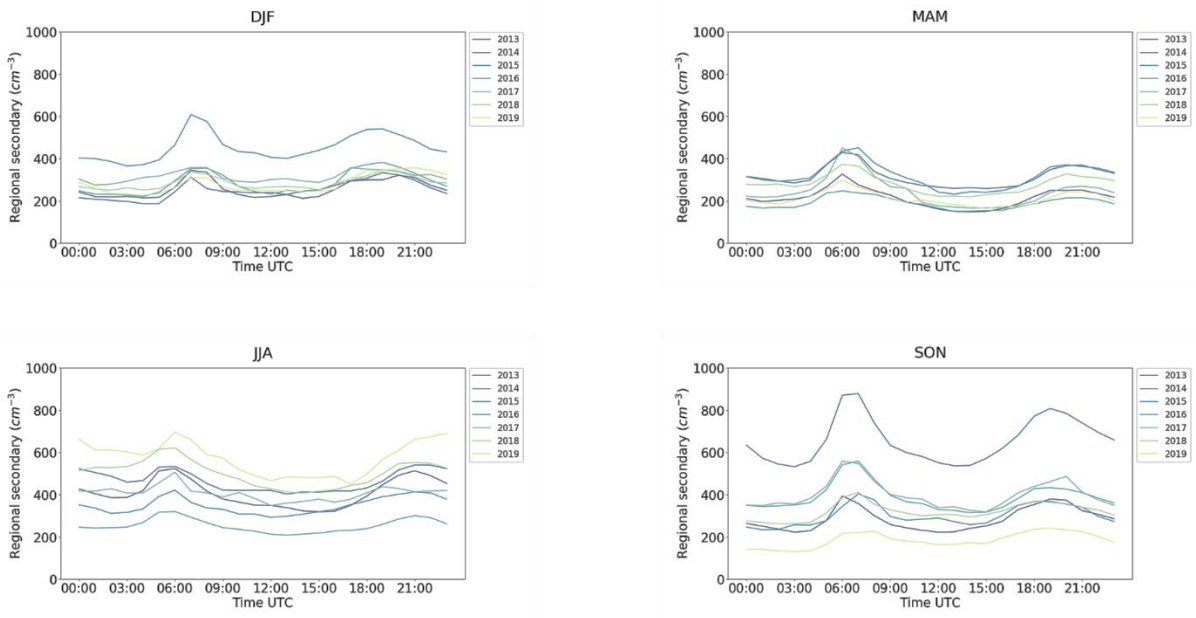

Figure S6: Seasonal average daily cycles for the "Regional secondary" factor contribution to the total particle number at Barcelona (urban background station), separating annual averages from 2013 to 2019.

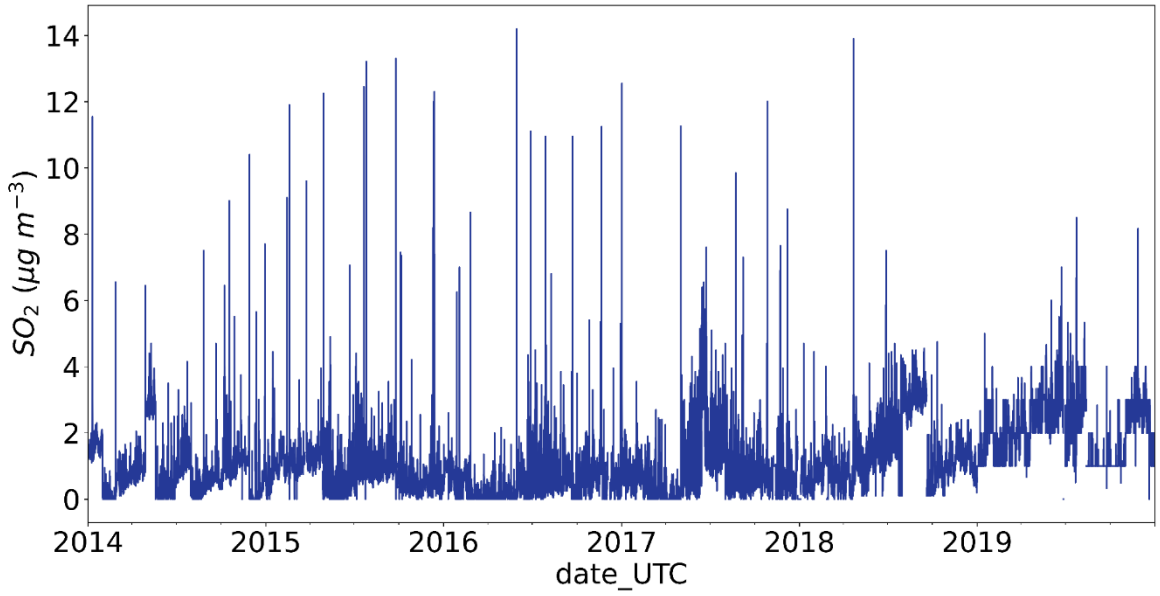

Figure S7: Time series of SO_2 concentrations at the regional background station Montseny before corrections. Errors that could be clearly linked to faulty instrument maintenance have been detected and corrected before calculating the trends. However, additional invalid data might still be present in the dataset used for SO_2 trend calculations.

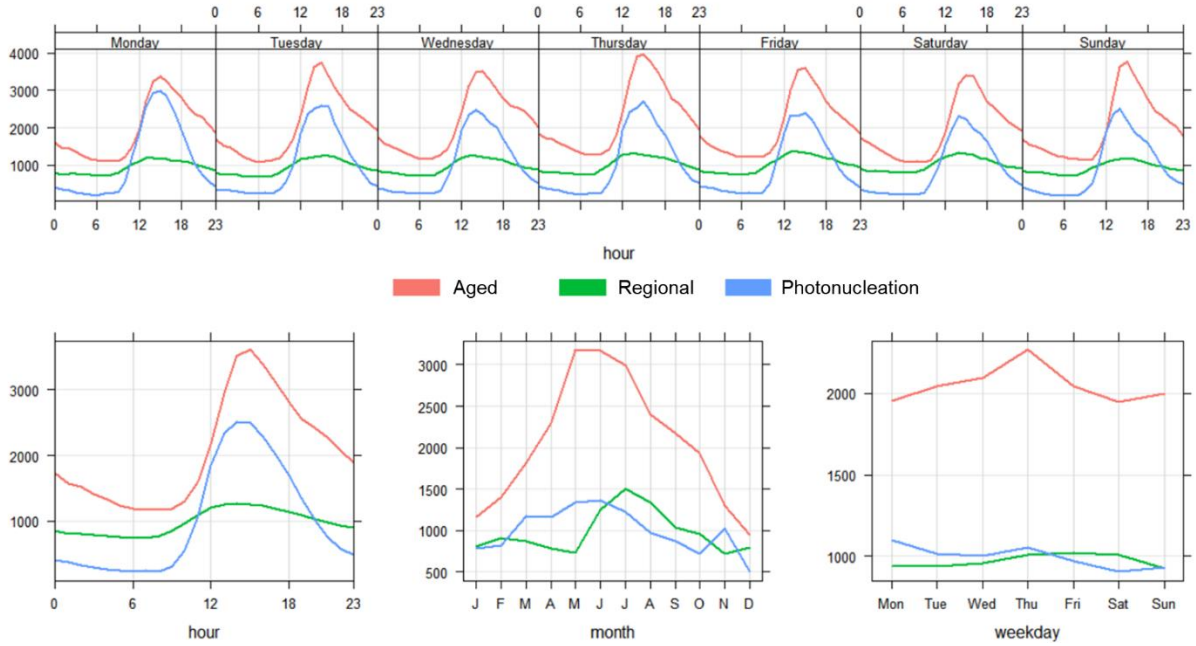

Figure S8: Average daily, weekly and monthly cycles of the contributions of each PMF factor to the total particle number at Montseny (regional background station) from 2014 to 2019.

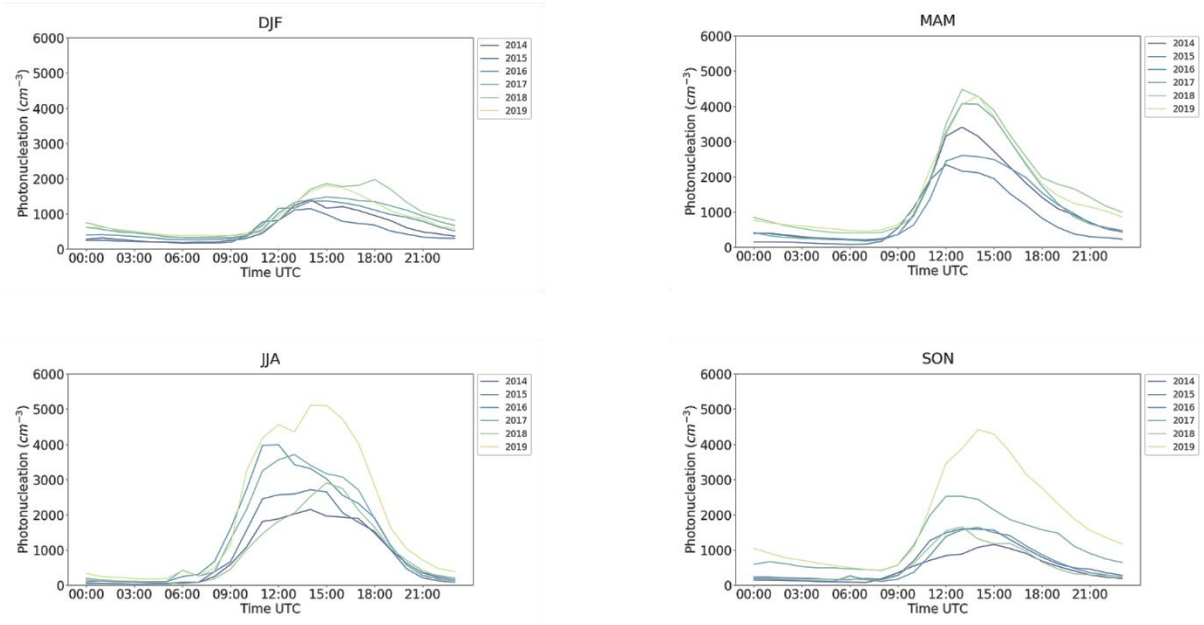

Figure S9: Seasonal average daily cycles for the "Photonucleation" factor contribution to the total particle number at Montseny (regional background station), separating annual averages from 2014 to 2019

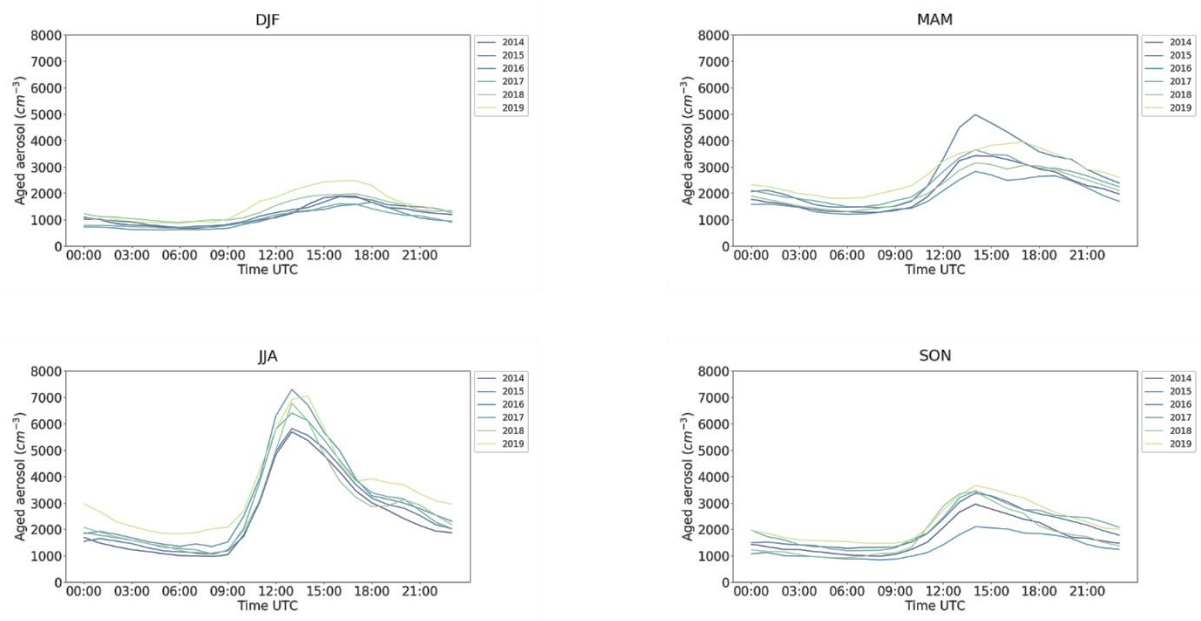

Figure S10: Seasonal average daily cycles for the "Aged aerosol" factor contribution to the total particle number at Montseny (regional background station), separating annual averages from 2014 to 2019.

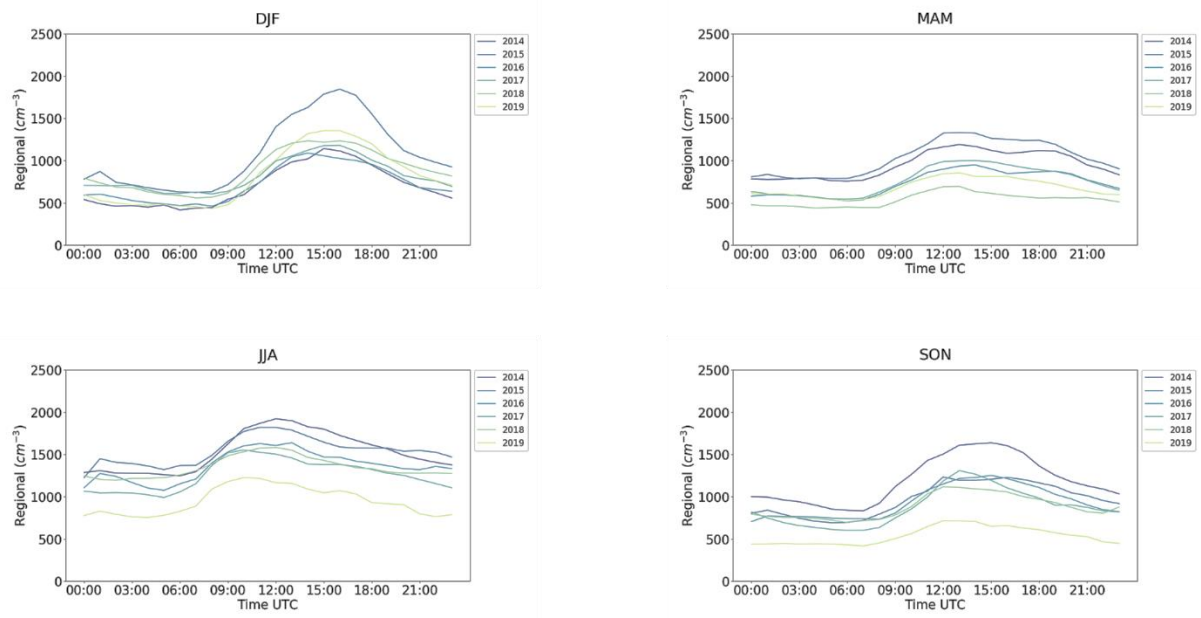

Figure S11: Seasonal average daily cycles for the "Regional" factor contribution to the total particle number at Montseny (regional background station), separating annual averages from 2014 to 2019.

4 DISCUSSION

The results of this thesis have provided an in-depth analysis of the spatial and temporal evolution of UFPs and O_3 in different environments and under diverse environmental conditions. The intensive measurement campaigns have allowed investigating the vertical distribution of aerosols and O_3 in two different environments, suburban and regional background; the horizontal distribution of regional events in urban and suburban locations; and the characterization of particular UFPs, NPF and O_3 events with the help of advanced instrumentation. Additionally, the analysis of long-term measurement datasets at an urban background and a regional background stations has allowed characterizing the temporal evolution of UFPs, the sources and processes that contribute to their concentrations and their relation with other pollutants and atmospheric conditions, as well as an exhaustive trend analysis of all of these.

In order to characterize the dynamics of UFPs episodes and their connection with O_3 episodes (Objective 1), it is necessary to determine under which conditions these episodes are favored, and to identify what contributes to their formation and transport. This analysis is detailed next in Section 4.1, by means of a conceptual model that aims to help understanding the physical processes that take place under different atmospheric conditions, which has been developed based on the results reported in the scientific publications presented in this thesis. Section 4.2 discusses the connections between UFPs and O_3 episodes (Objective 2). Finally, Section 4.2 also examines what factors are contributing to the concentrations of UFPs, while also discussing how these have evolved in recent years (Objective 3).

4.1 Conceptual Model

The results of this thesis revealed two distinct scenarios that govern local and regional UFPs and O_3 concentrations by controlling their local formation and transport: vertical recirculation of air masses and venting scenarios. The occurrence of either scenario is mainly determined by synoptic and mesoscale meteorological conditions (see e.g. Gangoiti et al., 2001). On the other hand, the increase in the magnitude of UFP and O_3 concentrations in each scenario is modulated by the availability of precursors and by local atmospheric and orographic conditions. In general, each of these two scenarios persists for a few days and are constantly alternating in spring and summer.

The alternation from one scenario to the other may occur on consecutive days, although typically there is a transition period that may last several days. Whereas the recirculation and venting scenarios are relatively easy to identify and characterize, the transition periods are harder to describe because the atmospheric patterns are less definite. For this reason, this section focuses only in the description of the recirculation and venting scenarios, because UFPs and O_3 episodes generally occur during these and not during the transition periods. It also has to be noted that the conditions during any of the scenarios may be evolving throughout the days in which the event occurs. This makes it sometimes difficult to distinguish the exact time when one scenario ends and a transition period or a different scenario starts. Yet, each scenario has specific characteristics that usually allow distinguishing from one another. Table 4.1 summarizes the general environmental patterns of recirculation and venting scenarios. Figure 4.2 and Figure 4.4 illustrate an interpretation of the conditions and atmospheric processes taking place in recirculation and venting scenarios, respectively.

Table 4.1: General characteristics of recirculation and venting scenarios.

Characteristic	Recirculation scenario	Venting scenario
Occurrence	Most favored in summer	All year
Synoptic signature	Influence of the Azores anticyclone	Passage of fronts
Conditions	Stagnation, accumulation of pollutants	Changes of air masses, dispersion of pollutants
Temperature	High	Relatively low in summer and spring
Wind	Breeze, jet-type mesoscale winds	Strong synoptic and mesoscale winds
Concentration of UFPs	High	Intermediate or low
Type of UFPs	Primary + secondary	Mostly secondary
NPF	Disfavored	Favored in summer and spring. Regional events detected at surface and throughout the mixing layer
NPF precursors	High	Variable
Particle sinks	High	Low
Concentration of O_3	High	High but relatively lower than in recirculation
Concentration of nucleation-mode particles	High	Variable
Vertical features	Transport of pollutants + mixing layer	Homogeneous mixing layer + residual layer

4.1.1 Vertical recirculation scenario

In periods with high insolation, common in the area of study, the ultraviolet solar radiation heats the surfaces facing the sun, which in turn transfer part of the heat to the air at ground level. As a result, the air parcels close to the surface are warmer than the parcels above. Warmer air parcels are less dense and therefore more buoyant than colder parcels above them, which puts them in motion (thermal convection). The heated air parcels start ascending and cooling adiabatically, i.e., without heat transfer, until they have the same buoyancy than the air surrounding them, while colder air parcels are displaced downwards. This results in a well-mixed atmospheric boundary layer, named mixing layer (Figure 4.1; Stull, 1988). The stronger the heating is, the higher the air will arrive, which determines the height of the mixing layer. Therefore, the layer is usually deepest at midday, when the solar radiation is most intense. However, several other factors may influence the height of the layer. For instance, the mixing layer is higher in drier environments because dry air is heated more rapidly than moist air. However, the evaporation of plant moisture (evapotranspiration) into drier surrounding air increases the buoyancy of air parcels, which results in deeper layers in vegetated areas (Troen and Mahrt, 1986). Rough terrain, such as mountains or tall buildings in cities, increase the friction of the air parcels (mechanical convection), resulting in a more turbulent flow that increases the height of the layer (Arnfield, 2003).

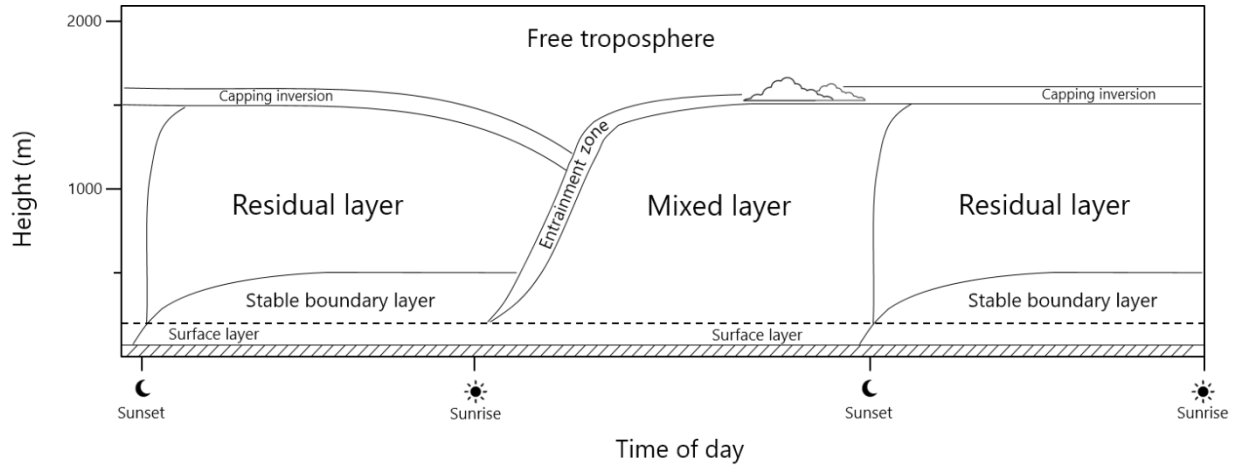

Figure 4.1: Schematic of the typical structure and diurnal cycle of the convective atmospheric boundary layer. Not to scale. Adapted from Stull (1988).

If the surfaces being heated have slopes, for example in mountains and systems with complex orography, the parcels of air adjacent to the surface are warmer than those next to them at the

same altitude. In this case, the movement of the air parcels causes an upslope flow, known as anabatic wind or valley breeze (Seinfeld and Pandis, 2006).

When the sun stops heating the surfaces, the earth emits long-wave radiation resulting in the cooling of the air parcels at ground level at a higher rate than the surrounding parcels of air, resulting in the termination of the rising motions. This causes the atmospheric boundary layer to shrink and become stable at night (Figure 4.1; Stull, 1988). In the case of complex terrain, when the sun stops heating the slopes, the air in the surface cools faster than the surrounding air, leading to katabatic winds or mountain breezes with a downslope flow opposed to that during daytime (Seinfeld and Pandis, 2006).

In areas with large bodies of water, the different heat capacities of water and land create pressure differences that result in a system of breezes. During daytime, the land heats faster than water, thus the air parcels at ground level rise and are replaced by air above the sea, producing a flow from the water to the land. The strength of the breeze is proportional to the temperature difference between the body of water and the land (Atkinson, 1982). Aloft, the flow has an opposing direction and there is a descent of air above the water due to the differences in air pressure (subsidence).

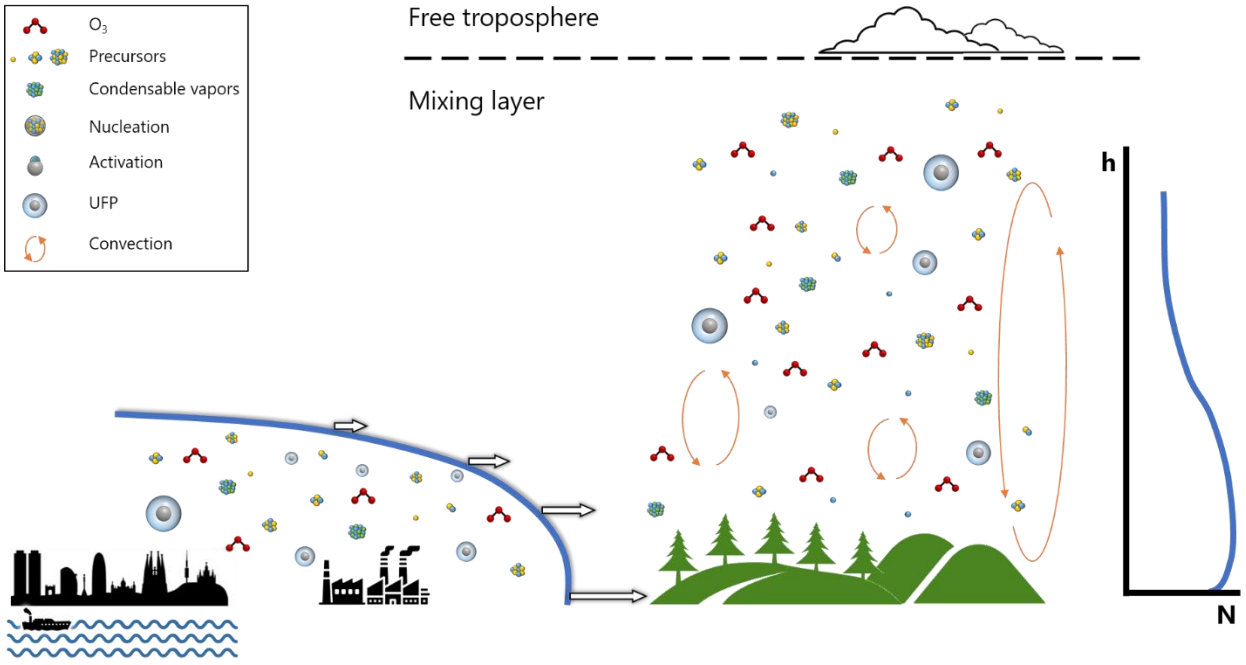

Figure 4.2: Conceptualization of the vertical and horizontal distribution of pollutants and vertical profile (see also Figure 4.3) of the total number of particles during a recirculation episode in a rural environment affected by urban and industrial plumes, as reported in Montseny in **Paper II**.

In the Western Mediterranean basin, the sea breeze creates a flow of pollutants from the polluted coastal areas towards the land that adds to the flow of valley breezes caused by the complex Mediterranean orography in the absence of strong synoptic flows (Drobinski et al., 2006). The superposition of sea and land breezes is sometimes referred to as *combined breeze* (Millán et al., 1996). When the solar radiation is intense and the temperature difference is very high, the combination breeze may transport pollutants from the coastline to more than 100 km inland. The air masses then reach the Pyrenees mountain range, which inject them in the mid-troposphere at 2000–4000 m a.s.l., creating a stratified reservoir layer of aged pollutants (Millán et al., 1996). There, the prevailing westerly winds transport the air masses back to the Mediterranean, where they sink to compensate the typical thermal lows that form at surface during the warm periods (subsidence) (Gangoiti et al., 2001; Millán et al., 1991). In addition, northerly jet-like winds associated with the Azores anticyclone, channeled in the geographical gap between the Pyrenees and the Alps, add to the downslope nocturnal winds, transporting the pollutants southwards to the sea at night. During daytime, this flow is deflected eastwards, as a consequence of the formation of diurnal high pressure systems in the Mediterranean basin associated with mesoscale sinking (Gangoiti et al., 2001). The repetition of this cycle for 2 to 5 days causes the accumulation and ageing of pollutants (Gangoiti et al., 2001). In general, the influence of the Azores anticyclone over southern Europe is more frequent in summer (Millán et al., 1997). However, the influence of the anticyclone in the area is not uncommon in spring and autumn as well, or even in winter. Therefore, this scenario can be active during any time of the year, although it is most favorable in late spring and early summer (**Papers II** and **III**), when the synoptic configuration favors this closed-loop circulation and the high insolation is highest, coinciding also with the period with the highest temperatures and lowest relative humidity.

Similar recirculation patterns have been observed in areas beyond the Mediterranean. In Madrid, the Guadarrama mountain range to the north of the city may create a closed-loop circulation of air masses similar to that of the Mediterranean basin, under certain conditions (Querol et al., 2018).

The vertical recirculation of air masses and accumulation of pollutants lead to very high concentrations of UFPs, which grow in diameter as the air masses age. In this case, UFPs are both primary and secondary, with the proportion of primary and secondary particles depending on the type of environment (regional background, urban, traffic…), the time of the day and season. Although the high number concentration of pre-existing particles prevents efficient NPF (**Papers II** and **III**), the concentration of nucleation-mode particles is very high. These particles are most probably primary, although it cannot be discarded that they are formed elsewhere and have been transported afterwards. In this scenario, early stages of particle formation are often detected as increases in sub-3 nm number concentrations and sub-10 nm bursts around sunrise, but the fresh

particles very rarely grow to larger sizes. There are two likely causes for this: either the incoming polluted air masses increase the scavenging of these small fresh particles, or the breeze carries away the local air mass enriched with freshly formed particles, which may continue to grow further outside our measuring bounds. In the rare cases when freshly formed particles are observed to grow further in this scenario, growth rates are higher than in cleaner days. This suggests that the transported air masses are enriched with condensable vapors that overcome the scavenging by the high number of pre-existing particles. This has also been observed in Chinese megacities, where growth rates are higher during more polluted events (Kulmala et al., 2017; Qi et al., 2015; Wu et al., 2007).

The high insolation in this scenario, added to the accumulation of precursors and vertical recirculation of air masses also favor the formation of O_3. Additionally, fumigation processes related to convective activity bring O_3 accumulated in high-altitude reservoirs down to surface level (Millán et al., 2002). Despite deposition and O_3 consumption at night, the daily formation and the vertical recirculation of O_3 formed on previous days, as well as external contributions, lead to very high O_3 concentrations that often exceed the air quality standards and guidelines (Section 1.3), as described in **Paper II**.

Vertical soundings carried out during this scenario in **Paper II** clearly showed that the combined breeze transports air masses enriched with UFPs and O_3 (Figure 4.2). Their vertical distributions are similar to that of the wind speed — with higher values in the lower levels, but low values just above the surface — and increase towards midday (Figure 4.3). Additionally, there is significant O_3 formation during the day, apparently independent of the transported air masses. The high number concentration of pre-existing particles is probably responsible for the absence of NPF during the soundings. However, the instrumentation used in the soundings only measured the size distribution of particles greater than 10 nm in diameter. Thus, it remains unclear whether the first stages of nucleation occur in the mixing layer in these cases.

4.1.2 Venting scenario

In contrast to the recirculation scenario, the venting scenario is characterized by strong or moderate synoptic and mesoscale winds that favor the dilution of pollutants, mainly in periods with atmospheric instability, during the passage of fronts or cold air masses aloft that may cause precipitation. The strong winds prevent the formation of well-developed breezes, thus the atmospheric circulation is not a closed loop as in the recirculation scenario, and the air masses change frequently. These conditions are opposite to those governing recirculation episodes, in

which the influence of the Azores anticyclone blocks the passage of fronts in the area. For this reason, the two scenarios cannot occur simultaneously and they are constantly alternating.

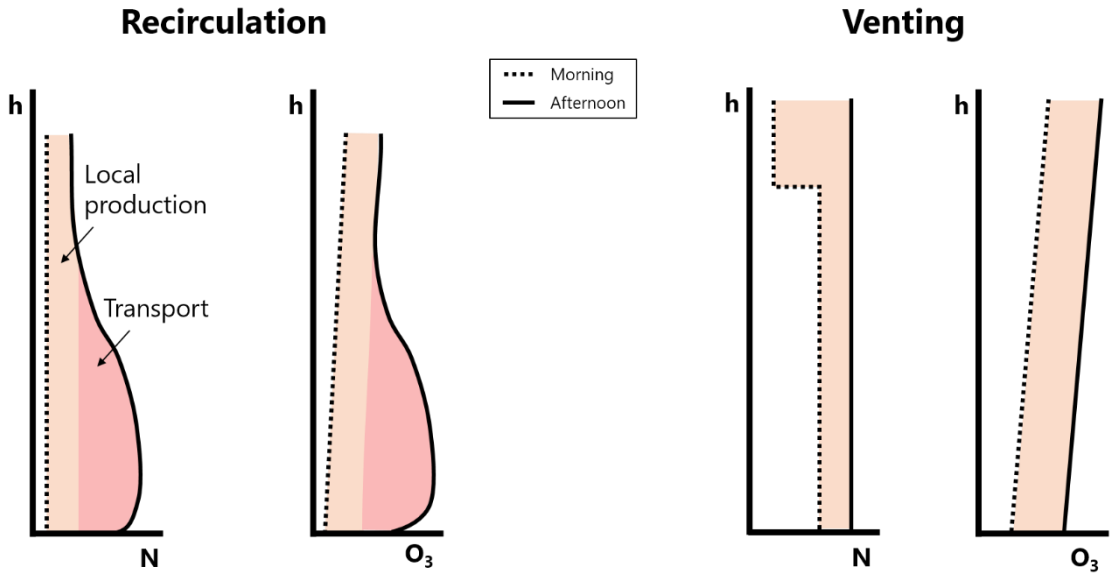

Figure 4.3: Schematic of the vertical profile of the particle number concentration (N) and ozone concentration (O_3) during recirculation and venting episodes, according to the balloon sounding measurements reported in **Papers I** and **II**. Dotted lines represent the distribution in the morning and solid lines represent the distribution in the afternoon. The O_3 profile in venting scenarios has been conceptualized after the measurements reported by Querol et al. (2018), which were carried out simultaneously during the intensive campaign reported in **Paper I**.

The absence of stagnation prevents the accumulation of pollutants and precursors, which leads to relatively low CS and O_3 formation. In spite of this, O_3 levels may still be high in these conditions, compared to the rest of the year. Additionally, the lack of strong breezes transporting pollutants and precursors leads to relatively clean atmospheres in remote areas that are usually affected by polluted air masses during recirculation episodes.

It is important to bear in mind that O_3 is a high oxidant with an important role in oxidizing gaseous pollutants involved in NPF. In these summer-spring venting episodes the O_3 levels are much lower than during the recirculation scenario, but markedly high compared with the rest of the year. The concentrations might be high enough to favor the occurrence of NPF in conditions with low CSs.

The balance between the availability of precursors and particle sinks determines the concentration of UFPs and the occurrence of NPF. If the concentrations of precursors are high enough, NPF takes place with formation rates sufficient to compensate the losses to the pre-existing aerosol. Those days had the highest negative ion and sub-3nm particle concentrations. However, growth rates in these cases are lower than during events that took place in recirculation

scenarios. This agrees with cleaner air masses, which would have lower particle sinks but also less condensable vapors, thus slowing down the growth processes. In this case, the concentration of UFPs is intermediate, with mainly secondary particles. By contrast, in some days, the availability of precursors may be too low due to lower emissions or atmospheric conditions that wash out the precursors or prevent the transport of nearby sources (**Paper II**). In these cases, the formation rates are lower than loss rates, thus the formation of particles is inefficient and the concentration of UFPs is very low. In general, the origin of UFPs in this scenario includes both primary and secondary particles. The contribution of secondary particles may dominate over primary particles, although the balance depends on the time of the day and local conditions.

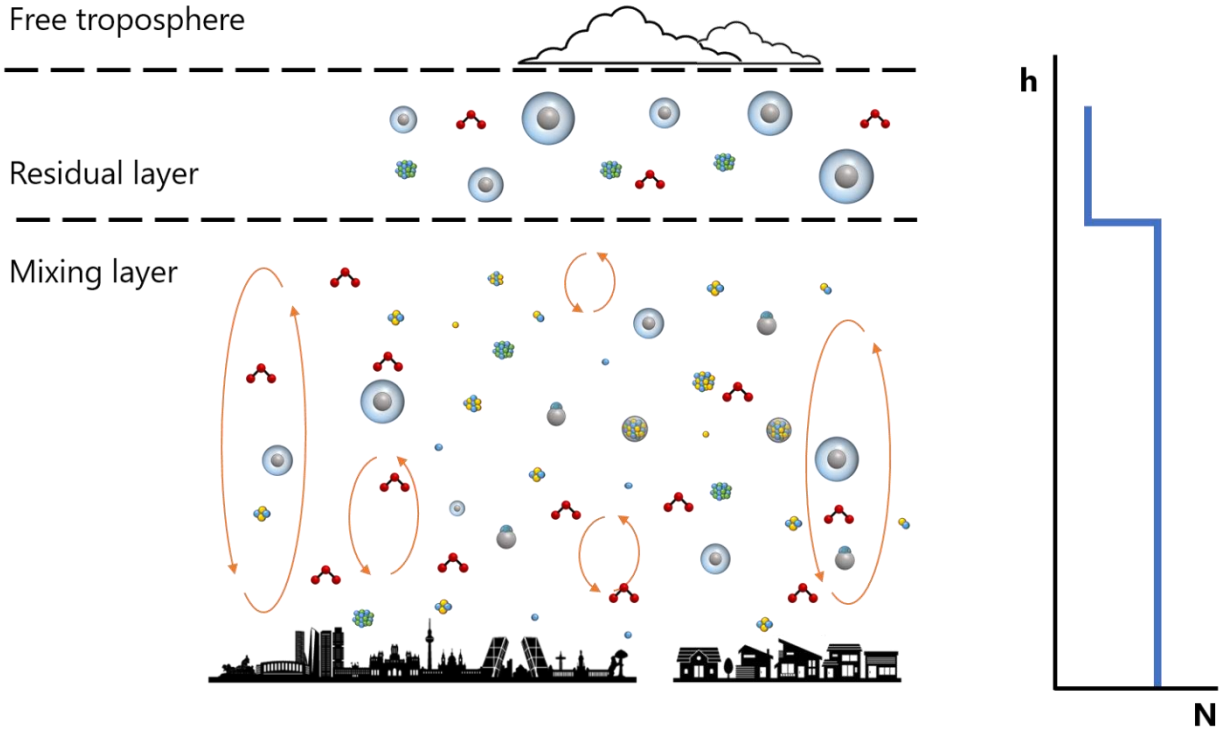

Figure 4.4: Conceptualization of the vertical and horizontal distribution of pollutants and vertical profile (see also Figure 4.3) of the total number of particles during a venting episode in urban and suburban environments, as reported in Madrid in **Paper I**. See legend in Figure 4.2.

NPF episodes in this scenario may be regional episodes, i.e., episodes take place simultaneously over large areas and even in different environments at the same time. As reported in **Paper I**, condensational growth starts simultaneously in the different environments and it coincides with the beginning of increasing O_3 concentrations, which peak in the afternoon. Nucleation-mode particles — including those related to traffic emissions — may be detected at any time in urban environments, even at night. By contrast, in cleaner locations such as suburban or regional

environments, nucleation-mode particles are only detected at daytime before midday, shortly before condensational growth is observed. Accordingly, it may be concluded that, in this scenario, particles may be formed or emitted locally depending on the environment, whereas the growth of particles is not caused by local precursors, but by precursors homogeneously distributed in an air mass covering a relatively wide area.

The formation of particles leads to maximum UFPs concentrations at midday, coinciding with the lowest BC concentrations at urban locations. However, rural locations affected by breezes may register the maximum UFP concentrations coinciding with the highest BC concentrations, because there are no local emissions of BC, it is transported and is usually maximum in the afternoon, shortly after the breeze has reached the maximum strength.

The total number concentration of particles starts increasing at sunrise simultaneously at urban and suburban locations, coinciding with the typical traffic rush emissions. This causes the particle sinks to increase as well at the same time, which inhibits the activation of freshly formed particles until around 9 UTC (11 local time), when particle sinks are at a relative minimums and the intensity of solar radiation is around its daily maximum. Particles then grow for a few hours up to around 50 nm in the afternoon. At that point, nucleation and Aitken mode particles may start shrinking coinciding with increases in wind speed and the decline of solar radiation. The subsequent dilution favors the evaporation of semi-volatile vapors. Shrinking seems to be a regional phenomenon and was previously reported by Cusack et al. (2013) in Montseny and Alonso-Blanco et al. (2017) in Madrid during warm periods. According to the observations reported in **Paper I**, larger particles (D_p > 40 nm) seem to have higher shrinking rates than smaller particles (D_p < 40 nm). Shrinking was not observed in accumulation mode particles. Focusing only on the particle diameter, this result may seem in apparent contradiction to the Kelvin effect (4.1), according to which the vapor pressure — an indication of the evaporation rate — is higher over a curved surface than over a flat surface (Thomson, 1871):

$$e_{sc}(T) = e_s(T) \cdot \exp\left(\frac{4\sigma}{n\,R\,T\,D_p}\right), \tag{4.1}$$

where e_{sc} is the vapor pressure over a curved surface, e_s is the vapor pressure over a flat surface, σ is the surface tension, n is the number of moles of the condensed phase per unit volume, R is the universal gas constant and D_p is the surface diameter.

Therefore, according to (4.1), molecules on the surface of small particles should evaporate more easily and have higher shrinking rates than those on the surface of larger particles, which have less curvature than small particles. There are several possible explanations of the discrepancy of this effect with our results. Firstly, the curvature effect decreases exponentially with the particle diameter, mainly affecting particles with less than around 20 nm in diameter, thus having a

negligible impact in the size ranges in which shrinking was observed in **Paper I**. Secondly, it is plausible that the densities of large particles are different from those of small particles. Kannosto et al. (2008) reported that nucleation mode particles have higher densities than Aitken mode particles, but are less dense than accumulation mode particles. The authors attributed the differences between nucleation and Aitken mode particles to the condensation of lighter compounds during growth stages. Accordingly, less densely distributed molecules over the surface of larger particles evaporate more easily than the more dense condensed molecules on smaller particles. This could also explain why shrinking was not observed in accumulation mode particles, which may be too dense. In the size ranges measured with our instrumentation, the differences in density probably have a bigger impact on the shrinking rate compared to the Kelvin effect. Finally, it is important to bear in mind that the shrinking rates of only a few regional events were calculated (16 occurrences in 8 days). It cannot be ruled out that a higher number of observations could lead to different results.

Another important result is the frequent detection of an Aitken mode that corresponds to particles formed on previous days. These particles are first detected as fresh particles in the nucleation mode one day and then alternate stages of growth and shrinkage over consecutive days until they are diluted or grow beyond the detection limit of the instrumentation. The fact that this phenomenon is observed during a venting scenario suggests that these particles are regional particles present in a vast area because, despite the local changes of air masses due to the strong winds, the particles are detected uninterruptedly throughout multiple days.

Balloon soundings performed in venting scenarios (**Paper I**) revealed the structure of the atmospheric boundary layer (Figure 4.3 and Figure 4.4), which evolved during the day. At sunrise, convective activity starts to develop a mixing layer that deepens towards midday. The concentration of UFPs also increases throughout the day, with homogenous concentrations in all of the vertical extension of the layer. Therefore, as convection heightens the mixing layer, particles emitted or formed at ground level are detected at higher altitudes. On the other hand, the vertical distribution of O_3 does not seem to be influenced by the vertical structure of the atmospheric boundary layer or the height of the mixing layer, although it does affect the magnitude of O_3 concentrations (Querol et al., 2018).

NPF is observed throughout the mixing layer, simultaneous with regional events registered at surface level (**Paper I**). The fact that these suburban events are registered almost simultaneously at surface level at the urban locations suggests that the vertical distribution of atmospheric processes conceptualized in Figure 4.4 is similar in urban and suburban environments that are nearby. Growth rates were very similar aloft and at surface, which points to a homogeneous distribution of condensable vapors throughout the mixing layer. Particle shrinking was also observed aloft, related to increases of wind speed that enhanced evaporation of the particles, as

observed at surface. The regional growth of particles formed in previous days is also detected throughout the mixing layer.

As in the recirculation scenario, the concentrations of UFPs in the venting scenario are higher on days with shallower mixing layers (**Paper I**), i.e., days with lower convective activity, which also have higher formation rates. Thus, the higher UFPs concentrations in days with lower mixing layer heights owe to both a more intense NPF and to less volume in which the particles are vertically distributed.

Above the mixing layer, the balloon soundings revealed a layer that is probably the remnant of the mixing layer of the previous day (residual layer, see Figure 4.1). Once the convective activity stops, a shallow stable layer forms at surface layer, and the remaining previously mixed layer becomes the residual layer, which is detached from the surface. When the sun rises again on the following day, convective cells develop a new mixing layer that heightens throughout the day. This makes the lower limit of the residual layer be detected at higher altitudes as the mixing layer develops. In the boundary between the mixing and residual layers, the concentration of UFPs decreased sharply. In the residual layer, the particle size distribution was considerably different to that in the mixing layer. Particles in the residual layer were larger, more aged, than in the mixing layer. Additionally, no nucleation-mode particles were detected in the residual layer and NPF was not observed at any time at this higher altitude. However, Aitken-mode particles, some of them probably formed in the mixing layer on previous days, were observed to grow in the residual layer. Our results show that particles in the residual layer have lower growth rates than in the mixing layer, probably due to a lower concentration of vapors that are able to condense onto particles, compared to the mixing layer. Accordingly, it may be concluded that the vapors are emitted at the surface and are vertically mixed during the day via convection inside the mixing layer. When convective activity ceases at sunset, the residual layer contains leftover vapors that were not able to condense onto particles during the day. These vapors may be involved in particle growth inside the residual layer, but since the layer is isolated from surface emissions, no additional vapors are introduced in the layer and the concentration of vapors eventually diminishes.

In summer, venting episodes are registered with relatively low temperatures in all environments. However, our results lead to different conclusions regarding the relative humidity, which depends on the location and type of analysis used to identify NPF episodes. In the urban and suburban locations in Madrid (**Paper I**) and the regional background in Montseny (**Paper II**), the NPF episodes coincided with periods with high relative humidity. However, in the urban and regional backgrounds of Barcelona and Montseny (**Paper III**), days in which NPF dominate the total number of particles, which is considered as a proxy of venting episodes in that study, occurred with low relative humidity. The latter is contrary to the findings of **Paper II** for the relative

humidity at Montseny and with the result of **Paper I** in Madrid. However, it is consistent with previous studies that have reported that low relative humidity enhances NPF (Brines et al., 2015; Kulmala et al., 2004; Kulmala and Kerminen, 2008). The fact that the relative humidity was found to be higher in periods with NPF events in **Paper I** may be related to the fact that the relative humidity depends on the temperature and, accordingly, it is not a direct representation of the amount of water in the atmosphere, which could be the actual factor that influences NPF. Another possible explanation that could also explain the inconsistency of the findings in Montseny could be the fact that the conditions during a venting scenario can be very diverse conditions, as discussed here earlier. It is possible that the different circumstances causing NPF events in venting scenarios (concentrations of H_2SO_4 and O_3, insolation, type of VOCs…) are linked to different atmospheric conditions that are compatible with both low and high relative humidity.

4.2 How are UFPs and O_3 Episodes Connected?

It is well known that O_3 favors NPF by acting as an oxidant, for example by favoring the oxidation of SO_2 into H_2SO_4, and by producing OH that enhance particle formation rates (Hao et al., 2009). Additionally, ozonolysis contributes to the condensational growth of particles (Hao et al., 2009). Thus, it is not evaluated here if O_3 is relevant for NPF, but rather if intense O_3 episodes coincide with high UFPs concentrations, and specifically with NPF. Accordingly, one of the main objectives of this thesis was to elucidate the relationship between UFPs episodes and O_3 episodes (Objective 2), determining whether they are occurring simultaneously driven by the same processes, influencing each other, occurring in parallel with the same seasonality pattern or are unrelated (see Section 1.4).

The findings from this thesis, especially those summarized in the conceptual model described in Section 4.1, suggest that there may be a link between UFPs and O_3 episodes. In particular, it seems that the conditions leading to recirculation events favor both UFPs and O_3 episodes (*case a* in Section 1.4), and these often occur during the same day.

Nevertheless, the previous conclusion does not rule out all the other possibilities. For instance, it cannot be cannot discarded the fact that, on specific days, the conditions that favor the UFPs episodes disfavor O_3 episodes, or vice versa (*case c* in Section 1.4). In fact, during venting episodes, when the formation of O_3 is low compared to recirculation episodes, but high enough to favor the oxidation of precursors, the formation of new particles is most favored. Although the concentration of UFPs in these cases is not as high as during recirculation events, this inverse connection has to be considered too. Thus, during the summer recirculation episodes it is not the acute O_3 pollution that inhibits the formation of particles, but that these maximal O_3

concentrations occur with environmental conditions that disfavor NPF, such as a high CS due to the recirculation and aging of air masses.

In summary, UFPs episodes are undoubtedly related to O_3 episodes, but the connection between them is rather complex. Both pollutants are higher in spring and summer, but the episodes may or may not be simultaneous on the same day during this warm period, depending on the atmospheric conditions. The occurrence of an O_3 episode on a given day seems to be always concurrent with an UFPs episode caused by accumulation of primary and secondary particles. However, high UFPs concentrations caused by NPF are mostly occurring with relatively lower O_3 concentrations (but still high in absolute concentration) during venting periods. In any case, both UFPs and O_3 concentrations and episode occurrences have a similar evolution throughout the year, when considering months or seasons instead of separate days. As stated in Section 1.4, this result has been widely reported in the literature, but it is difficult to elaborate on the relationship between both episodes when doing statistical analysis that use long-term series. Previous studies failed to explore the complex dynamics of the episodes of both pollutants that are exposed here.

4.3 Contributions to the Concentration of UFPs

To better understand how UFPs concentrations evolve and to identify the factors that are influencing their evolution (Objective 3) it is important to identify and apportion the different sources and processes that contribute to the aerosol population.

Regarding the contribution of NPF, our research found that, on days with NPF events, the number of UFPs related to NPF is higher than the number of particles related to traffic emissions (**Paper I**). However, when considering long-time series, the majority of days do not have NPF events (**Papers II** and **III**). For this reason, when considering the average annual UFPs concentrations, our results show that primary emissions (mainly from traffic) have a greater contribution to the total number of particles in urban locations than NPF (**Paper III**). In fact, NPF takes place in only 7–14% of the days at the locations with long-term measurements considered in this thesis (**Papers II** and **III**). These results agree with the 10–30% reported for European urban and rural locations in the literature (Kerminen et al., 2018). Nonetheless, with the generalized decreasing anthropogenic emissions reported in **Paper III** and references therein, the number of days with NPF events is increasing. Therefore, the contribution of NPF to the number of UFPs is increasing as well. The total number of UFPs, however, may either increase or decrease, depending on the local conditions and precursor emissions (natural and anthropogenic). On one hand, the decline in anthropogenic emissions would reduce the number of primary UFPs, consequently reducing

the total number of UFPs. On the other hand, decreasing UFPs leads to a decline in condensation and coagulation sinks, thus NPF is more favored, which could increase the number of UFPs.

In rural environments, primary UFPs anthropogenic emissions are minor contributors to the total number of particles. Despite a decline in transported anthropogenic precursors, the local natural precursors are able to form new particles because of the decrease in sinks. Moreover, the increasing temperatures are probably enhancing the emission of natural precursors (Lathière et al., 2006). Thus, NPF becomes more favorable and the concentrations of UFPs increase in rural environments (**Paper III**). On the other hand, our results show that in rural environments NPF is more favored in weekdays than in weekends (**Paper III**), revealing that anthropogenic emissions enhance the formation of new particles not only in urban locations, but also in nearby environments affected by the transport of urban emissions. This is in apparent contradiction with the fact that NPF increases when anthropogenic emissions decrease. A possible explanation for this inconsistency might be that a certain amount of anthropogenic precursors is required for efficient NPF. If the emissions are below that threshold, for example during weekends, NPF is disfavored. However, if the emissions during the weekdays decrease but are above that threshold, NPF becomes more favorable because there are enough precursors to form particles but there are less sinks scavenging those particles.

In urban environments, where anthropogenic primary particles have a major contribution to the total number of particles, the decline in anthropogenic emissions leads to a direct decrease in the total number of UFPs. These results suggest that, in urban environments, the decrease in anthropogenic emissions of atmospheric pollutants reduces both the precursors and sinks in a similar proportion. The number of days with conditions favorable for NPF increase only slightly compared to the marked increase in regional environments.

In summary, reducing anthropogenic emissions of atmospheric pollutants in urban areas results in a decrease of the total number particle concentrations in these locations. In rural environments, the trend is inverse: the declining trend in anthropogenic emissions results in an increase of the total number of particles (**Paper III**). There are several explanations for the contrasting results between urban and rural environments. Firstly, the generally rising temperatures may play an important role in this result, since the local emission of biogenic precursors may be increasing. The different influence of biogenic emissions is also evident when looking at the different seasonality of NPF episodes in different environments. At the regional background, NPF events are most frequent in spring, when biogenic emissions are expected to be maximal, whereas at urban locations, which are not expected to be influenced by biological processes, NPF episodes are most favorable in summer. Nonetheless, increasing biogenic emissions could also increase the CS to a point where NPF is inhibited. Although this does not seem to be the case, further research

is needed to investigate and quantify the differences in the composition of precursors, specifically those related to biogenic emissions.

Secondly, the policies implemented in recent years aiming at decreasing primary emissions have had a notable impact in the total number of particles at urban environments, given that primary vehicle exhaust particles dominate the total aerosol budget there. However, since primary particles have a lesser contribution at rural environments, these policies probably have not significantly diminished the total number of particles in the regional background.

Thirdly, the fact that secondary particles increase at the regional background, whereas these show no trend at the urban background, may indicate that there is a significant increase in NPF at the regional background — probably favored by the reduction of particles transported from urban and industrial areas — that is contributing to increasing the total number particle concentration. However, this does not explain why the reduction of particle sinks does not lead to significantly increasing NPF and the number concentration of secondary particles at the urban background.

Lastly, it is important to bear in mind the different measuring ranges of the instrumentation used in our studies. In the data analysis reported in **Paper III**, the lower range of particle size distributions (10–15 nm) had to be discarded at the urban background station due malfunctioning instrumentation for a considerable length of the long-term series. The issue could not be fully identified and, accordingly, the correction of the series was not possible. The exclusion of the lower size range may have had a great impact in the analysis of the contribution of NPF to the aerosol population in urban areas. Thus, these results should be interpreted with caution, since an underestimation of the total and nucleation-mode number particle concentrations cannot be excluded at the urban background.

5 CONCLUSIONS

The main objective of this thesis was to characterize the main environmental patterns governing UFPs episodes and offer some insights on their connection with those of tropospheric O_3. Intensive campaigns carried out during UFPs and O_3 episodes have contributed to advance the understanding of how the concentrations of these pollutants vary in time and space. Additionally, the evaluation of long-term datasets at fixed locations has revealed the seasonality of UFPs and O_3 episodes. The latter has also provided insights on the factors driving the trends on UFPs concentrations over the last decade. The following main conclusions were extracted from this thesis:

- The formation and transport of UFP and O_3 at local and regional scales are governed by two distinct scenarios: vertical recirculation of air masses and venting scenarios. Typically, each of these scenarios persists for a few days and are constantly alternating in summer and spring. The occurrence of either scenario is mainly determined by large-scale meteorological conditions, whereas the increase in the magnitude of UFP and O_3 concentrations in each scenario is modulated by the availability of precursors and by local atmospheric and orographic conditions.

- In the recirculation scenario, the closed-loop recirculation causes the accumulation of pollutants and leads to very high concentrations of UFPs — which grow in diameter by condensation of vapors as the air masses age — and O_3, with simultaneous episodes on the same day. UFPs are both primary and secondary, with contributions to bulk number particle concentrations depending on the type of environment, time of the day and season. The large number of pre-existing particles caused by accumulation of pollutants generally prevents efficient NPF in this scenario.

- In the venting scenario, strong winds prevent the formation of well-developed breezes, thus the atmospheric circulation is not a closed loop as in the recirculation scenario, and the air masses change frequently. The absence of stagnation and recirculation prevents the accumulation of pollutants and precursors, which leads to intermediate or low concentrations of UFPs and relatively low particle condensation and coagulation sinks and O_3 formation. Yet, these relatively low O_3 concentrations, but high in absolute values, are

high enough to favor the occurrence of NPF in conditions with low sinks, given its important role in oxidizing gaseous pollutants involved in nucleation processes.

- During NPF events measured in venting scenarios, particles may be formed or emitted locally, whereas the growth of these particles by condensation of vapors may be simultaneous in large areas. Thus, it can be concluded that the formation of particles is a local process and particle growth is a regional process, each of them controlled by different gaseous precursors. In any case, the precursors of both processes are emitted or formed at surface level and are vertically well mixed inside the mixing layer during the day.
- When considering the average annual UFPs concentrations, primary emissions (mainly from traffic) have a greater contribution to the total number particle concentrations in urban areas than NPF. However, on days with NPF events, the contribution of NPF to bulk number concentration is higher than that of traffic emissions.
- When considering long-time series, NPF events occur only in a low proportion of days per year. Nonetheless, the number of days with NPF events is increasing due to a general decreasing trend in anthropogenic emissions of atmospheric pollutants. Therefore, the contribution of NPF to the number concentration of UFPs is increasing as well.
- The total number concentration of UFPs may either increase or decrease, depending on the type of environment. In urban areas, the decline in anthropogenic emissions causes a direct decrease in the total number concentration of UFPs. In rural environments, NPF becomes more favored and the total concentration of UFPs increases. This is probably caused by an increase in the local biogenic emission of precursors caused by the rising temperatures, as well as by a reduction of condensation and coagulation sinks due to the decline in the transported air pollutants as a result of emission abatement policies. Nonetheless, a potential slight increase of specific anthropogenic precursors (SO_2) could have enhanced NPF to some extent in the rural environment evaluated in this thesis.
- NPF events have a different seasonality in rural and urban environments. In rural environments, NPF are most favored in spring, when the emission of biogenic precursors is at its maximum. In urban environments, where biogenic emissions do not play an important role, NPF is found to be most favored in summer, probably due to higher insolation and slightly higher SO_2.
- UFPs episodes are undoubtedly linked with tropospheric O_3 episodes. However, the connection between the two pollutants is complex. In particular, it seems that the conditions leading to vertical air mass recirculation events favor both UFPs and O_3 episodes, and these often occur during the same day. Yet, on specific days, the conditions that favor the UFPs episodes disfavor O_3 episodes, or vice versa.

- The concentrations and frequency of episodes of UFPs and O_3 have a similar pattern when considering months or seasons instead of separate days. The concentrations and frequencies of episodes of both pollutants are higher in spring and summer, but the episodes may or may not be simultaneous on the same day during this warm period, depending on the atmospheric conditions and patterns of the emission of precursors. The occurrence of an O_3 episode on a given day seems to be always concurrent with an UFPs episode caused by a regional accumulation of primary and secondary particles. However, high UFPs concentrations caused by NPF are mostly occurring with relatively low O_3 concentrations during venting periods (low for spring and summer, but high in absolute levels). During the summer recirculation episodes it is not the acute O_3 pollution that inhibits the formation of new particles, but that these maximal O_3 concentrations occur with environmental conditions that disfavor NPF, such as a high CS due to the increase of the concentration of atmospheric particulate matter caused by recirculation and aging of air masses.
- The policies implemented in recent years aiming at decreasing primary emissions of particulate matter and gaseous pollutants have had a notable positive impact in abating the total number particle concentrations in urban environments. However, these policies probably have not significantly diminished the total number of particles in the regional background.
- Abatement policies have had a general positive effect in the reduction of pollutant concentrations. Nonetheless, the air quality might decay in certain areas by increasing the total number particle concentrations, as observed in the regional background. Still, taking into account the human exposure to these changes, it is recommended that abatement policies continue to be applied and reinforced, given that the more densely populated urban areas would benefit from them.
- There is a clear increasing trend in NPF at the regional background. In urban locations, the increase in the number of NPF events is small but not insignificant. Therefore, it is important to continue monitoring the concentration of UFPs and periodically inspecting the evolution and occurrences of NPF events, because they may eventually lead to an increase in the number particle concentrations in urban locations. The health effects of particles from NPF have not been studied enough to this date, but an increase of these particles might have adverse effects for a large number of inhabitants, since these areas are usually densely populated. In addition, future research should address the global changes in particle number concentrations due to the changes in anthropogenic emissions. A global increase in the number of particles could have severe effects not only in human health but also in climate.

6 FUTURE RESEARCH

The following list provides suggestions for future research that could allow addressing the limitations and gaps of knowledge that have been identified in this thesis.

- The measurements of hourly VOCs concentrations were performed only during intensive field campaigns at Madrid, Barcelona and Montseny using a PTR-TOF-MS. Unfortunately, these measures provided data for only short periods of time. Consequently, there is a lack of continuous measurements of VOCs precursors of secondary organic particles and O_3 influencing the UFP and O_3 episodes described in this thesis. Given the crucial role that these play in NPF and O_3 formation, it is of critical importance to have continuous measurements of VOCs concentrations for future research on this topic. Recently, a PTR-MS has been installed at Montseny, which will provide valuable information on UFPs and O_3 episodes at this location, specifically on biogenic precursors, and a new PTR-TOF-MS will be installed in Barcelona.

- A general limitation in some of the results presented in this thesis is the measuring size range of the instruments used. Although in **Paper I** instrumentation that is more precise was used for the intensive campaign, the typical size cut-off of the particle sizers used in long-term measurements is around 10 nm. Moreover, the particle size distribution below 15 nm at Barcelona had to be discarded in the analysis of **Paper III** due to an unknown instrument malfunction. Given that the initial — and perhaps most important — stages of NPF events occur below this size, the use of instruments with a lower size detection limit is strongly recommended for future research. This would allow for a better identification of NPF events, some of which might be underestimated or even overlooked with the instrumentation currently in use.

- On a similar note, future experiments using balloon soundings should try to use instruments with a lower size detection limit. This, coupled with earlier morning flights before convection becomes efficient could help elucidate whether NPF takes place all over the mixing layer at any time or it is limited to happen at the surface and the particles are later mixed to upper levels.

- Future experimental campaigns aimed at measuring the vertical distribution of pollutants could explore alternative sounding systems that are easier to operate and transported and are less dependent of meteorological conditions. Drone soundings may be a good alternative, although the limited payload capacity, compared to balloon soundings, may pose difficulties in experiments measuring with multiple instruments at the same time. Additionally, some authorities may require specific licenses to operate drones and airfield limitations in restricted areas. Finally, the effect of the air displacement generated by the drone wings, which could influence the sampling, should be taken into account if drones are used for this type of soundings.

- Improving the identification of NPF episodes would benefit future research. On the one hand, the classification of episodes chosen in this thesis is rather limited due to the instrumentation available to measure particle size distributions. With the method and instrumentation used, a considerable number of days are classified as undefined events, which are not considered for analysis. A large number of these events could have been properly classified if instrumentation with lower size detection limits would have been used. On the other hand, future studies could benefit from a routine classification of NPF events at all stations that measure the size distribution of aerosols. Accordingly, a comparison between multiple stations would allow studying the extent and characteristics of regional UFPs episodes. However, this classification is time-consuming and ideally requires a group of at least two scientists manually classifying each day. Moreover, the traditional visual methods have inherently a subjective component. For all of this, this field of study would benefit from more research in the development of NPF classification schemes that use machine learning and data mining to reduce time costs and subjectivity.

- Moreover, the choice of the methodology used to estimate the contribution of NPF to UFPs concentrations, i.e., event classification in **Papers I** and **II** and source apportionment in **Paper III**, might lead to different results. Each of these methods has intrinsic uncertainties and limitations that require cautious interpretation of the results. Future studies should consider the suitability of each method, and choose one or the other depending on the type of analysis needed and the resources available.

- Another limitation of this thesis is that the studies are based exclusively on experimental measurements and the subsequent data analysis. Future studies combining experimental data with meteorological, emission and/or photochemical models would certainly offer valuable insight into this field of study.

- Finally, given that NPF is becoming more favorable in recent years, future studies should evaluate the effects of these secondary UFPs on health effects and climate, considering their effects on cloud formation and composition, the duration of the events and the associated radiative forcing.

REFERENCES

Note that the scientific publications included in the compendium have their own list of references and are not included here.

Alonso-Blanco, E., Gómez-Moreno, F. J., Núñez, L., Pujadas, M., Cusack, M. and Artíñano, B.: Aerosol particle shrinkage event phenomenology in a South European suburban area during 2009–2015, Atmos. Environ., doi:10.1016/j.atmosenv.2017.04.013, 2017.

Arnfield, A. J.: Two decades of urban climate research: a review of turbulence, exchanges of energy and water, and the urban heat island, Int. J. Climatol., 23(1), 1–26, doi:10.1002/joc.859, 2003.

Atkinson, B. W.: Mesoscale atmospheric circulations, Academic Press, London., 1982.

Avnery, S., Mauzerall, D. L., Liu, J. and Horowitz, L. W.: Global crop yield reductions due to surface ozone exposure: 2. Year 2030 potential crop production losses and economic damage under two scenarios of O3 pollution, Atmos. Environ., doi:10.1016/j.atmosenv.2011.01.002, 2011.

Bianchi, F., Kurtén, T., Riva, M., Mohr, C., Rissanen, M. P., Roldin, P., Berndt, T., Crounse, J. D., Wennberg, P. O., Mentel, T. F., Wildt, J., Junninen, H., Jokinen, T., Kulmala, M., Worsnop, D. R., Thornton, J. A., Donahue, N., Kjaergaard, H. G. and Ehn, M.: Highly Oxygenated Organic Molecules (HOM) from Gas-Phase Autoxidation Involving Peroxy Radicals: A Key Contributor to Atmospheric Aerosol, Chem. Rev., 119(6), 3472–3509, doi:10.1021/acs.chemrev.8b00395, 2019.

Birmili, W., Berresheim, H., Plass-Dülmer, C., Elste, T., Gilge, S., Wiedensohler, A. and Uhrner, U.: The Hohenpeissenberg aerosol formation experiment (HAFEX): a long-term study including size-resolved aerosol, H2SO4, OH, and monoterpenes measurements, Atmos. Chem. Phys., 3(2), 361–376, doi:10.5194/acp-3-361-2003, 2003.

Bond, T. C., Doherty, S. J., Fahey, D. W., Forster, P. M., Berntsen, T., Deangelo, B. J., Flanner, M. G., Ghan, S., Kärcher, B., Koch, D., Kinne, S., Kondo, Y., Quinn, P. K., Sarofim, M. C., Schultz, M. G., Schulz, M., Venkataraman, C., Zhang, H., Zhang, S., Bellouin, N., Guttikunda, S. K., Hopke, P. K., Jacobson, M. Z., Kaiser, J. W., Klimont, Z., Lohmann, U., Schwarz, J. P., Shindell, D., Storelvmo, T., Warren, S. G. and Zender, C. S.: Bounding the role of black carbon in the climate system: A scientific assessment, J. Geophys. Res. Atmos., doi:10.1002/jgrd.50171, 2013.

Brean, J., Beddows, D. C. S., Shi, Z., Temime-Roussel, B., Marchand, N., Querol, X., Alastuey, A., Minguillon, M. C. and Harrison, R. M.: Molecular insights into new particle formation in Barcelona, Spain, Atmos. Chem. Phys., doi:10.5194/acp-20-10029-2020, 2020.

Brines, M., Dall'Osto, M., Beddows, D. C. S., Harrison, R. M., Gómez-Moreno, F., Núñez, L., Artíñano, B., Costabile, F., Gobbi, G. P., Salimi, F., Morawska, L., Sioutas, C. and Querol, X.: Traffic and nucleation events as main sources of ultrafine particles in high-insolation developed world cities, Atmos. Chem. Phys., 15(10), 5929–5945, doi:10.5194/acp-15-5929-2015, 2015.

Buenrostro Mazon, S., Riipinen, I., Schultz, D. M., Valtanen, M., Maso, M. D., Sogacheva, L., Junninen, H., Nieminen, T., Kerminen, V. M. and Kulmala, M.: Classifying previously undefined days from eleven years of aerosol-particle-size distribution data from the SMEAR II station, Hyytiälä, Finland, Atmos. Chem. Phys., doi:10.5194/acp-9-667-2009, 2009.

Cassee, F. R., Mills, N. L. and Newby, D.: Cardiovascular Effects of Inhaled Ultrafine and Nanosized Particles, John Wiley & Sons, Inc., Hoboken, NJ, USA., 2011.

Cassee, F. R., Morawska, L., Peters, A., Wierzbicka, A., Buonanno, G., Cyrys, J., SchnelleKreis, J., Kowalski, M., Riediker, M., Birmili, W., Querol, X., Yildirim, A. Ö., Elder, A., Yu, I. J., Øvrevik, J., Hougaard, K. S., Loft, S., Schmid, O., Schwarze, P. E., Stöger, T., Schneider, A., Okokon, E., Samoli, E., Stafoggia, M., Pickford, R., Zhang, S., Breitner, S., Schikowski, T., Lanki, T. and Tobias, A.: Ambient ultrafine particles: evidence for policy makers [White paper], , 1–23 [online] Available from: https://efca.net/files/WHITE PAPER-UFP evidence for policy makers (25 OCT).pdf, 2019.

Charron, A. and Harrison, R. M.: Primary particle formation from vehicle emissions during exhaust dilution in the roadside atmosphere, Atmos. Environ., doi:10.1016/S1352-2310(03)00510-7, 2003.

Cusack, M., Alastuey, A. and Querol, X.: Case studies of new particle formation and evaporation processes in the western Mediterranean regional background, Atmos. Environ., 81, 651–659, doi:10.1016/j.atmosenv.2013.09.025, 2013.

Dada, L., Chellapermal, R., Buenrostro Mazon, S., Paasonen, P., Lampilahti, J., E Manninen, H., Junninen, H., Petäjä, T., Kerminen, V. M. and Kulmala, M.: Refined classification and characterization of atmospheric new-particle formation events using air ions, Atmos. Chem. Phys., doi:10.5194/acp-18-17883-2018, 2018.

Dada, L., Ylivinkka, I., Baalbaki, R., Li, C., Guo, Y., Yan, C., Yao, L., Sarnela, N., Jokinen, T., Daellenbach, K. R., Yin, R., Deng, C., Chu, B., Nieminen, T., Wang, Y., Lin, Z., Thakur, R. C., Kontkanen, J., Stolzenburg, D., Sipilä, M., Hussein, T., Paasonen, P., Bianchi, F., Salma, I., Weidinger, T., Pikridas, M., Sciare, J., Jiang, J., Liu, Y., Petäjä, T., Kerminen, V.-M. and Kulmala, M.: Sources and sinks driving sulfuric acid concentrations in contrasting environments: implications on proxy calculations, Atmos. Chem. Phys., 20(20), 11747–11766, doi:10.5194/acp-20-11747-2020, 2020.

Dal Maso, M., Kulmala, M., Riipinen, I., Wagner, R., Hussein, T., Aalto, P. P., Lehtinen, K. E. J., Maso, D., Kulmala, M., Riipinen, M., Wagner, I., Hussein, R., Aalto, T. and Lehtinen, P. P. &: Formation and growth of fresh atmospheric aerosols: eight years of aerosol size distribution data from SMEAR II, Hyytiälä, Finland, Boreal Environ. Res., 10, 323–336, 2005.

Dall'Osto, M., Querol, X., Alastuey, A., O'Dowd, C., Harrison, R. M., Wenger, J. and Gómez-Moreno, F. J.: On the spatial distribution and evolution of ultrafine particles in Barcelona, Atmos. Chem. Phys., 13(2),

741–759, doi:10.5194/acp-13-741-2013, 2013.

Donahue, N. M., Kroll, J. H., Pandis, S. N. and Robinson, A. L.: A two-dimensional volatility basis set – Part 2: Diagnostics of organic-aerosol evolution, Atmos. Chem. Phys., 12(2), 615–634, doi:10.5194/acp-12-615-2012, 2012.

Drinovec, L., Močnik, G., Zotter, P., Prévôt, A. S. H., Ruckstuhl, C., Coz, E., Rupakheti, M., Sciare, J., Müller, T., Wiedensohler, A. and Hansen, A. D. A.: The "dual-spot" Aethalometer: An improved measurement of aerosol black carbon with real-time loading compensation, Atmos. Meas. Tech., doi:10.5194/amt-8-1965-2015, 2015.

Drobinski, P., Bastin, S., Dabas, A., Delville, P. and Reitebuch, O.: Variability of three-dimensional sea breeze structure in southern France: Observations and evaluation of empirical scaling laws, Ann. Geophys., 24(7), 1783–1799, doi:10.5194/angeo-24-1783-2006, 2006.

EC: Directive 2008/50/EC of 21 May 2008 on ambient air quality and cleaner air for Europe. [online] Available from: https://eur-lex.europa.eu/legal-content/EN/TXT/HTML/?uri=CELEX:32008L0050&from=ES, 2008.

EEA: Air quality in Europe - 2020 report. [online] Available from: https://www.eea.europa.eu/ds_resolveuid/XZWO12PVGN, 2020.

Ehn, M., Kleist, E., Junninen, H., Petäjä, T., Lönn, G., Schobesberger, S., Dal Maso, M., Trimborn, A., Kulmala, M., Worsnop, D. R., Wahner, A., Wildt, J. and Mentel, T. F.: Gas phase formation of extremely oxidized pinene reaction products in chamber and ambient air, Atmos. Chem. Phys., 12(11), 5113–5127, doi:10.5194/acp-12-5113-2012, 2012.

Ehn, M., Thornton, J. A., Kleist, E., Sipilä, M., Junninen, H., Pullinen, I., Springer, M., Rubach, F., Tillmann, R., Lee, B., Lopez-Hilfiker, F., Andres, S., Acir, I.-H., Rissanen, M., Jokinen, T., Schobesberger, S., Kangasluoma, J., Kontkanen, J., Nieminen, T., Kurtén, T., Nielsen, L. B., Jørgensen, S., Kjaergaard, H. G., Canagaratna, M., Maso, M. D., Berndt, T., Petäjä, T., Wahner, A., Kerminen, V.-M., Kulmala, M., Worsnop, D. R., Wildt, J. and Mentel, T. F.: A large source of low-volatility secondary organic aerosol, Nature, 506(7489), 476–479, doi:10.1038/nature13032, 2014.

ETC/ACM: Ozone in Southern Europe - Assessment and effectiveness of measures, , (April), 77, 2018.

Fernández-Camacho, R., Rodríguez, S., de la Rosa, J., Sánchez de la Campa, A. M., Viana, M., Alastuey, A. and Querol, X.: Ultrafine particle formation in the inland sea breeze airflow in Southwest Europe, Atmos. Chem. Phys., 10(19), 9615–9630, doi:10.5194/acp-10-9615-2010, 2010.

Fuchs, N. A. and Sutugin, A. G.: Highly dispersed aerosols, in Topics in Current Aerosol Research., 1971.

Fuchs, N. A., Daisley, R. E., Fuchs, M., Davies, C. N. and Straumanis, M. E.: The Mechanics of Aerosols, Phys. Today, 18(4), 73–73, doi:10.1063/1.3047354, 1965.

Gangoiti, G., Millán, M. M., Salvador, R. and Mantilla, E.: Long-range transport and re-circulation of pollutants in the western Mediterranean during the project Regional Cycles of Air Pollution in the West-Central Mediterranean Area, Atmos. Environ., 35(36), 6267–6276, doi:10.1016/S1352-2310(01)00440-

X, 2001.

Giere, R. and Querol, X.: Solid Particulate Matter in the Atmosphere, Elements, 6(4), 215–222, doi:10.2113/gselements.6.4.215, 2010.

Gordon, H., Kirkby, J., Baltensperger, U., Bianchi, F., Breitenlechner, M., Curtius, J., Dias, A., Dommen, J., Donahue, N. M., Dunne, E. M., Duplissy, J., Ehrhart, S., Flagan, R. C., Frege, C., Fuchs, C., Hansel, A., Hoyle, C. R., Kulmala, M., Kürten, A., Lehtipalo, K., Makhmutov, V., Molteni, U., Rissanen, M. P., Stozkhov, Y., Tröstl, J., Tsagkogeorgas, G., Wagner, R., Williamson, C., Wimmer, D., Winkler, P. M., Yan, C. and Carslaw, K. S.: Causes and importance of new particle formation in the present-day and preindustrial atmospheres, J. Geophys. Res. Atmos., 122(16), 8739–8760, doi:10.1002/2017JD026844, 2017.

Graus, M., Müller, M. and Hansel, A.: High resolution PTR-TOF: Quantification and formula confirmation of VOC in real time, J. Am. Soc. Mass Spectrom., 21(6), 1037–1044, doi:10.1016/j.jasms.2010.02.006, 2010.

Hansel, A., Jordan, A., Holzinger, R., Prazeller, P., Vogel, W. and Lindinger, W.: Proton transfer reaction mass spectrometry: on-line trace gas analysis at the ppb level, Int. J. Mass Spectrom. Ion Process., doi:10.1016/0168-1176(95)04294-U, 1995.

Hao, L. Q., Yli-Pirilä, P., Tiitta, P., Romakkaniemi, S., Vaattovaara, P., Kajos, M. K., Rinne, J., Heijari, J., Kortelainen, A., Miettinen, P., Kroll, J. H., Holopainen, J. K., Smith, J. N., Joutsensaari, J., Kulmala, M., Worsnop, D. R. and Laaksonen, A.: New particle formation from the oxidation of direct emissions of pine seedlings, Atmos. Chem. Phys., 9(20), 8121–8137, doi:10.5194/acp-9-8121-2009, 2009.

Hirsikko, A., Bergman, T., Laakso, L., Dal Maso, M., Riipinen, I., Hõrrak, U. and Kulmala, M.: Identification and classification of the formation of intermediate ions measured in boreal forest, Atmos. Chem. Phys., doi:10.5194/acp-7-201-2007, 2007.

Hoek, G., Krishnan, R. M., Beelen, R., Peters, A., Ostro, B., Brunekreef, B. and Kaufman, J. D.: Long-term air pollution exposure and cardio-respiratory mortality: A review, Environ. Heal. A Glob. Access Sci. Source, doi:10.1186/1476-069X-12-43, 2013.

Hopke, P. K.: Review of receptor modeling methods for source apportionment, J. Air Waste Manag. Assoc., doi:10.1080/10962247.2016.1140693, 2016.

Hussein, T., Dal Maso, M., Petaja, T., Koponen, I. K., Paatero, P., Aalto, P. P., Hameri, K. and Kulmala, M.: Evaluation of an automatic algorithm for fitting the particle number size distributions, Boreal Environ. Res., 10(5), 337–355, 2005.

ICP Vegetation: Ozone Pollution: A hidden threat to food security. [online] Available from: https://icpvegetation.ceh.ac.uk/sites/default/files/Ozone Pollution - A hidden threat to food security.pdf, 2011.

IPCC: Climate Change 2013: The Physical Science Basis. Contribution of Working Group I to the Fifth Assessment Report of the Intergovernmental Panel on Climate Change., 2013.

IUPAC: Compendium of Chemical Terminology, 2nd ed., Blackwell Scientific Publications, Oxford., 2009.

Jaenicke, R.: Chapter 1 Tropospheric Aerosols, in Aerosol-cloud-climate interactions, pp. 1–31., 1993.

Joutsensaari, J., Ozon, M., Nieminen, T., Mikkonen, S., Lähivaara, T., Decesari, S., Facchini, M. C., Laaksonen, A. and Lehtinen, K. E. J.: Identification of new particle formation events with deep learning, Atmos. Chem. Phys., 18(13), 9597–9615, doi:10.5194/acp-18-9597-2018, 2018.

Junkermann, W. and Hacker, J. M.: Ultrafine Particles in the Lower Troposphere: Major Sources, Invisible Plumes, and Meteorological Transport Processes, Bull. Am. Meteorol. Soc., 99(12), 2587–2602, doi:10.1175/BAMS-D-18-0075.1, 2018.

Kalabokas, P., Hjorth, J., Foret, G., Dufour, G., Eremenko, M., Siour, G., Cuesta, J. and Beekmann, M.: An investigation on the origin of regional springtime ozone episodes in the western Mediterranean, Atmos. Chem. Phys., 17(6), 3905–3928, doi:10.5194/acp-17-3905-2017, 2017.

Kalabokas, P. D., Mihalopoulos, N., Ellul, R., Kleanthous, S. and Repapis, C. C.: An investigation of the meteorological and photochemical factors influencing the background rural and marine surface ozone levels in the Central and Eastern Mediterranean, Atmos. Environ., 42(34), 7894–7906, doi:10.1016/j.atmosenv.2008.07.009, 2008.

Kannosto, J., Virtanen, A., Lemmetty, M., Mäkelä, J. M., Keskinen, J., Junninen, H., Hussein, T., Aalto, P. and Kulmala, M.: Mode resolved density of atmospheric aerosol particles, Atmos. Chem. Phys., 8(17), 5327–5337, doi:10.5194/acp-8-5327-2008, 2008.

Kerminen, V.-M., Chen, X., Vakkari, V., Petäjä, T., Kulmala, M. and Bianchi, F.: Atmospheric new particle formation and growth: review of field observations, Environ. Res. Lett., 13(10), 103003, doi:10.1088/1748-9326/aadf3c, 2018.

Kirkby, J., Curtius, J., Almeida, J., Dunne, E., Duplissy, J., Ehrhart, S., Franchin, A., Gagné, S., Ickes, L., Kürten, A., Kupc, A., Metzger, A., Riccobono, F., Rondo, L., Schobesberger, S., Tsagkogeorgas, G., Wimmer, D., Amorim, A., Bianchi, F., Breitenlechner, M., David, A., Dommen, J., Downard, A., Ehn, M., Flagan, R. C., Haider, S., Hansel, A., Hauser, D., Jud, W., Junninen, H., Kreissl, F., Kvashin, A., Laaksonen, A., Lehtipalo, K., Lima, J., Lovejoy, E. R., Makhmutov, V., Mathot, S., Mikkilä, J., Minginette, P., Mogo, S., Nieminen, T., Onnela, A., Pereira, P., Petäjä, T., Schnitzhofer, R., Seinfeld, J. H., Sipilä, M., Stozhkov, Y., Stratmann, F., Tomé, A., Vanhanen, J., Viisanen, Y., Vrtala, A., Wagner, P. E., Walther, H., Weingartner, E., Wex, H., Winkler, P. M., Carslaw, K. S., Worsnop, D. R., Baltensperger, U. and Kulmala, M.: Role of sulphuric acid, ammonia and galactic cosmic rays in atmospheric aerosol nucleation, Nature, doi:10.1038/nature10343, 2011.

Kirkby, J., Duplissy, J., Sengupta, K., Frege, C., Gordon, H., Williamson, C., Heinritzi, M., Simon, M., Yan, C., Almeida, J., Tröstl, J., Nieminen, T., Ortega, I. K., Wagner, R., Adamov, A., Amorim, A., Bernhammer, A.-K., Bianchi, F., Breitenlechner, M., Brilke, S., Chen, X., Craven, J., Dias, A., Ehrhart, S., Flagan, R. C., Franchin, A., Fuchs, C., Guida, R., Hakala, J., Hoyle, C. R., Jokinen, T., Junninen, H., Kangasluoma, J., Kim, J., Krapf, M., Kürten, A., Laaksonen, A., Lehtipalo, K., Makhmutov, V., Mathot, S., Molteni, U., Onnela, A., Peräkylä, O., Piel, F., Petäjä, T., Praplan, A. P., Pringle, K., Rap, A., Richards,

N. A. D., Riipinen, I., Rissanen, M. P., Rondo, L., Sarnela, N., Schobesberger, S., Scott, C. E., Seinfeld, J. H., Sipilä, M., Steiner, G., Stozhkov, Y., Stratmann, F., Tomé, A., Virtanen, A., Vogel, A. L., Wagner, A. C., Wagner, P. E., Weingartner, E., Wimmer, D., Winkler, P. M., Ye, P., Zhang, X., Hansel, A., Dommen, J., Donahue, N. M., Worsnop, D. R., Baltensperger, U., Kulmala, M., Carslaw, K. S. and Curtius, J.: Ion-induced nucleation of pure biogenic particles, Nature, 533(7604), 521–526, doi:10.1038/nature17953, 2016.

Knutson, E. O. and Whitby, K. T.: Aerosol classification by electric mobility: apparatus, theory, and applications, J. Aerosol Sci., 6(6), 443–451, doi:10.1016/0021-8502(75)90060-9, 1975.

Kucera, V. and Fitz, S.: Direct and indirect air pollution effects on materials including cultural monuments, Water, Air, Soil Pollut., 85(1), 153–165, doi:10.1007/BF00483697, 1995.

Kulmala, M. and Kerminen, V.-M.: On the formation and growth of atmospheric nanoparticles, Atmos. Res., 90(2–4), 132–150, doi:10.1016/j.atmosres.2008.01.005, 2008.

Kulmala, M., Dal Maso, M., Mäkelä, J. M., Pirjola, L., Väkevä, M., Aalto, P., Miikkulainen, P., Hämeri, K. and O'Dowd, C. D.: On the formation, growth and composition of nucleation mode particles, Tellus, Ser. B Chem. Phys. Meteorol., doi:10.3402/tellusb.v53i4.16622, 2001.

Kulmala, M., Vehkamäki, H., Petäjä, T., Dal Maso, M., Lauri, A., Kerminen, V. M., Birmili, W. and McMurry, P. H.: Formation and growth rates of ultrafine atmospheric particles: A review of observations, J. Aerosol Sci., doi:10.1016/j.jaerosci.2003.10.003, 2004.

Kulmala, M., Petäjä, T., Nieminen, T., Sipilä, M., Manninen, H. E., Lehtipalo, K., Dal Maso, M., Aalto, P. P., Junninen, H., Paasonen, P., Riipinen, I., Lehtinen, K. E. J., Laaksonen, A. and Kerminen, V.-M.: Measurement of the nucleation of atmospheric aerosol particles, Nat. Protoc., 7(9), 1651–1667, doi:10.1038/nprot.2012.091, 2012.

Kulmala, M., Kontkanen, J., Junninen, H., Lehtipalo, K., Manninen, H. E., Nieminen, T., Petaja, T., Sipila, M., Schobesberger, S., Rantala, P., Franchin, A., Jokinen, T., Jarvinen, E., Aijala, M., Kangasluoma, J., Hakala, J., Aalto, P. P., Paasonen, P., Mikkila, J., Vanhanen, J., Aalto, J., Hakola, H., Makkonen, U., Ruuskanen, T., Mauldin, R. L., Duplissy, J., Vehkamaki, H., Back, J., Kortelainen, A., Riipinen, I., Kurten, T., Johnston, M. V., Smith, J. N., Ehn, M., Mentel, T. F., Lehtinen, K. E. J., Laaksonen, A., Kerminen, V.-M. and Worsnop, D. R.: Direct Observations of Atmospheric Aerosol Nucleation, Science (80-.)., 339(6122), 943–946, doi:10.1126/science.1227385, 2013.

Kulmala, M., Petäjä, T., Ehn, M., Thornton, J., Sipilä, M., Worsnop, D. R. and Kerminen, V.-M.: Chemistry of Atmospheric Nucleation: On the Recent Advances on Precursor Characterization and Atmospheric Cluster Composition in Connection with Atmospheric New Particle Formation, Annu. Rev. Phys. Chem., 65(1), 21–37, doi:10.1146/annurev-physchem-040412-110014, 2014.

Kulmala, M., Kerminen, V.-M., Petäjä, T., Ding, A. J. and Wang, L.: Atmospheric gas-to-particle conversion: why NPF events are observed in megacities?, Faraday Discuss., 200, 271–288, doi:10.1039/C6FD00257A, 2017.

Kulmala, M., Dada, L., Daellenbach, K. R., Yan, C., Stolzenburg, D., Kontkanen, J., Ezhova, E., Hakala, S.,

Tuovinen, S., Kokkonen, T. V., Kurppa, M., Cai, R., Zhou, Y., Yin, R., Baalbaki, R., Chan, T., Chu, B., Deng, C., Fu, Y., Ge, M., He, H., Heikkinen, L., Junninen, H., Liu, Y., Lu, Y., Nie, W., Rusanen, A., Vakkari, V., Wang, Y., Yang, G., Yao, L., Zheng, J., Kujansuu, J., Kangasluoma, J., Petäjä, T., Paasonen, P., Järvi, L., Worsnop, D., Ding, A., Liu, Y., Wang, L., Jiang, J., Bianchi, F. and Kerminen, V.-M.: Is reducing new particle formation a plausible solution to mitigate particulate air pollution in Beijing and other Chinese megacities?, Faraday Discuss., doi:10.1039/D0FD00078G, 2021.

Kumar, P., Morawska, L., Birmili, W., Paasonen, P., Hu, M., Kulmala, M., Harrison, R. M., Norford, L. and Britter, R.: Ultrafine particles in cities, Environ. Int., 66, 1–10, doi:10.1016/J.ENVINT.2014.01.013, 2014.

Lathière, J., Hauglustaine, D. A., Friend, A. D., De Noblet-Ducoudré, N., Viovy, N. and Folberth, G. A.: Impact of climate variability and land use changes on global biogenic volatile organic compound emissions, Atmos. Chem. Phys., 6(8), 2129–2146, doi:10.5194/acp-6-2129-2006, 2006.

Lehtipalo, K., Yan, C., Dada, L., Bianchi, F., Xiao, M., Wagner, R., Stolzenburg, D., Ahonen, L. R., Amorim, A., Baccarini, A., Bauer, P. S., Baumgartner, B., Bergen, A., Bernhammer, A.-K., Breitenlechner, M., Brilke, S., Buchholz, A., Mazon, S. B., Chen, D., Chen, X., Dias, A., Dommen, J., Draper, D. C., Duplissy, J., Ehn, M., Finkenzeller, H., Fischer, L., Frege, C., Fuchs, C., Garmash, O., Gordon, H., Hakala, J., He, X., Heikkinen, L., Heinritzi, M., Helm, J. C., Hofbauer, V., Hoyle, C. R., Jokinen, T., Kangasluoma, J., Kerminen, V.-M., Kim, C., Kirkby, J., Kontkanen, J., Kürten, A., Lawler, M. J., Mai, H., Mathot, S., Mauldin, R. L., Molteni, U., Nichman, L., Nie, W., Nieminen, T., Ojdanic, A., Onnela, A., Passananti, M., Petäjä, T., Piel, F., Pospisilova, V., Quéléver, L. L. J., Rissanen, M. P., Rose, C., Sarnela, N., Schallhart, S., Schuchmann, S., Sengupta, K., Simon, M., Sipilä, M., Tauber, C., Tomé, A., Tröstl, J., Väisänen, O., Vogel, A. L., Volkamer, R., Wagner, A. C., Wang, M., Weitz, L., Wimmer, D., Ye, P., Ylisirniö, A., Zha, Q., Carslaw, K. S., Curtius, J., Donahue, N. M., Flagan, R. C., Hansel, A., Riipinen, I., Virtanen, A., Winkler, P. M., Baltensperger, U., Kulmala, M. and Worsnop, D. R.: Multicomponent new particle formation from sulfuric acid, ammonia, and biogenic vapors, Sci. Adv., 4(12), doi:10.1126/sciadv.aau5363, 2018.

Merikanto, J., Spracklen, D. V., Mann, G. W., Pickering, S. J. and Carslaw, K. S.: Impact of nucleation on global CCN, Atmos. Chem. Phys., doi:10.5194/acp-9-8601-2009, 2009.

Millán, M., Salvador, R., Mantilla, E. and Artíñano, B.: Meteorology and photochemical air pollution in Southern Europe: Experimental results from EC research projects, Atmos. Environ., 30(12), 1909–1924, doi:10.1016/1352-2310(95)00220-0, 1996.

Millán, M. M., Artíñano, B., Alonso, L., Navazo, M. and Castro, M.: The effect of meso-scale flows on regional and long-range atmospheric transport in the western Mediterranean area, Atmos. Environ. Part A. Gen. Top., 25(5–6), 949–963, doi:10.1016/0960-1686(91)90137-V, 1991.

Millán, M. M., Salvador, R., Mantilla, E. and Kallos, G.: Photooxidant dynamics in the Mediterranean basin in summer: Results from European research projects, J. Geophys. Res. Atmos., 102(D7), 8811–8823, doi:10.1029/96JD03610, 1997.

Millán, M. M., José Sanz, M., Salvador, R. and Mantilla, E.: Atmospheric dynamics and ozone cycles related

to nitrogen deposition in the western Mediterranean, in Environmental Pollution., 2002.

Minguillón, M. C., Brines, M., Pérez, N., Reche, C., Pandolfi, M., Fonseca, A. S., Amato, F., Alastuey, A., Lyasota, A., Codina, B., Lee, H.-K., Eun, H.-R., Ahn, K.-H. and Querol, X.: New particle formation at ground level and in the vertical column over the Barcelona area, Atmos. Res., 164–165, 118–130, doi:10.1016/j.atmosres.2015.05.003, 2015.

Minoura, H. and Takekawa, H.: Observation of number concentrations of atmospheric aerosols and analysis of nanoparticle behavior at an urban background area in Japan, Atmos. Environ., 39(32), 5806–5816, doi:10.1016/J.ATMOSENV.2005.06.033, 2005.

Mirme, A., Tamm, E., Mordas, G., Vana, M., Uin, J., Mirme, S., Bernotas, T., Laakso, L., Hirsikko, A. and Kulmala, M.: A wide-range multi-channel air ion spectrometer, Boreal Environ. Res., 12(3), 247–264, 2007.

Monks, P. S., Archibald, A. T., Colette, A., Cooper, O., Coyle, M., Derwent, R., Fowler, D., Granier, C., Law, K. S., Mills, G. E., Stevenson, D. S., Tarasova, O., Thouret, V., von Schneidemesser, E., Sommariva, R., Wild, O. and Williams, M. L.: Tropospheric ozone and its precursors from the urban to the global scale from air quality to short-lived climate forcer, Atmos. Chem. Phys., 15(15), 8889–8973, doi:10.5194/acp-15-8889-2015, 2015.

Müller, T., Henzing, J. S., De Leeuw, G., Wiedensohler, A., Alastuey, A., Angelov, H., Bizjak, M., Collaud Coen, M., Engström, J. E., Gruening, C., Hillamo, R., Hoffer, A., Imre, K., Ivanow, P., Jennings, G., Sun, J. Y., Kalivitis, N., Karlsson, H., Komppula, M., Laj, P., Li, S. M., Lunder, C., Marinoni, A., Martins Dos Santos, S., Moerman, M., Nowak, A., Ogren, J. A., Petzold, A., Pichon, J. M., Rodriquez, S., Sharma, S., Sheridan, P. J., Teinilä, K., Tuch, T., Viana, M., Virkkula, A., Weingartner, E., Wilhelm, R. and Wang, Y. Q.: Characterization and intercomparison of aerosol absorption photometers: Result of two intercomparison workshops, Atmos. Meas. Tech., doi:10.5194/amt-4-245-2011, 2011.

Ogulei, D., Hopke, P. K., Chalupa, D. C. and Utell, M. J.: Modeling Source Contributions to Submicron Particle Number Concentrations Measured in Rochester, New York, Aerosol Sci. Technol., 41(2), 179–201, doi:10.1080/02786820601116012, 2007.

Ohlwein, S., Kappeler, R., Kutlar Joss, M., Künzli, N. and Hoffmann, B.: Health effects of ultrafine particles: a systematic literature review update of epidemiological evidence, Int. J. Public Health, doi:10.1007/s00038-019-01202-7, 2019.

Paasonen, P., Kupiainen, K., Klimont, Z., Visschedijk, A., Denier van der Gon, H. A. C. and Amann, M.: Continental anthropogenic primary particle number emissions, Atmos. Chem. Phys., 16(11), 6823–6840, doi:10.5194/acp-16-6823-2016, 2016.

Paatero, P.: Least squares formulation of robust non-negative factor analysis, in Chemometrics and Intelligent Laboratory Systems, vol. 37, pp. 23–35, Elsevier., 1997.

Park, K., Park, J. Y., Kwak, J.-H., Cho, G. N. and Kim, J.-S.: Seasonal and diurnal variations of ultrafine particle concentration in urban Gwangju, Korea: Observation of ultrafine particle events, Atmos. Environ., 42(4), 788–799, doi:10.1016/j.atmosenv.2007.09.068, 2008.

Pey, J., Querol, X., Alastuey, A., Rodríguez, S., Putaud, J. P. and Van Dingenen, R.: Source apportionment of urban fine and ultra-fine particle number concentration in a Western Mediterranean city, Atmos. Environ., 43(29), 4407–4415, doi:10.1016/J.ATMOSENV.2009.05.024, 2009.

Pikridas, M., Riipinen, I., Hildebrandt, L., Kostenidou, E., Manninen, H., Mihalopoulos, N., Kalivitis, N., Burkhart, J. F., Stohl, A., Kulmala, M. and Pandis, S. N.: New particle formation at a remote site in the eastern Mediterranean, J. Geophys. Res. Atmos., 117(12), doi:10.1029/2012JD017570, 2012.

Pirjola, L., Kulmala, M., Wilck, M., Bischoff, A., Stratmann, F. and Otto, E.: Formation of sulphuric acid aerosols and cloud condensation nuclei: An expression for significant nucleation and model comparison, J. Aerosol Sci., doi:10.1016/S0021-8502(98)00776-9, 1999.

Plaza, J., Pujadas, M. and Artíñano, B.: Formation and Transport of the Madrid Ozone Plume, J. Air Waste Manag. Assoc., doi:10.1080/10473289.1997.10463938, 1997.

Qi, X. M., Ding, A. J., Nie, W., Petäjä, T., Kerminen, V.-M., Herrmann, E., Xie, Y. N., Zheng, L. F., Manninen, H., Aalto, P., Sun, J. N., Xu, Z. N., Chi, X. G., Huang, X., Boy, M., Virkkula, A., Yang, X.-Q., Fu, C. B. and Kulmala, M.: Aerosol size distribution and new particle formation in the western Yangtze River Delta of China: 2 years of measurements at the SORPES station, Atmos. Chem. Phys., 15(21), 12445–12464, doi:10.5194/acp-15-12445-2015, 2015.

Querol, X., Alastuey, A., Reche, C., Orio, A., Pallares, M., Reina, F., Dieguez, J. J., Mantilla, E., Escudero, M., Alonso, L., Gangoiti, G. and Millán, M.: On the origin of the highest ozone episodes in Spain, Sci. Total Environ., 572, 379–389, doi:10.1016/j.scitotenv.2016.07.193, 2016.

Querol, X., Gangoiti, G., Mantilla, E., Alastuey, A., Minguillón, M. C., Amato, F., Reche, C., Viana, M., Moreno, T., Karanasiou, A., Rivas, I., Pérez, N., Ripoll, A., Brines, M., Ealo, M., Pandolfi, M., Lee, H.-K., Eun, H.-R., Park, Y.-H., Escudero, M., Beddows, D., Harrison, R. M., Bertrand, A., Marchand, N., Lyasota, A., Codina, B., Olid, M., Udina, M., Jiménez-Esteve, B., Soler, M. R., Alonso, L., Millán, M. and Ahn, K.-H.: Phenomenology of high-ozone episodes in NE Spain, Atmos. Chem. Phys., 17(4), 2817–2838, doi:10.5194/acp-17-2817-2017, 2017.

Querol, X., Alastuey, A., Gangoiti, G., Perez, N., Lee, H. K., Eun, H. R., Park, Y., Mantilla, E., Escudero, M., Titos, G., Alonso, L., Temime-Roussel, B., Marchand, N., Moreta, J. R., Revuelta, M. A., Salvador, P., Artíñano, B., García dos Santos, S., Anguas, M., Notario, A., Saiz-Lopez, A., Harrison, R. M., Millán, M. and Ahn, K.-H.: Phenomenology of summer ozone episodes over the Madrid Metropolitan Area, central Spain, Atmos. Chem. Phys., 18(9), 6511–6533, doi:10.5194/acp-18-6511-2018, 2018.

Reche, C., Querol, X., Alastuey, A., Viana, M., Pey, J., Moreno, T., Rodríguez, S., González, Y., Fernández-Camacho, R., de la Rosa, J., Dall'Osto, M., Prévôt, A. S. H., Hueglin, C., Harrison, R. M. and Quincey, P.: New considerations for PM, Black Carbon and particle number concentration for air quality monitoring across different European cities, Atmos. Chem. Phys., 11(13), 6207–6227, doi:10.5194/acp-11-6207-2011, 2011.

Riccobono, F., Rondo, L., Sipilä, M., Barmet, P., Curtius, J., Dommen, J., Ehn, M., Ehrhart, S., Kulmala, M., KArten, A., Mikkilä, J., Paasonen, P., Petäjä, T., Weingartner, E. and Baltensperger, U.:

Contribution of sulfuric acid and oxidized organic compounds to particle formation and growth, Atmos. Chem. Phys., doi:10.5194/acp-12-9427-2012, 2012.

Riipinen, I., Yli-Juuti, T., Pierce, J. R., Petäjä, T., Worsnop, D. R., Kulmala, M. and Donahue, N. M.: The contribution of organics to atmospheric nanoparticle growth, Nat. Geosci., doi:10.1038/ngeo1499, 2012.

Rivas, I., Beddows, D. C. S., Amato, F., Green, D. C., Järvi, L., Hueglin, C., Reche, C., Timonen, H., Fuller, G. W., Niemi, J. V., Pérez, N., Aurela, M., Hopke, P. K., Alastuey, A., Kulmala, M., Harrison, R. M., Querol, X. and Kelly, F. J.: Source apportionment of particle number size distribution in urban background and traffic stations in four European cities, Environ. Int., 135, 105345, doi:10.1016/j.envint.2019.105345, 2020.

Rose, C., Zha, Q., Dada, L., Yan, C., Lehtipalo, K., Junninen, H., Mazon, S. B., Jokinen, T., Sarnela, N., Sipilä, M., Petäjä, T., Kerminen, V.-M., Bianchi, F. and Kulmala, M.: Observations of biogenic ion-induced cluster formation in the atmosphere, Sci. Adv., 4(4), doi:10.1126/sciadv.aar5218, 2018.

Salma, I., Németh, Z., Kerminen, V.-M., Aalto, P., Nieminen, T., Weidinger, T., Molnár, Á., Imre, K. and Kulmala, M.: Regional effect on urban atmospheric nucleation, Atmos. Chem. Phys., 16(14), 8715–8728, doi:10.5194/acp-16-8715-2016, 2016.

Salvador, P., Artíñano, B., Viana, M. M., Alastuey, A. and Querol, X.: Multicriteria approach to interpret the variability of the levels of particulate matter and gaseous pollutants in the madrid metropolitan area, during the 1999-2012 period, Atmos. Environ., doi:10.1016/j.atmosenv.2015.03.008, 2015.

Schobesberger, S., Junninen, H., Bianchi, F., Lönn, G., Ehn, M., Lehtipalo, K., Dommen, J., Ehrhart, S., Ortega, I. K., Franchin, A., Nieminen, T., Riccobono, F., Hutterli, M., Duplissy, J., Almeida, J., Amorim, A., Breitenlechner, M., Downard, A. J., Dunne, E. M., Flagan, R. C., Kajos, M., Keskinen, H., Kirkby, J., Kupc, A., Kürten, A., Kurtén, T., Laaksonen, A., Mathot, S., Onnela, A., Praplan, A. P., Rondo, L., Santos, F. D., Schallhart, S., Schnitzhofer, R., Sipilä, M., Tomé, A., Tsagkogeorgas, G., Vehkamäki, H., Wimmer, D., Baltensperger, U., Carslaw, K. S., Curtius, J., Hansel, A., Petäjä, T., Kulmala, M., Donahue, N. M. and Worsnop, D. R.: Molecular understanding of atmospheric particle formation from sulfuric acid and large oxidized organic molecules, Proc. Natl. Acad. Sci. U. S. A., doi:10.1073/pnas.1306973110, 2013.

Schraufnagel, D. E.: The health effects of ultrafine particles, Exp. Mol. Med., 52(3), 311–317, doi:10.1038/s12276-020-0403-3, 2020.

Seinfeld, J. H. and Pandis, S. N.: Atmospheric Chemistry and Physics, 2nd ed., John Wiley & Sons, New York., 2006.

Sillman, S.: The relation between ozone, NOx and hydrocarbons in urban and polluted rural environments, Atmos. Environ., 33(12), 1821–1845, doi:10.1016/S1352-2310(98)00345-8, 1999.

Sipila, M., Berndt, T., Petaja, T., Brus, D., Vanhanen, J., Stratmann, F., Patokoski, J., Mauldin, R. L., Hyvärinen, A. P., Lihavainen, H. and Kulmala, M.: The role of sulfuric acid in atmospheric nucleation, Science (80-.)., doi:10.1126/science.1180315, 2010.

Soler, M. R., Arasa, R., Merino, M., Olid, M. and Ortega, S.: Modelling Local Sea-Breeze Flow and

Associated Dispersion Patterns Over a Coastal Area in North-East Spain: A Case Study, Boundary-Layer Meteorol., doi:10.1007/s10546-011-9599-z, 2011.

Spracklen, D. V., Carslaw, K. S., Kulmala, M., Kerminen, V. M., Mann, G. W. and Sihto, S. L.: The contribution of boundary layer nucleation events to total particle concentrations on regional and global scales, Atmos. Chem. Phys., doi:10.5194/acp-6-5631-2006, 2006.

Squizzato, S., Masiol, M., Emami, F., Chalupa, D., Utell, M., Rich, D. and Hopke, P.: Long-Term Changes of Source Apportioned Particle Number Concentrations in a Metropolitan Area of the Northeastern United States, Atmosphere (Basel)., 10(1), 27, doi:10.3390/atmos10010027, 2019.

Stolzenburg, M. R. and McMurry, P. H.: An Ultrafine Aerosol Condensation Nucleus Counter, Aerosol Sci. Technol., 14(1), 48–65, doi:10.1080/02786829108959470, 1991.

Stull, R. B.: An Introduction to Boundary Layer Meteorology, Kluwer Academic Publishers., 1988.

Syri, S., Amann, M., Schöpp, W. and Heyes, C.: Estimating long-term population exposure to ozone in urban areas of Europe, Environ. Pollut., doi:10.1016/S0269-7491(00)00157-3, 2001.

Thomson, W.: On the equilibrium of vapour at a curved surface of liquid , London, Edinburgh, Dublin Philos. Mag. J. Sci., 42(282), 448–452, doi:10.1080/14786447108640606, 1871.

Toll, I. and Baldasano, J. M.: Modeling of photochemical air pollution in the Barcelona area with highly disaggregated anthropogenic and biogenic emissions, Atmos. Environ., 34(19), 3069–3084, doi:10.1016/S1352-2310(99)00498-7, 2000.

Troen, I. B. and Mahrt, L.: A simple model of the atmospheric boundary layer; sensitivity to surface evaporation, Boundary-Layer Meteorol., 37(1–2), 129–148, doi:10.1007/BF00122760, 1986.

Tunved, P., Ström, J. and Krejci, R.: Arctic aerosol life cycle: Linking aerosol size distributions observed between 2000 and 2010 with air mass transport and precipitation at Zeppelin station, Ny-Ålesund, Svalbard, Atmos. Chem. Phys., doi:10.5194/acp-13-3643-2013, 2013.

U.S. EPA: Air Quality Criteria For Ozone and Related Photochemical Oxidants, Washington, DC. [online] Available from: https://cfpub.epa.gov/si/si_public_record_report.cfm?Lab=NCEA&count=10000&dirEntryId=149923&searchall=&showcriteria=2&simplesearch=0&timstype=, 2006.

UNECE: Mapping critical levels for vegetation, in Manual on methodologies and criteria for modelling and mapping critical loads and levels, United Nations Economic Comission for Europe, Geneva, Switzerland. [online] Available from: https://icpvegetation.ceh.ac.uk/get-involved/manuals/mapping-manual, 2011.

Vana, M., Ehn, M., Petäjä, T., Vuollekoski, H., Aalto, P., de Leeuw, G., Ceburnis, D., O'Dowd, C. D. and Kulmala, M.: Characteristic features of air ions at Mace Head on the west coast of Ireland, Atmos. Res., doi:10.1016/j.atmosres.2008.04.007, 2008.

Vanhanen, J., Mikkilä, J., Lehtipalo, K., Sipilä, M., Manninen, H. E., Siivola, E., Petäjä, T. and Kulmala, M.: Particle Size Magnifier for Nano-CN Detection, Aerosol Sci. Technol., 45(4), 533–542,

doi:10.1080/02786826.2010.547889, 2011.

Vehkamäki, H. and Riipinen, I.: Thermodynamics and kinetics of atmospheric aerosol particle formation and growth, Chem. Soc. Rev., 41(15), 5160, doi:10.1039/c2cs00002d, 2012.

Vu, T. V., Delgado-Saborit, J. M. and Harrison, R. M.: Review: Particle number size distributions from seven major sources and implications for source apportionment studies, Atmos. Environ., doi:10.1016/j.atmosenv.2015.09.027, 2015.

Wang, D., Zhou, B., Fu, Q., Zhao, Q., Zhang, Q., Chen, J., Yang, X., Duan, Y. and Li, J.: Intense secondary aerosol formation due to strong atmospheric photochemical reactions in summer: observations at a rural site in eastern Yangtze River Delta of China, Sci. Total Environ., 571, 1454–1466, doi:10.1016/J.SCITOTENV.2016.06.212, 2016.

Wang, M., Kong, W., Marten, R., He, X. C., Chen, D., Pfeifer, J., Heitto, A., Kontkanen, J., Dada, L., Kürten, A., Yli-Juuti, T., Manninen, H. E., Amanatidis, S., Amorim, A., Baalbaki, R., Baccarini, A., Bell, D. M., Bertozzi, B., Bräkling, S., Brilke, S., Murillo, L. C., Chiu, R., Chu, B., De Menezes, L. P., Duplissy, J., Finkenzeller, H., Carracedo, L. G., Granzin, M., Guida, R., Hansel, A., Hofbauer, V., Krechmer, J., Lehtipalo, K., Lamkaddam, H., Lampimäki, M., Lee, C. P., Makhmutov, V., Marie, G., Mathot, S., Mauldin, R. L., Mentler, B., Müller, T., Onnela, A., Partoll, E., Petäjä, T., Philippov, M., Pospisilova, V., Ranjithkumar, A., Rissanen, M., Rörup, B., Scholz, W., Shen, J., Simon, M., Sipilä, M., Steiner, G., Stolzenburg, D., Tham, Y. J., Tomé, A., Wagner, A. C., Wang, D. S., Wang, Y., Weber, S. K., Winkler, P. M., Wlasits, P. J., Wu, Y., Xiao, M., Ye, Q., Zauner-Wieczorek, M., Zhou, X., Volkamer, R., Riipinen, I., Dommen, J., Curtius, J., Baltensperger, U., Kulmala, M., Worsnop, D. R., Kirkby, J., Seinfeld, J. H., El-Haddad, I., Flagan, R. C. and Donahue, N. M.: Rapid growth of new atmospheric particles by nitric acid and ammonia condensation, Nature, doi:10.1038/s41586-020-2270-4, 2020.

Wang, S. C. and Flagan, R. C.: Scanning electrical mobility spectrometer, Aerosol Sci. Technol., doi:10.1080/02786829008959441, 1990.

WHO: Air quality guidelines for particulate matter, ozone, nitrogen dioxide and sulfur dioxide, World Heal. Organ. [online] Available from: http://whqlibdoc.who.int/hq/2006/WHO_SDE_PHE_OEH_06.02_eng.pdf?ua=1 (Accessed 1 June 2021), 2006.

WHO: Health risks of ozone from long-range transboundary air pollution. [online] Available from: https://www.euro.who.int/en/health-topics/environment-and-health/air-quality/publications/pre2009/health-risks-of-ozone-from-long-range-transboundary-air-pollution, 2008.

WHO: Review of evidence on health aspects of air pollution – REVIHAAP Project. [online] Available from: https://www.euro.who.int/en/health-topics/environment-and-health/air-quality/publications/2013/review-of-evidence-on-health-aspects-of-air-pollution-revihaap-project-final-technical-report, 2013.

WHO: WHO Expert consultation: Available evidence for the future update of the WHO Global air quality

guidelines (AQGs). [online] Available from: https://www.euro.who.int/__data/assets/pdf_file/0013/301720/Evidence-future-update-AQGs-mtg-report-Bonn-sept-oct-15.pdf?ua=1, 2016.

Wichmann, H. E., Spix, C., Tuch, T., Wölke, G., Peters, A., Heinrich, J., Kreyling, W. G. and Heyder, J.: Daily mortality and fine and ultrafine particles in Erfurt, Germany part I: role of particle number and particle mass., Res. Rep. Health. Eff. Inst., (98), 2000.

Wonaschütz, A., Demattio, A., Wagner, R., Burkart, J., Zíková, N., Vodička, P., Ludwig, W., Steiner, G., Schwarz, J. and Hitzenberger, R.: Seasonality of new particle formation in Vienna, Austria – Influence of air mass origin and aerosol chemical composition, Atmos. Environ., 118, 118–126, doi:10.1016/J.ATMOSENV.2015.07.035, 2015.

Wu, Z., Hu, M., Liu, S., Wehner, B., Bauer, S., Ma ßling, A., Wiedensohler, A., Petäjä, T., Dal Maso, M. and Kulmala, M.: New particle formation in Beijing, China: Statistical analysis of a 1-year data set, J. Geophys. Res., 112(D9), D09209, doi:10.1029/2006JD007406, 2007.

Xiao, S., Wang, M. Y., Yao, L., Kulmala, M., Zhou, B., Yang, X., Chen, J. M., Wang, D. F., Fu, Q. Y., Worsnop, D. R. and Wang, L.: Strong atmospheric new particle formation in winter in urban Shanghai, China, Atmos. Chem. Phys., 15(4), 1769–1781, doi:10.5194/acp-15-1769-2015, 2015.

Yan, C., Dada, L., Rose, C., Jokinen, T., Nie, W., Schobesberger, S., Junninen, H., Lehtipalo, K., Sarnela, N., Makkonen, U., Garmash, O., Wang, Y., Zha, Q., Paasonen, P., Bianchi, F., Sipilä, M., Ehn, M., Petäjä, T., Kerminen, V.-M., Worsnop, D. R. and Kulmala, M.: The role of H2SO4-NH3 anion clusters in ion-induced aerosol nucleation mechanisms in the boreal forest, Atmos. Chem. Phys., 18(17), 13231–13243, doi:10.5194/acp-18-13231-2018, 2018.

Yan, C., Yin, R., Lu, Y., Dada, L., Yang, D., Fu, Y., Kontkanen, J., Deng, C., Garmash, O., Ruan, J., Baalbaki, R., Schervish, M., Cai, R., Bloss, M., Chan, T., Chen, T., Chen, Q., Chen, X., Chen, Y., Chu, B., Dällenbach, K., Foreback, B., He, X., Heikkinen, L., Jokinen, T., Junninen, H., Kangasluoma, J., Kokkonen, T., Kurppa, M., Lehtipalo, K., Li, H., Li, H., Li, X., Liu, Y., Ma, Q., Paasonen, P., Rantala, P., Pileci, R. E., Rusanen, A., Sarnela, N., Simonen, P., Wang, S., Wang, W., Wang, Y., Xue, M., Yang, G., Yao, L., Zhou, Y., Kujansuu, J., Petäjä, T., Nie, W., Ma, Y., Ge, M., He, H., Donahue, N. M., Worsnop, D. R., Veli-Matti Kerminen, Wang, L., Liu, Y., Zheng, J., Kulmala, M., Jiang, J. and Bianchi, F.: The Synergistic Role of Sulfuric Acid, Bases, and Oxidized Organics Governing New-Particle Formation in Beijing, Geophys. Res. Lett., 48(7), doi:10.1029/2020GL091944, 2021.

Yao, L., Garmash, O., Bianchi, F., Zheng, J., Yan, C., Kontkanen, J., Junninen, H., Mazon, S. B., Ehn, M., Paasonen, P., Sipilä, M., Wang, M., Wang, X., Xiao, S., Chen, H., Lu, Y., Zhang, B., Wang, D., Fu, Q., Geng, F., Li, L., Wang, H., Qiao, L., Yang, X., Chen, J., Kerminen, V.-M., Petäjä, T., Worsnop, D. R., Kulmala, M. and Wang, L.: Atmospheric new particle formation from sulfuric acid and amines in a Chinese megacity, Science (80-.)., 361(6399), 278–281, doi:10.1126/science.aao4839, 2018.

Zaidan, M. A., Haapasilta, V., Relan, R., Junninen, H., Aalto, P. P., Kulmala, M., Laurson, L. and Foster, A. S.: Predicting atmospheric particle formation days by Bayesian classification of the time series features, Tellus B Chem. Phys. Meteorol., 70(1), 1–10, doi:10.1080/16000889.2018.1530031, 2018.

Zhang, R., Khalizov, A., Wang, L., Hu, M. and Xu, W.: Nucleation and growth of nanoparticles in the atmosphere, Chem. Rev., doi:10.1021/cr2001756, 2012.

Zhao, J., Ortega, J., Chen, M., McMurry, P. H. and Smith, J. N.: Dependence of particle nucleation and growth on high-molecular-weight gas-phase products during ozonolysis of α-pinene, Atmos. Chem. Phys., 13(15), 7631–7644, doi:10.5194/acp-13-7631-2013, 2013.